Punching shear and moment transfer in reinforced concrete flat slabs.

Khaled Kamaraldin

School of Electronics and Computer Science

PUNCHING SHEAR AND MOMENT TRANSFER IN REINFORCED CONCRETE FLAT SLABS

by

KHALED KAMARALDIN, CIVIL ENG., MSc

A thesis submitted to the council for
National Academic Award
for the Degree of Doctor of Philosophy
in the Faculty of Engineering.

The Polytechnic of Central London,

NOVEMBER 1990

D E D I C A T E D T O M Y P A R E N T S

ABSTRACT

==========

The behaviour of slab column junctions of reinforced concrete flat slab structures, subjected to various combinations of vertical load and moment was studied with regard to flexure, and punching shear.

Laboratory tests were made to study the behaviour of flat slabs supported by internal columns. Particular attention was paid to ultimate strength, slab-column rotations, and slab deflections. The principal variables in the ten slab specimens reported in the present work were the shape of the columns, slab aspect ratios, the ratio of reinforcement, and the eccentricity of applied loads.

Following from the experimental work a proposal is made for calculation of punching shear resistance of concentrically loaded slabs at internal columns. The same method is extended to eccentrically loaded slabs. The method of calculating punching shear resistance of internal flat slabs is based upon a realistic model of their internal behaviour. A method of finding the effective joint stiffness of cracked slabs subjected to eccentric loading is also developed.

The proposed method of shear resistance calculation is applied to the author's tests and to as many other slab tests as posible. Comparisons of the author's proposed method of predicting punching shear failure loads with various alternative methods are presented. A number of conclusions are

drawn from these comparisons as well as from the experimental observations. Some suggestions are also made for further research on the subject.

ACKNOWLEDGEMENTS

==========

The research work presented in this thesis was developed under the supervision of Prof.P.E. Regan, BSc.,D.I.C., Ph.D., S.V.R. (Sweden), Head of the School of Architecture and Engineering, Polytechnic of Central London,

The author is greatly indebted to Prof. Regan for his excellent guidance, constructive criticism, and help throughout the work.

Sincere gratitude is due to Dr. C.W.Yu, Ph.D.,D.I.C.,BSc, MASCE,MICE, my external supervisor, for his encouragement and valuable advice.

The author wishes to express his deepest gratitude to his brother Ahmed for his moral support.

CONTENTS

CHAPTER SIX

Test Analysis

LIST OF FIGURES

LIST OF TABLES

CHAPTER ONE

INTRODUCTION AND REVIEW OF PREVIOUS WORK ON METHODS OF OVERALL DESIGN AND SHEAR FAILURES OF REINFORCED CONCRETE FLAT SLABS.

1-1 INTRODUCTION

Reinforced concrete flat slabs are structures directly supported by columns, and are often preferred to conventional slab-beam construction from architectural and economic points of view.

Flat slab construction offers many advantages:

- Reduction of the storey height
- Simplicity of construction allowing reduction of the construction time
- Considerable reduction in formwork
- Reduction in finishing material
- Flexibility in the arrangement of partitions

However the absence of beams in flat slab structures creates the following problems:

- The structure has a relatively lower stiffness under lateral loading
- Vertical deflections are increased
- At slab-column connections high shear stresses are generated which may result in the punching shear mode of failure.

The lower lateral stiffness can be avoided by shear walls, lift shafts or external bracing. Prestressing can be employed to control the deflection. The main problem in flat slab structures is thus the punching resistance at slab-column connections.

1-2 THE OBJECT OF THE PROJECT

Punching shear resistance has been the subject of a number of research projects. Some investigators and codes of practice treat the problem empirically. Other investigators have treated it semi-theoretically for special cases. However no completely theoretical method of analysis exists for the problem of punching shear resistance under concentric or eccentric loading conditions. Most of the past work on the punching shear resistance of reinforced concrete flat slabs has been concerned with concentric loading conditions on simply supported slabs. In the experimentally based investigations (2,20,21,23,40, 43,52,63,71) which have addressed themselves to eccentric loading conditions, the test specimens have represented the part of a flat slab around a column spanning between points of contraflexure and the distance from the line of zero moment has been fixed and equal on the two sides. These conditions can not in general be true for connections transferring moments. For equal spans with equal vertical loads and wind loading the distance to the lines of contraflexure must be unequal at opposite sides of the column. The effects produced by such test arrangements are thus not fully compatible with those arising in real conditions in

terms of rotations at the slab-column junction and deflections within the slab. The test arrangement also suffers from the lack of any possibility of redistribution of moment between midspan and support sections. A more realistic set-up would be one which allowed redistribution of moments between midspan and supports. Long and Masterson (38) suggested that tests should be carried out on specimens with boundary conditions different from those mentioned above by extending the specimen beyond the line of contraflexure for shear loading.

<u>The main objects of the present research were to:</u>

-Develop a method of modelling a typical interior slab-column connection in which the actual boundary conditions would be simulated for all types of loading.

-Study the mechanism of failure in shear of reinforced concrete slabs

-Investigate the behaviour of slabs under concentric and eccentric loading conditions

-Develop a model and an analysis with sufficient accuracy to predict the punching failure load

-Investigate the deformations and develop expressions for use in assessing deflections of flat-slabs

-Verify the proposed analysis by an experimental programme allowing the validity of the assumptions used in the proposed method of analysis to be examined in the light of the results of these tests and other test results from various sources.

Since the punching shear mode of failure may occur in slabs with concentric or eccentric load the experimental programme was planned to study the behaviour of slabs under vertical loading, and combined vertical loading with moment transfer from slab to column.

1-3 REVIEW OF PREVIOUS WORK ON REINFORCED CONCRETE FLAT SLABS

In order to be able to design reinforced concrete flat slabs their flexural and punching shear strengths should be studied.

1-3-1 METHODS OF OVERALL DESIGN FOR FLAT SLABS.

1-3-1-1 Yield line theory

If a flat slab is to be analysed by yield line theory it is necessary to consider both overall and local mechanisms.

The simplest overall mechanisms for slabs under vertical loading are simple positive and negative yield lines traversing the full width in either direction as shown in Fig. (1-1). The separate mechanisms can also be combined as in Fig. (1-2). The consideration of such mechanisms alone provides no information on the way in which reinforcement should be distributed along the yield lines.

However a plastic solution for this can be obtained from a study of the collapse mode of Fig.(1-3).The dimensions 'a' and 'b' vary with the degree of concentration of reinforcement toward the column lines, and the normal objective of design is to provide a concentration sufficient to ensure that, with the

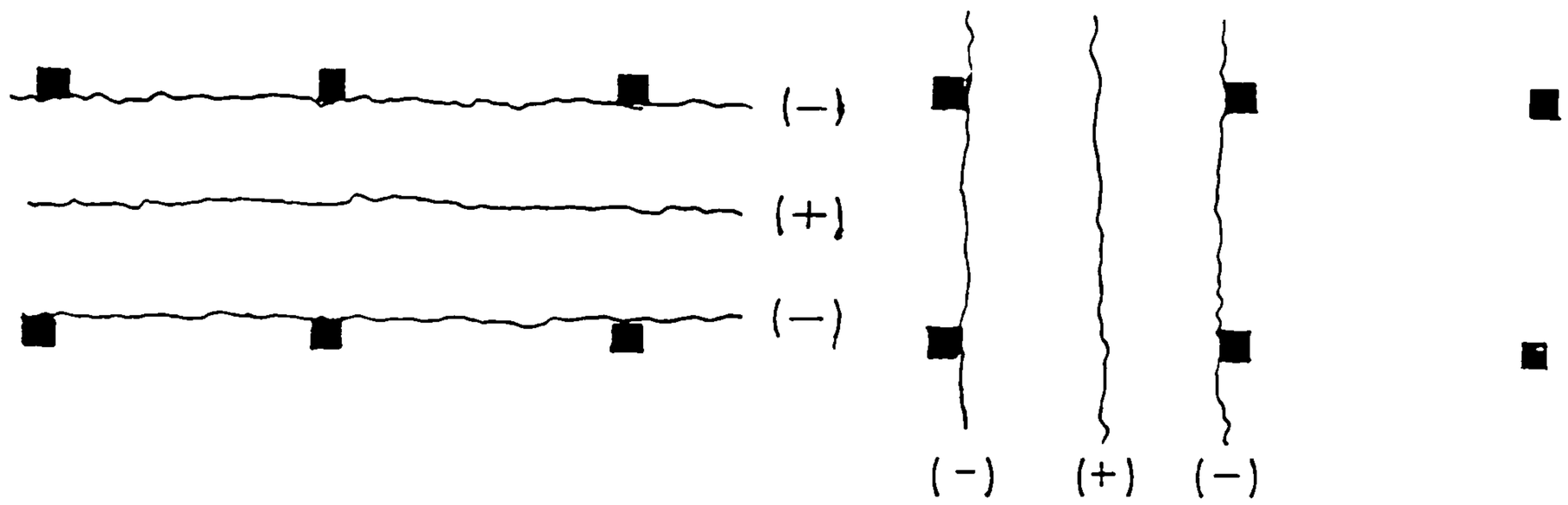

Fig.(1-1) Positive and negative yield lines
for slabs under vertical loading

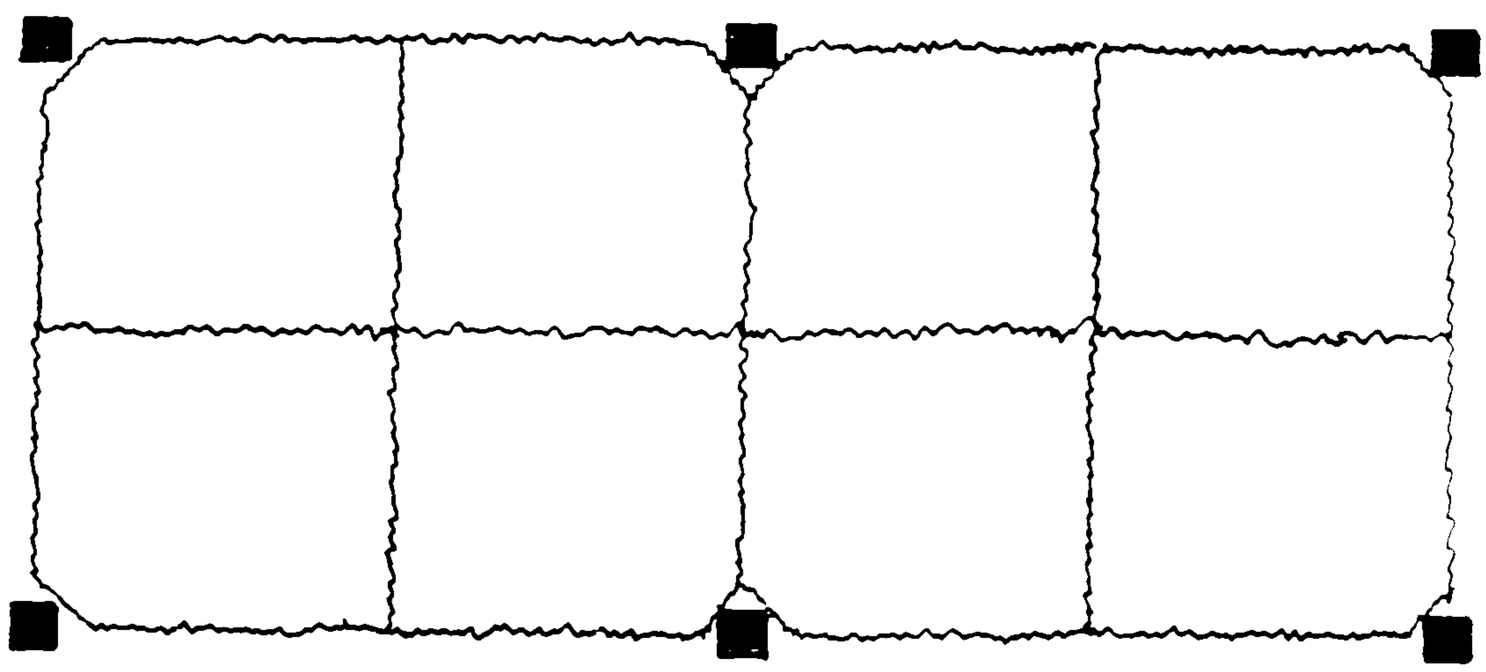

Fig.(1-2) Combined yield line mechanisms for
flat-slabs under vertical loading

corresponding critical dimensions 'a' and 'b' ,the resistance of the system is at least equal to that for the collapse modes in Figs.(1-1) and (1-2). To obtain this requires less concentration than is obtained from approximately elastic designs and for normal arrangements of reinforcement the collapse pattern of Fig.(1-3) is unlikely.

The mechanisms for edge and corner panels corresponding to those of Figs.(1-1) ,(1-2) and Fig.(1-3) for interior situations are shown in Figs.(1-4),(1-5) and (1-6).

Again the obvious objective of detailed design is to arrange the reinforcement in such a way that the different mechanisms give equal collapse loads. A further mechanism which should be Considered in this context is a variation on that in Fig.(1-4), where the full-width interior yield lines are accompanied at the edges by the local mechanism of Fig.(1-7). If the full yield line theory resistance to the mechanism of Fig.(1-7) is to be developed the detailing of the slab must provide adequate torsional resistance at its edge. In practice this necessitates a close spacing of U-bars or links at the edge to oppose the opening of torsion cracks indicated in Fig.(1-8).

The local mechanism of Fig.(1-7) and the corner yield line of Fig.(1-5) require the transfer of moments between the slab and the exterior columns. The transfer of moments to interior columns makes possible a number of local mechanisms not considered above, two of which are illustrated in Fig. (1-9). Some of the local mechanisms present particular problems if the

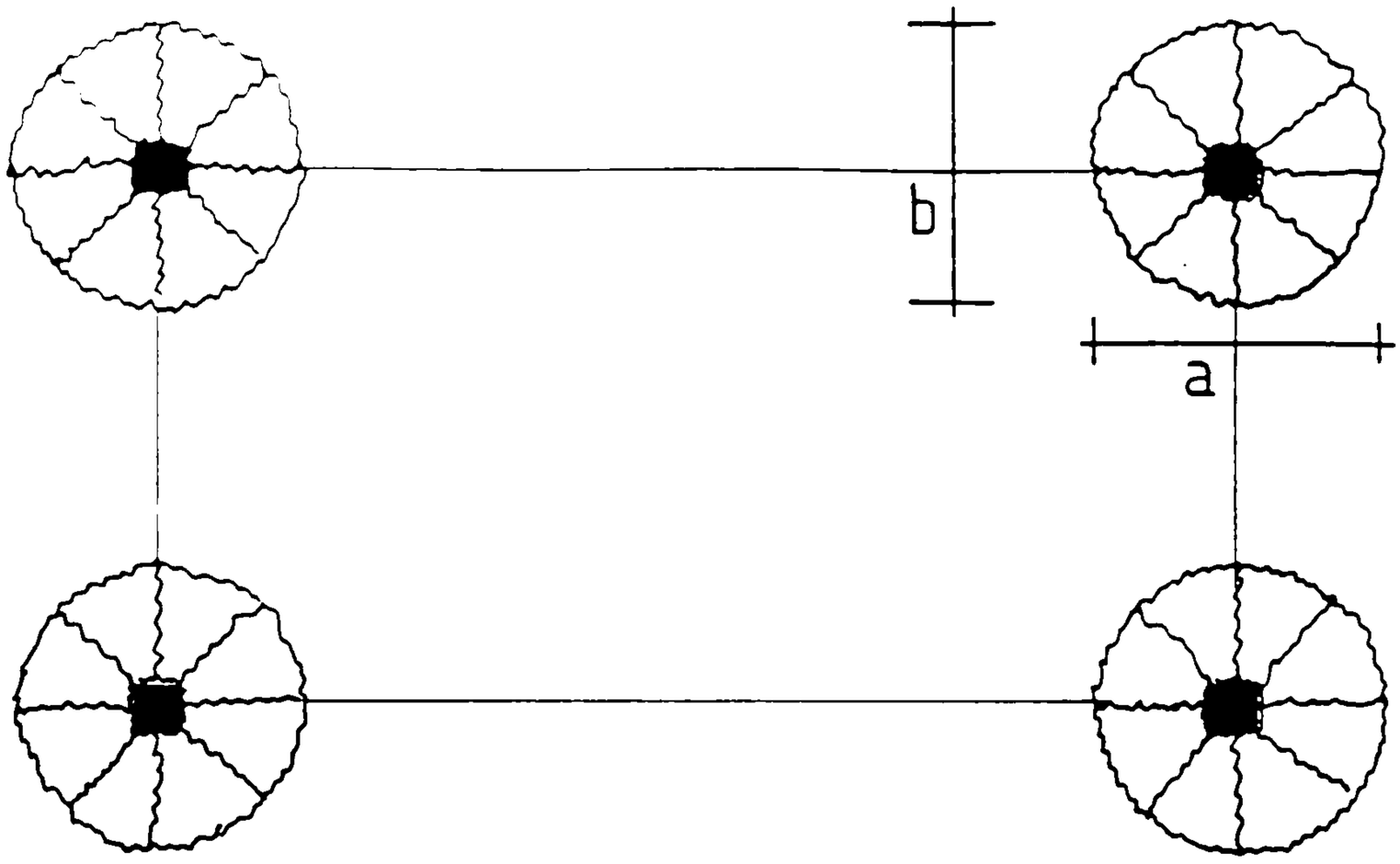

Fig.(1-3) Local collapse mechanisms of flat-slabs

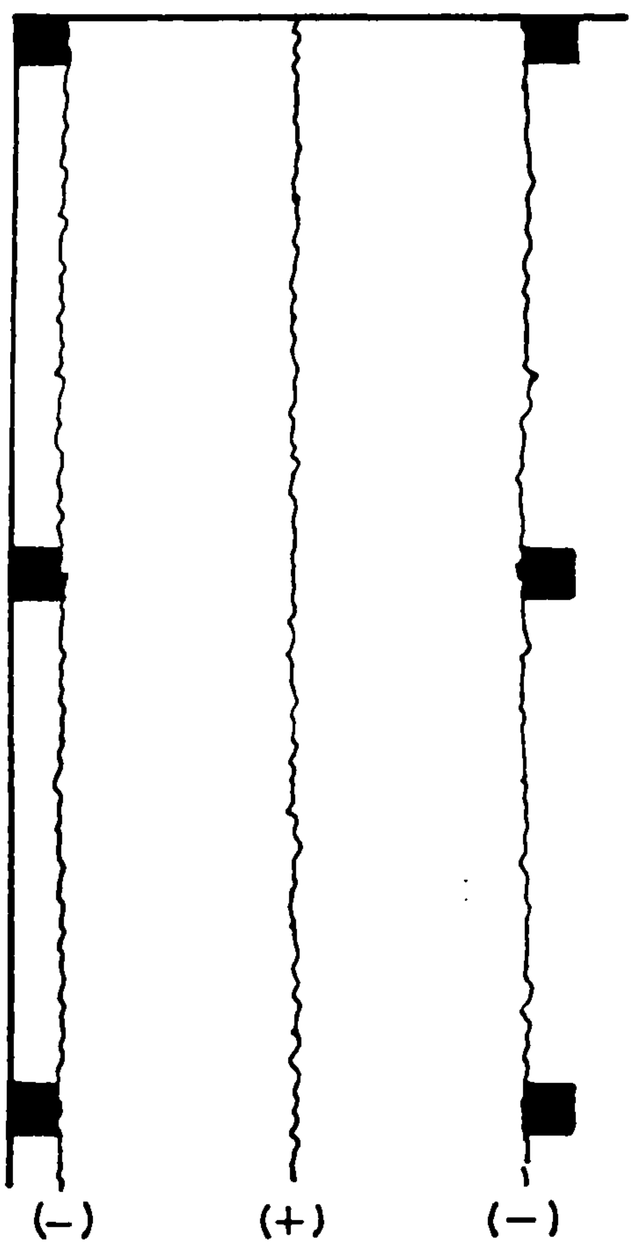

Fig.(1-4) Positive and negative yield lines for edge and corner panels of flat-slabs

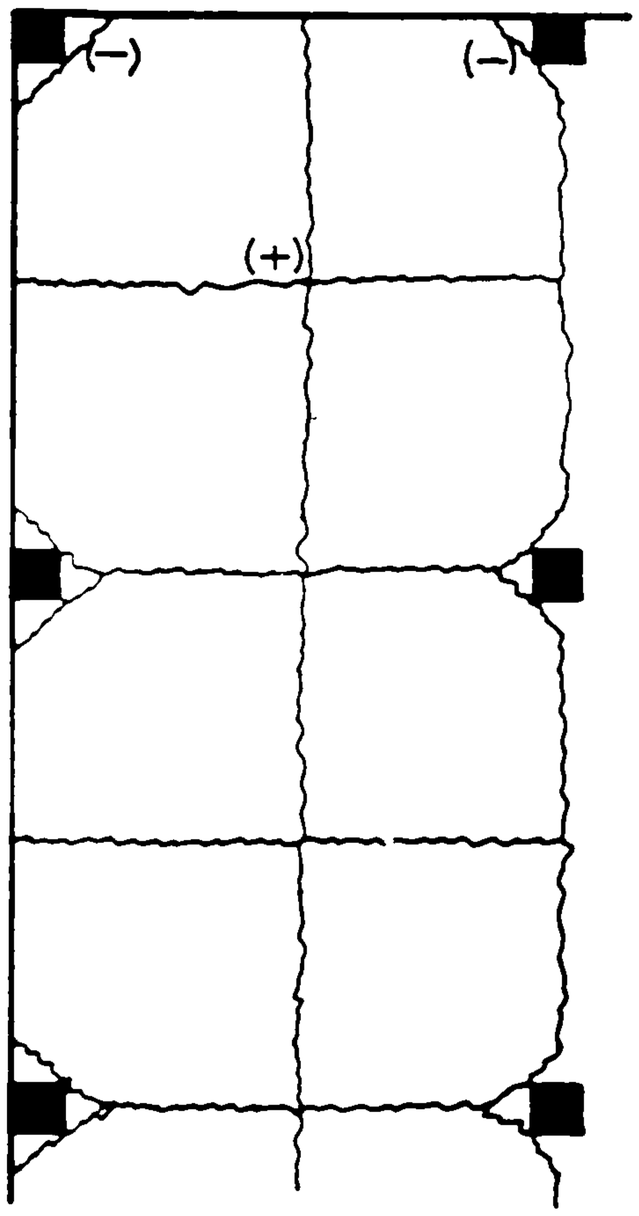

Fig.(1-5) Combined yield line mechanisms for edge and corner panels of flat-slabs

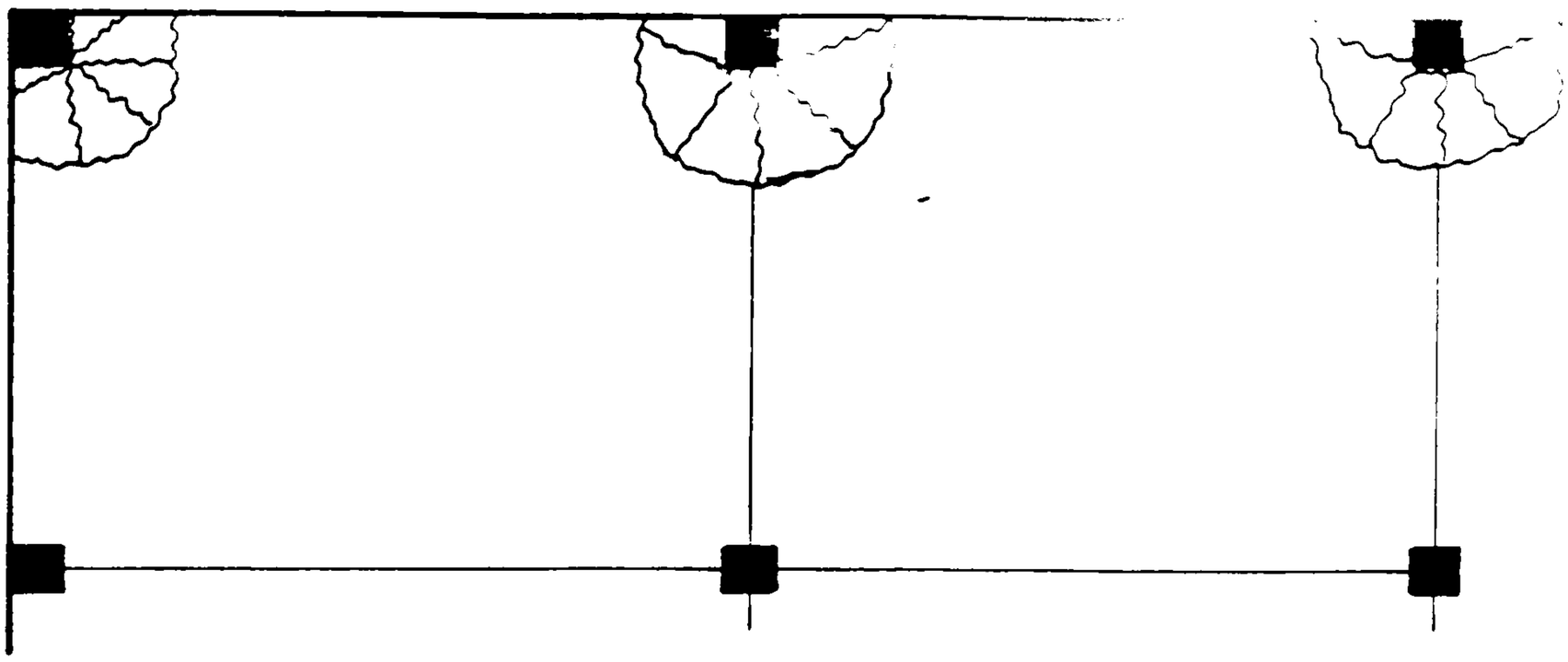

Fig.(1-6) Local collapse mechanisms of corner and edge panels of flat slabs

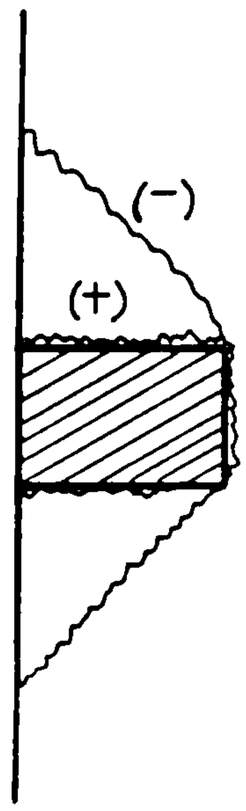

Fig.(1-7) Local mechanism at an edge column

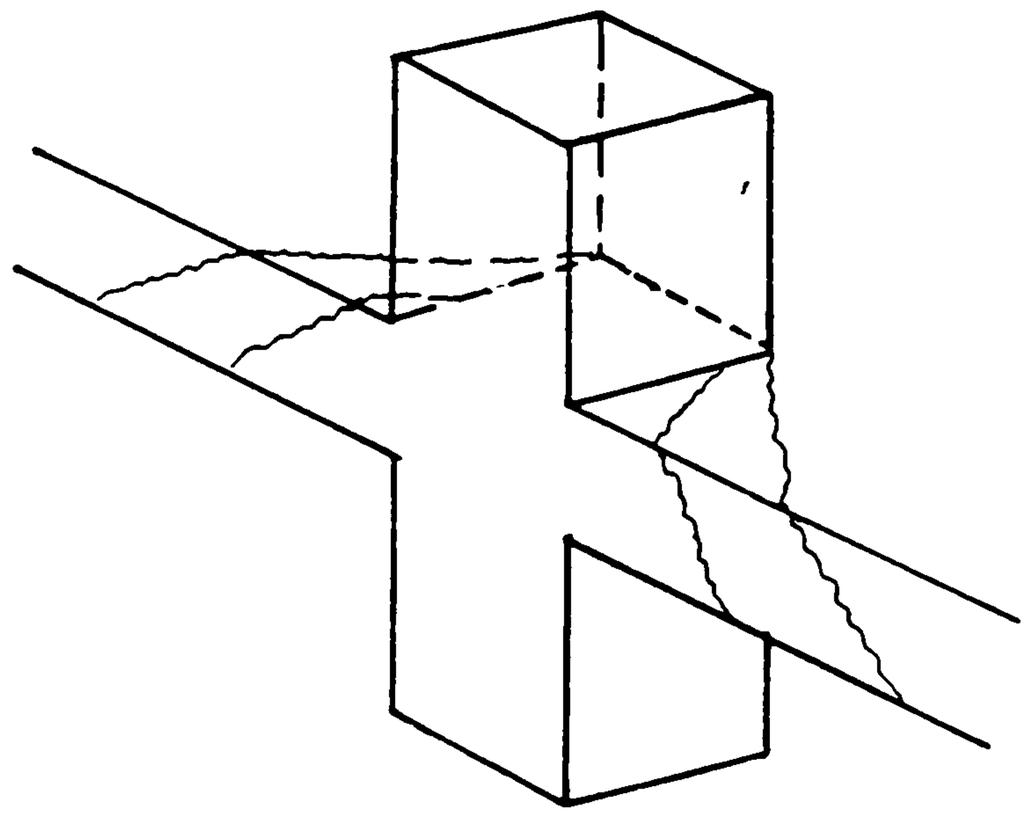

Fig.(1-8) Torsion cracks at an edge column

cracks associated with the yield lines are assumed to be vertical. A simple example is the situation at a corner column at roof level where the vertical yield line of Fig. (1-10a) may give an apparent resistance considerably greater than that Corresponding to the inclined yield line of Fig. (1-10b). The mechanism of Fig.(1-9a) also appears rather problematic in view of the very small area involved in the failure and the probabilities that

I: Inclined cracking will occur and

II: Highly significant membrane forces will be developed.

Some of these local mechanism problems could be serious but there are in any case other factors which seem to make yield-line theory unacceptable as a general approach to flat slab design.

The theory necessarily relies upon the plasticity of the slab and it is very uncertain whether there is actually sufficient ductility available in the negative moment regions around columns. There are numerous examples of test slabs of the type shown in Fig.(1-11) which have reached or almost reached the load predicted by yield-line theory and then failed by punching without developing large deformations. It seems very possible that the punching resistance declines markedly as soon as large plastic deformations occur.

The final and probably most important objection to the use of yield-line theory is that it involves no consideration of compatibility and can thus be used to produce designs in which

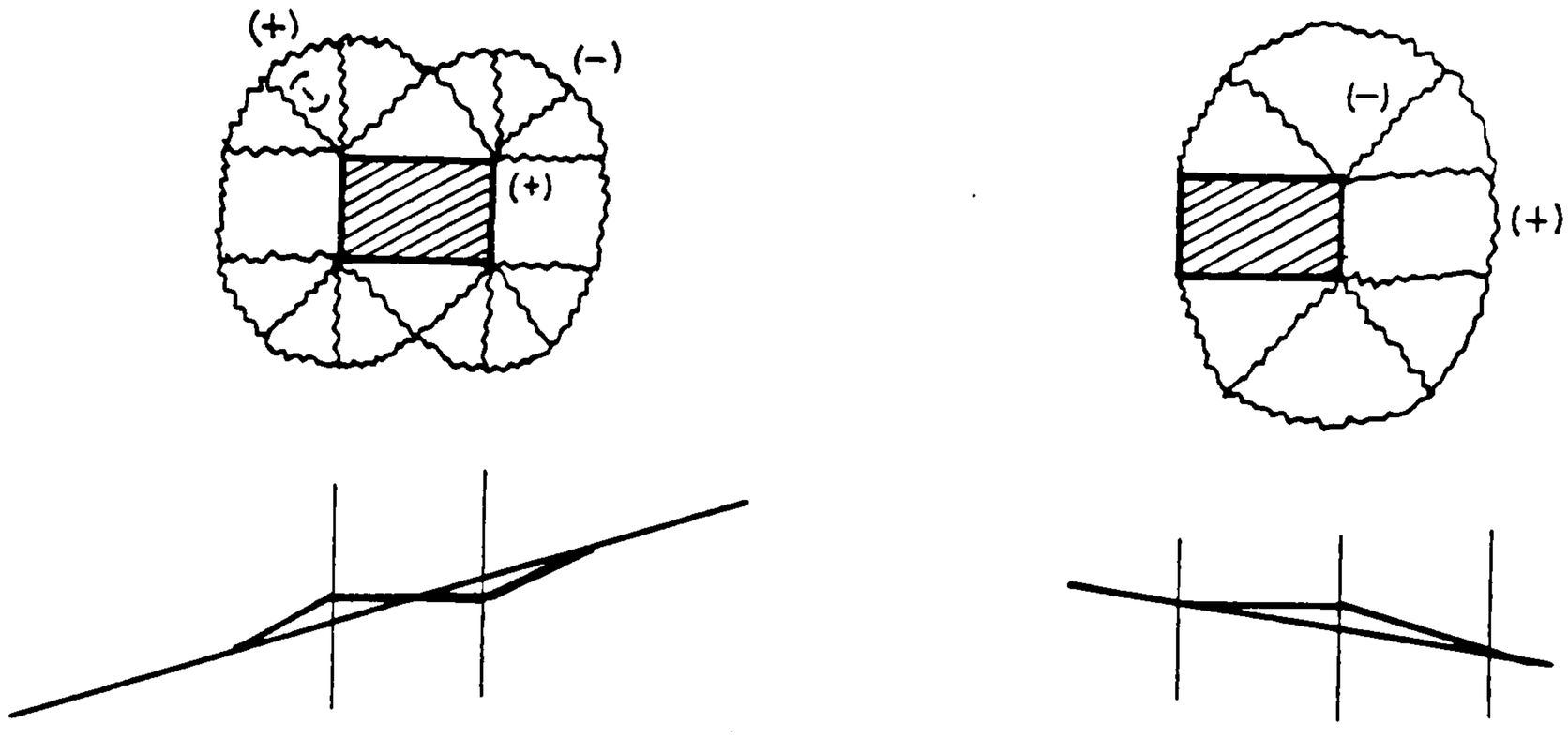

(a)

Fig.(1-9) L0cal mechanisms at an internal column

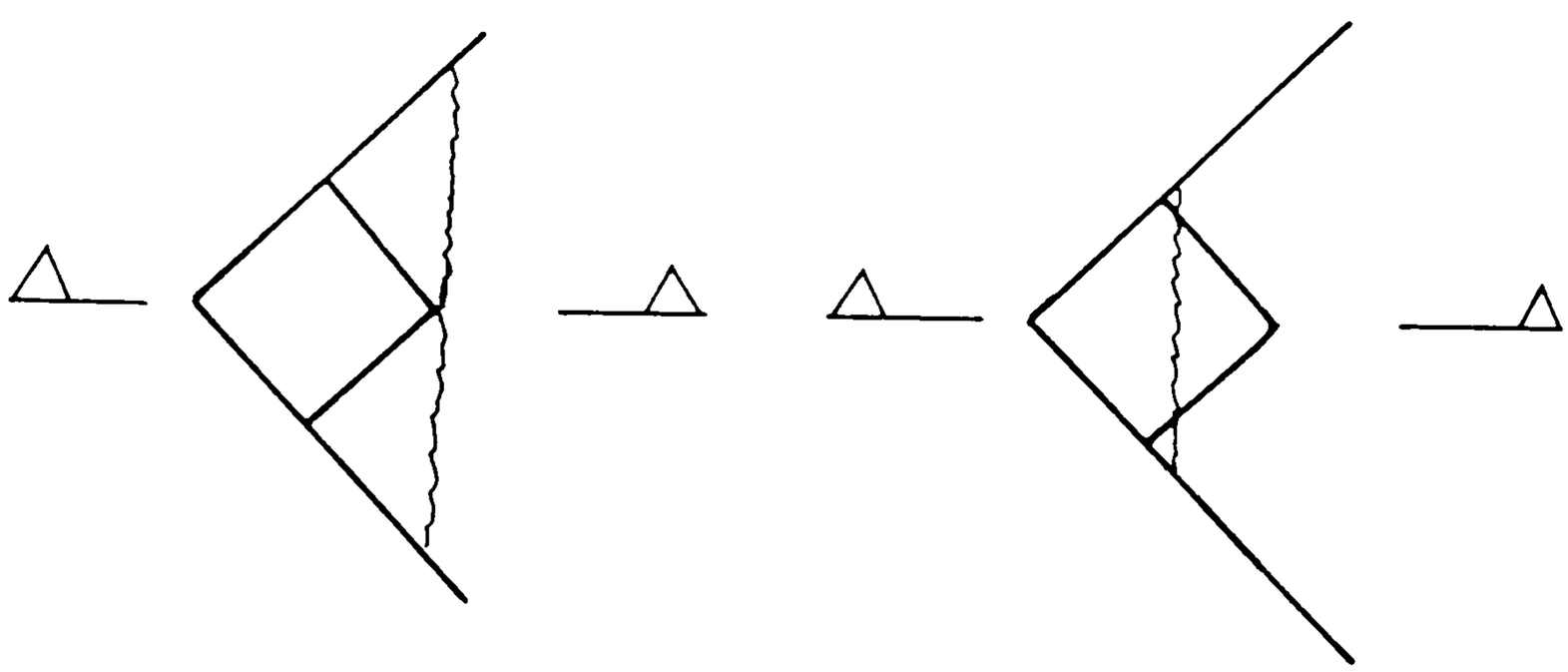

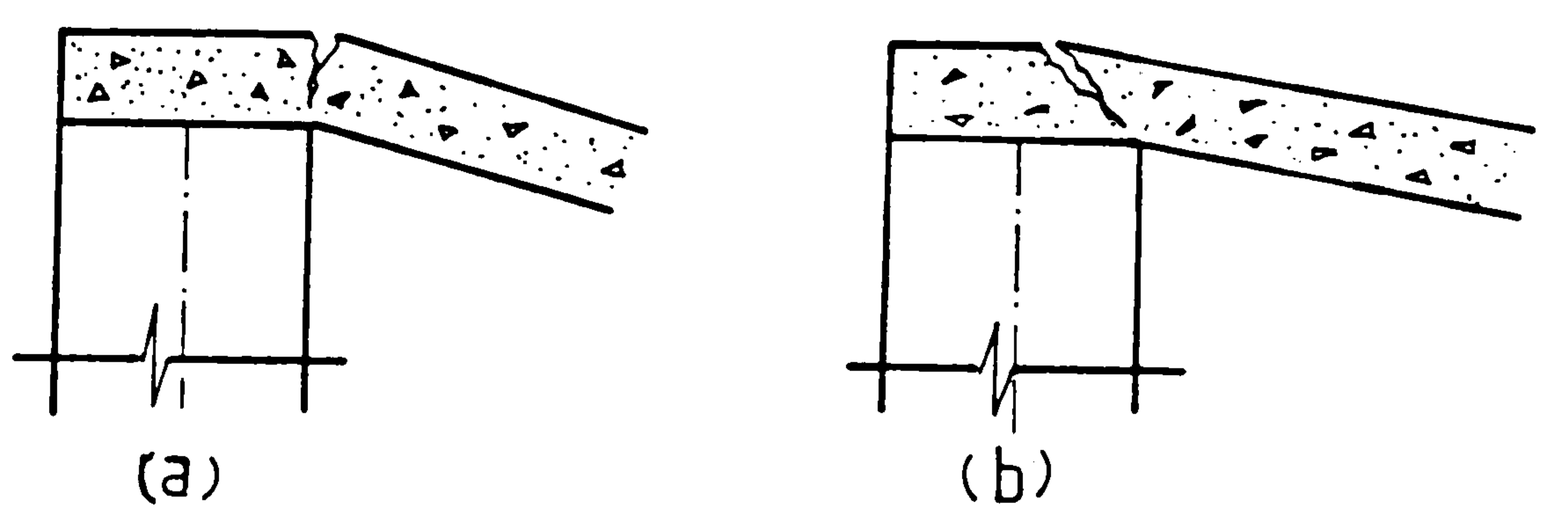

Fig.1-10) Local mechanism at a corner column at roof level

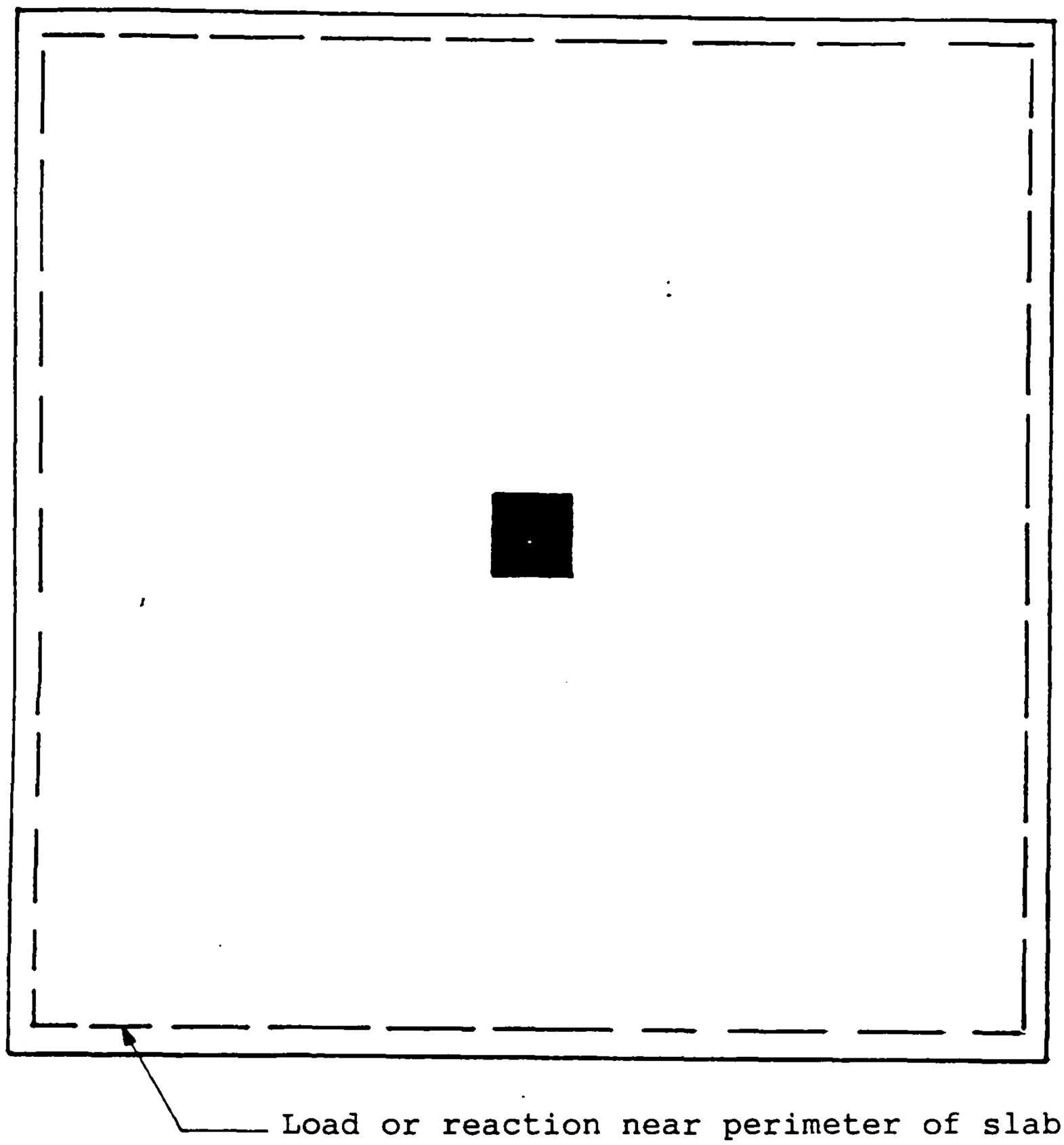

Fig.(1-11) Slab-column specimens

moment transfer to columns is ignored. This could lead to serious overestimations of the shear capacities of slab-column connections, as these are sensitive to moment transfer.

1-3-1-2 <u>Equivalent frame analysis</u>

The use of an equivalent frame approach is very attractive and it provides a reasonable representation of the true behaviour of flat slabs by systems of columns and beams analysed separately in two directions. It satisfies the absolute equilibrium requirements in any span of the structure.

$M + (M_1 + M_2)/2 = QL/8$

where M is the positive moment at midspan

M_1 , M_2 are the negative moments at supports

Q is the total (uniformly distributed) load on the span.

The difference between the frame of a flat slab and the equivalent beam-column frame is the relative lack of continuity between the slab and the columns which in some cases results in slab rotations greater than the equivalent beam rotations. As a result the moments transferred from the slabs to the columns in cases of vertical loading are over-estimated by the equivalent frame method. In cases of horizontal loading the moment distribution is less affected but the frame deformations are under-estimated.

The British Standard BS 8110 (11) divides the structure longitudinally and transversely into frames consisting of columns and strips of slabs. The width of the slab used to define the stiffness of the horizontal member of the frame

depends upon the aspect ratio of the panel and the type of loading. The stiffnesses of the members that could model the frame correctly would also depend on the details of the slab column connection. However in treating vertical loading the code uses actual column stiffness and slab widths defined by panel centre lines and overestimates the moments transferred to columns.

For horizontal loading it is recommended that the slab width be taken as the lesser of half the span and half the bay width. It seems surprising that the effective stiffness of the slab depends just on the aspect ratio of the panels and the type of loading, while according to elastic theory the column dimensions play a role in determining the effective stiffness of the slab.

The ACI equivalent frame method (4) (17) for vertical loading modifies the column flexural stiffness to account for the torsional flexibility of the slab-to-column connection which reduces its stiffness for the transmission of moments. The flexibility of an equivalent column may be taken as the sum of the flexibilities of the actual columns above and below the slab-beam and the flexibility of the torsional members (see Fig.(1-12)) as expressed by

$$\frac{1}{K_{ec}} = \frac{1}{\Sigma K_c} + \frac{1}{K_t}$$

where K_{ec} = Stiffness of equivalent column

ΣK_c = Sum of stiffnesses of actual columns above and below the joint

K_t = Stiffness of torsional member.

Computation of the torsional stiffness K_t of the torsional member requires several simplifying assumptions. The transfer of a moment between a slab and a column is assumed to be made by the imaginary torsional member shown in Fig.(1-12a). The width c of the torsional member is assumed to be equal to the width of the column, and it is assumed that no torsional rotation occurs in the beam over the width of the support.

The value of the torsional stiffness can be obtained by assuming the moment distribution along the torsional member to be linear as in Fig. (1-12b) so that the moment at a distance X<b/2 from the edge of the equivalent frame is

$$m_x = 4MX/b^2$$

and the torsion at section X Fig.(1-12c) is

$$T_x = \int_0^x m_x \, d_x = 2MX^2/b^2$$

The corresponding twist per unit length is

$$\phi x = \frac{T_x}{G_c} = \frac{2MX^2}{G_c b^2}$$

where G_c is the torsional rigidity of the member. The total twist at, point X is

$$\Phi_x = \int_0^x x d_x = 2MX^3/3G_c b^2$$

For the equivalent frame analysis an average value of Φ_x Fig. (1-12d) is used as the rotation of θ_t of the torsional beam

$$\theta_t = M(b-c_2)^2/36\ G_c\ b^2$$

and the stiffness of the torsional member is calculated by the following expression

$$K_t = \sum \frac{9E_{cs}C}{b(1-c_2/b)^3}$$

where c_2 is a column dimension and b relate to the transverse span see Fig. (1-12a). The constant C may be evaluated for any shape of cross section by dividing it in to separate rectangular parts and carrying out the following summation

$$C = \sum (1-0.63(X'/Y'))(X'^3Y'/3)$$

X' = shorter over-all dimension of a rectangular part of the cross section

Y' = longer over-all dimension of a rectangular part of the cross section.

There seem to be some disadvantages in the ACI approach.

The assumptions for determining the value of K_t in Fig. (1-12)

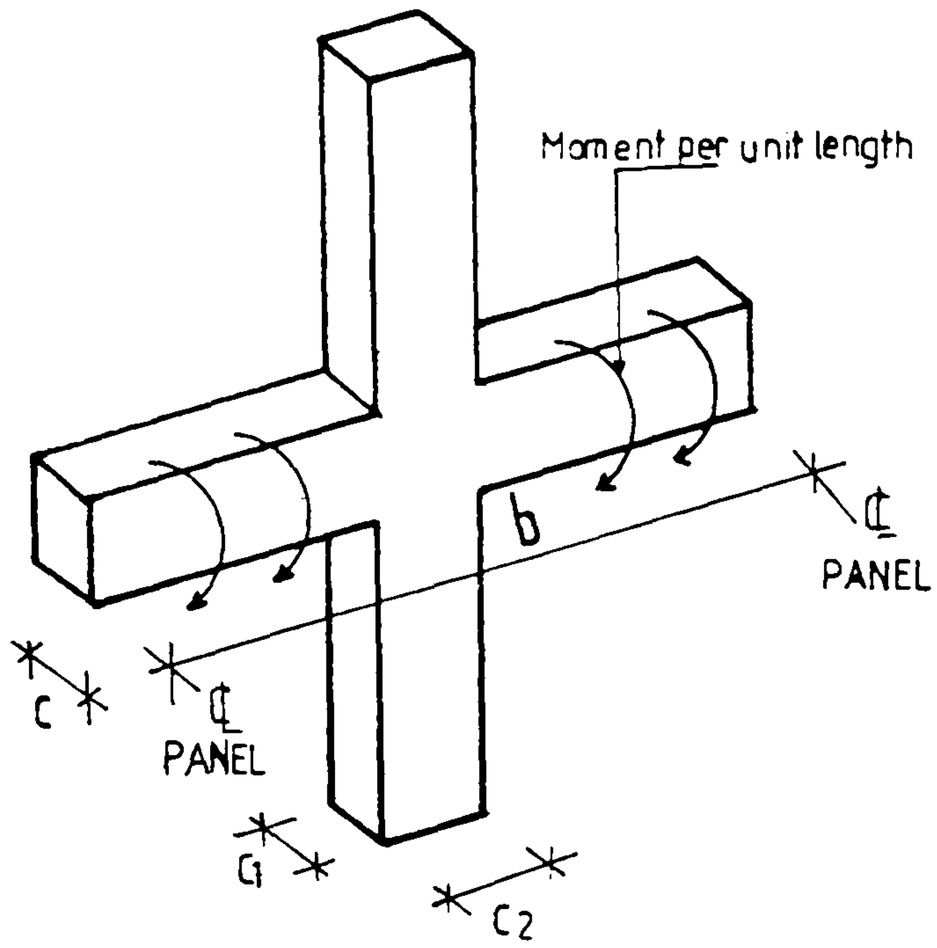

a) Simplified physical model of equivalent column

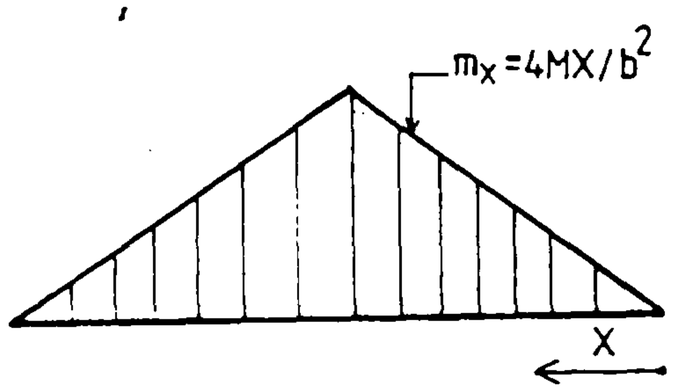

b) Distribution of moment along the column centre line

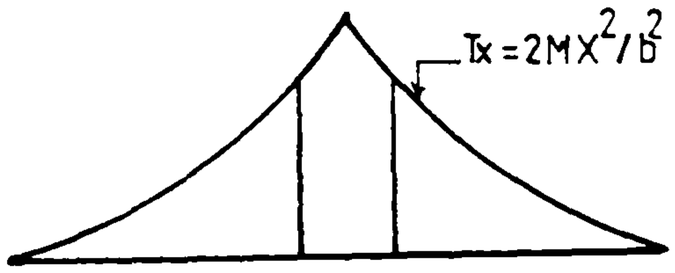

c) Twisting moment diagram

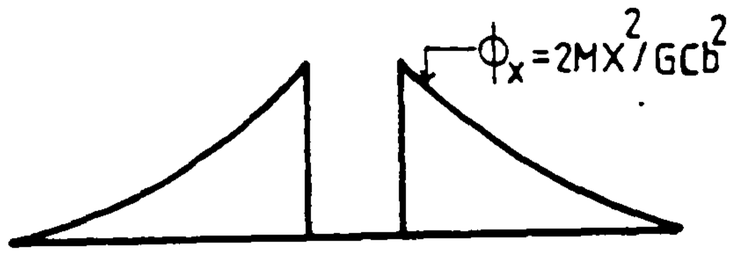

d) Twist per unit length of the edge strip

Fig.(1-12) ACI equivalent frame method

are unrealistic, and the average effective rotation of the torsional beam θ_t seems to be arbitrary.

A portion of the slab equal to the width of the column is assumed to offer the torsional resistance. If a slab is connected to only the inner face of an exterior column, the ACI joint stiffness becomes zero, while, according to elastic theory a significant moment can be transferred to the column.

For rectangular panels, where the moments are in the long span direction, the distribution of the moment along the column centre line is unrealistic and the moments need not to drop to zero at the strip edge.

For horizontal loading, it is difficult to use the ACI method, in its entirety. The torsional member can be retained but the device of an equivalent column is not applicable.

In view of the ACI method's disadvantages Regan(53) proposed a new treatment of the equivalent frame analysis for vertical and horizontal loading.

A- <u>Regan's method for vertical loading</u>

Regan noted that the rotation of a simply supported slab on columns is greater than that for a slab supported across its full width. He treated the increase in rotation by the use of an effective slab width less than or equal to the full value defined such that $\theta_s=(2bl^3)/(24b_eD)$ Fig.(1-13)

θ_s is the rotation of the slab at the columns according to elastic plate theory.

l is the span of the slab

b is the full width of the equivalent frame (i.e the width from which the loading is determined)

D is the slab rigidity $D = E_c\ h^3/12$

b_e is the effective slab width equal to the lesser of b and l

q is the load per unit area of the slab

Also he considered the same slab structure but with the vertical loading removed and replaced by the moments M acting on the slab at the positions of the columns. As before the rotations of the slab at the columns are greater than the uniform rotation produced if the same total moments were distributed along the edges of the slab. For uniform edge moments the corresponding rotation is Ml/2bD and the slab rotation at the column can be expressed

$$\theta_s = \theta_b + \theta_j = (Ml/2b_eD) + (M/K_j)$$

Where K_j is the stiffness of the joint between the slab and column. The values of K_j obtained as approximations to the results of elastic analysis of plates are shown in Fig.(1-14). These K_j values can then be incorporated in the analysis in the same way as the ACI's K_t

B- <u>Regan's method for horizontal loading</u>

When horizontal loading is considered in stiffness analysis

the slab stiffness should be reduced according to

$$(1/K_{se}) = (1/K_s) + (1/K_j)$$

Where K_s = slab stiffness over the effective panel width

K_{se} = effective slab stiffness for horizontal loading

$$\theta_s = \frac{q\,b\,l^3}{24\,b_e D}$$

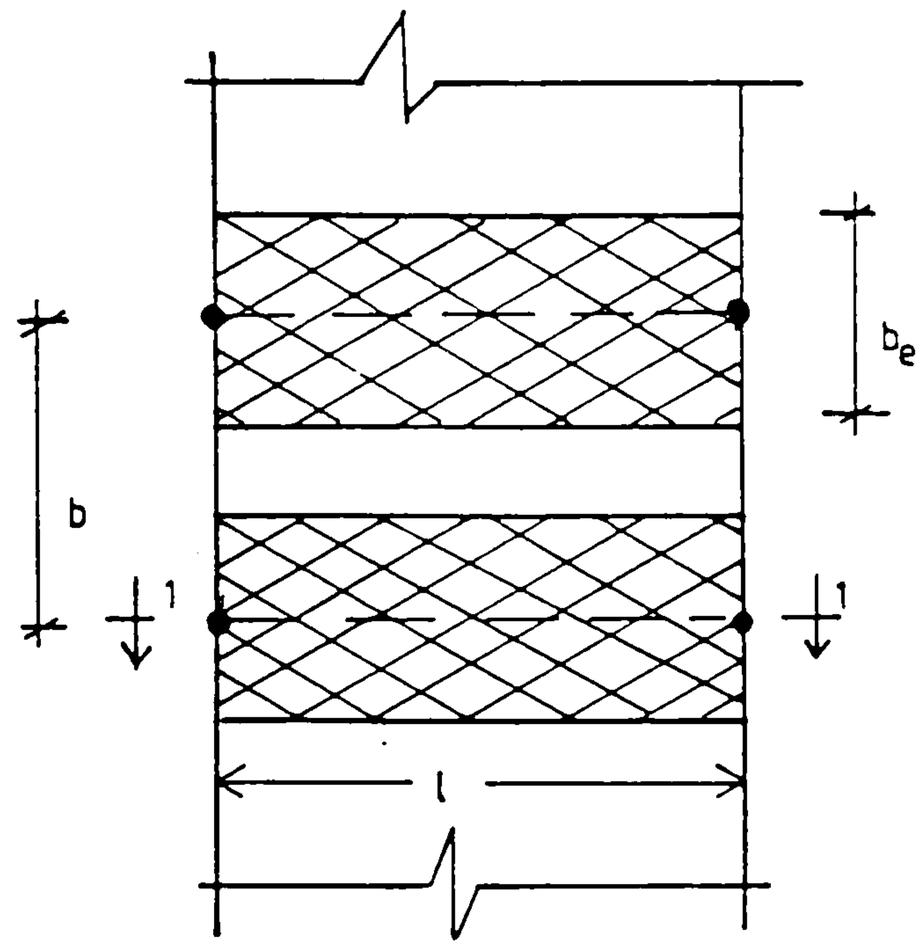

SECTION 1–1

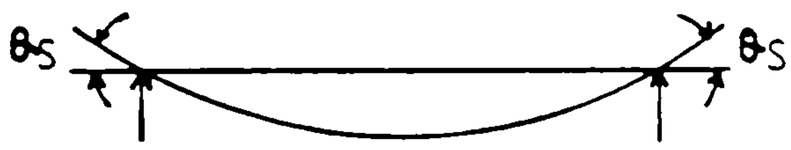

Fig.(1-13) Rotation at the edge of a simply supported slab strip

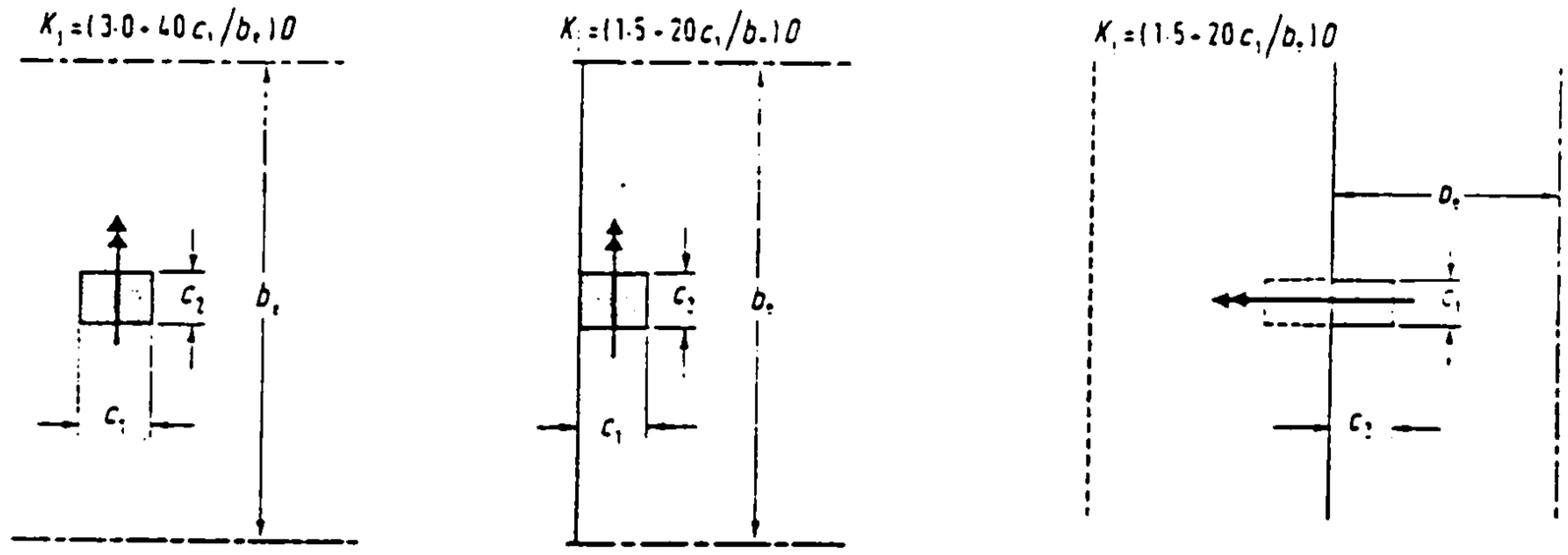

Fig.(1-14) Joint stiffness

The above equation is directly applicable at an end column but at an internal column two separate effective stiffnesses are required, one for each span. Thus the effective slab stiffness (K_{sle}) on one side of the column is given by

$$\frac{1}{K_{sle}} = \frac{1}{K_{s1}} + \left(\frac{K_{s1} + K_{s2}}{K_{s1}}\right)\left(\frac{1}{K_j}\right)$$

Where the suffices apply to spans 1 and 2 respectively.

Although this method dose offer an approach to horizontal loading which is a sort of parallel to that for vertical loading, the device adopted is clumsy. With contemporary use of small computers it is not difficult to include the felexible slab - column connection as a separate member in the analysis. This technique would be equally applicable with the ACI's torsion member or Regan's flexible joint.

1-3-1-3 <u>Grillage analysis</u>

In CIRIA Report 110 (66) Whittle developed a computer program to be used in the grillage analysis of a slab, the program contains its own mesh generator of the member lay-out as follows.

1- The lay-out should be largely based on the centre-lines of the columns with each column represented by a point support and the slab-to-column connection represented by members connecting to this point (A1 and A2) Fig.(1-15).

2- The stiffness of members connected to the columns should be calculated for a width of slab equal to or a little greater than that of the column.

3- Lines of members should connect centre-lines of panels (D1 and D2).

4- Members should be positioned at quarter panel lines (C1 and C2).

5- A line of members should be positioned at about a column width from the column centre-line (B1 and B2).

The column stiffness should normally assume fixity at its remote end and be equal to 4EI/L (3EI/L if the remote end acts as a pin).

The Grillage analysis may be carried out to model both the ultimate and serviceability limit states using the appropriate member properties. Various sections of the slab are likely to be cracked in flexure and torsion and realistic estimates of their reduced stiffness for input to the grillage analysis is required. It is recommended that the rigidity of the concrete slab can be assumed to reduce by half when cracked and that the torsional stiffness of the elements connected to the column is small.

1-3-1-4 Plate theory.

Plate theory is likely to predict the behaviour of a flat slab under working load conditions. For the ultimate limit state it can give a valid lower bound plastic solution and in some cases an economic one if the reinforcement is suitably disposed.

1-3-2 ESTIMATION OF RESISTANCE TO SYMMETRIC PUNCHING.

The following paragraphs review methods of calculating resistance to concentric punching. Treatments of punching under eccentric loading are described in section 1-3-3.

1-3-2-1 EMPIRICAL APPROACHES.

Most research on the shear strength of flat slabs has been concerned with the generation of experimental data, and the development of empirical formulae for design. Varying answers can be obtained from the variety of empirical methods proposed for computing shear strength. These methods fall into two broad groups.

1. Those in which the amount of flexural reinforcement is the prime variable.
2. Those in which the concrete strength is the major factor.

1 - WHITNEY

Whitney (65) presented an ultimate strength theory for shear in which he assumed that the shear strength is primarily a function of the ultimate resisting moment of the slab per unit width inside the pyramid of rupture. The ultimate shearing strength was given by the equation.

$$q=100 \text{ p.s.i} + 0.75\ m/d^2\ \sqrt{d/r_3}$$

Where q is computed at a distance d/2 from the perimeter of the loaded area r_3 is the shear span, i.e. distance from column face to the point of contraflexure, and m is the flexural resistance per unit width.

2- HOGNESTAD, ELSTNER And HANSON

Hognestad, Elstner and Hanson (26) tested 6ft. square slabs with 6in. total depth supported along four edges and related the shear strength of the slab to the splitting tensile strength f_t of the concrete. They presented the following equation for the shearing strength q.

$$q = \frac{V}{4cd} = \frac{2.24(1 - 0.075c/d)f_t}{1 +(3.136cdf_t/V_{flex})} \qquad \text{(p. s. i)}$$

Where V_{flex} is the flexural capacity of the slab computed by yield line theory. c is the side length of a square column. The critical section is assumed to be located at the perimeter of the loaded area.

3- MOE

Moe (40) tested 31 slabs under concentric loading and 12 slabs under eccentric loading. All the slabs were 6ft. square with an overall thickness of 6in. The slabs were simply supported along all four edges with the corners free to lift. The main variables were the concrete strength, the percentage of tensile reinforcement and the column dimensions. The ultimate shearing strength of symmetrically loaded slabs was found to be

$$q = \frac{V}{bd} = \frac{15(1 - 0.075c/d)}{1 + (5.25bd\sqrt{f_c})/V_{flex}} \sqrt{f_c} \qquad \text{(p.s.i)}$$

Where b = width of critical section in shear and is equal to 4c
for a square column

c = side length of loaded area of square shape

d = effective depth of slab

The constants were determined on the basis of statistical analysis of available test data. Moe also limited the shear stresses for flexural strength to govern in design to

$q = (9.23 - 1.12\ c/d)\ \sqrt{fc}$ for $c/d \leq 3$ (p.s.i)

$q = (2.5 + 10\ d/c)\ \sqrt{fc}$ for $c/d > 3$ (p.s.i)

4-REGAN

Regan (53) made empirical proposals derived from data for the basic case of an internal column, or load free from unbalanced moments. The expression proposed for the punching strength of a slab at an internal column is

$Vu = K_a\ K_{SC}\ \xi_s \sqrt{(100A_s f_{cu})/bd}\ \ 2.69d(\ \Sigma c + 7.85d\ )$

Where K_a =0.13 for normal dense concrete and 0.105 for light-weight aggregate concrete with a density of about 1700 kg/m^3

$K_{SC} = 1.15 \sqrt{4\pi * \text{column area} / (\text{column perimeter})^2}$

$\xi_s = \sqrt[4]{300/d}$ with d in mm

$100A_s/bd$ is the average of the percentages of tensile reinforcement in two orthogonal directions

f_{cu} is the cube strength of concrete N/mm^2

d is the effective depth of the slab

Σc is the perimeter of the column or loaded area in mm.

5-PETCU, STANCULESCU AND PANCALDI

Petcu, Stanculescu and Pancaldi (50) proposed a formula for the punching load of two-way reinforced concrete slabs based on two assumptions. Firstly, the punching load for slabs without transverse reinforcement is in equilibrium with the vertical component of the resultant force of the tensile concrete stresses acting on the lateral surface of the truncated cone, at incipient failure. Secondly the angle between the slab surface and the generatrix of the surface of the punching cone is variable and less than 45^{o}, its value depending on the mean bending reinforcement percentage. The design punching load P_s is

$$P_s = m_c \cdot s_o \cdot f_t$$

Where:

m_c = 0.135 is the shape factor of the diagram of the vertical tensile concrete stresses acting on the lateral surface of the punching cone

s_o = projection of the lateral surface of the punching cone on the plane of the slab. The surface s_o represented in Fig.(1-16a) may be computed using the formula

$$s_o = (\pi/4).(D^2 - r^2)$$

D is the diameter of the great base of the punching cone

r is the diameter of the smaller end of the punching cone

The diameter r may be determined depending on the shape of the area to which the punching load is applied as follows

- If the loaded area is circular of diameter $2r_o$, $r = 2r_o$
- If the loaded area is a square with side equal to c, r=1.27c
- If the loaded area is a rectangle with sides equal to a and b

$r = 0.64(a+b)$

The diameter D may be determined depending on the value of the bending reinforcement percentage as follows

If the mean value of the bending reinforcement percentage is less than unity

$D = r + 2d\ (1 + 3\sqrt{p})$

If the mean value of the bending reinforcement percentage is greater than unity

$D = r + 8d$

Where d is the effective depth of the slab

p is the percentage of the bending reinforcement of the slab.

If the distance between the periphery of the small end of the punching cone and the inner face of the nearest slab support is smaller than (D-r)/2 the surface s_o is that shaded in Fig.(1-16b). This means that the punching resistance is reduced if the load is near the support, while tests results are against this. Regan (55) indicates that the punching resistance is increased if the load is near the support.

6-CODES OF PRACTICE

Codes of practice in general have treated the problem of punching empirically by limiting the nominal shear stress at a critical perimeter.

In the ACI code (3) (4) the unfactored ultimate shear stress is a function of the aspect ratio of the loaded area, and is equal to

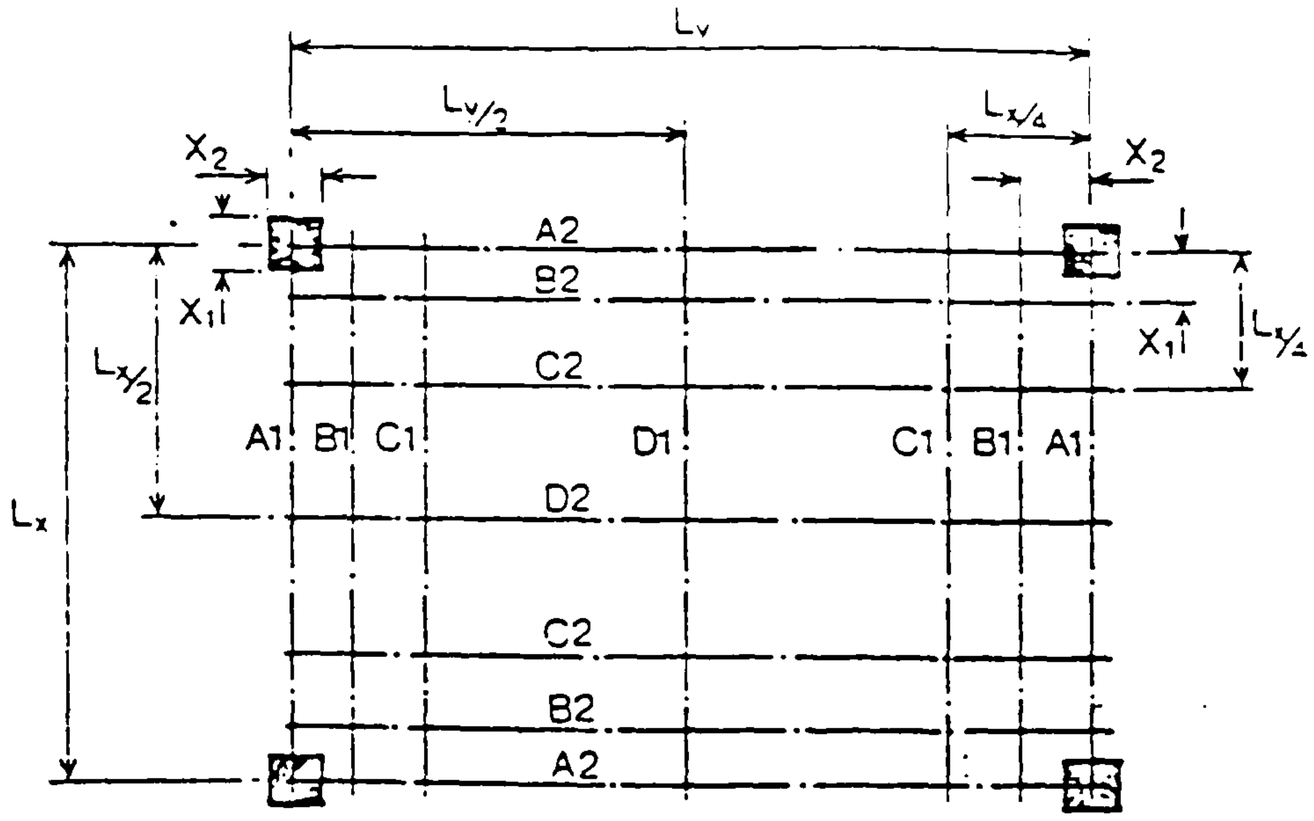

Fig.(1-15) Member lay-out for grillage analysis

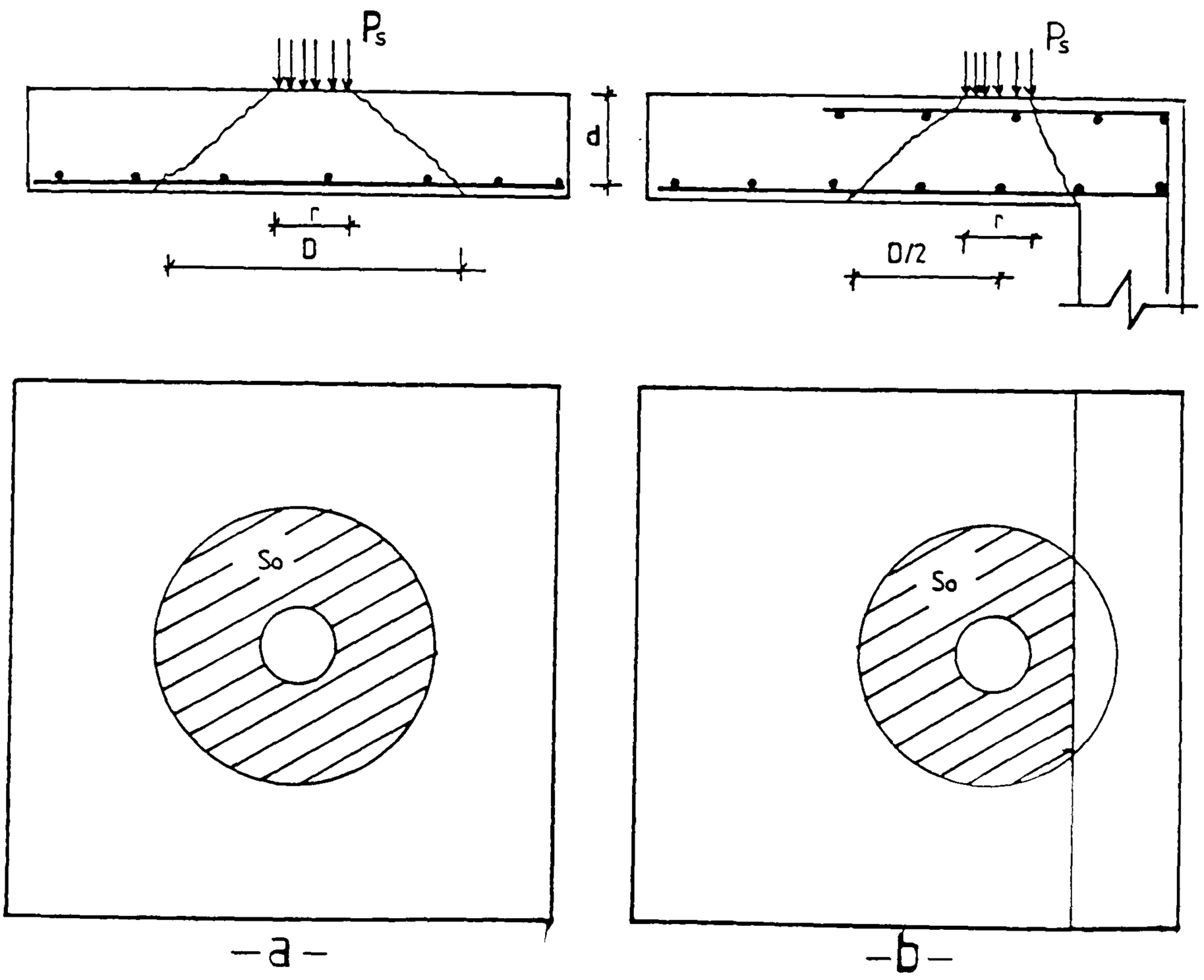

Fig.(1-16) The projection of the surface of the punching cone

$v_c = (1 + 2/\beta c)\ (\sqrt{f_c}/6)$ but not greater than $(\sqrt{f_c}/3)$ N/mm^2

βc is the ratio of long side to short side of the concentrated load or reaction area

The shear resistance $V = v_c \cdot u \cdot d$

u is the perimeter of the critical section defined by straight lines drawn parallel to and at a distance d/2 from the edges of a rectangular area. For a circular loaded area the critical perimeter is circular and at a distance d/2 from the outline of the load or support.

British Standard BS 8110, (11) limits the maximum design shear stress at the column face to 0.8 $\sqrt{f_{cu}}$ or 5 N/mm^2 if less. The design ultimate concrete shear stress at a perimeter 1.5d from the column is

$$v_c = 0.79(100A_s/(xd))^{1/3} \cdot (400/d)^{1/4}/\gamma m \quad N/mm^2$$

100As/xd should not be taken greater than 3

Where

x is the length of the side of the shear perimeter considered

$(400/d)^{1/4}$ should not be taken as less than 1

$\gamma m = 1.25$

For a characteristic concrete cube strength greater than 25 N/mm^2 the value of v_c may be multiplied by $(f_{cu}/25)^{1/3}$. The value of f_{cu} should not be taken greater than 40. The design shear resistance $V = v_c \cdot u \cdot d$ where, u is the control perimeter

distance 1.5d from the loaded area and has square corners whether the loaded area is rectangular or circular.

The CEB-FIP, (15) code for concrete structures defines the nominal shear stress as $v_c = V/ud$ where the control perimeter u is the length of the shortest curve at a minimum distance of 0.5d from the loaded area. The concrete shear strength v_c is

$v_c = 1.6\ R_c\ K\ (1+50\rho)$

Where R_c is a function of the characteristic concrete compressive strength f_c, $R_c = (0.035f_c)^{2/3}$

$K = 1.6 - d \not< 1$ (d in m)

$\rho = \sqrt{\rho_x \cdot \rho_y} \not> 0.008$

ρ_x and ρ_y correspond to the reinforcement parallel to x and y

$d = (1/2)\ (d_x+d_y)$, where d_x and d_y are the effective depths in x and y directions.

The CEB uses different shear stresses on different parts of the perimeters around large columns. For a circular loaded area with a diameter r>3.5d the active punching length of the perimeter is $u=4.5\pi \cdot d$, and for a rectangular loaded area with sides a and b < a the effective part of the linear section is limited to the lengths, b_i = min.(b,2.8d) and a_i = min.(a,2b,5.6d-b1) located near rounded corners see Fig.(1-17). The remaining parts of the control surface are assumed to carry one-way shear only. The CEB-FIP expression for v_c includes a partial safety factor of 1.5 applied to the shear resistance.

1-3-2-2 THEORETICAL METHODS OF ANALYSIS OF PUNCHING SHEAR

1- Kinnunen and Nylander

Kinnunen and Nylander (30) developed a theoretical analysis for punching shear based on tests of circular slabs, centrally supported on circular columns, and loaded at the free edges. The theoretical method of analysis was based on the mechanical model shown in Fig.(1-18) and primarily considered slabs with ring reinforcement only. It considers the slab to be divided by radial cracks into segments bounded by the shear crack and slab edge. The segments are regarded as rigid bodies and each segment rotates around a centre of rotation C.R located at the root of shear crack see Fig.(1-18d). The central truncated cone bounded by the shear crack and the loaded area remains undeformed. The segments are assumed to be carried on a imaginary conical shell, between the column and the root of the shear crack Fig.(1-18c). Each segment is acted on by the resultant forces shown in Fig.(1-18b). The internal forces are functions of the angle of rotation ψ Fig.(1-18d), and the mechanical properties of the concrete and steel. Failure is assumed to occur when the tangential strains at the bottom of the slab below the root of the shear crack reach a characteristic value ε_{ct} which is dependent on B/d, at the same time as the concrete stress in the imaginary conical shell is at the characteristic value. At failure $\psi = \varepsilon_{ct} (1+(B/2x))$ and the yield stress fy is reached in the reinforcement within a radius r_s, where

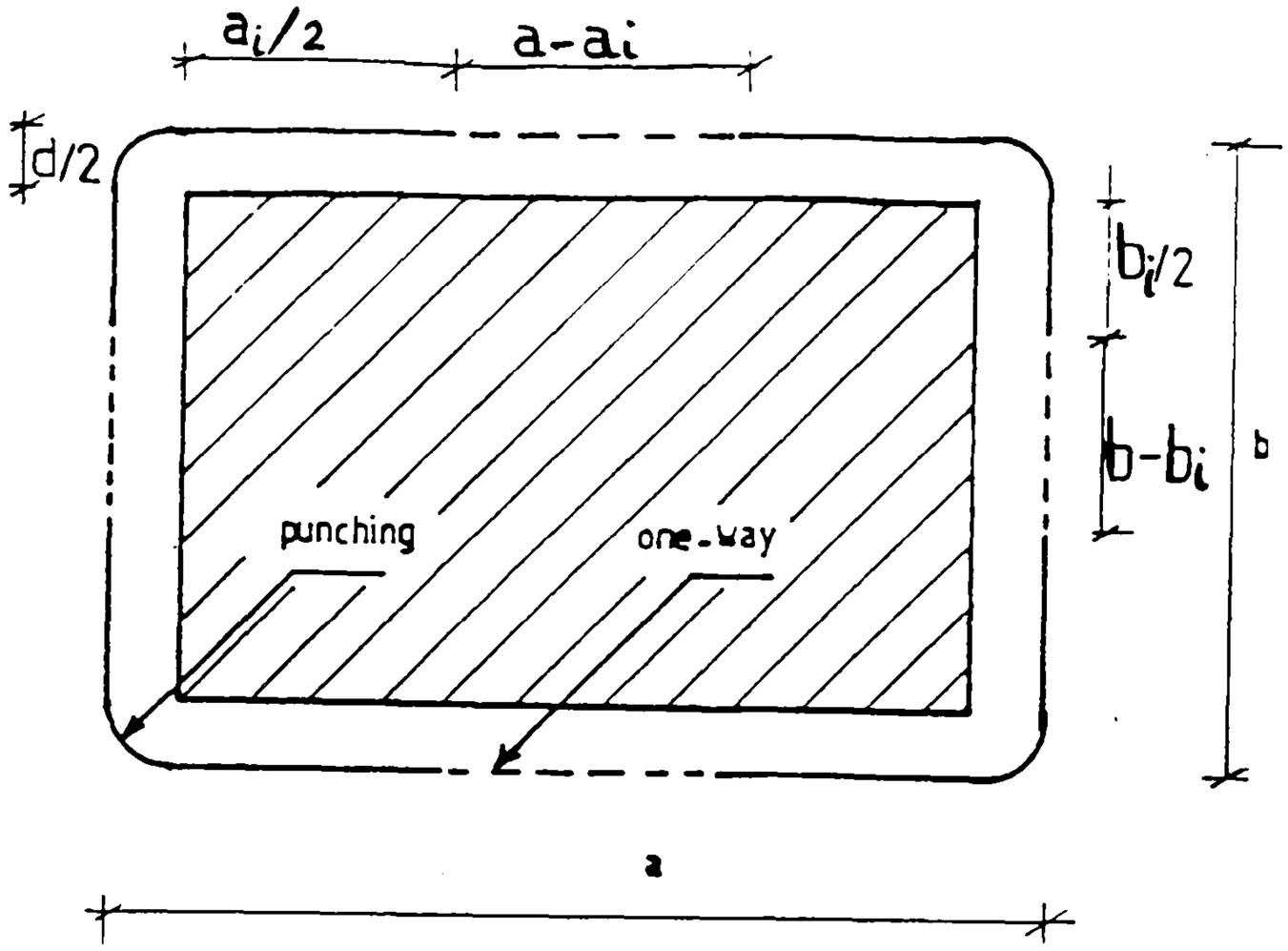

Fig.(1-17) CEB subdivision of perimeter

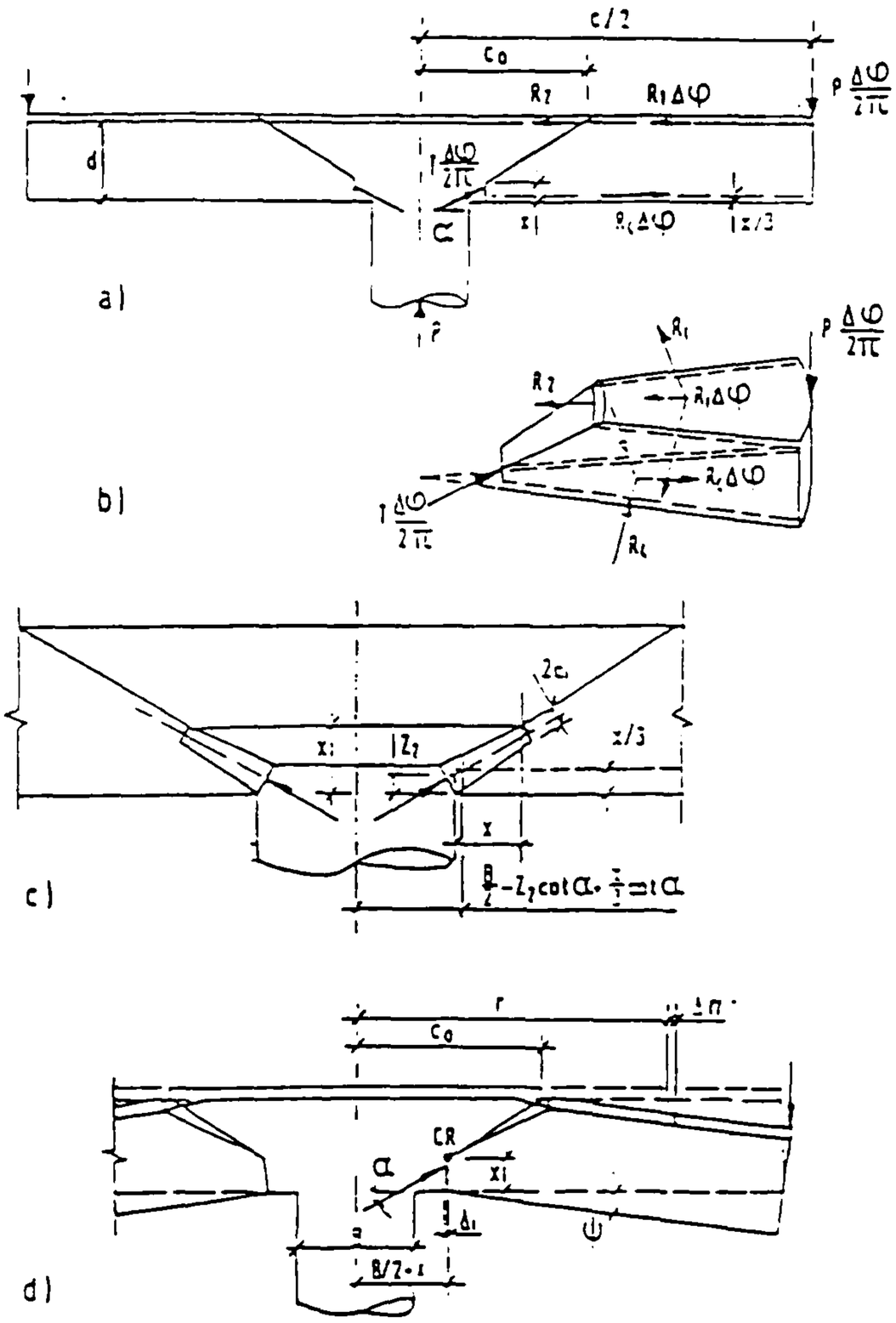

Fig.(1-18) Kinnunen and Nylander model

$r_s = \psi \cdot (d-x)\ E_s/f_y$.

By applying the conditions of equilibrium the punching load can be estimated by means of a trial an error process.
The method is able to predict the ultimate load irrespective of whether the type of failure is flexural or punching. In 1963 Kinnunen (31) presented an extension of the theory of Kinnunen and Nylander to apply to slabs with two-way reinforcement. In this dowel forces and tensile membrane effects were considered in estimating the increased load-carrying capacity of the slab as compared with the ring reinforced slabs considered in the original theory. Regarding the part of the slab inside the shear crack remaining undeformed the test results of Kinnunen and Nylander (30), only support this assumption in cases of slabs with ring reinforcement. For two-way reinforced slabs the part inside the shear crack is deformed by the membrane and dowel forces, and the difference between the steel forces at the column face and at the shear crack together with the radial component of the tangential steel forces in that part are all transmitted through the part of the slab which is attached to the column.

2-Anis

Anis (2) used the Kinnunen and Nylander mechanical model to describe punching shear resistance. The major difference between his approach and that of Kinnunen and Nylander was, the

assumption by Anis that the failure occurs when the radial compressive strain in the section located at the column face reaches a limiting value.

Anis's method is not easy to use for design purposes.

3-<u>Shehata</u>

Shehata's (62) theory is along the general lines proposed by Kinnunen and Nylander. He assumed that the front part of the radial segment fails to support the bearing force at the column face when one of the following three critical states is reached.

a- If the angle α of the compressive force at the front part of the segment reaches 20^{o}.

b- If the average radial strain on the compressed face reaches a value of 0.0035 in a plastic length starting from the column face. The plastic length is taken to be 150 mm for two-way and 75 mm for ring reinforced slabs.

c- If the tangential strain on the compressed face reaches a value of 0.0035 at a distance from the column face equal to x, the neutral axis depth.

It is necessary to assess the bearing strength of a truncated pyramidal element with an apex angle approximately equal to 20^{o} representing the front of a radial segment supported at a column face and this was determined as a function of the stress gradient in the failure zone

$$\sigma_{c1}/f_c = 1 + \lambda_c \, SG$$

$$SG = ((\sigma_{c1} - \sigma_{c2})/\lambda a_1) \cdot (a_1/f_c)$$

Fig.(1-19). This condition could be true when σc1 acts parallel to the axis of the pyramid, but as described in criterion (a) above the angle can vary from 10^o to 20^o. Where the force is not concentric with the pyramid it would seem that σ_{c1}/f_c could be less than that calculated above for concentric loading resulting in under estimating the neutral axis depth.

In the criterion of failure the plastic length is taken to be dependent on the reinforcement lay-out in order to find the failure rotation, while in fact the failure rotation is dependent on the material properties of the concrete and the depth of the compression zone.

4- <u>Plasticity approach</u>

Braestrup (8) developed a plastic solution for the punching shear strength of slabs. It is based upon the failure mechanism shown in Fig.(1-20). The deformations are assumed to be concentrated in a rotationally symmetric failure surface, the rest of the slab remaining rigid. The relative deformation rate v is perpendicular to the slab, therefore the main reinforcement does not contribute to the resistance and the punching force depends only on geometric factor and the strength of the concrete.

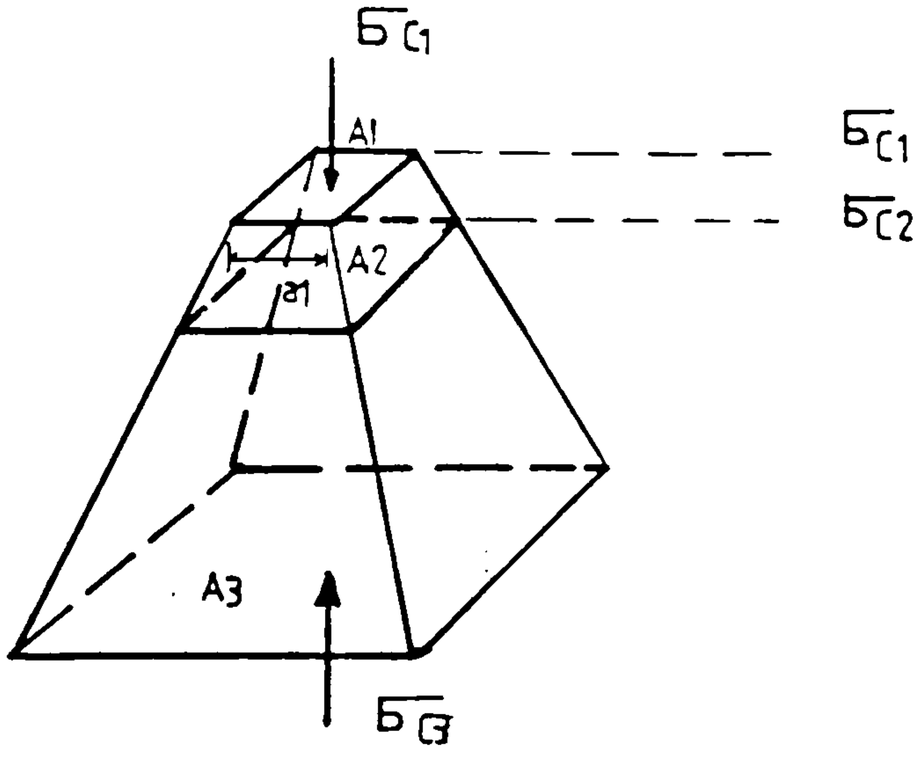

Fig.(1-19) Truncated pyramid

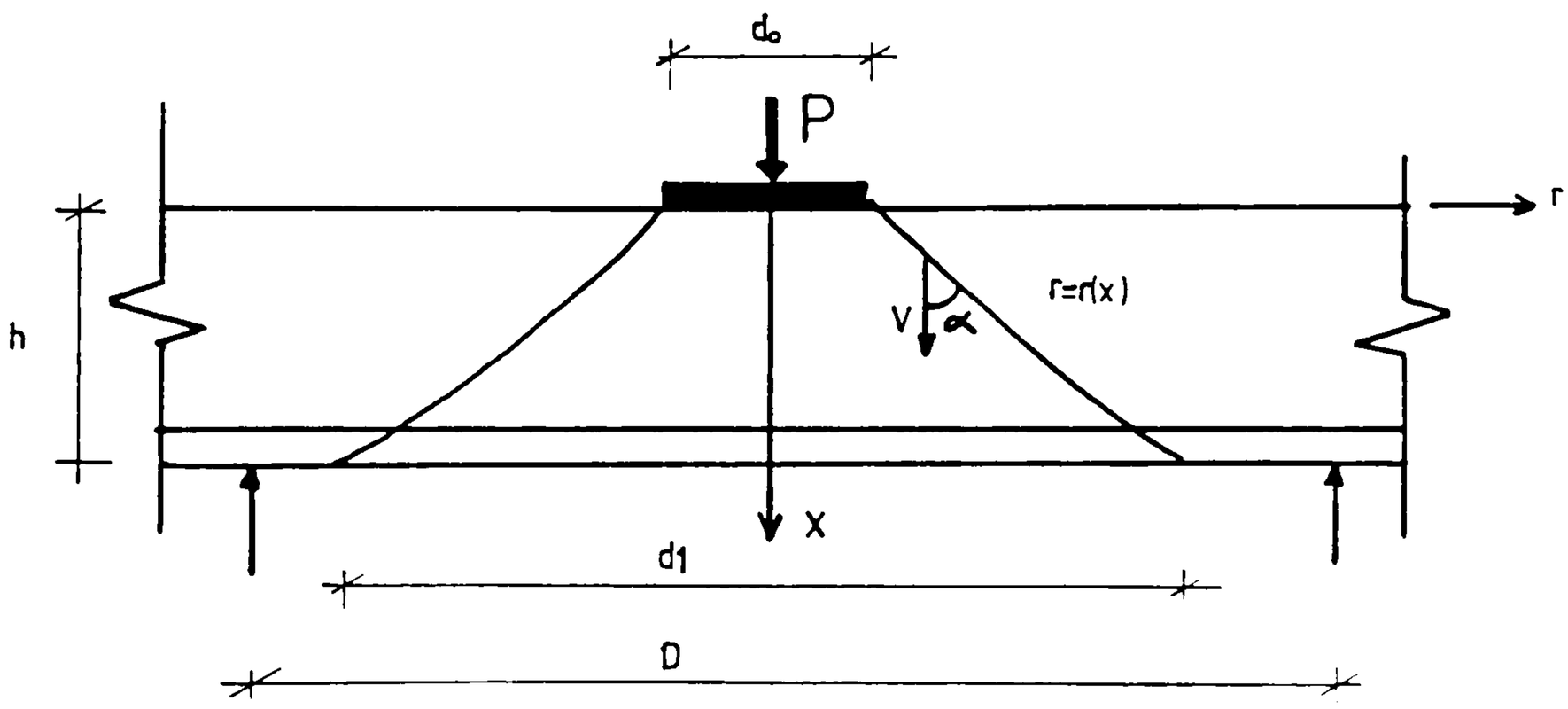

Fig.(1-20) Failure mechanism of Braestrup

Many tests reported in the literature as punching shear failures show a dependence of strength upon the amount of tension reinforcement.

To find an estimate for the ultimate punching load Braestrup applied the upper bound theorem, equating the rate of external work done by the load with the rate of internal work dissipated in the failure surface. As a constitutive model for concrete Braestrup used the modified Coulomb failure criterion as a yield condition Fig.(1-21) with the associated flow rule indicated in the figure. This constitutive model has three material parameters, the tensile strength f_t, the compressive strength f_c, and the angle of internal fraction φ, determining the parameter K Fig.(1-21). The upper bound solution for the failure of Fig.(1-20) yields

$$P = \pi f_c \int_0^h (l\sqrt{1 + (r')^2} - mr')r\,dx$$

Where h is the slab thickness, r= r(x) is the equation for the failure surface generatrix and r' = dr/dx. The parameters l and m are defined as

$l = 1-(K-1)\ f_t/f_c$ and

$m = 1-(K+1)\ f_t/f_c$

where $K = (1+\sin\varphi)/(1-\sin\varphi)$

The above solution is subject to the condition $r' \geqslant \tan\varphi$ and the lowest upper bound is determined by minimisation of the

functional at $x=h_o$. The optimal failure surface is consequently described by the generatrix $r=r(x)$ where

$r(x)=r_o+x\tan\varphi$ for $0 \leqslant x \leqslant h_o$

$r = a \cosh (x-h_o/c) + b \sinh (x-h_o/c)$ for $h_o \leqslant x < h$

The corresponding upper bound $P = P_1 + P_2$ where the contributions P_1 and P_2 for the straight line and catenary part respectively are found to be

$$P_1 = 0.5\ \pi\ f_c\ h_o\ (d_o + h_o\tan\varphi\ )(1-\sin\varphi)/(\cos\varphi)$$

$$P_2 = 0.5\ \pi\ f_c\ [l_c\ (h-h_o) + l(r_1\ \sqrt{(r_1)^2-c^2}\ -ab)-m(r^2-a^2)]$$

The constants a,b,c and h_o are determined by the equations

$$c^2 = a^2 - b^2$$

$$a = r_o + h_o\ \tan\varphi$$

$$b/c = \tan\varphi$$

$$r_1 = a\ \cosh(h-h_o)/c + b\ \sinh(h-h_o)/c$$

This solution requires an assumed value of the opening diameter d_1, and the lowest upper bound is found by minimisation with respect to this parameter. The punching force is a function of the diameter d_o and the slab depth h, and the load may be represented by the parameter τ/f_c where $\tau = P/\pi h(d_o+2h)$ Fig.(1-22a). The solution is very dependent upon the value of the concrete tensile strength Fig.(1-22b).

The plastic solution developed so far is an upper bound only. To establish it as a complete solution it would be necessary to specify a stress distribution in the entire slab which:

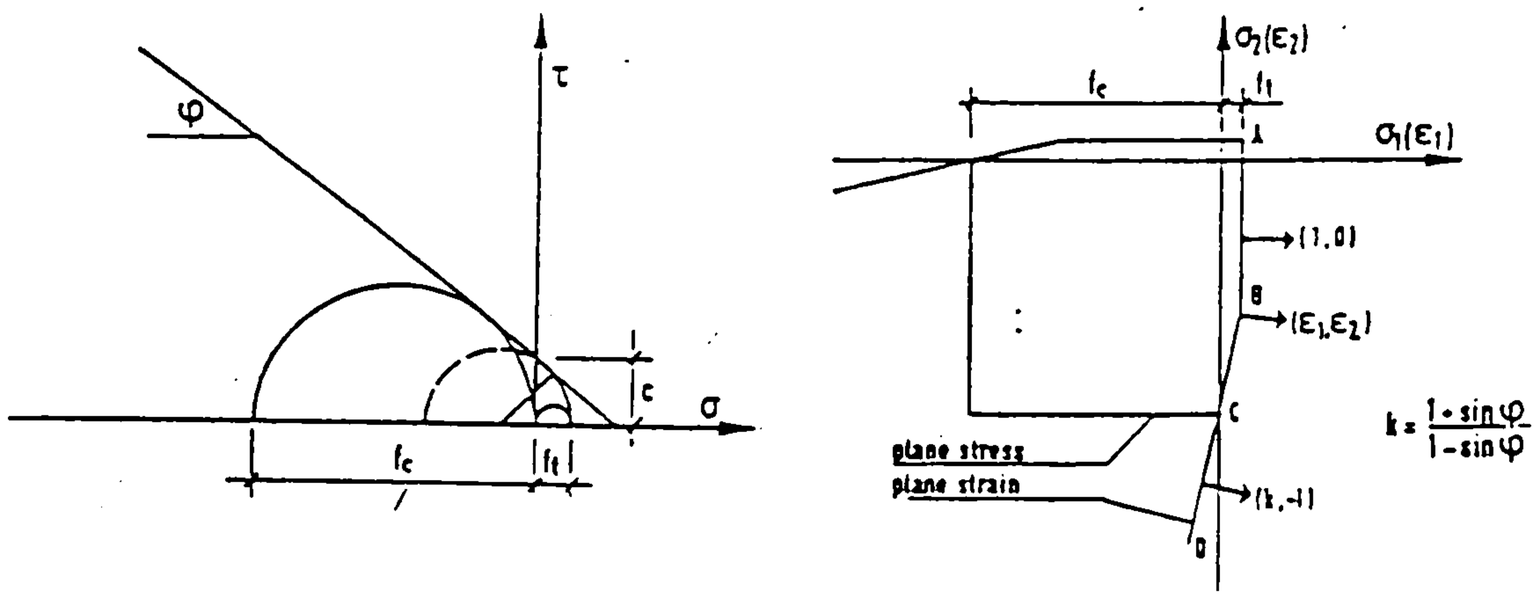

Fig.(1-21) Modified coulomb failure criterion

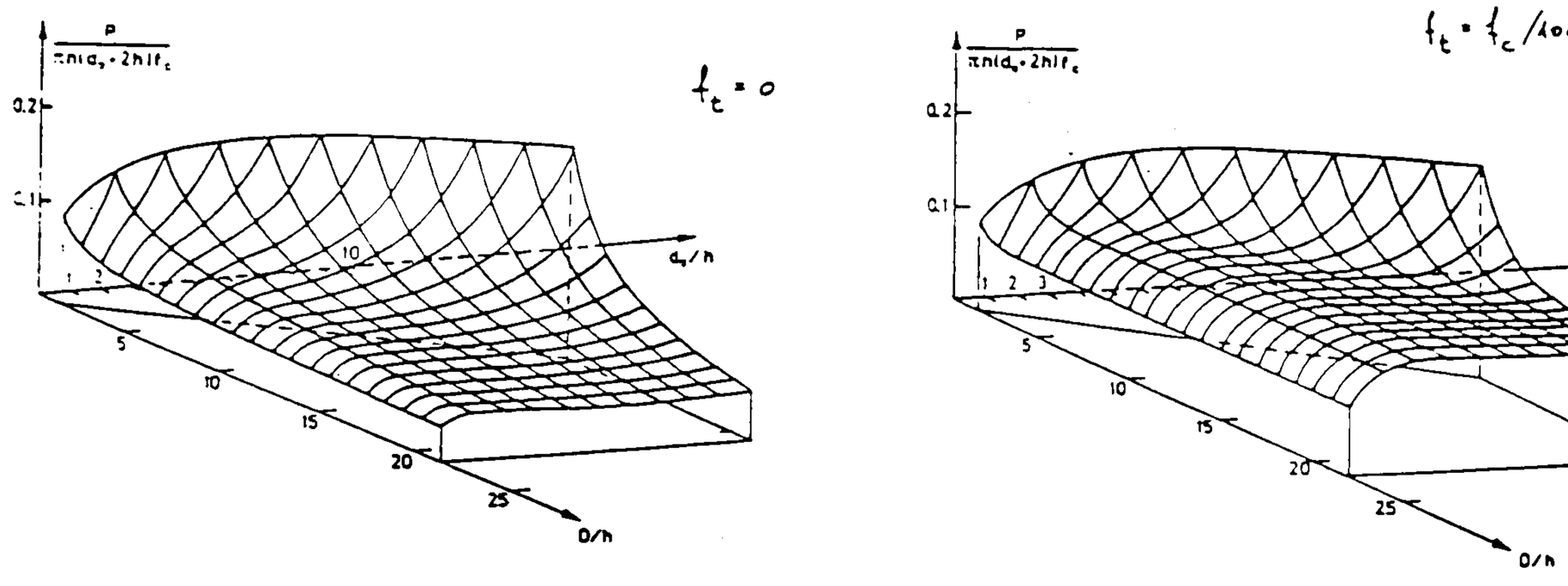

-a- -b-

Fig.(1-22) Variation of punching resistance according to plastic theory (Brastrup)

-Satisfies the equilibrium equations and the statical boundary conditions

-Corresponds to a yield line along the optimal failure surface generatix

-Does not violate the yield condition at any point. The prospects of an exact solution are brighter if the tensile strength is neglected, and for simplicity it is further assumed that the geometry is such that the optimal failure surface generatrix is a catenary without any linear part Fig.(1-23).

The failure surface generatix

$$\rho = r(xX) = a \cosh(xX/c) + b \sinh(xX/c)$$

Assuming the function $\theta = \theta(xX, \rho)$

$$\cot\theta = (\rho + \sqrt{\rho^2 - c^2})/c$$

The circumferential stress $\sigma\varphi$

$$\sigma\varphi = \frac{\rho + \sqrt{\rho^2 - c^2}}{2\sqrt{\rho^2 - c^2}} f_c$$

This is numerically greater than the compressive strength f_c, and thus violates the yield condition. The lack of a corresponding lower bound suggests that there may be an error in the upper bound solution.

5- Andrä

Andrä (1) made a theoretical study of the punching of a circular slab with ring reinforcement. He derived his model by using a finite element analysis. The model considers a radial segment rotated as a rigid body around a centre of rotation,

located at the face of the column at the neutral axis depth Fig.(1-24). From the rigid body rotation, the tangential forces on a ring element dr in the elastic stage are

$$Fs = \rho d\ d_s\ Es\ \psi\ (d/r)(1-(x/d))$$

$$Fc = 0.5\ d_r\ (E_s/\alpha_e)\ \psi\ (x/r)\ x$$

Each segment is analysed using a truss model Fig.(1-25) for the part beyond the shear crack, with 45^o tension and compression members representing the behaviour of the uncracked concrete. Assuming that $Fs/Fc > 1$ and

$$x/d < \sqrt{(\rho\alpha_e)^2 + 2\rho\alpha_e} - \rho\alpha_e$$

where $\alpha_e = Es/Ec$, resolving the forces Fs and Fc in the direction of the struts and normal to them, and equating stresses due to the normal components to the tensile strength of concrete f_t, the radius r_1 of Fig.(1-25) can be found. For the elastic stage:

$$r_1^3 - r_1 r_o = (z/f_t)\ \psi\ E_s[\rho d(d-x) - (X^2/2\alpha_e)]$$

For the yielding stage of the reinforcement

$$r_1 = \frac{r_o}{2} + \sqrt{\frac{r_o^2}{4} + \frac{Z}{f_t}\ (\rho d f_y)}$$

The radius r_2 of Fig.(1-25) is calculated on the basis of the limit $\tan\alpha = 0.2$ i.e $r_2 = r_o + 5z$. In the absence of yielding, the punching force can be estimated by integrating the vertical components of the strut forces:

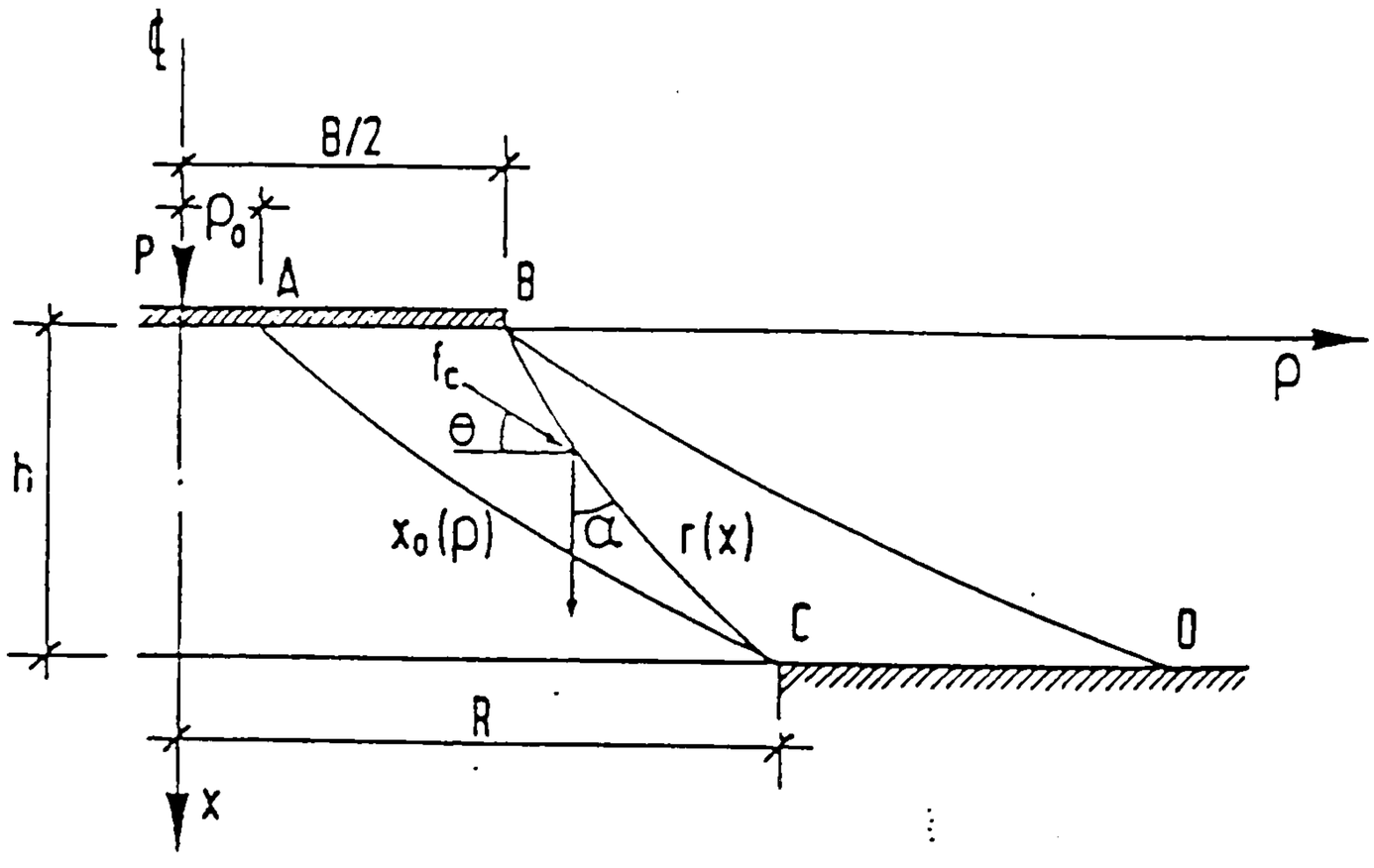

Fig.(1-23) Lower bound stress field

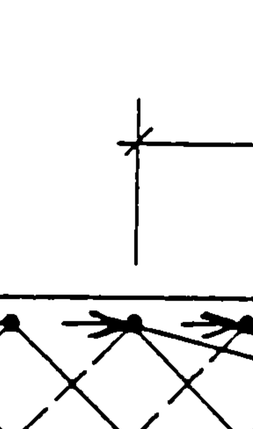

Fig.(1-24) Rigid body rotation model adopted by Andrä

Fig.(1-25) Andrä's truss idealization of
a radial segment

$$P_{up} = \pi\ r_v\ Es\ \psi\ [\rho d(d-x)\ -\ (x^2/2\alpha_e)]\cdot[(1/r_1)-(1/r_2)]$$

$$r_v = 2\ (0.4r_o + 0.8z)$$

Where r_v is a particular radius, and r_1 should not be less than r_v

$\psi = 0.003\ d/x$ for ring reinforcement

$\psi = 0.0035\ d/x$ for two-way reinforcement

In the case when the reinforcement yields, the integration is done in two parts

Part 1 for $r_1 < r < r_y$

Part 2 for $r_y < r < r_2$

Where $r_y = \psi\ (d-x)/\varepsilon_y$

the two integrations lead to:

$$P1_{up} = 2\ \pi\ r_o\ \rho\ d\ f_y\ (r_v/2r_o)\ \ln(r_y/r_1)$$

$$P2_{up} = 2\ \pi\ r_o\ Es\ \psi\ [\rho d(d-x)-(x^2/2\alpha_e)]\cdot(r_v/2r_o)[(1/r_y)-(1/r_2)]$$

The punching load will be

$$P_{up} = P1_{up} + P2_{up}$$

The horizontal component of the strut forces H_u is calculated in the same manner as P_u for reinforcement in the elastic stage

$$H_u = 2\ \pi\ r_o\ E_s\ (\psi/r_o)[\rho d(d-x)-(x^2/2\alpha_e)]\cdot\ln(r_2/r_1)$$

If the reinforcement is yielding

$$H_u^1 = 2\ \pi\ r_o\ (d/\rho_o)\rho f_y(r_y-r_1)$$

$$H_u^2 = 2\ \pi\ r_o\ (E_s\psi/r_o)[\rho d(d-x)-(x^2/2\alpha e)]\ln(r_2/r_y)$$

$$H_u = H_u^1 + H_u^2$$

The total inclined force F can be expressed as

$$F = \sqrt{(P_{up})^2 + (H_u)^2}$$

at an angle $\alpha_o = \tan^{-1}(P_{u,p}/H_u)$ as shown in Fig.(1-26). The bearing stress at the support of the struts is

$\sigma_b = F/(2\ \pi\ r_o\ x\ \cos\alpha_o)$

Failure is assumed to occur when this bearing stress is equal to the limit local bearing stress f_{bu} defined as

$f_{bu} = f_c \sqrt{(r_o+d)/r_o} \leqslant 1.4\ f_c$ for two-way reinforcement

$f_{bu} = f_c \sqrt{(r_o+0.5d)/r_o} \leqslant 1.4\ f_c$ for ring reinforcement

6- <u>Nölting</u>

Using the inclined compression approach, Nölting (46) proposed a method for calculating the punching strength. He assumed that all failures at inclined cracks around concentrated loads or supports can be regarded as forms of punching, irrespective of the state of the reinforcement in terms of yield. Nölting adopted a limiting strain in the direction of the inclined compression around the loaded area as a criterion of failure. The strain can be calculated using three relationships between:

-The load and the critical moment at the column or loaded area
-The moment and the horizontal strain of the concrete
-The horizontal and inclined strain of the concrete

The critical moment is determined on the basis of the elastic theory as used in the German code (19) and code manual (18). A simple equation with numerical coefficients dependent on the slab geometry and loading conditions was developed by Nölting

for concentric loading

$m = P / K_4 \ (1+K_5 \ b_q/l_m)$

Where m is the critical moment per unit width and l_m is a length dependent on the slab geometry. K_4 and K_5 are numerical coefficients. The values of l_m, K_4, and K_5 are given in Fig.(1-27). The horizontal strain of the concrete (ε_{bh}) is determined for three stages.

For a load less than that causing yield m < my, P < P_y, ε_{bh} is determined from cracked elastic analysis of the cross-section as in the DIN code (19)

At the yield load P = P_y

$\varepsilon_{bdy} = \varepsilon_{bh}\psi/f(\lambda)$

where ε_{bd} is the strain of the concrete in the diagonal direction

ε_{bh} is the strain of the concrete in the horizontal direction

$f(\lambda)$ is a function of the slenderness λ of the slab as illustrated by Fig.(1-28)

$f(\lambda) = 1 - (1/\sqrt{\lambda})$

For loads beyond yield P > Py

$\varepsilon_{bd} = \varepsilon_{bdy}(P/P_y)^2$

The criterion of failure is expressed as $\varepsilon_{bdu} = 4.5‰$.

Combining the above

$$P_u = P_y \sqrt{\frac{4.5‰}{\varepsilon_{bhy}}} \left(1 - \frac{1}{\sqrt{\lambda}}\right) \qquad \text{or}$$

$$\left(1 - \frac{1}{\sqrt{\lambda}}\right) = \frac{P_u}{P_y} \sqrt{\frac{\varepsilon_{bhy}}{4.5‰}}$$

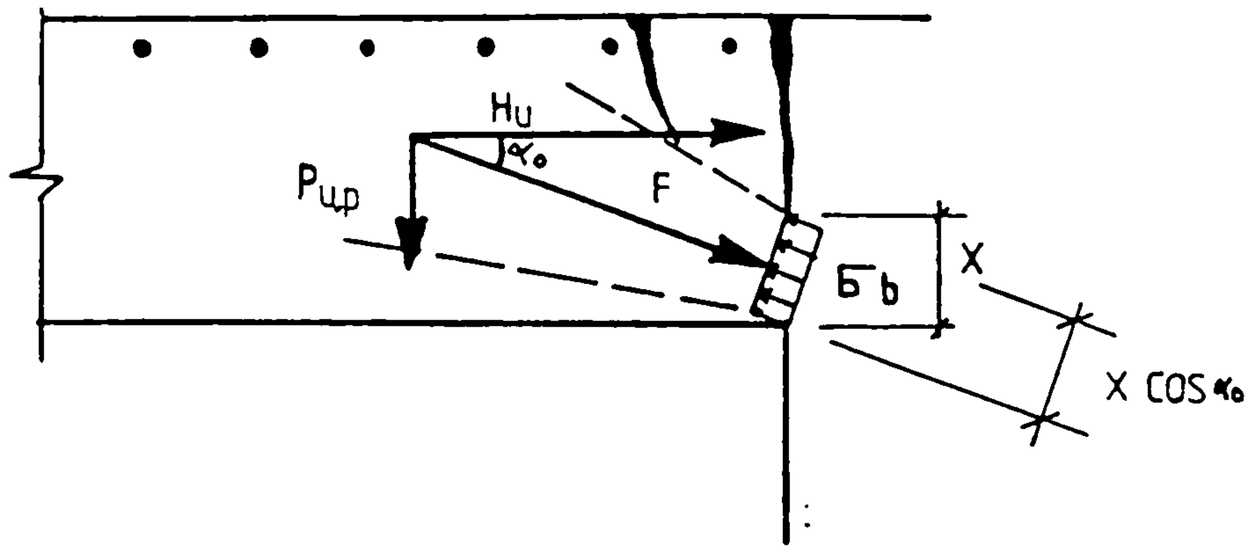

Fig.(1-26) Force and stress at the column face according to Andrä's approach

	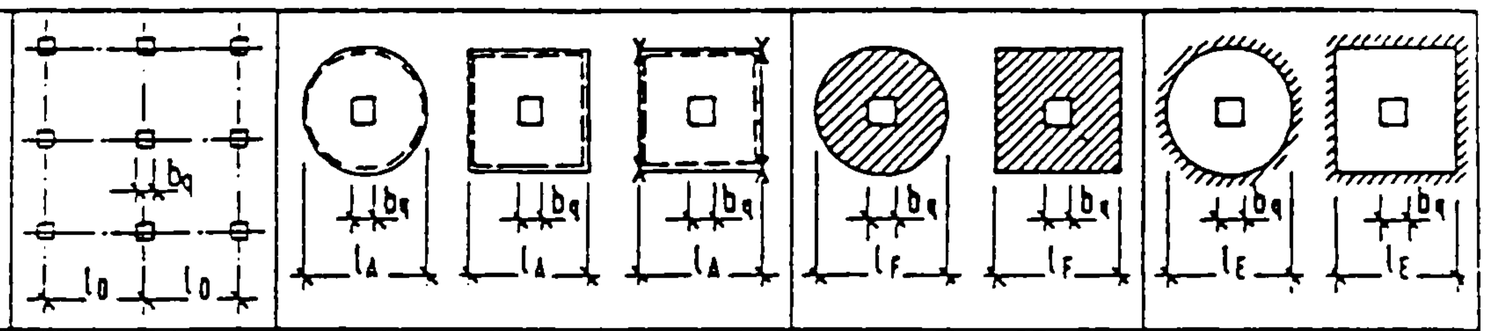			
	FLAT SLAB	SIMPLE MODELS	FOOTINGS	ENCASTRÉ SLABS
l_m	$0.46 l_0$	l_A l_A $0.8 l_A$	l_F $1.13 l_F$	l_E $1.13 l_E$
k_1		- 0 0159	-0.0477	- 0.0637
k_4		2.65	1.90	2.00
k_5		6	20	22

Fig.(1-27) Data for moment calculations in Nölting's theory (46)

The punching failure load according to the method described above can be approximated as

$$P_u = 4.75 \sqrt{\rho\ f_c}\ \ d^2\ \alpha_o$$

where f_c is the cylinder compressive strength of the concrete and α_o is a function describing the geometry of the slab.

For a flat slab α_o = (0.65+9.4 B/L)-(2.2+70 B/L)d/L as illustrated in Fig.(1-29).

1-3-3 TREATMENTS OF LOAD ECCENTRICITY

Where an eccentric load is transferred from a slab to an internal column a part of the moment (M=e.P) is likely to be provided by an uneven distribution of the vertical shear at perimeters around the column. The distribution of the shear can be estimated by a variety of methods. Plate analysis can give theoretical shear distributions and the results are relatively simple, provided they are restricted to the elastic range. There are considerable problems involved in their use for the prediction of punching resistances, and it is difficult to allow for redistribution of effects following flexural cracking and yielding.

The nominal shear stress due combined shear and moment transfer in the elastic can be expressed as

$$v = (P/ud)(1+ Ke/c)$$

Provided the behaviour is idealized to that of a column and an infinite plate

FLAT SLAB	SIMPLE MODELS	FOOTINGS
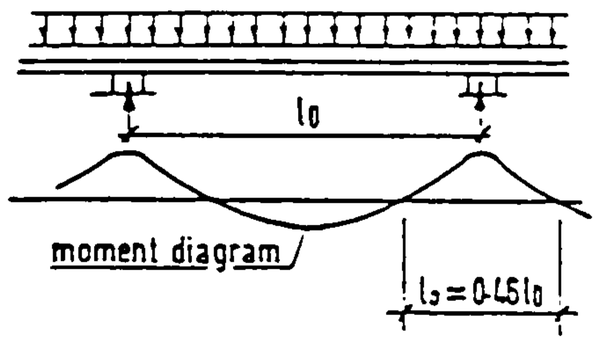	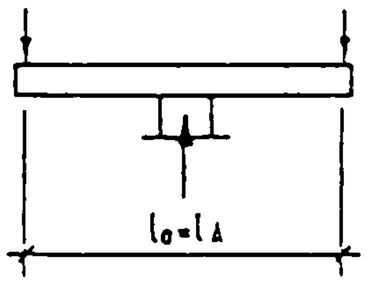 but note for square slabs with corners held $l_0 = 0.8\, l_A$	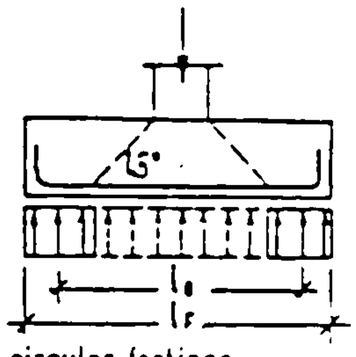 for circular footings $l_0 = \frac{2}{3} l_F \frac{1-\beta^3}{1-\beta^2}$ for square footings $l_0 = \frac{2}{3}\sqrt{\frac{\pi}{4}}\, l_F \frac{1-\beta^3}{1-\beta^2}$ where $\beta = A_K / A_F$ A_K = area of base of punching cone A_F = area of base of footing
SLENDERNESS $\lambda = [l_0 - B]/d$		

Fig.(1-28) Definitions of slenderness in Nölting's theory

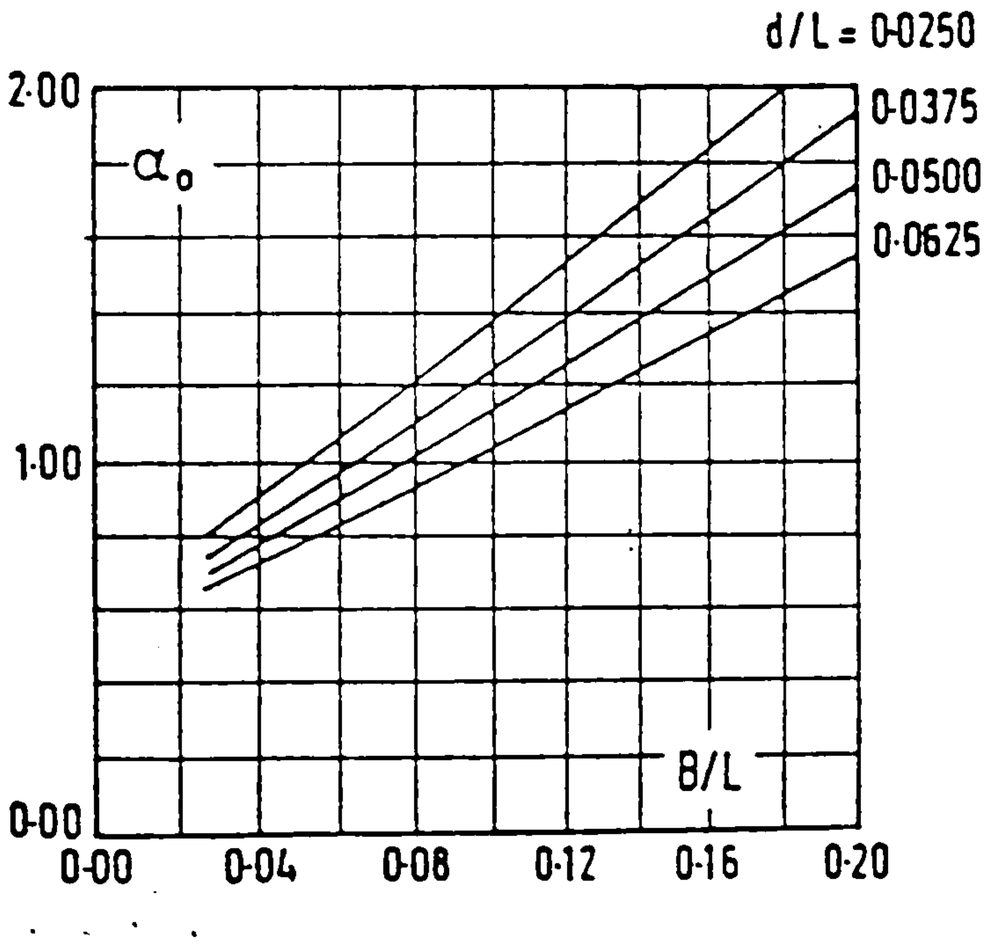

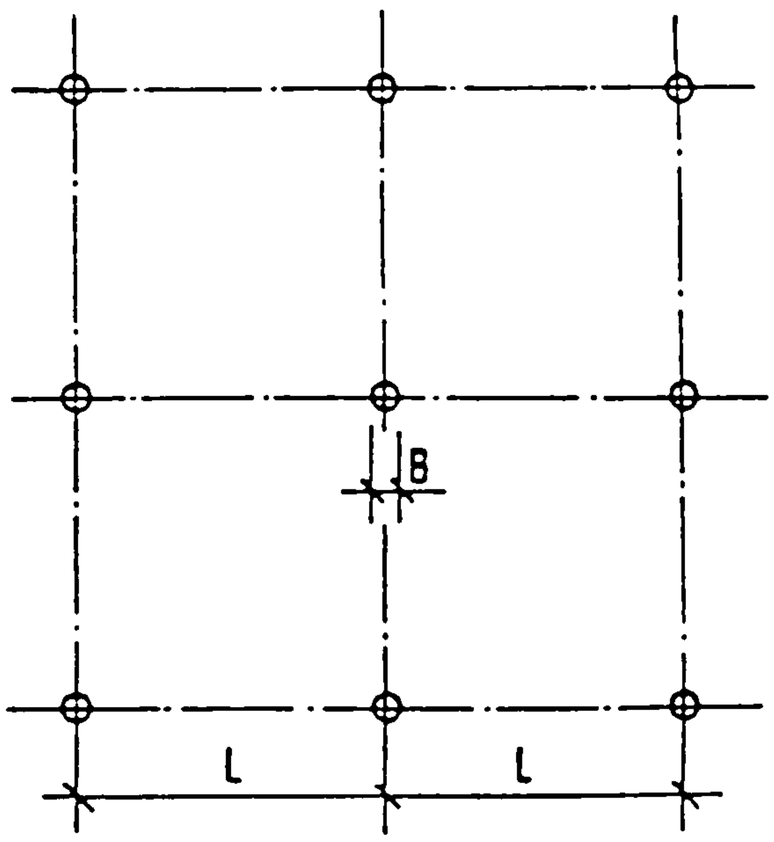

Fig.(1-29) Nölting's function α_o for flat slabs (46)

Where

u = the length of the control perimeter

K = a numerical coefficient

e = the eccentricity (M/P) of the load

M = the unbalanced moment

c = a dimension dependent on the column dimensions and the slab thickness

For slabs with short spans 1, the span length can be included in the previous equation.

Another approach to express the shear stresses due to moment transfer is to assume a value for the proportion of the moment provided by uneven shear and then to assume the resulting shear stress to vary linearly around the control perimeter, thus.

$V = P/A + KM \cdot c/J$

where

$A = u.d$

KM = the part of the moment resisted by shear

c = the distance from the column centre to the furthest part of the control perimeter

J = the moment of inertia of the control surface. If X and Y are the plan dimensions of a rectangular control perimeter

$J = (X^3d/6) + (Xd^3/6) + (X^2Yd/2)$ with torsional effects included

$J = (X^2Yd/2) + (X^3d/6)$ with vertical shear alone considered

1- THE BUILDING CODE RULES

a- ACI-318-83

The stress distribution assumed is illustrated in Fig.(1-30). The factored shear force V and unbalanced moment M are determined at the centroidal axis c-c of the critical section. The maximum factored shear stress may be calculated from.

$$v_{(AB)} = (V/A_c) + (\gamma_v \cdot Mc_{AB}/J_c)$$

or

$$v_{(CD)} = (V/A_c) - (\gamma_v \cdot Mc_{CD}/J_c)$$

where

$$\gamma_v = 1 - \frac{1}{1 + (2/3)\sqrt{(c_1+d)/(c_2+d)}}$$

is the fraction of the moment between the slab and column that is considered to be transferred by eccentricity of the shear about the centroid of the assumed critical section.

$$A_c = 2d(c_1 + c_2 + 2d)$$

$$J_c = \frac{d(c_1+d)^3}{6} + \frac{(c_2+d)d^3}{6} + \frac{d(c_1+d)(c_2+d)^2}{2}$$

b- British standard BS 8110

$$v_{\cdot max} = \frac{P}{u \cdot d}\left[1 + \frac{1.5e_x}{C_x+3d}\right]$$

where c_x is the column dimension in the direction of the eccentricity e_x

c- CEP-FIP

$$v_{\cdot max} = \frac{P}{u \cdot d} \left[1 + \frac{1.5[e_1] + 1.5[e_2]}{\sqrt{(c_1 + d)(c_2 + d)}} \right]$$

2- Regan

Regan (53) assumed the distribution of shear corresponding to pure moment loading can be visualized as in Fig.(1-31). The lever arm between the forces reaching on to the faces c_2 of the column is approximately (c_1+2d).

The maximum vertical stress on the inclined surface due to the moment M is then

$$v_{\cdot max} = \frac{\alpha M}{d \sqrt{1 + \cot^2\theta}\ (c_1+2d)[c_2+0.5\pi \cdot d \cdot \cot\theta + c_1\ (3c_1+6d)]}$$

Combining this with a stress resulting from concentric shear V and with e = M/V results in

$$\frac{V_{ue}}{V_{uo}} = \frac{1}{1 + \beta[e/(c_1+2d)]}$$

where

V_{ue} = ultimate shear capacity for an eccentric load

V_{uo} = ultimate concentric load shear capacity

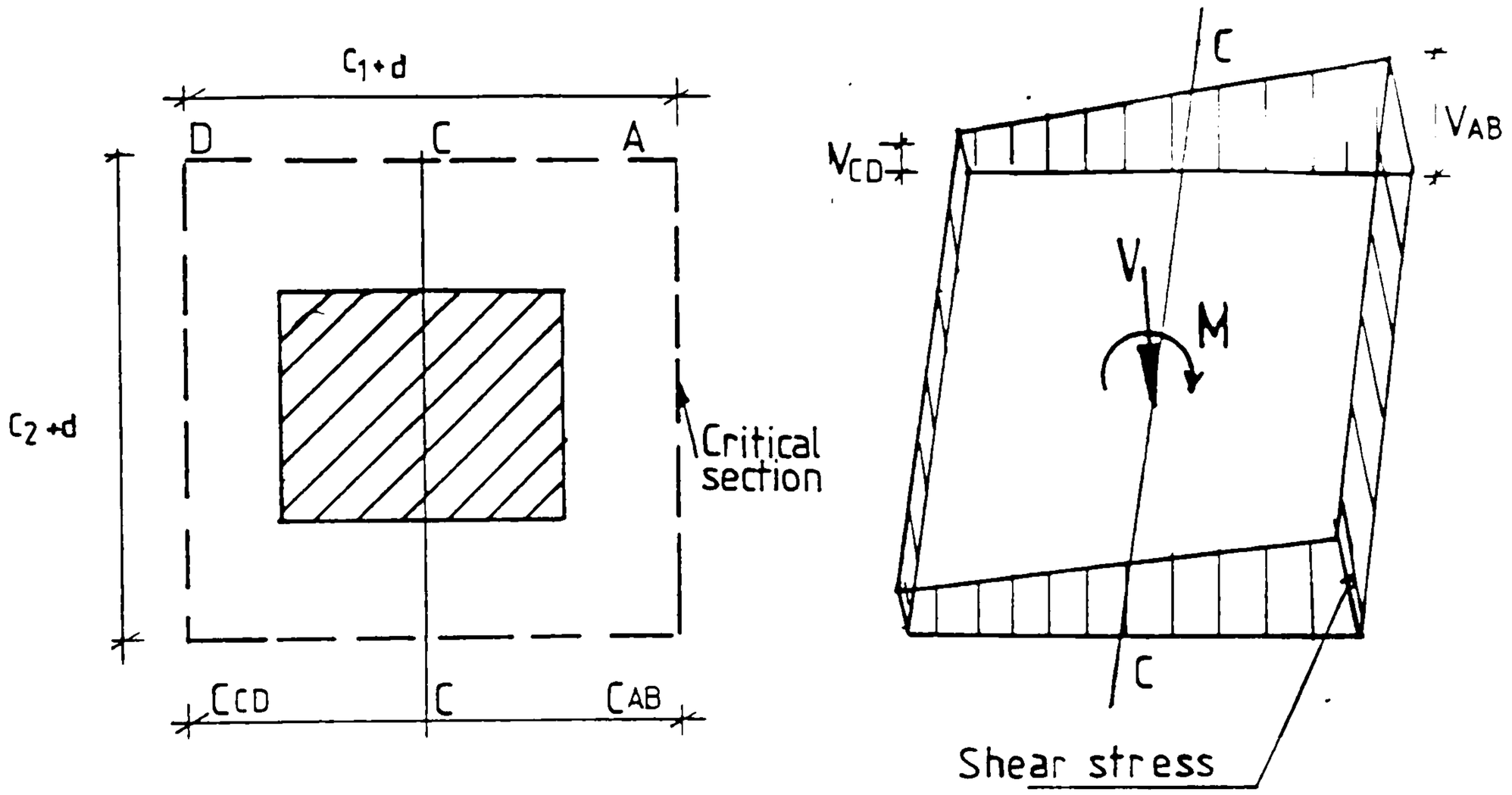

Fig.(1-30) ACI Assumed distribution of shear stress

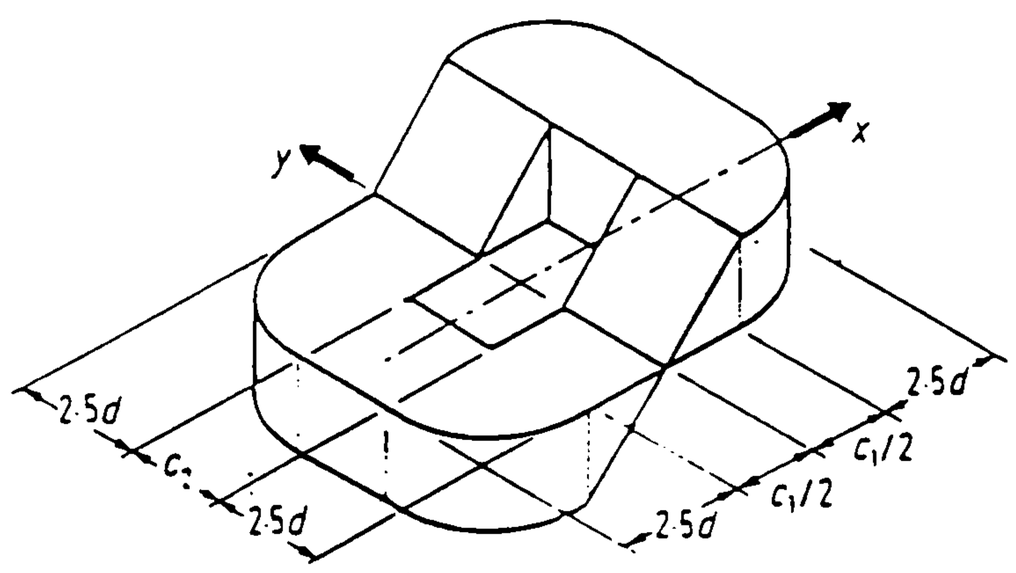

Fig.(1-31) Distribution of stresses on fracture surface due to unbalanced column moment loading (Regan)

$$\beta = 2\alpha \left[\frac{\frac{c_2}{c_1} + \frac{\pi}{2} \cdot \frac{d \cot\theta}{c_1} + 1}{\frac{c_2}{c_1} + \frac{\pi}{2} \cdot \frac{d \cot\theta}{c_1} + \frac{1}{3[1+(2d/c_1)]}} \right]$$

3- ANIS

Anis (2) indicates that the criteria of failure of slabs under concentric load can be used for slabs under eccentric load. He assumed that the side toward the eccentricity fails first when the maximum concrete strain is reached, and he assumed the shear stress distribution around the critical section with radius r_{cr} in the region of a circular column stub loaded with a vertical force V and moment M to be as in Fig.(1-32).

Anis presented the ultimate load P as a function of the shear cracking load

$V_{cr} = 0.6P$

For combined load the critical shear cracking stresses are assumed to be

$q_{cr} = q_1 + q_2$

The shear stress q_1 due to the vertical load V is

$$q_1 = \frac{V_{cr}}{2\pi\, r_{cr}\, d}$$

The equilibrium equation of the external moment and the shear

stresses gives the magnitude of q_2 as follows. The resultant of the shear stresses of one half of the cone is Q

$$Q = \frac{3}{4} \pi r_{cr} d q_2$$

the moment of these stresses is

$$M_{cr} = \frac{3}{4} \pi r_{cr} d q_2 Z$$

where $M_{cr} = V_{cr} \cdot e$ = the applied moment corresponding to shear cracking

Z = distance between the resultants of the shear stresses as Shown in Fig.(1-32)

$$q_2 = \frac{V_{cr} \cdot e}{1.15 \pi r_{cr}^2 d}$$

$$q_{cr} = \frac{V_{cr}}{2\pi r_{cr} d} + \frac{V_{cr} \cdot e}{1.15\pi r_{cr} d}$$

$$q_{cr} = 6\sqrt[3]{f_{cu}(p\%)} \qquad lbs/in^2$$

the value of r_{cr} can be given as

$$r_{cr} = \frac{V_{cr} + \sqrt{V_{cr}^2 + 44d\, q_{cr}\, V_{cr}\, e}}{12.56\, d\, q_{cr}}$$

4- <u>STAMENKOVIC and CHAPMAN</u>

Stamekovic and Chapman (63) suggested that the ultimate shear strength under vertical load only can

be calculated from a modified version of Moe'S (40) formula

$$V_u = 0.9 \left[4rd \sqrt{(f_c/145)} \cdot \left(\frac{15(1-0.075r/d)}{1 + 5.25 \frac{4rd \sqrt{f_c/145}}{V_{flex}}} \right) \right] \quad f_c \text{ in } N/mm^2$$

and the ultimate moment strength at the column head under horizontal loading only is due to the combined action of the bending resistances developed at by compression stress blocks the vertical slab-column interfaces normal to the moment plane, the couple due to the bond of reinforcement passing through the column, the couple due to the vertical shears at the faces normal to the moment plane, and of the torsional resistance developed at the vertical slab-column interfaces parallel to the moment plane Fig.(1-33). The ultimate moment strength can be calculated as.

$$M_u = K_c f_{cu} r(h/2)^2 + 0.13 f_{cu} \Sigma_o b a_s + K_s f_{cu} rdb + 0.5n K_t \frac{A_s f_y}{bh} h^2 \left(b - \frac{h}{3}\right)$$

where k_c, K_s, K_t, n are 1, 0.1, 1 and 2 respectively

a_s - distance between top and bottom bars

h - slab depth

r - side length of column section normal to moment plane

b - side length of column section parallel to moment plane. The ultimate strength under combined loading can be calculated from the following proposed interaction formula

$$\frac{V}{V_u} + \frac{M}{M_u} = 1$$

5-Long

Long (37) suggested that, flat slabs share two basic modes of failure, a flexural mode, when the steel yields before the concrete fails, and a shear mode of failure, when the concrete fails before the steel yields.

For concentric loading, Long presented the predicted punching load for a slab to be the lesser of P_1 and P_2

$$P_1 = \frac{\rho\ f_y\ d^2\ (1-0.59(\rho f_y/f_c))}{(0.2\ -\ 0.9(C/L))}$$

$$P_2 = \frac{1.66(c+d)\ d\ (100\rho)^{0.25}\ \sqrt{f_c}}{(0.75\ +\ 4(C/L))} \qquad \text{Newtons}$$

Where P_1 = The predicted punching load for the flexural mode

P_2 = The predicted punching load for the shear mode

c = Side length of a square column

L = Span between columns

For combined loading the punching capacity is

$$P = \frac{P_v}{(1\ +\ 15(e/L))} \qquad \text{Or} \qquad \frac{P_v}{(1\ +\ 0.9(e/C))}$$

Where P_v is the lesser of P1 and P2

e is the eccentricity with respect to the column centre line.

Longs expressions are based on equal spans and on square columns.

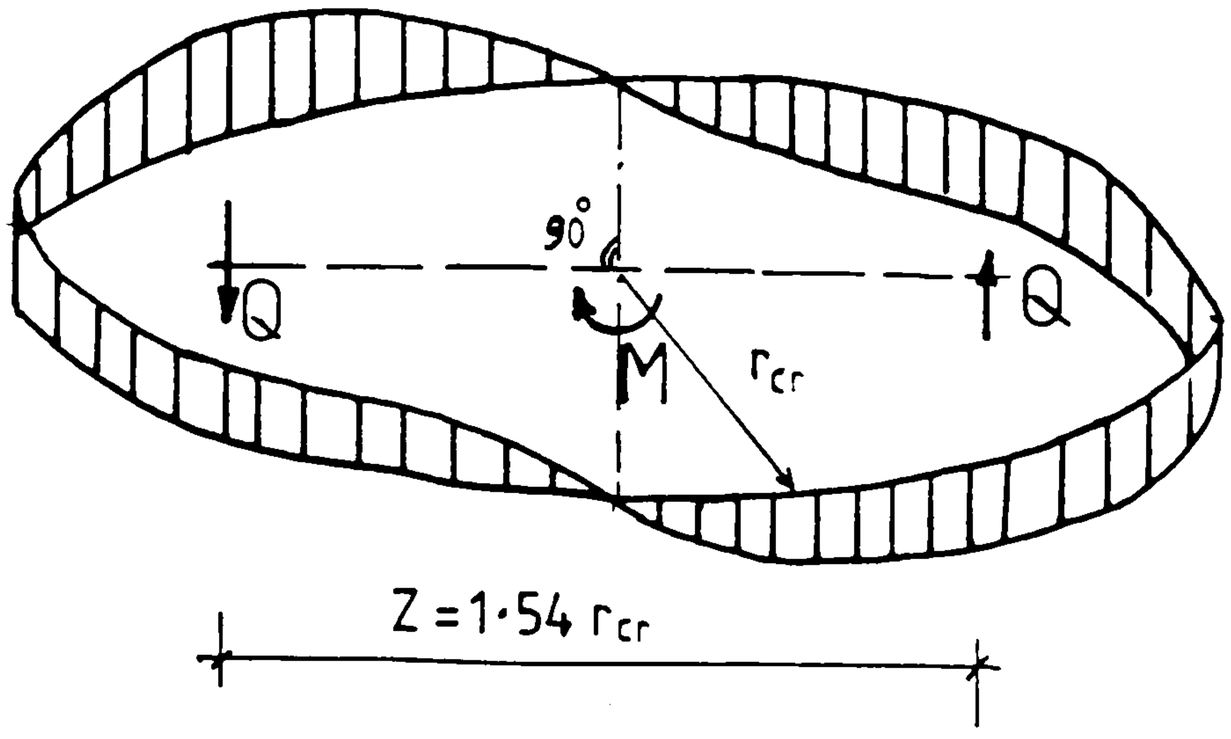

Fig.(1-32) Assumed distribution of shear stresses due to a pure couple (Anis)

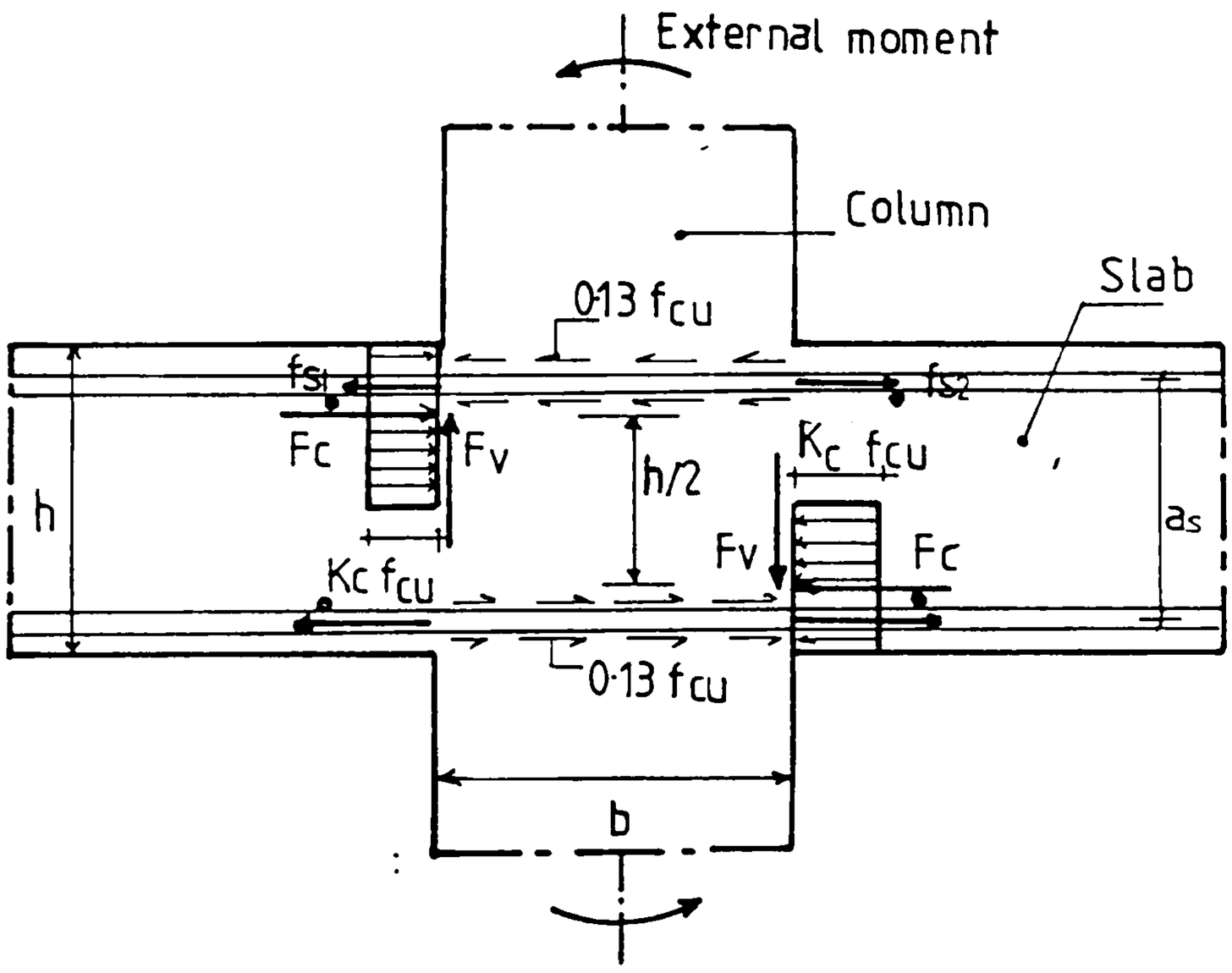

Fig.(1-33) internal forces balancing the external moment (Stamenkovic)

6- Other Methods

There have been various attempts to treat slab-column connections as crosses of beam-column joints. There are considerable difficulties in such approaches with the division of the loading into bending moments, shears and torsions in the four pseudo-beams meeting at an internal column. Furthermore the methods are inherently illogical as they must assume that the regions of the slab near the corners of the column are ineffective. This can not be true with regard to shear as the concentric punching capacity of a slab is much greater than the sum of the shear strengths of four beams with widths equal to the column's side dimensions.

1-4 CONCLUSION

This chapter has reviewed the methods of overall design for flat slabs and the treatments of concentric and eccentric punching. Some of the important aspects the present review are summarised below

Overall Analysis

1- Yield line theory is inappropriate as a general approach to flat slab design as it provides no basis for assessing moments transmitted to columns, while these moments are important as determinants of punching resistance.

2- Equivalent Frame analysis provides a reasonable representation of the behaviour of flat slabs by systems of column and beams analysed separately in two directions.

3- The difference between the frame of a flat slab and the simple equivalent beam-column frame is partial lack of continuity between the slabs and the columns. To estimate the moment transfer to the columns it is reasonable to use the ACI model of a connection in which a torsional member is inserted between the slab and column. The analysis should then be made of a frame directly including the torsion member, rather than hiding it in an "equivalent column" since the equivalent column technique can not be used for horizontal loading. Regans flexible joint would be an alternative to the ACI's torsion member but the later is widely known and there is no obvious advantage in Regan's variant. As currently used both formulations are based on the elastic theory of uncracked plates but either could be extended to allow consideration of the effects of cracking.

Symmetric Punching

With regards to symmetric punching there is a measure of agreement on the physical model proposed by Kinnunen and Nylander. The slab is divided in to segments by radial flexural cracks and the parts of the segments outside the shear crack rotate as rigid bodies. At the periphery of the column the concrete resists transverse load by an inclined radial compression. Near the column the compression zone is subjected to a condition of complex and high stresses which makes a fully theoretical treatment very difficult. The theories proposed to date are difficult to use in practice.

Eccentric Punching

Eccentric punching resistance is presently described by empirical equations based on simple factoring of the resistance of slabs under concentric loading. There are rather wide discrepancies between the equations used and there is generally little or no theoretical background to them. The sole exception is Stamenkovic's approach in which the pure moment capacity of a connection is treated more or less theoretically. The pure shear and pure moment capacities are then used to construct a shear-moment interaction diagram. This approach is an interesting one. From what has been reviewed above it is clear that more work needs to be done:

a- On concentric punching to improve the method of predicting shear resistance based on the physical model proposed by Kennunen and Nylander. Some improvement in accuracy would be desirable but the greater concern is to derive a more readily usable formulation.

b- To develop an analysis with sufficient accuracy for the prediction of eccentric punching resistance.The analyses should be verified not only for the square columns and square slabs considered in almost all the work to date, but should also be checked for rectangular columns and slabs. Ideally the analysis should be fully based on a physical model but even a rather empirical approach could represent considerable progress here.

c- To study the real deformations in the regions of slab-column connections transmitting moments. The results could be used directly in calculations of deflections and might be applied in non-linear analysis of equivalent frames.

CHAPTER TWO

EXPERIMENTAL STUDY

2-1 CHOICE OF SPECIMEN TYPE

2-1-1 INTRODUCTION

The range of types of specimen which can have been used for punching tests is quite large, and any reinforced model, in which a failure of the right type can be produced, is a legitimate subject of study. A complete theory would take account of the differences between different models and should be able to be checked, albeit only partially, by comparisons between its predictions and the experimental results from any model.

However the present state of knowledge is such that a complete theory is unlikely to be developed in the near future and actual theoretical approaches are likely to be incomplete and reliant on empirical data. In these circumstances it is necessary to consider the suitability of experimental models in terms of their ability to simulate conditions in prototypes -in the present case primarily flat slab or flat plate floors.

One extreme of modelling is to use specimens comprising several complete panels. Such models are highly realistic and avoid the problems associated with arbitrary boundary conditions, but they are expensive and must either occupy a very large area or

be to a very small scale. The number of tests possible and thence the number of variables that can be investigated is generally small.

At the other extreme there is the conventional punching specimen intend to model the negative moment region around a single symmetrically loaded column. Such models can allow relatively large numbers of tests to be made to a quite large scale but do involve very arbitrary boundary conditions.

In order to make some judgement on the relative merits of the various models between these extremes it seems useful to consider the main issues involved.

2-1-2 Possible Collapse Mechanisms

Punching is not an entirely separate mode of failure and the behaviour of many slabs reported in the literature suggests that punching can occur, after the development of the full yield-line flexural capacity, but apparently without the large defections generally associated with a truly flexural mode of failure. In these circumstances it seems important that any model should be able to develop the yield lines that would be associated with flexural failure and should be able to undergo large deflections due to rotations at the yield lines.

From this point of view, models in which load is applied to a column while reactions are provided by an undeflecting boundary frame are unsatisfactory. They force the yield line pattern to be that of Fig. (2-1 a) instead of the normal one of Fig.(2-1b) Additionally large defections are associated with a tensile

membrane action in the slab adjacent to the column while this is not the case for a simple folding mechanism.

Models in which loads are applied to the slab at discrete points by a deformable loading arrangement are able to replicate the behaviour of Fig. (2-1b) and it was therefore decided to adopt a system of this type.

The difference between systems with the eventual mechanisms of Figs. (2-1a) and (2-1b) should be small if the failure loads are distinctly below flexural capacities, but could be significant where the ultimate load is more or less equal to the flexural strength. The model of Fig. (2-1c) would then be likely to appear to fail by punching, while that of Fig. (2-1d) would probably have a purely flexural collapse.

2-1-3 Compressive Membrane Action

It has been argued that models with free boundaries relatively close to columns (column to edge distance 0.2 or 0.25 x prototype span) are unsatisfactory because they do not allow the development of realistic compressive membrane actions.

Compressive membrane action can have two effects in a slab subjected to a concentrated load or reaction. One is the development of a shallow 'dome-like' resistance. The effect can be considerable in a thick slab with rigid restraints against lateral expansion at its boundaries. The other which is more probable in slabs of normal floor proportions is a load increase in the depth of the compression zone around a column. Rankin and Long (70) claim that compressive membrane action can

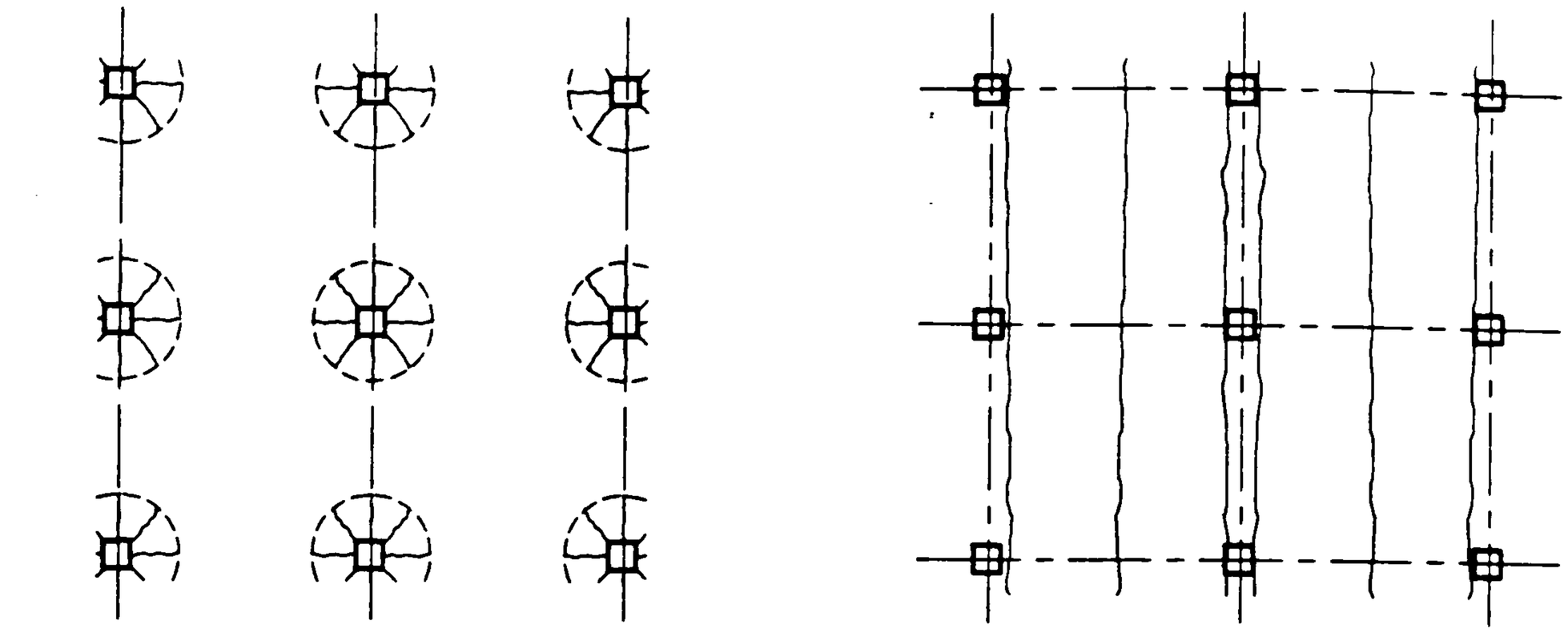

Fig.(2-1) Collapse mechanisms

produce a considerable enhancement of punching resistance in flat slabs. The claim is based on a comparison of the results of tests of the type illustrated by Fig 2-2. The data from the main group of tests is shown in the same figure as a graph of the ratio of the experimental ultimate load to the characteristic strength according to BS 8110 plotted against the ratio R of the slab size to the size of the periphery at which the loading has applied-the code's upper limit on f_{cu} was ignored in the calculation

so that : $V_{BS} = 0.79 \sqrt[3]{100\,\rho \cdot f_{cu}} \cdot \zeta \cdot ud$

with $\zeta = \sqrt[4]{400/d}$ for d in mm

It should be noted that the test model is not very appropriate as the provision of an increasing unloaded overhang reduces the moments in the slab for any given load. In the extreme with R=2 the yield line capacity of the slab is increased by 50%. inspite of test model thus tending to overestimate the effect of any membrane action, the increase of the ratio V_u/V_{BS} with R can be seen to be very modest.

In an earlier paper Long and Masterson (71) compared results from tests of models of the simple 'line of contraflexure' type and the type model shown in Fig. 2-3. In the majority of the tests the loading was eccentric and the results for the specimens with larger eccentricities are confused by the lack of ability of the test frame used for the smaller models to provide downward reactions. From the two slabs with concentric loading the larger specimen gave a slight increase of about 20%.

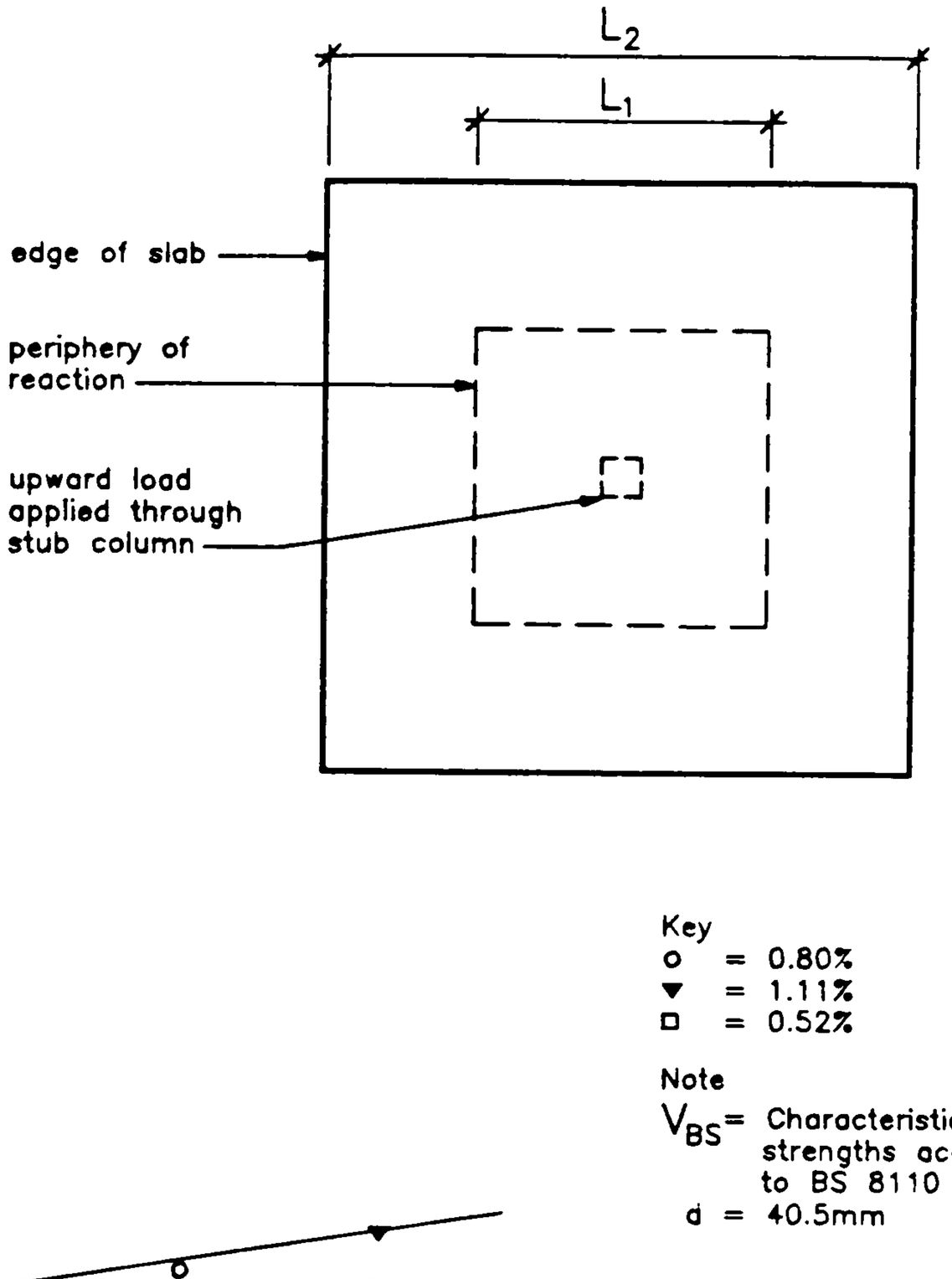

Fig.(2-2) Effect of compressive membrane action on punching strength according to tests by Rankin and Long.

Some further information on membrane effects can be inferred from the results of multi-panel test specimens reviewed by Regan and Braestrup (16). Their original comparison were based on a draft version of BS 8110 in which the depth factor ζ was $(500/d)^{0.25}$. The table below presents the results updated with $\zeta = (400/d)^{0.25}$.

Original source	Column size	Slab effective depth (mm)	Eccentricity (mm)	V_u V_{BS}
Guralnick & La Fraug	457x457	109.5	64	1.04
Tankut (slab 1)	203x203	76.0	71	0.97
Tankut (slab 2)	203x203	76.0	105	1.06
P C A	660x660	476.0	0	1.37

In the first three tests all the panels were loaded and there appears to have been no strength enhancement attributable to compressive membrane action. In the fourth test only a part of the slab was loaded and a large undamaged outer "ring" was available to provide in-plane restraint.

In conclusion here it seems that for slabs of proportions normal for flat plate floors compressive membrane action has little if any effect on punching resistance unless a large part of the slab is unloaded and able to provide a retraining ring around the test area. Thus in the design of test specimens the possibility of membrane effects was considered to be fairly unimportant.

2-1-4 Boundary Moments and Deformations

From the above discussion of membrane effects it would seem that the use of specimens modelling 0.4 to 0.5 l of a typical span could be satisfactory if only concentric load were to be considered. They would have some disadvantage due to the impossibility of redistributing moments from the negative to a positive moment region and this might mean that punching failures could not be obtained with low reinforcement ratios.

Once eccentric loading is considered there is more of a problem. If the moments transferred to the columns arise from wind effects the sections of contraflexure move away from the columns and toward midspan as the eccentricity increase. This movement cannot be replicated in the very simple specimens bounded by lines of radial contraflexture for vertical loading. To be realistic the specimen has to represent more of the slab and have positive moments applied at its boundaries to correspond to the effects of the symmetric vertical loading. The type of specimen developed by Long and shown in Fig.(2-3) is one solution. For concentric loading the edges of the specimen, which correspond to mid-panel lines are restrained so that there is no rotation perpendicular to the edge. Another possibility is to apply predetermined bounding moments, and this approach was adopted in the present work.The modelling of a prototype is less good than in Long's method but in compensation the test arrangements are simplified and the magnitudes of the boundary moments are known.

For moment loading Long's system correctly obliges the edges

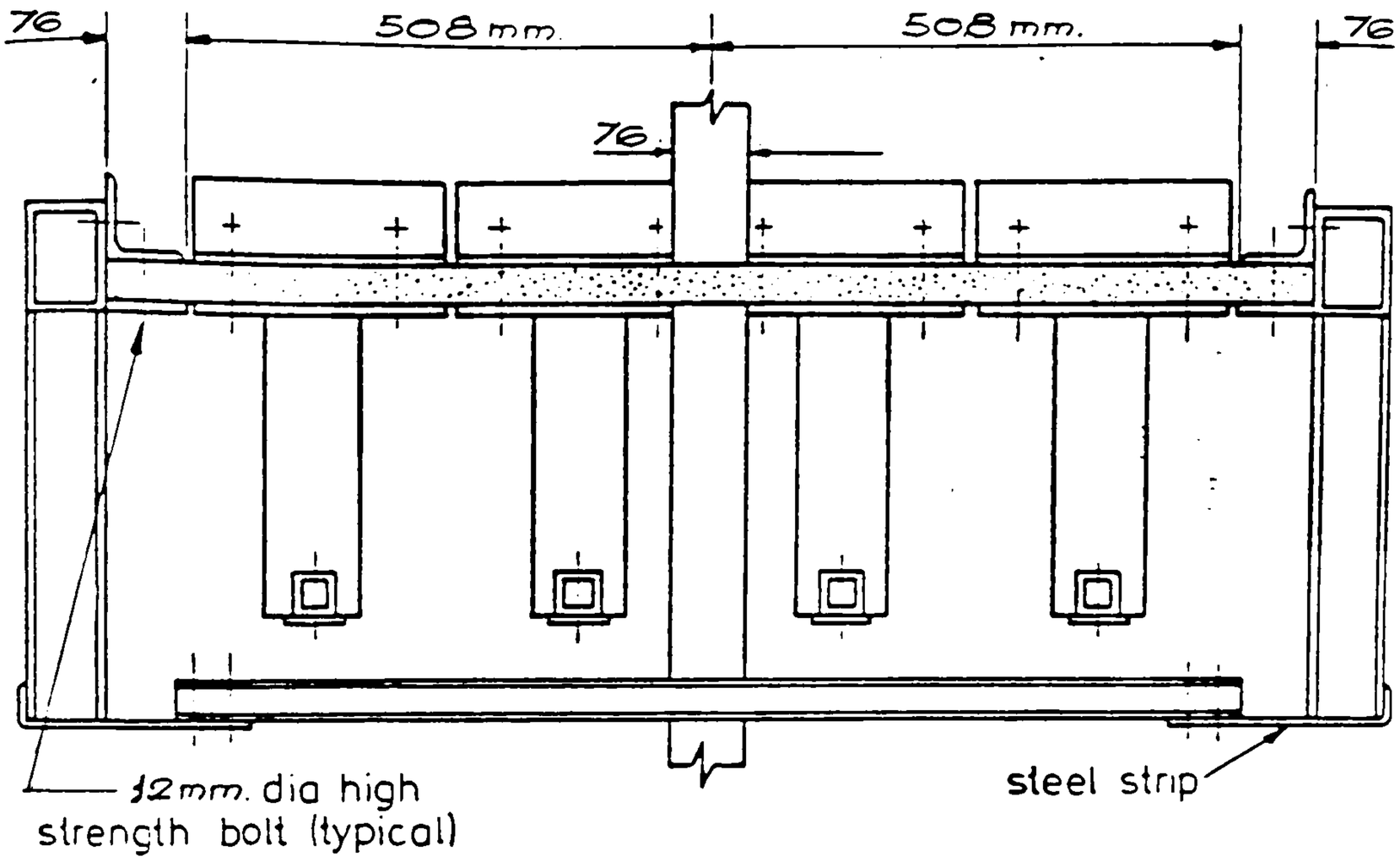

(a) Details of edge restraining system (series L)

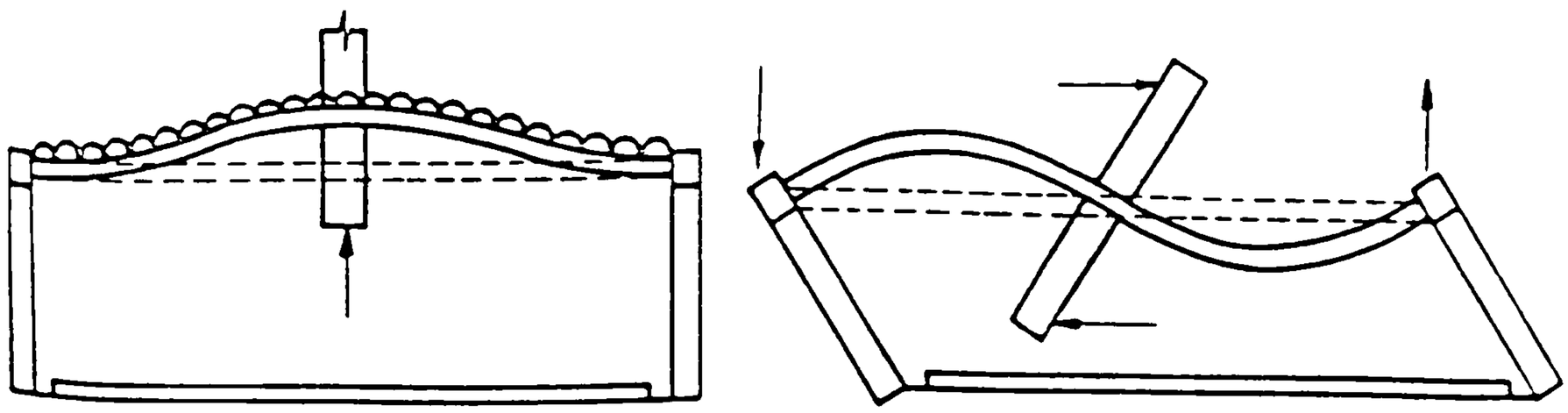

Shear Loading. Transfer of moment loading

(b) Idealized function of edge restraints.

Fig.(2-3) System of Edge Restraints

perpendicular to the eccentricity to undergo equal rotations, but the restraint system for the other two edges would seem to prevent their developing realistic deflected profiles.
The system adopted for the present tests left these edges free to the form while being subjected to moments corresponding to the concentric loading.

2-1-5 Ratios of Moments and Shears

The moments considered here are the total (or average) moments at the column lines and at panel centre lines is a prototype or at the edges of a model.
Considering square panels of side length 'l' subjected to uniformly distributed loading 'Q' per panel, the elastic moment distribution for the prototype gives:

Column line moment M'= 0.083 Ql

Centre line moment M = 0.042 Ql

M'/M = 2.0

In the test arrangement adopted (see Figs.(2-4) and (2-5))

M = 0.063 Ql

M'= 0.101 Ql

M'/M = 1.60

The arrangement thus simulated a modest redistributions of moments away from the column lines (a redistribution less than implied in BS 8110's empirical design method). The total moment (M+M') was 31% higher than that for of the prototype. This is a result of applying the loading close to the boundary rather than distributing it over the slab. In terms of reproducing the

a)

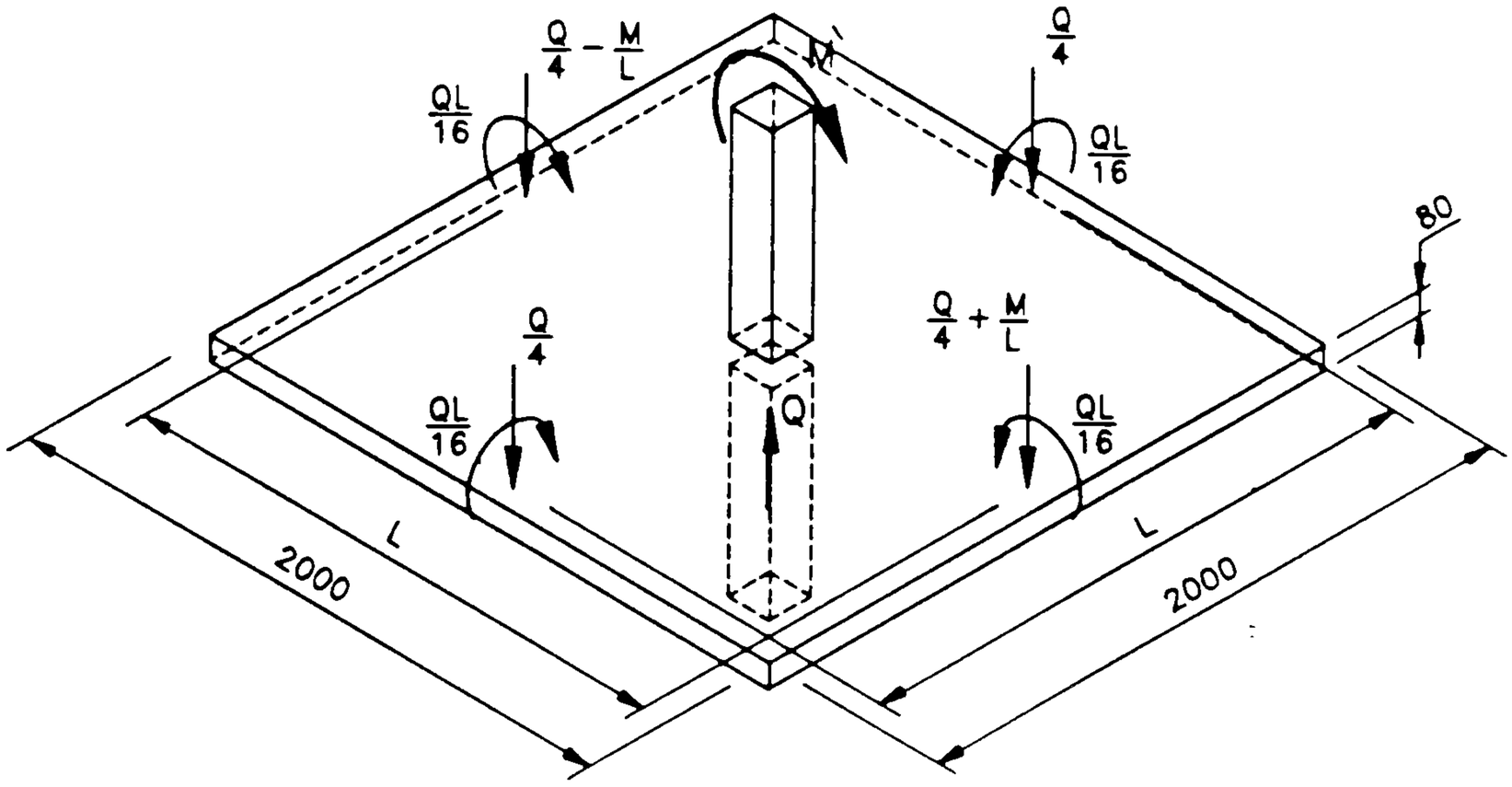

b)

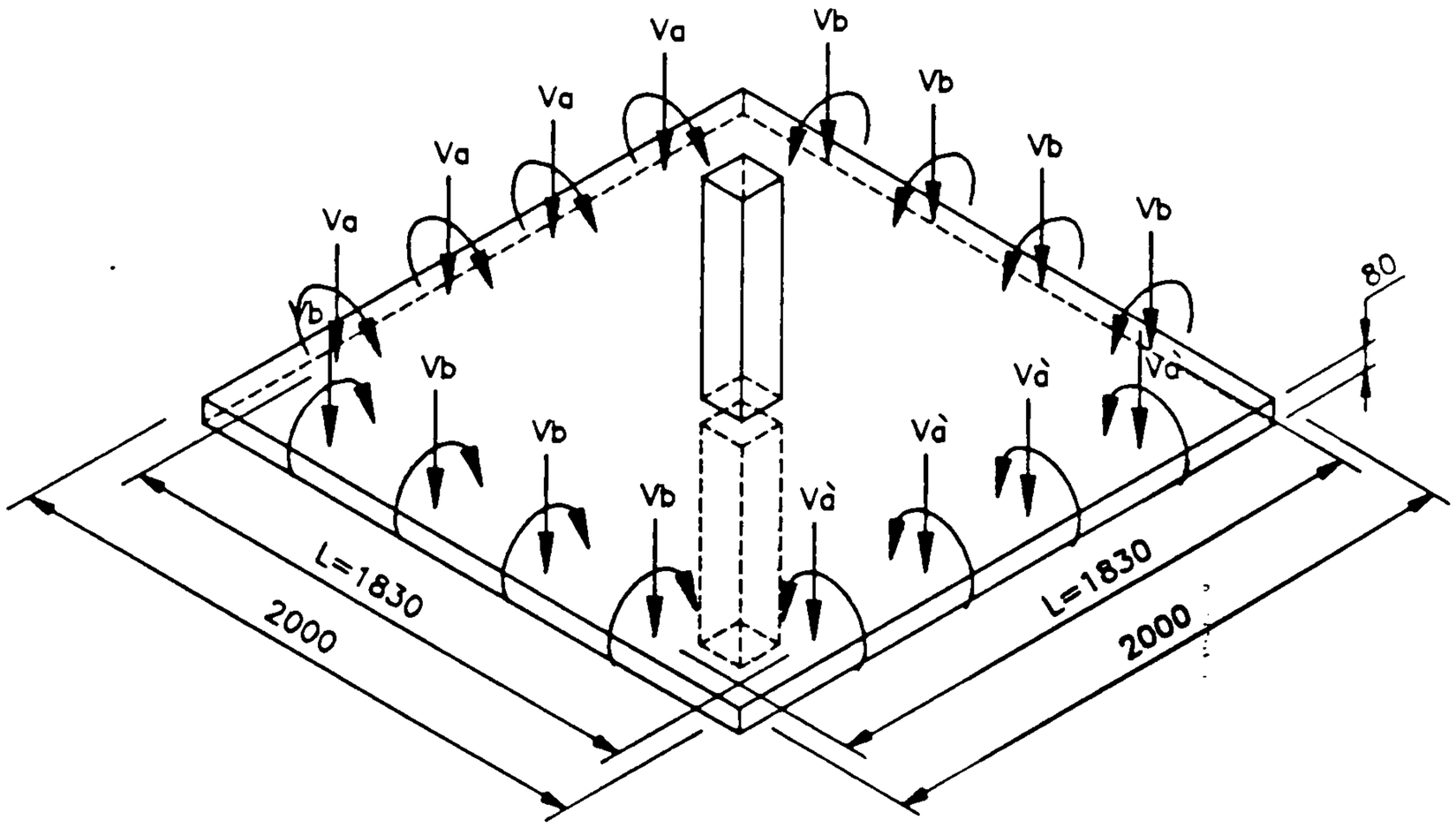

Fig.(2-4) Slab-Column specimens (square slabs)

a)

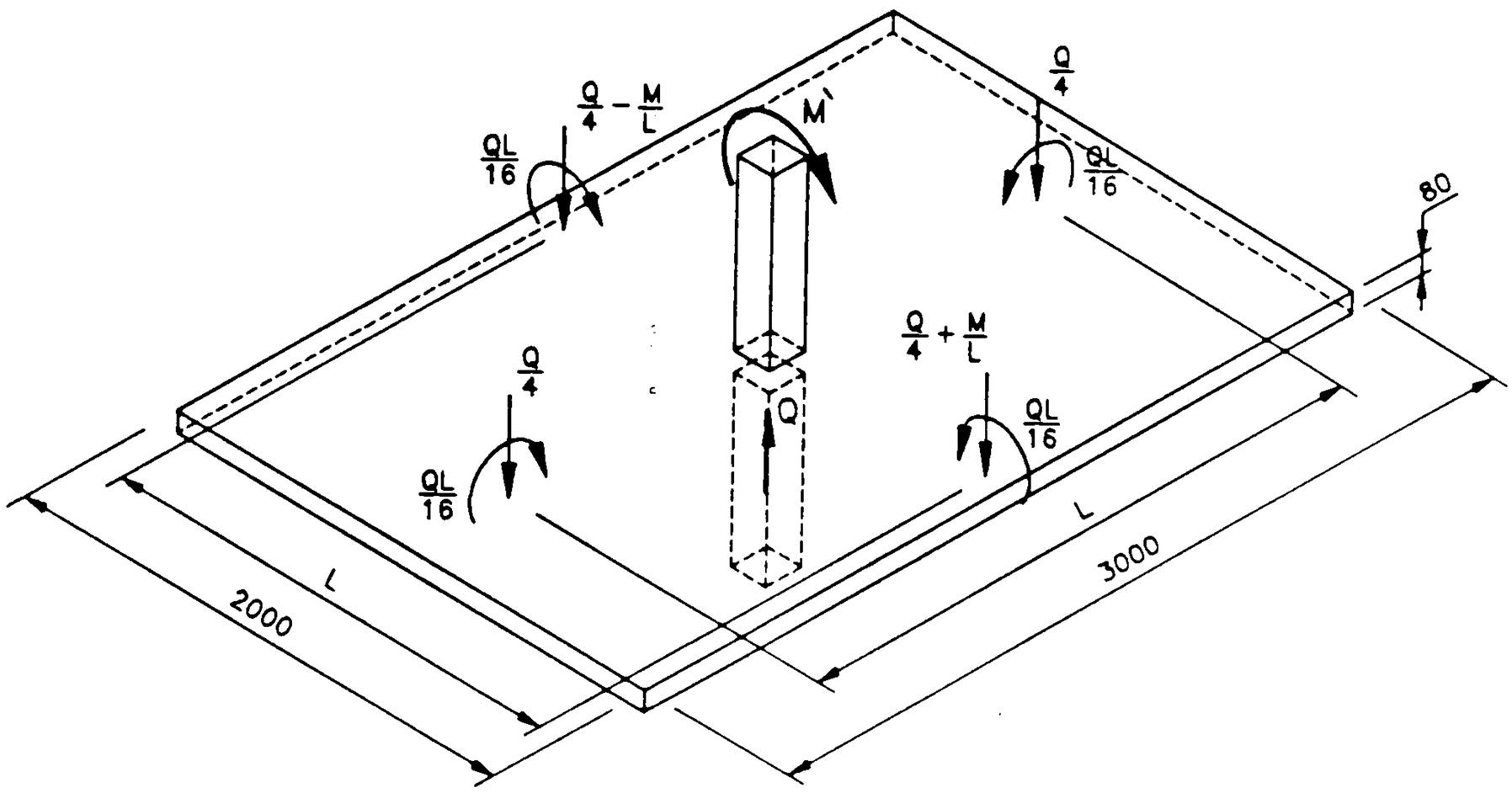

b)

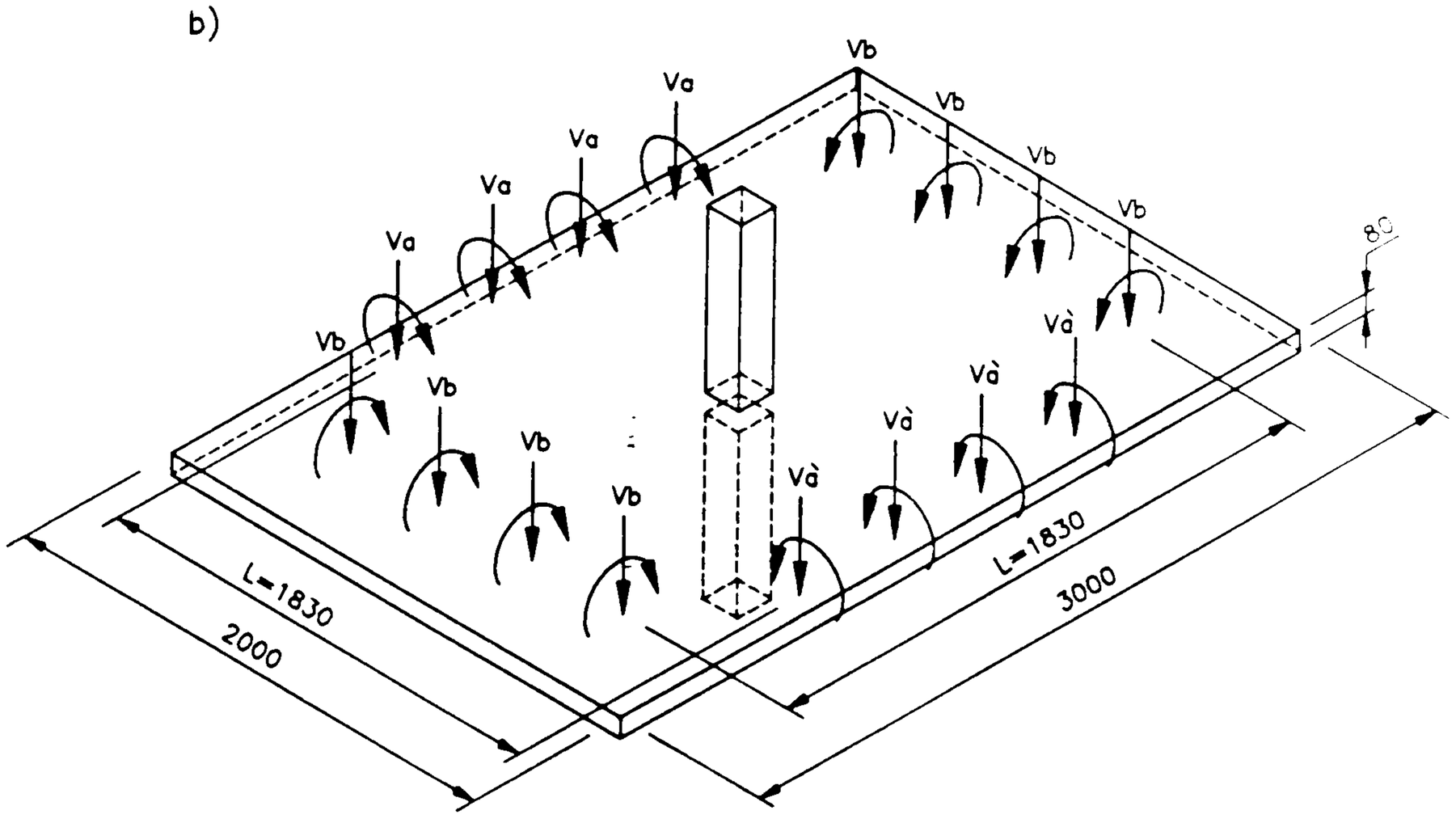

Fig.(2-5) Slab-Column specimens (rectangular slabs)

behaviour of a prototype it is clearly something of a disadvantage, but the boundary loading system was adopted to allow the same points to be used for both the vertical and the moment transfer loading and also to leave the top surface of the slab free for observation.

For combined (shear + moment) tests the vertical loading was viewed as comprising two parts. One corresponded to the shear and required equal loads at each boundary. The other corresponded to the moment and involved an increase of the load at one edge and a numerically equal decrease at the opposite boundary.

In terms of the positions of lines of contraflexure this system is a correct representation of a situation of equal loading acting on equal spans together with horizontal loading.

Where the slab panels were rectangular the vertical loading was none-the-less applied at a square perimeter. This was done to model elastic behaviour for which the active width of slab in the short span direction is effectively limited to the dimension of the span and not the slab breadth.

2-1-6 Rationale of the Test Arrangements Used

The test arrangements adopted for the present work are illustrated by Fig.(2-4) and (2-5). Further details are described in section (2-3).

In terms if scale with an overall slab depth of 80mm the specimen were large enough to allow the use of concrete, rather than mortar or micro-concrete, and that of normal reinforcement. The scale factor of about 2.0 between the models

and typical prototypes was seen as being sufficiently small for numerically meaningful results to be obtained.

The spreader system by which vertical loads were applied was deformable and could have allowed flexual failures to occur by the formation of full-width yield lines parallel to the slab edges.

It has already been noted that compressive membrane action is unlikely to be of much significance in realistic flat slabs and the extent to which such action might be developed was not a major concern. The model adopted should in principle be intermediate between the simple form in which the slab is bounded by lines of contraflexure and the Long and Masterson model extending to panel centre lines.

All the boundaries of the slabs were free to deform and in this respect as well as that of scale the arrangements seem preferable to those of Long and Masterson.

The application of somewhat arbitrary boundary moments may be seen as a disadvantage in comparison with the system of Fig. (2-3) in which the rotations perpendicular to the edges are correctly controlled. In terms of pure modelling this is true, but the system used appeared to have two advantages. Firstly it was simpler and secondly it allowed the magnitudes of the boundary moments to be known.

The treatment of combined loading cases as the superposition of a concentric system and a moment applied by forces at two edges represents what is probably the commonest situation in prototypes. Unavoidably it does not correctly model other

cases, eg. unequal spans or equal spans with unequal vertical loads.

2-2 OUTLINE OF TESTS.

The ten slabs reported here are divided in four groups each concerned with one or two parameters thought to influence the punching resistance.

GROUP -SA-

Four slabs were included in this group, they were all 2000 mm square and 80 mm thick. The ratio of tension reinforcement in the punching area was 0.8% in both directions and the slabs were supported on 150 mm square columns at their centres as shown in Fig. (2-4). The main variable in this group was the ratio of horizontal to vertical loads (i.e.the eccentricity of the load), the ratio was varied by applying vertical loads of different magnitudes to the edges of each slab see Fig.(2-4a).

GROUP -SB-

Two slabs were included in this group, they were both 2000 mm square and 80 mm thick and each was supported on a 150 mm square column. The ratio of tension reinforcement in the punching area was 1.45% in both directions. The first slab was tested under eccentric loading conditions while the second was loaded concentrically.

GROUP -SC-

Two slabs were included in this group they were 3000x2000x80mm and were supported on 150 mm square columns see Fig.(2-5). The ratio of tension reinforcement in the punching area was 1.35% parallel to the eccentricity and 1.62% in the perpendicular

direction. The first slab was tested under concentric load and the second was tested under eccentric loading conditions.

GROUP -SD-

Group -SD- consisted of two 3000x2000x80 mm slabs, each supported centrally on a 200x100 mm rectangular column.
The ratio of the tension reinforcement in the punching area was 1.35% parallel to the eccentricity and 1.62% in the perpendicular direction. The first slab was tested under concentric load and the second was tested under eccentric loading.

The average ratios of tension reinforcement in the slabs were:

SA- 25 T6 in 2 m with d=64 mm ρ =0.55%

SB- 25 T8 in 2 m with d=62 mm ρ =1.00%

SC&SD Transversal 12 T8+12 T6 in 3 m with d=62 ρ =0.5%

Main 23 T8 in 2 m with d=62 mm ρ =0.93%

More details of the test specimens are given in table 2-1 and Fig. (2-8).

2-3 TEST ARRANGEMENT

Each slab was supported on one single central column which rested on a rocker/roller bearing with rotation and horizontal movement allowed only in the direction of eccentricity see Fig.(2-6). Two small rockers were fixed on the column faces on opposite sides and at opposite ends at distances 500 mm above and below the slab surfaces Fig. (2-6). The rockers bore against horizontal load cells attached to the

TABLE 2-1 details of the test specimens

Slab No	Slab Dimension mm			Column Dimensions		Reinforcement				e mm
	Breadth	Length / with eccent.	Thickness h	Breadth b	Depth a// with eccent.	Top Tension		Bottom Compression		
						main	tran.	main	tran.	
SA1	2000	2000	80	150	150	0.55	0.55	0.55	0.55	52
SA2	2000	2000	80	150	150	0.55	0.55	0.55	0.55	0
SA3	2000	2000	80	150	150	0.55	0.55	0.55	0.55	100
SA4	2000	2000	80	150	150	0.55	0.55	0.55	0.55	336
SB1	2000	2000	80	150	150	1.00	1.00	1.00	1.00	0
SB2	2000	2000	80	150	150	1.00	1.00	1.00	1.00	360
SC1	3000	2000	80	150	150	0.93	0.50	0.50	0.93	0
SC2	3000	3000	80	150	150	0.93	0.50	0.50	0.93	337
SD1	3000	2000	80	100	200	0.93	0.50	0.50	0.93	0
SD2	3000	2000	80	100	200	0.93	0.50	0.50	0.93	310

Note. Eccentricities were in the 2.0 m width direction in all cases.

All dimensions are in mm

Reinforcement ratios given are averages for the full breadth/length of the slab.

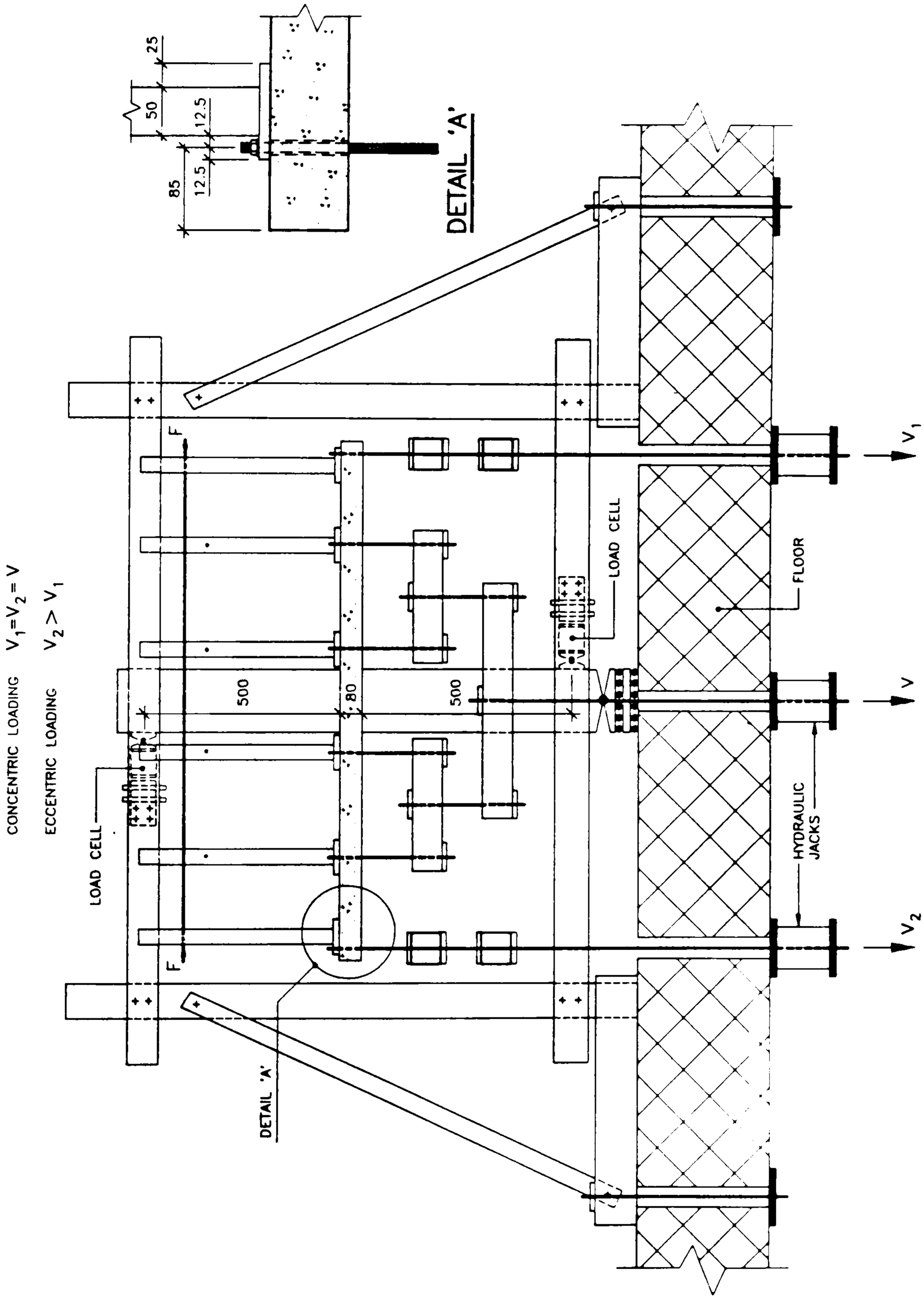

Fig.(2-6) Test set-up

framework shown in Fig. (2-6) and provided the restoring moment to counter the eccentricity of the loading. The vertical force was applied in stages using 100 kN hydraulic jacks and spreader beams to divide the loads equally between the four loading points in each line. The loads were measured using 100 kN load cells. The horizontal forces on the column were achieved by a variation in the vertical forces at parallel lines Fig.(2-6). The "edge" moments were applied as shown in Fig. (2-6) using bars passed through hollow square steel sections fixed on the slab edges. The force in each bar was measured using two strain gauges fixed on the bar. The loads and moments were applied to the 2m x 3m slabs in the 3m direction at distances of 915mm from the column centre on each side Fig. (2-5).

The deflections of each slab were measured along the centre lines by the means of dial gauges situated at distances of 300, 600, 900 mm from the column centre for the square slabs and at distances of 300, 600, 900, 1300 mm from the column centre for the long spans in the rectangular slabs. The dial gauges were fixed on a steel frame which was supported on the laboratory floor. To measure the rotations, spirit level inclinometers were used. They were situated adjacent to the column faces. In the eccentrically loaded slabs the column rotation was measured by the means of a spirit level inclinometer supported on wooden box which was fixed on the

column face at about 50mm from the slab surface.

2-4 MATERIALS

The materials used were similar for all specimens. Three batches of concrete were used for each specimen. The mix proportions by weight were:

-Rapid hardening portland cement.....1

-Sand (5 mm down)..... 2

-10 mm maximum size gravel aggregate.....3

-Water/cement ratio.....0.5

In order to assess the concrete strength, three 150 mm cubes and one 150 by 300 mm cylinder were made with each specimen, compacted by poker vibrators and cured with the slab. Each slab specimen was cast in one stage. After casting the specimens were covered with polythene sheets for approximately two days, after which the formwork was removed. The specimens were then left under wet hessian in the laboratory until testing at ages of 7 to 10 days.

All the reinforcement was high yield deformed steel, the diameters of the bars were 6 and 8 mm and stress-strain curves are shown in Fig. (2-7). The bottom bars were supported on 10 mm plastic cover chairs and the space between the top and bottom bars was controlled by plastic spacers, the reinforcement details for all the specimens are shown in Fig. (2-8).

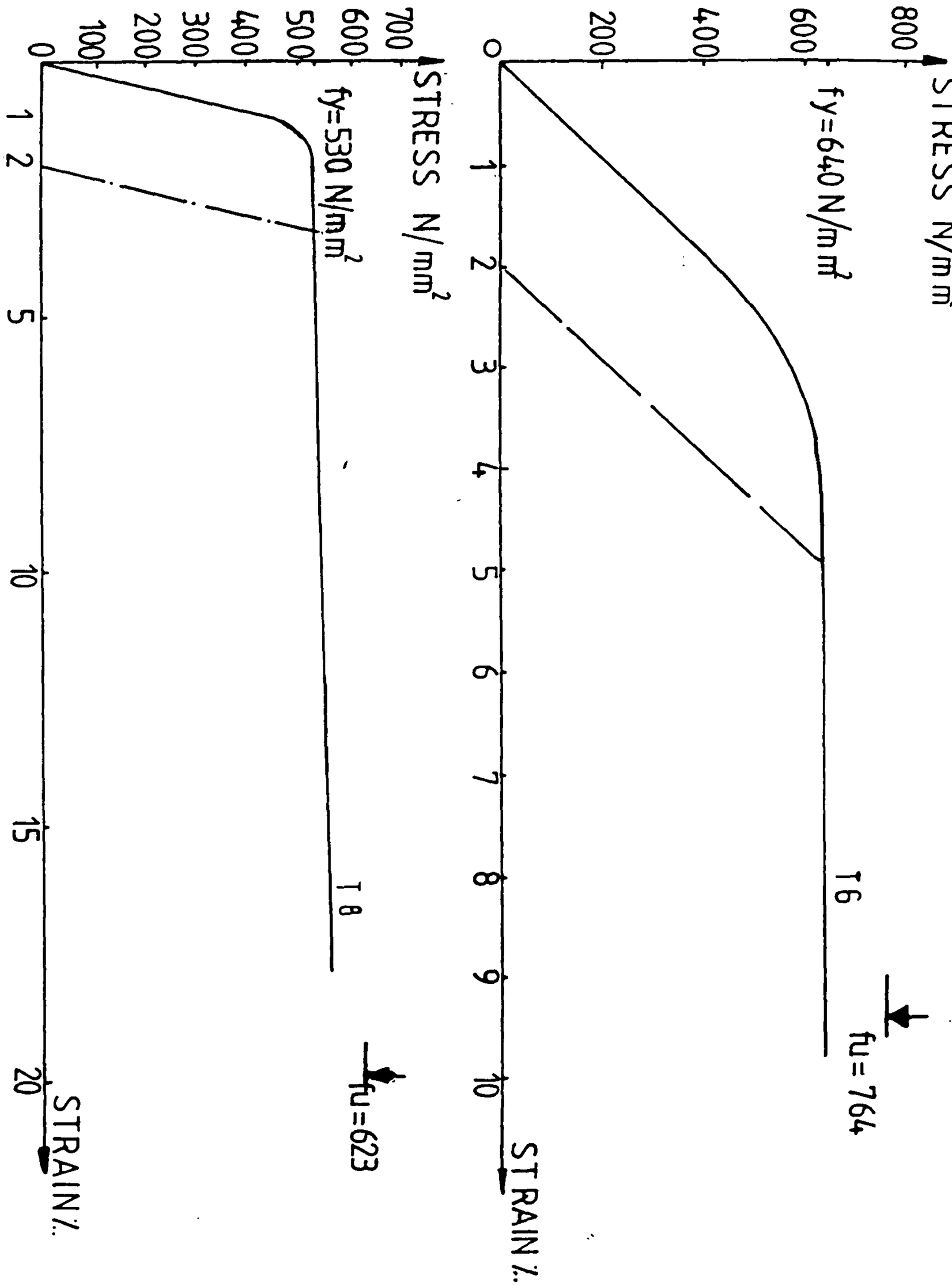

Fig.(2-7) Steel stress-strain curves

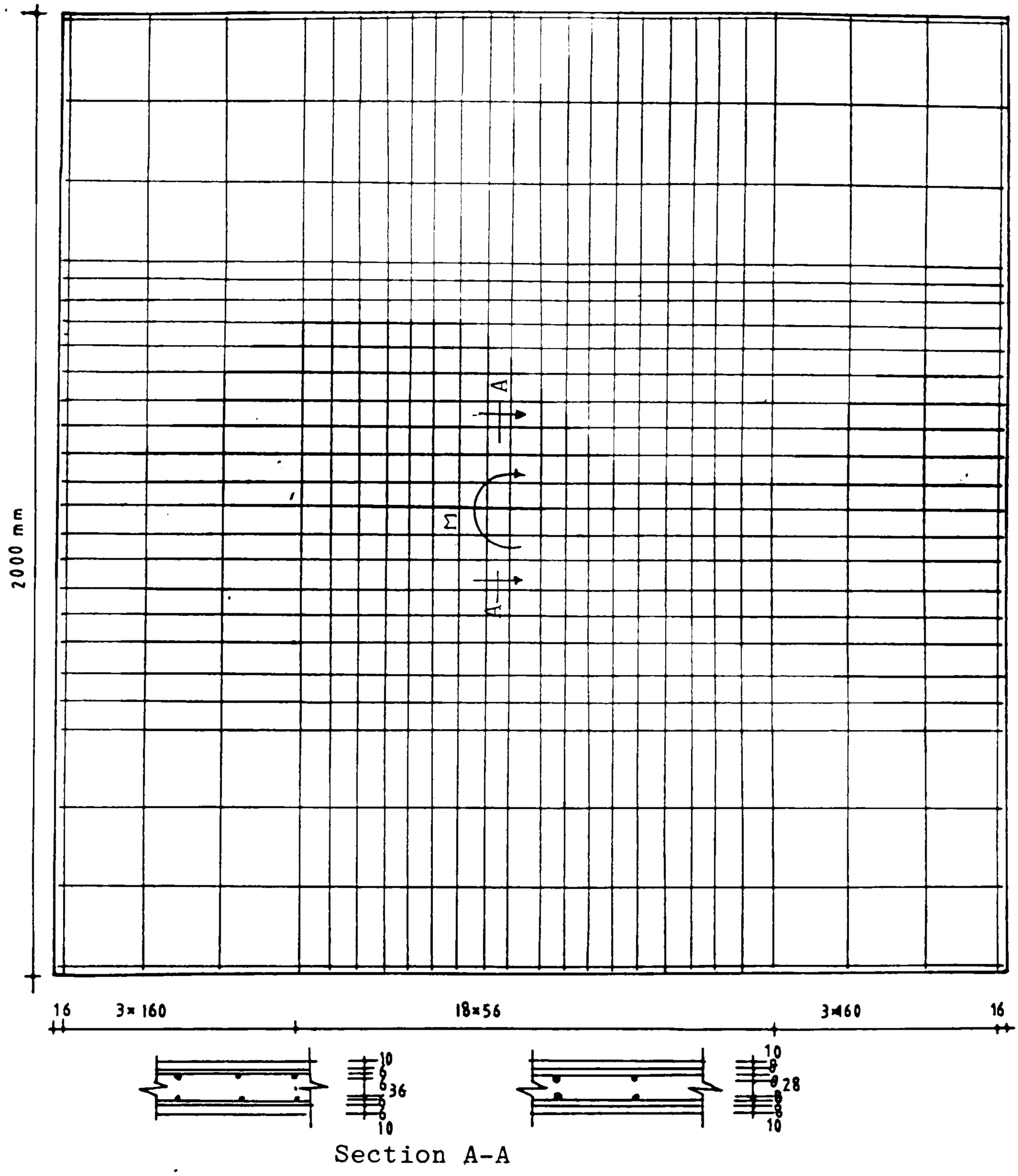

Section A-A

Fig.(2-8a) Reinforcement details

Top and bottom reinforcement for slabs

SA1,SA2,SA3,SA4 (All the bars were 6 mm)

SB1,SB2 (All the bars were 8 mm)

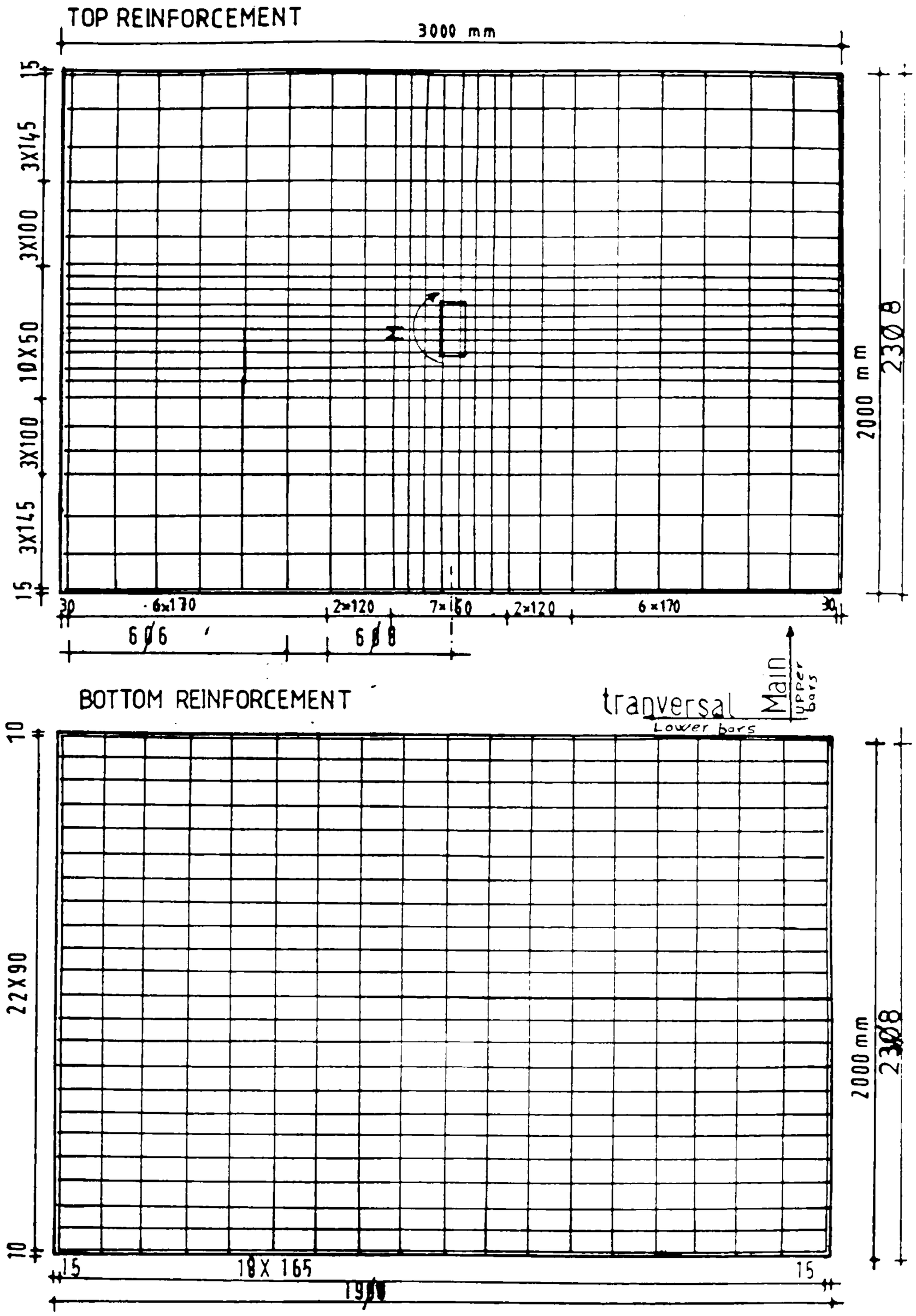

Fig.(2-8b) Reinforcement details for slabs SC1,SC2,SD1,SD2

CHAPTER THREE

GENERAL BEHAVIOUR OF THE SLABS

Four slabs were tested under concentric load, and six slabs were tested under eccentric load. All ten slabs failed in shear. The average concrete strengths and slab failure loads are shown in Table (3-1)

Table 3-1 Concrete strengths and slab failure loads

Slab No	SA1	SA2	SA3	SA4	SB1	SB2	SC1	SC2	SD1	SD2
f_c N/mm^2	33	34	36	32	27	28	36	37	36	31
P kN	109	141	85	49	133	61	129	65	127	56

f_c = cylinder crushing strength of concrete taken as $0.8f_{cu}$

3-1 Load deflection characteristics.

3-1-1 Slabs tested under concentric load.

Four slabs (SA2, SB1, SC1, SD1) were tested under concentric load. The deflections of

each slab were measured along the centre lines. The average deflections of each slab along the centre lines at about 95% of the ultimate load are shown in Fig.(3-1). At the first stage of loading no cracks were observed on the slab surface. As the load increased cracks appeared on the tension face and upon further increase of load the cracks opened up reducing the slab stiffness Fig.(3-2). The deflections were symmetric in the four quarters of the square slabs. Finally the slab failed when the central cone pushed through the slab. Fig.(3-1) shows that the load deflection curve of the slab part which is situated outside the shear crack is an almost linear function of radius.

It is hard to say which of the slab properties has the most effect on deflections near failure but it appears from Fig(3-1) slabs SA2 (0.79%) and SB1 (1.45%) that an increase in the ratio of reinforcement reduces the ultimate deflection.

3-2-1 Slabs tested under eccentric load.

Slabs (SA1, SA3, SA4, SB2, SC2, SD2) were tested under eccentric load. The deflection of each test slab was measured along the entre lines of the slab on the top surface by means of dial gauges, which were located symmetrically with respect to the centre of the slab. The deflected shapes of the slabs in the eccentricity direction at about 90% of the ultimate load are shown in Fig.(3-3). As the load increased the tensile cracks on the surface of the slab opened up resulting in large

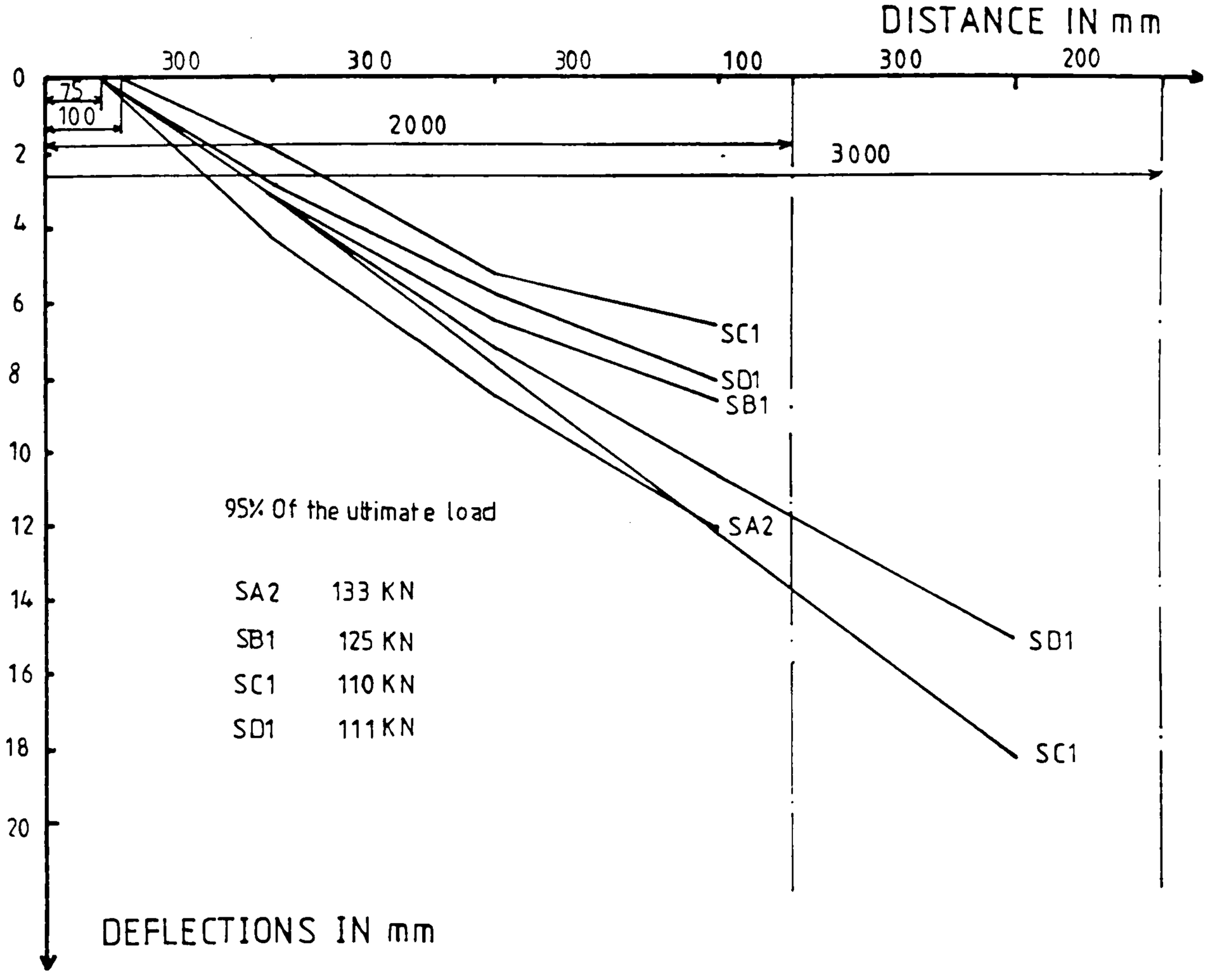

Fig.(3-1) The deflected shapes of the slabs tested under concentric load

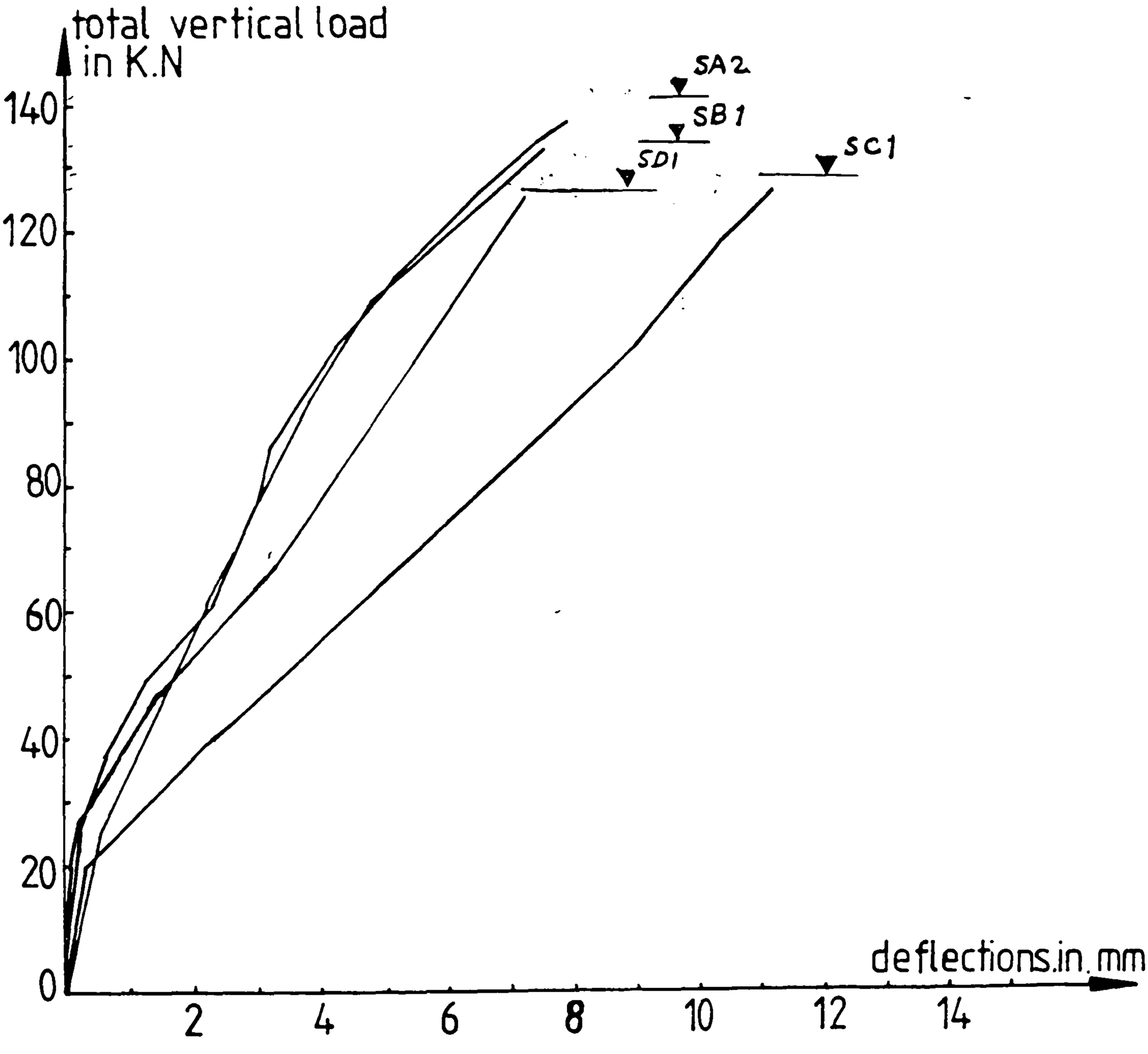

Fig.(3-2) Load deflection curves at 600 mm from the column centre, on the centre-linesof the slabs

deflections Fig. (3-4). The part of the slab bounded by the shear crack and the edge of the slab behaved as a rigid body. The maximum deflection was located on the side of the eccentricity, the deflection of the other side was relatively small or even changed to negative i.e. upwards, for slabs (SA3, SB2, SC2, SD2) Fig. (3-3). Finally the slab failed when the tensile part bounded by the shear crack and the column face pushed through. the slab. (i.e. unsymmetric punching) see Figures (3-5),(3-7).

In slabs SB2 and SD2 the load on the eccentric quarter was similar to that on the same quarter in the concentrically loaded slabs SB1, SD1, but the deflection in a slab quarter tested under eccentric loading was greater than that in a slab tested under concentric loading see Figures (3-1),(3-3).

3-2 Crack patterns.

In slabs subjected to concentric loading the first cracks appeared around the column face at approximately 25% of the failure load. The cracking loads for eccentrically loaded slabs were approximately 35 to 40% of the failure loads. In the slabs of group -SA- where the ratio of reinforcement was 0.79%, and was less than in the other groups, the first cracks appeared at approximately 30% of the failure load. Radial cracks started in the central part and extended to the edge of the slab with increasing loads Fig.(3-5) and (3-6).Further cracks then appeared in the vicinity of the column and along the column

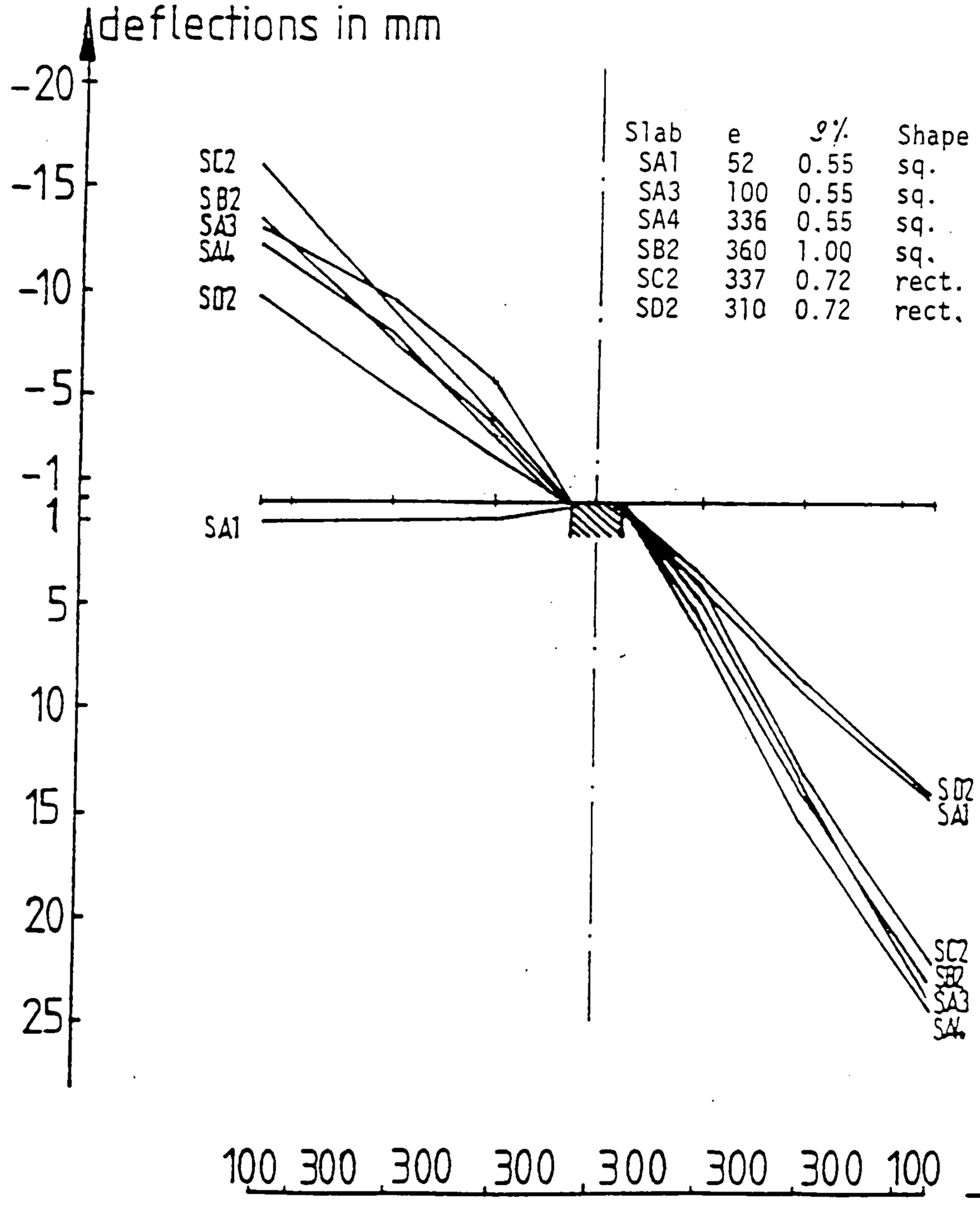

Slab	e	ρ%	Shape	Load KN
SA1	52	0.55	sq.	105
SA3	100	0.55	sq.	77
SA4	336	0.55	sq.	49
SB2	360	1.00	sq.	61
SC2	337	0.72	rect.	57
SD2	310	0.72	rect.	49

Fig.(3-3) The deflected shapes of the slabs tested under eccentric load relative to the horizontal

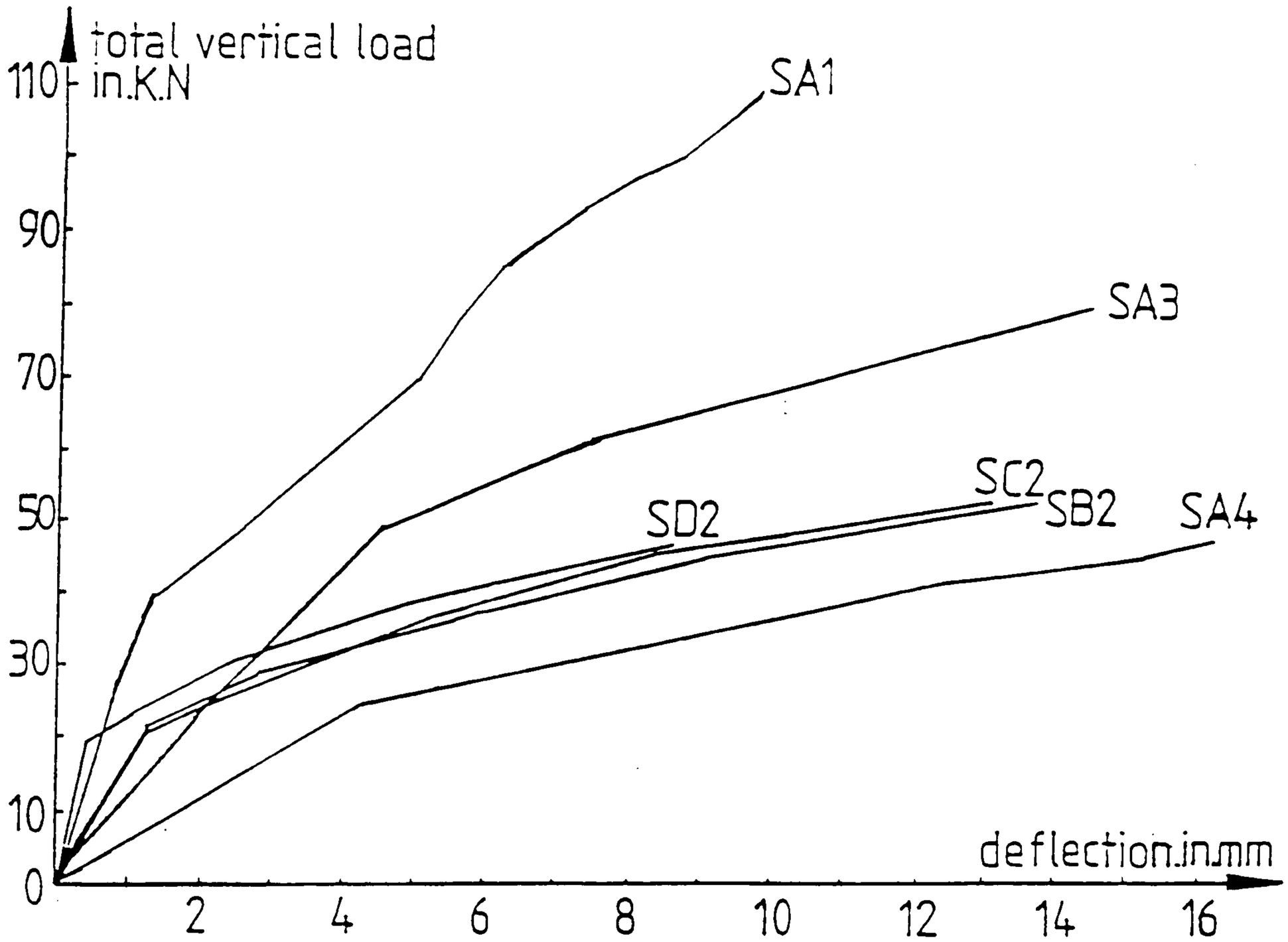

Fig.(3-4) Load deflection curves at 600 m m from the column centre in the quadrants with the highest loads

lines while existing cracks became wider. Some tangential cracks also appeared at various distances from the column face in the punching area Fig. (3-6) C,D. The crack patterns for the slabs tested under concentric load were symmetric Fig.(3-6). In slabs tested under larger eccentricities of the load no cracks formed at the side opposite to the eccentricity and the cracking radiated from the column face nearest the eccentric load. Finally failure occurred in the shape of a wide inclined crack running to the column face at the bottom of the slab as in Fig.(3-7). The exact positions of the initial shear cracks and the loads at which they appeared within the depth of the slab were not determined. As a rule it is not possible to observe the shear cracking in a slab and to find a completely unique value of the load at which the shear cracks begin to open up.

3-3 Strains in the test slabs

In the present work,the strain in the tensile reinforcement was measured in slab SB1 at some points of interest. Curves representing the relation between the observed values of the strains in the flexural reinforcement of the slab and the load P are shown in Fig. (3-8). The strains in gauges 2,3,5,6 were negative (i.e. compression in the top reinforcement from the edge moment action) at the first stage of loading. As the load increased the strain became positive (i.e. tension in the top reinforcement). However the maximum strains were small (about 0.0001) and this is consistent .with the lack of tangential cracking away from the column and the part of the

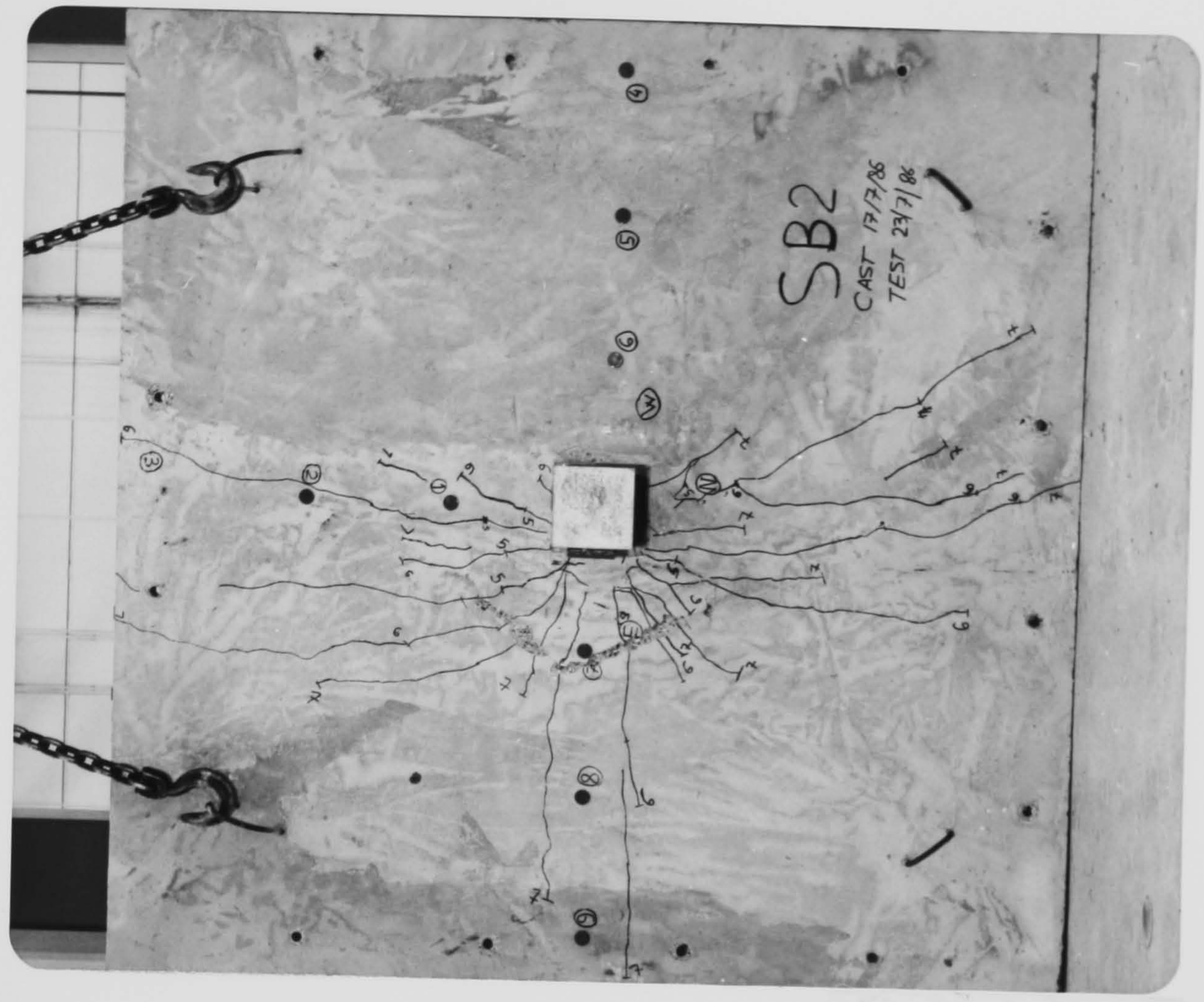

B e=360 mm

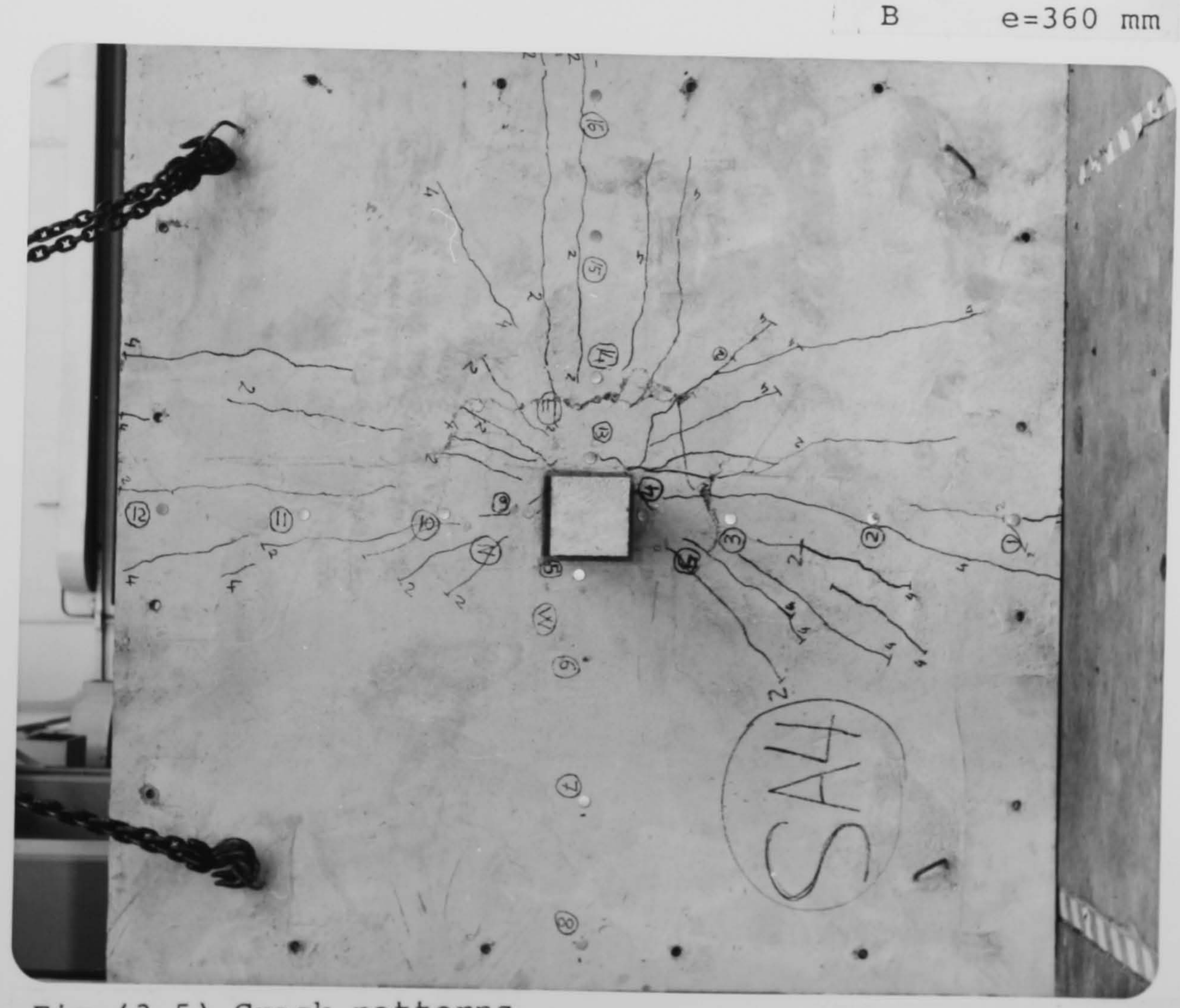

Fig.(3-5) Crack patterns

A e=336 mm

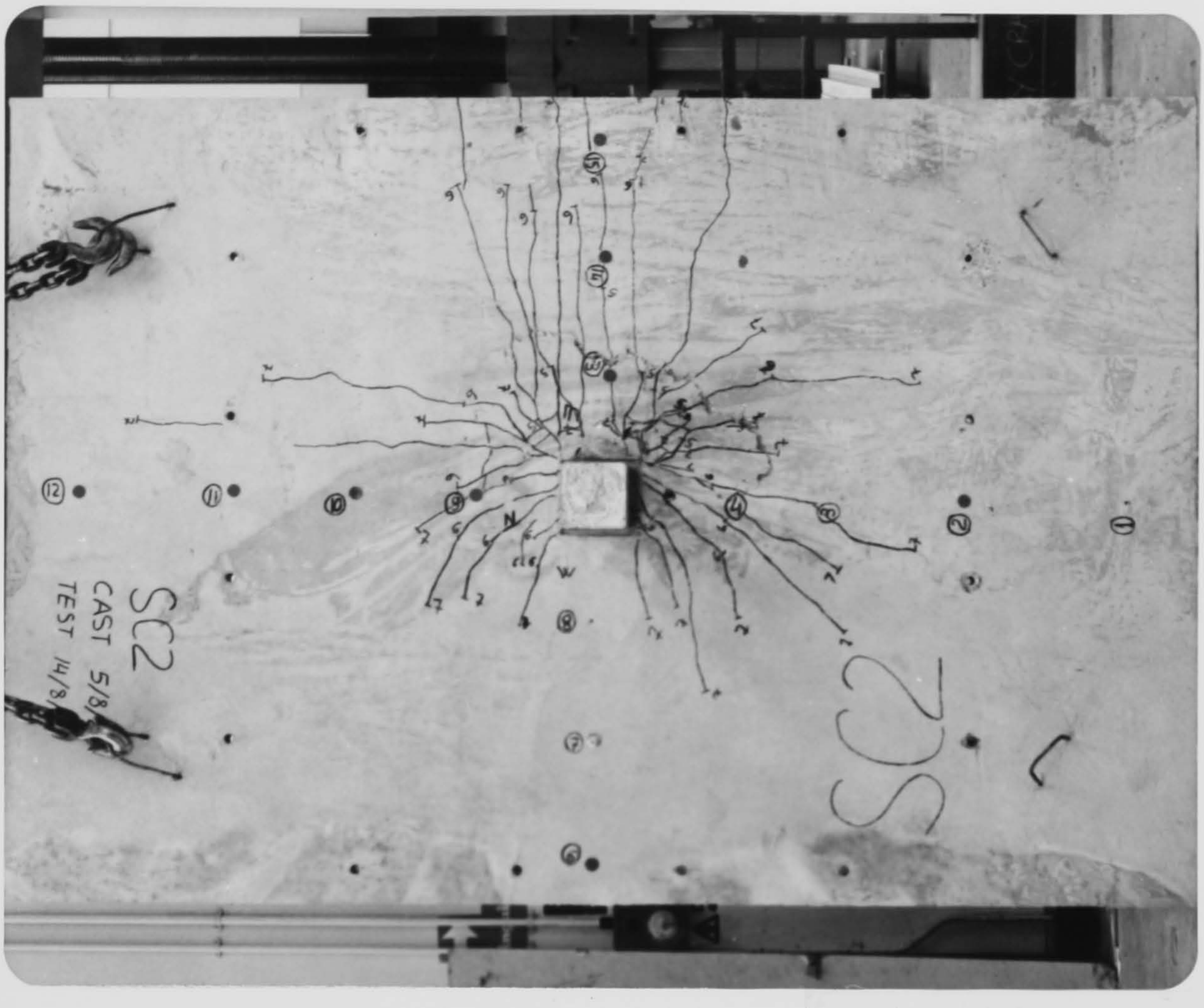

C e=337 mm

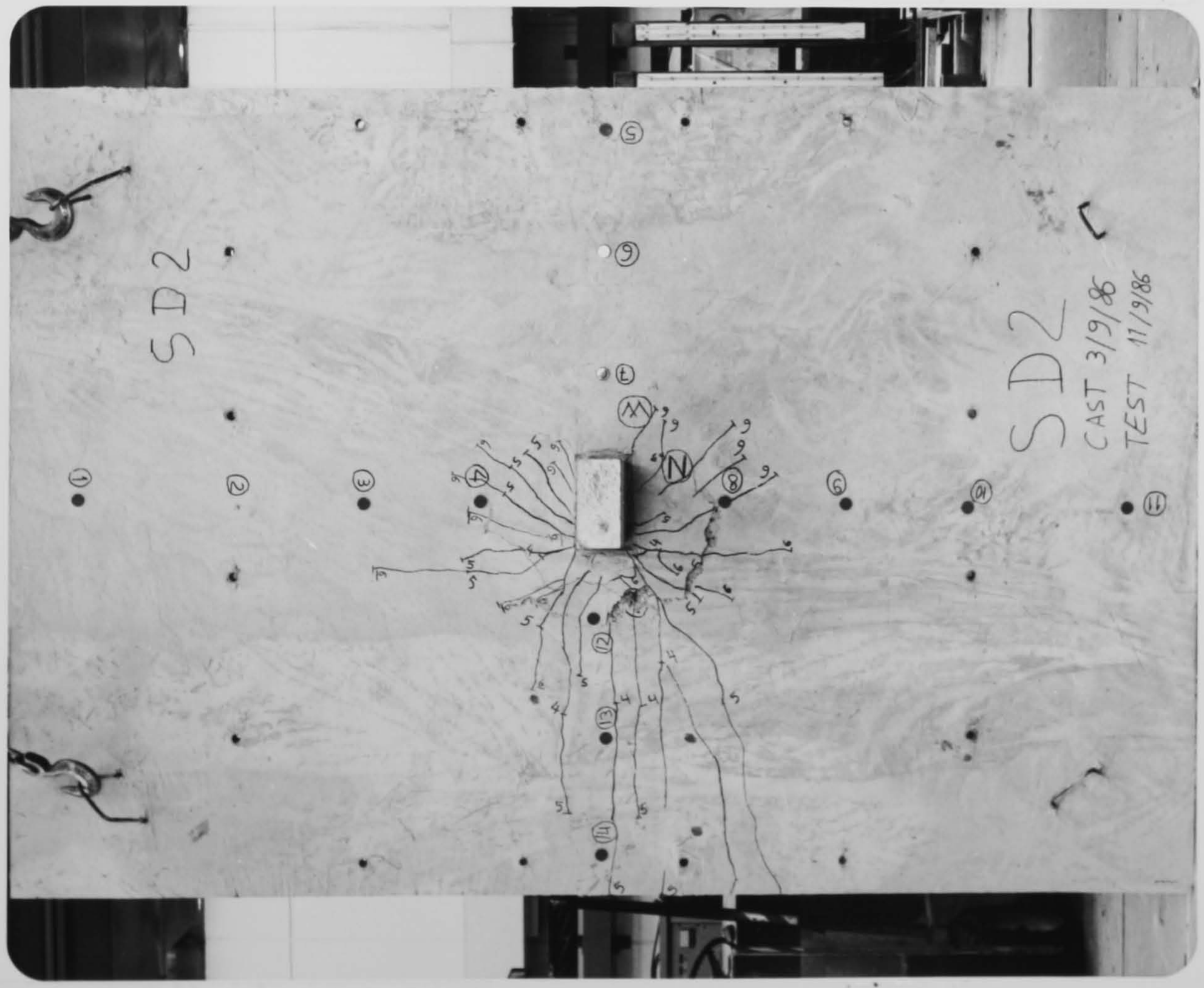

Fig.(3-5) Crack patterns

D e=310 mm

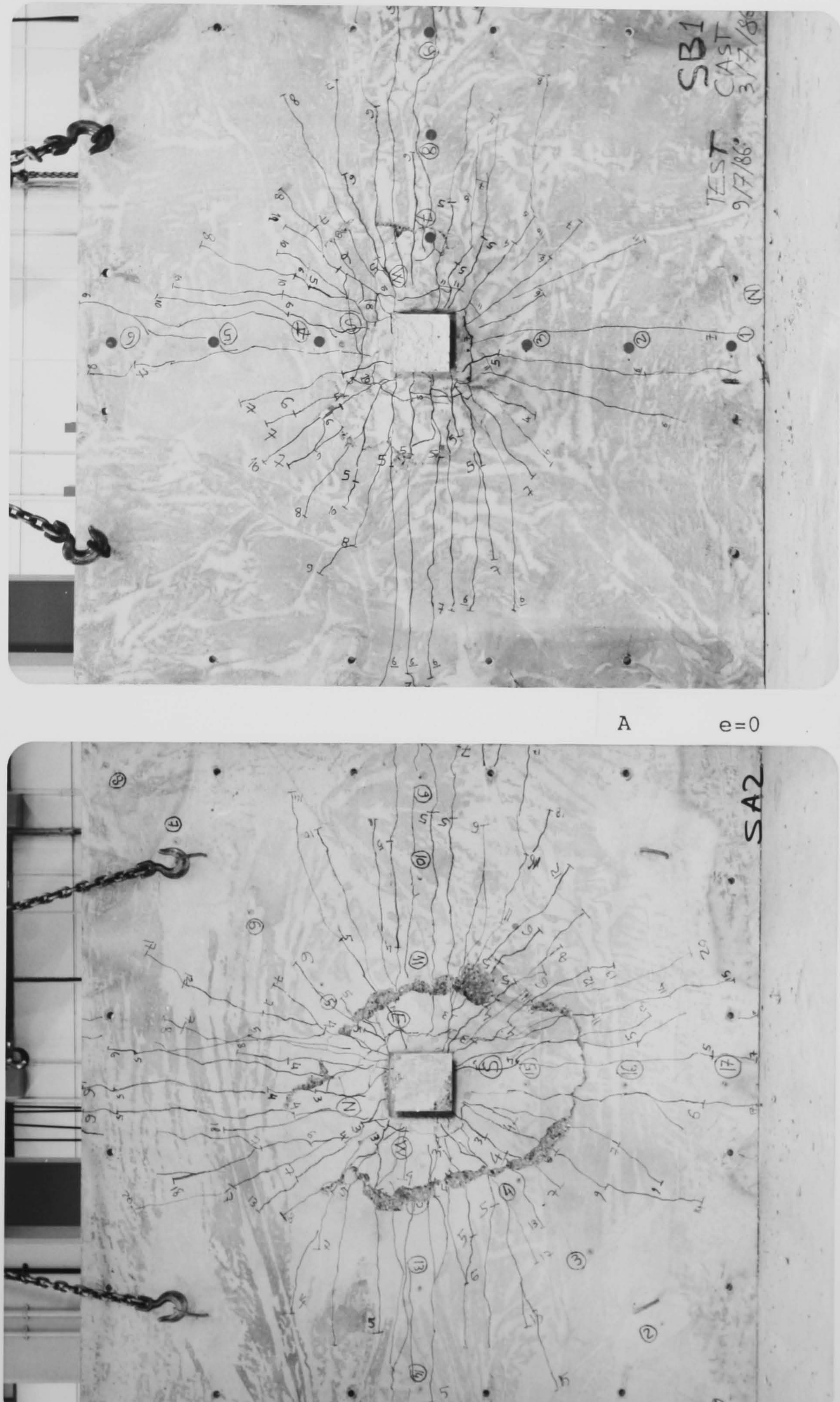

Fig.(3-6) Crack patterns

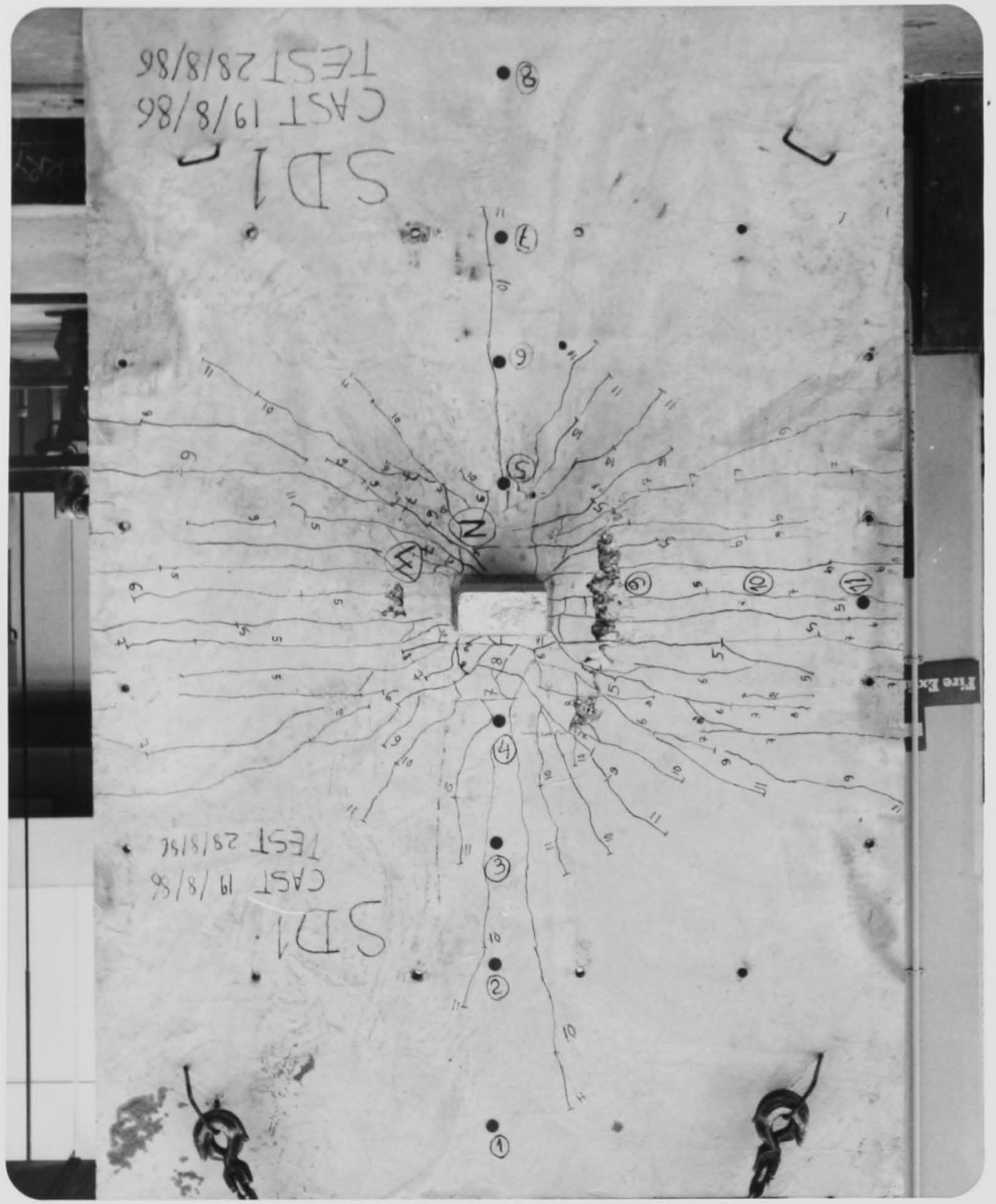

C e=0

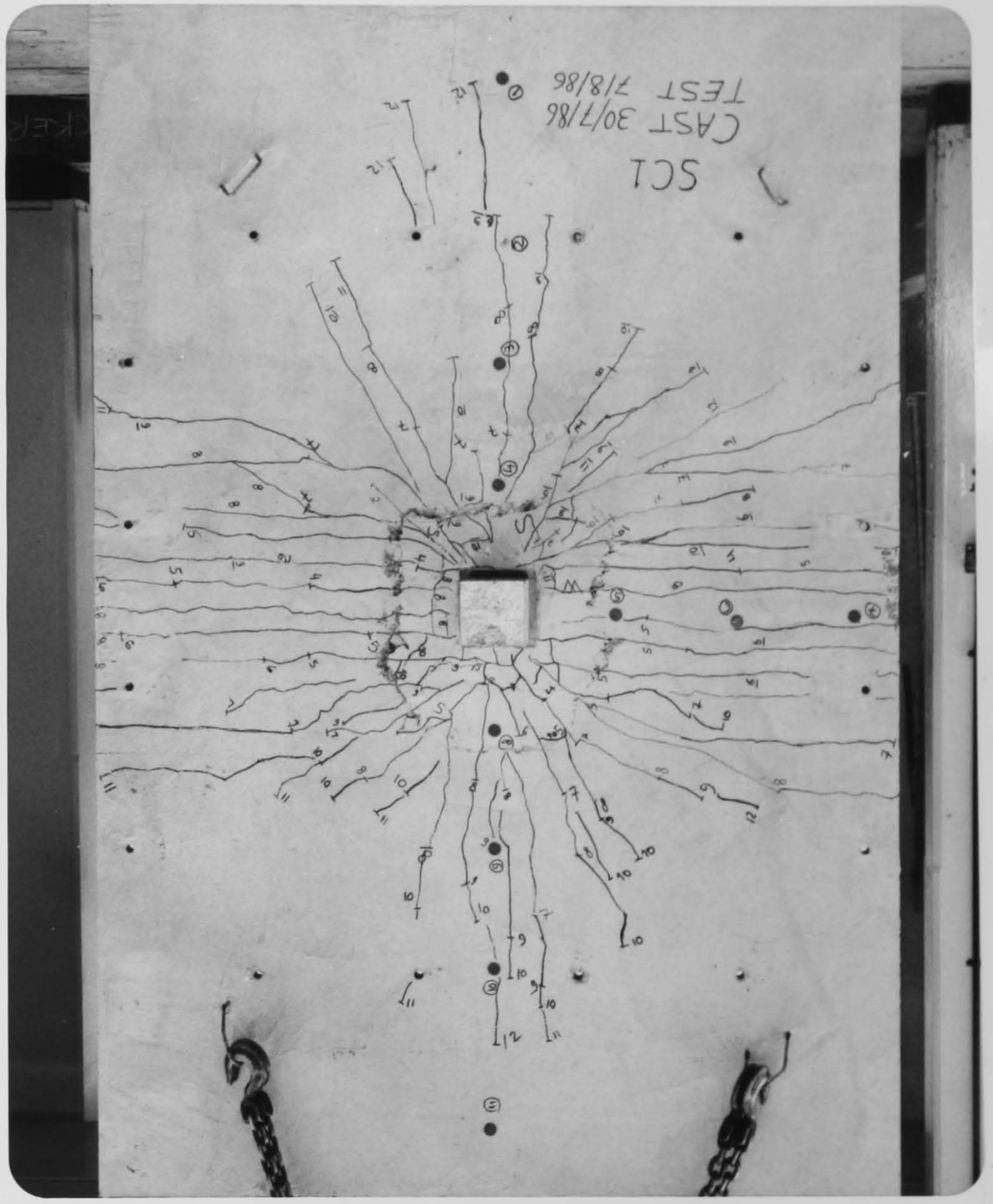

D e=0

Fig.(3-6) Crack patterns

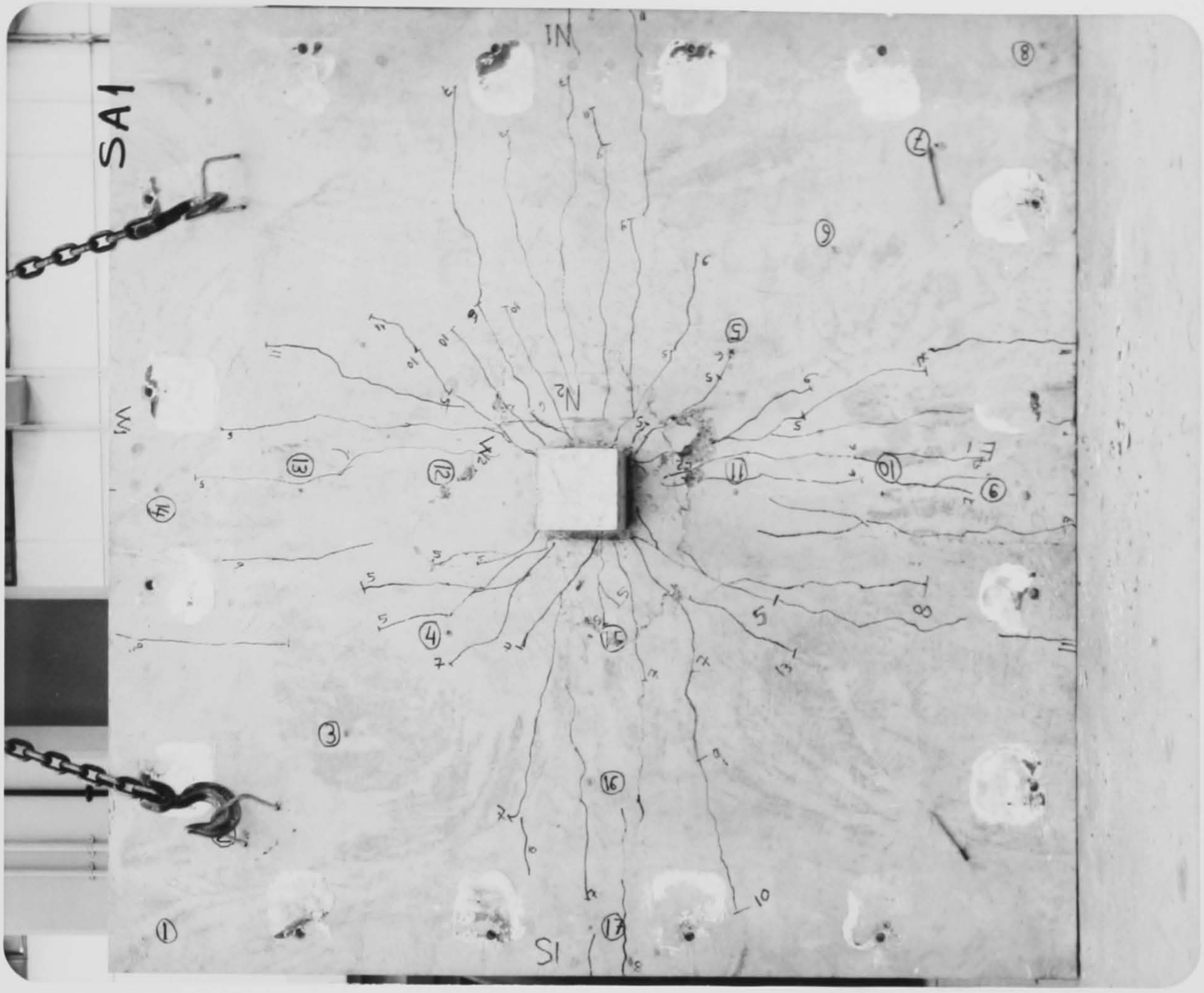

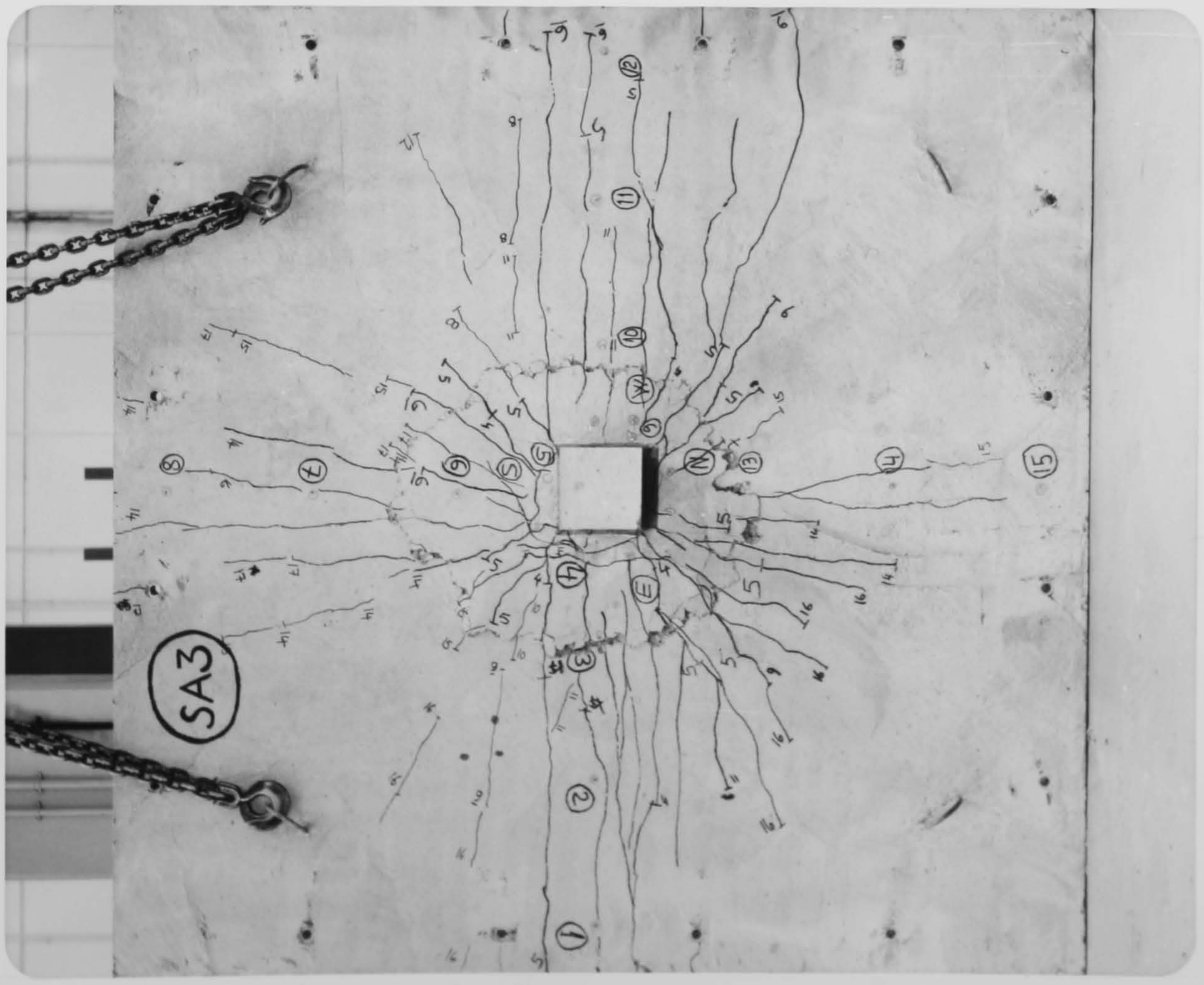

Fig.(3-6) Crack patterns

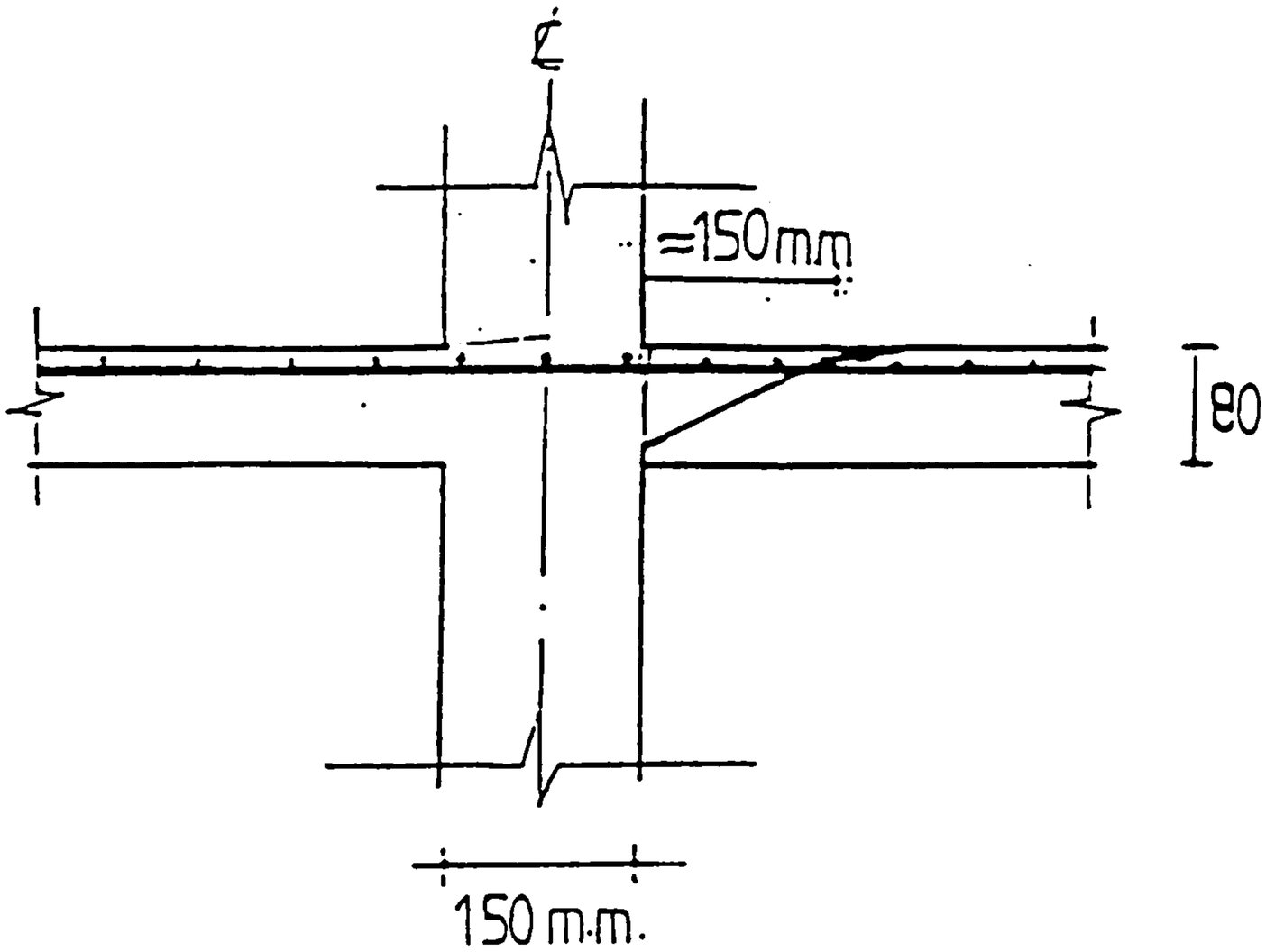

Fig.(3-7) Failure surface of slab-column junction

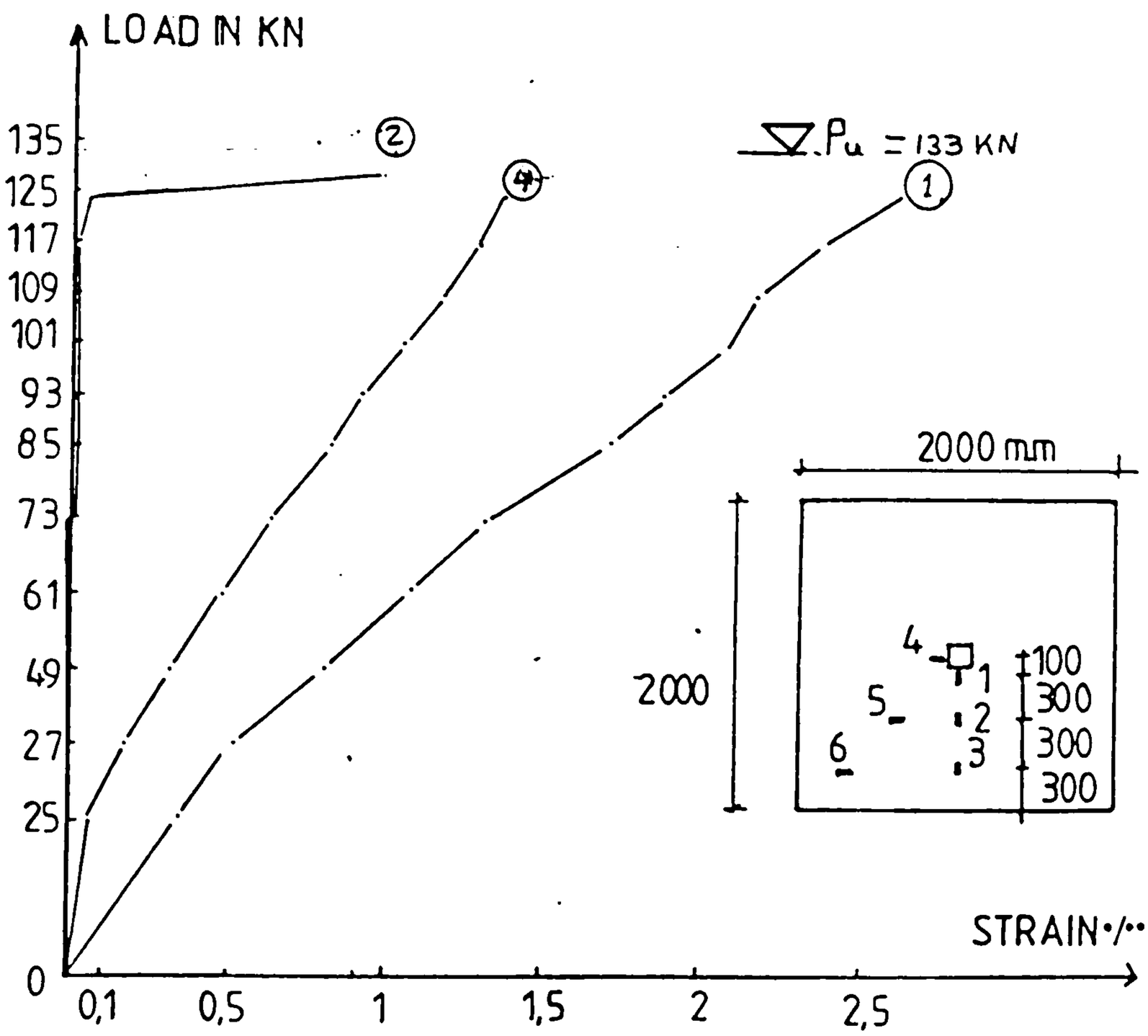

Fig.(3-8) Radial strain in the steel slab SB1

slab outside the shear crack behaving as a rigid body. The strain in gauge 1 near the column face reached the yield strain of the reinforcement.

3-4 Rotations in the test slabs

The rotations of the slabs were measured by means of spirit level inclinometers situated adjacent to the column faces. Figures (3-9) and (3-10) show the rotations of the slab at the column for the four tests of concentrically loaded specimens.It seems surprising that for slabs SA2 and SB1 which had different ratios of reinforcement, the ratio of reinforcement had relatively little effect on slab rotation see Fig. (3-9).

The curves of Fig. (3-10) are rotations of rectangular slabs with two column shapes. Slab SC1 had a square column while slab SD1 had a rectangular column, it seems that the column shape has a small effect on the slab rotation see Fig. (3-10).

Figs.(3-11),(3-12),(3-13) and (3-14) show the rotations of the slabs which were eccentrically loaded. The rotation on the side of the eccentricity was greater than on the other sides. The rotation on the side opposite to the eccentricity was relatively small or negative see Figs. (3-13) and (3-14).

The rotations on the sides perpendicular to eccentricity were nearly symmetric see Fig. (3-12), and greater than the rotations of the concentrically loaded slabs at the same

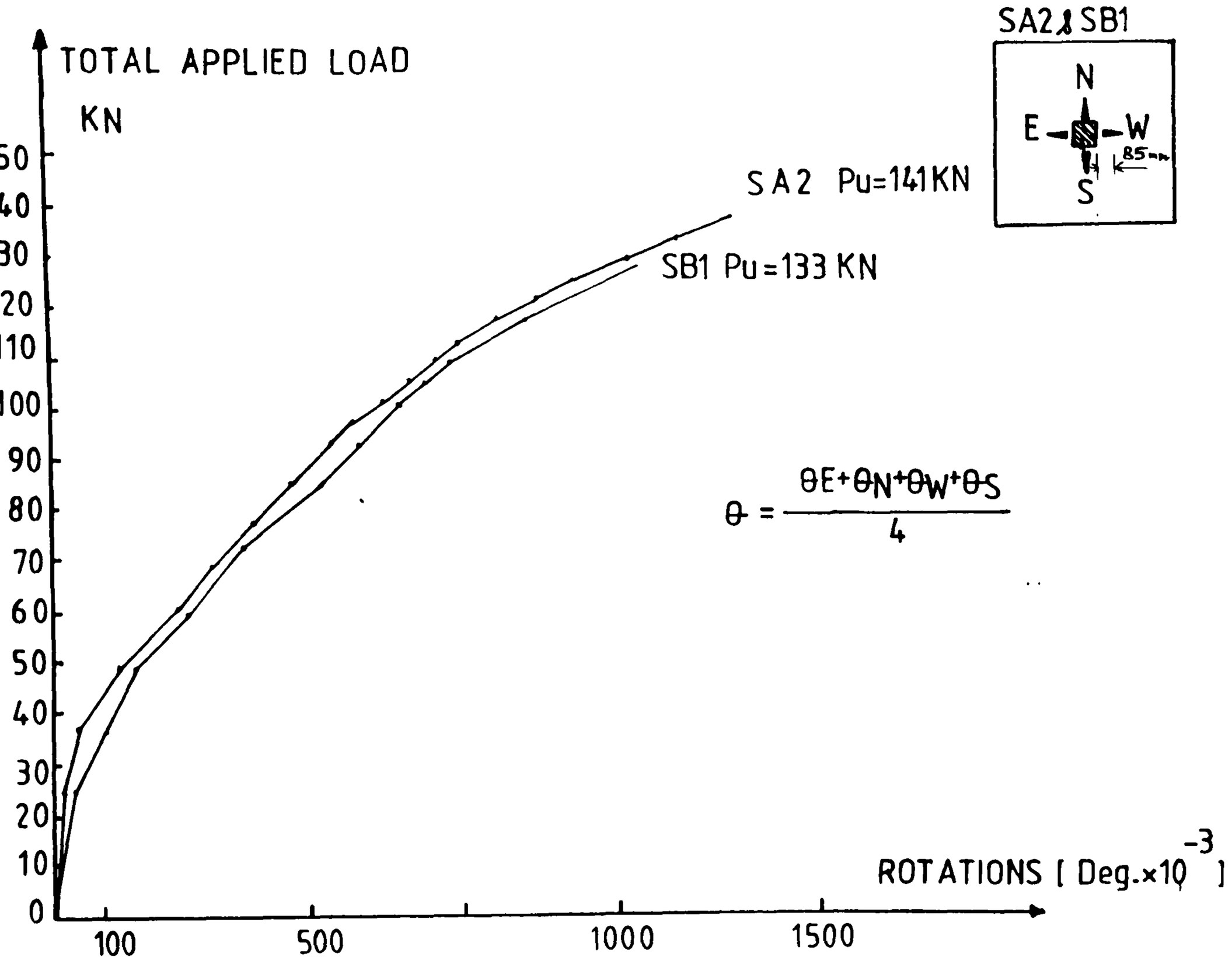

Fig.(3- 9) Slab rotations, Slabs with concentric loading

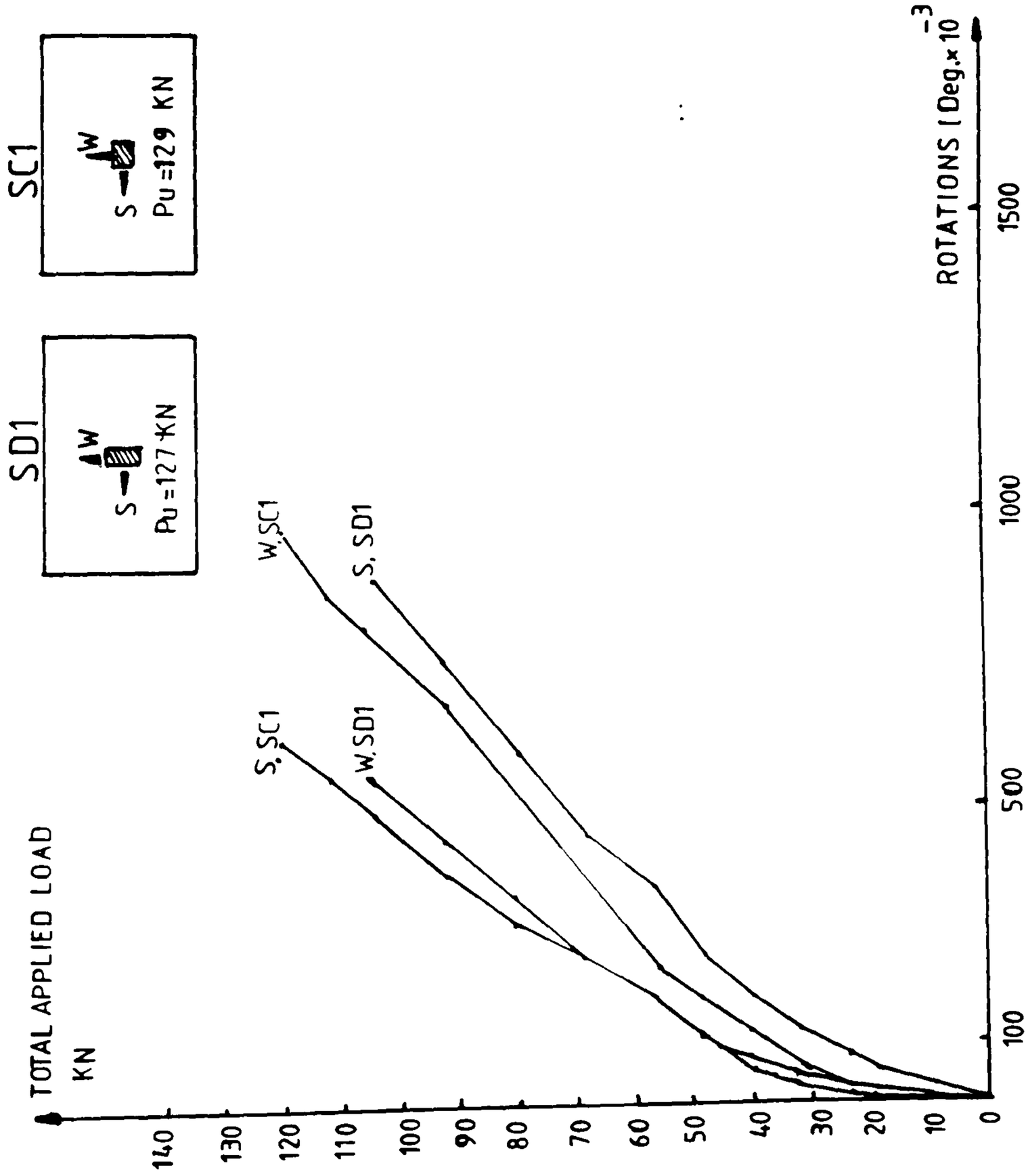

Fig.(3-10) Slab rotations -slabs with concentric loading

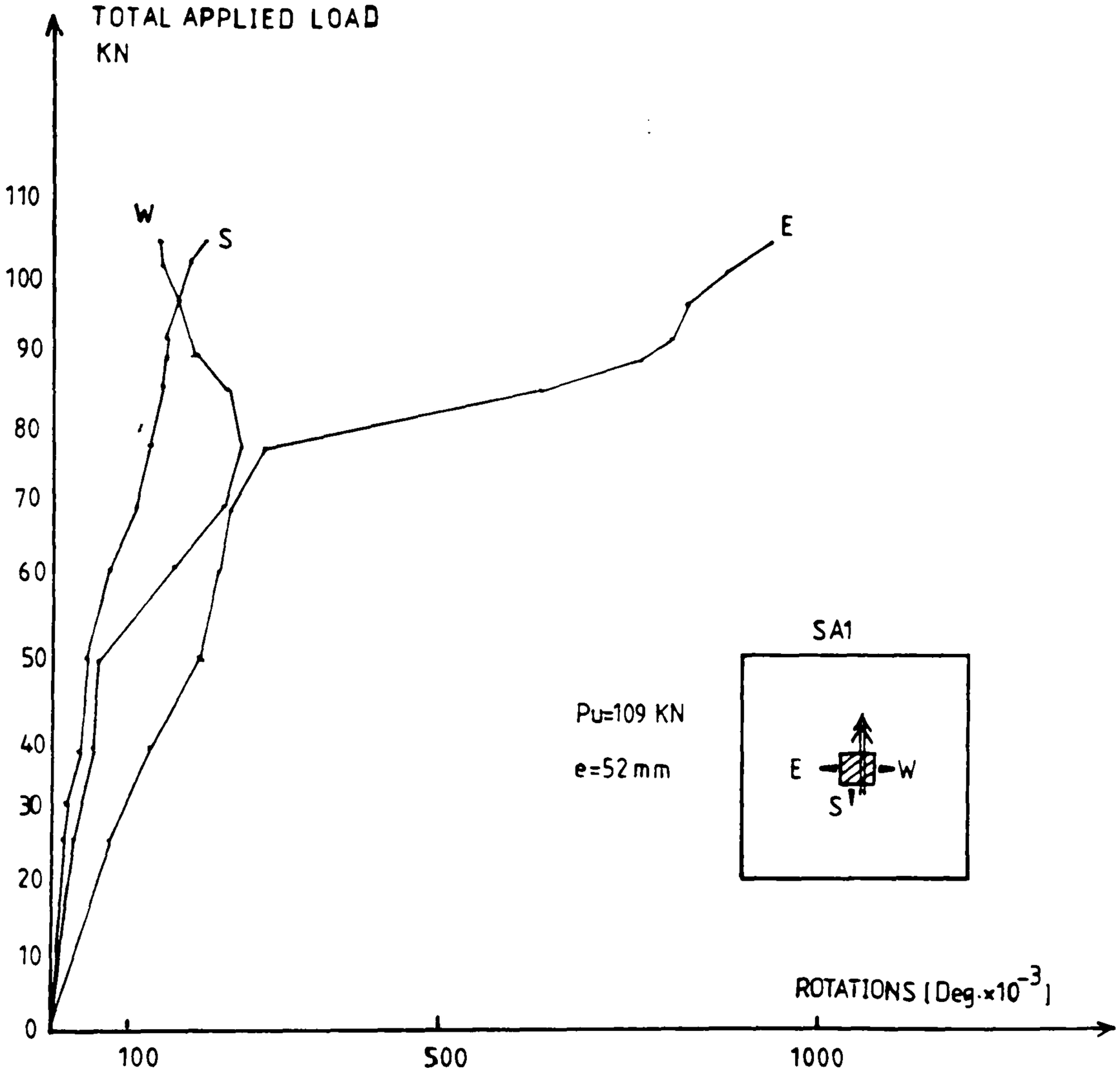

Fig.(3-11) Slab rotations

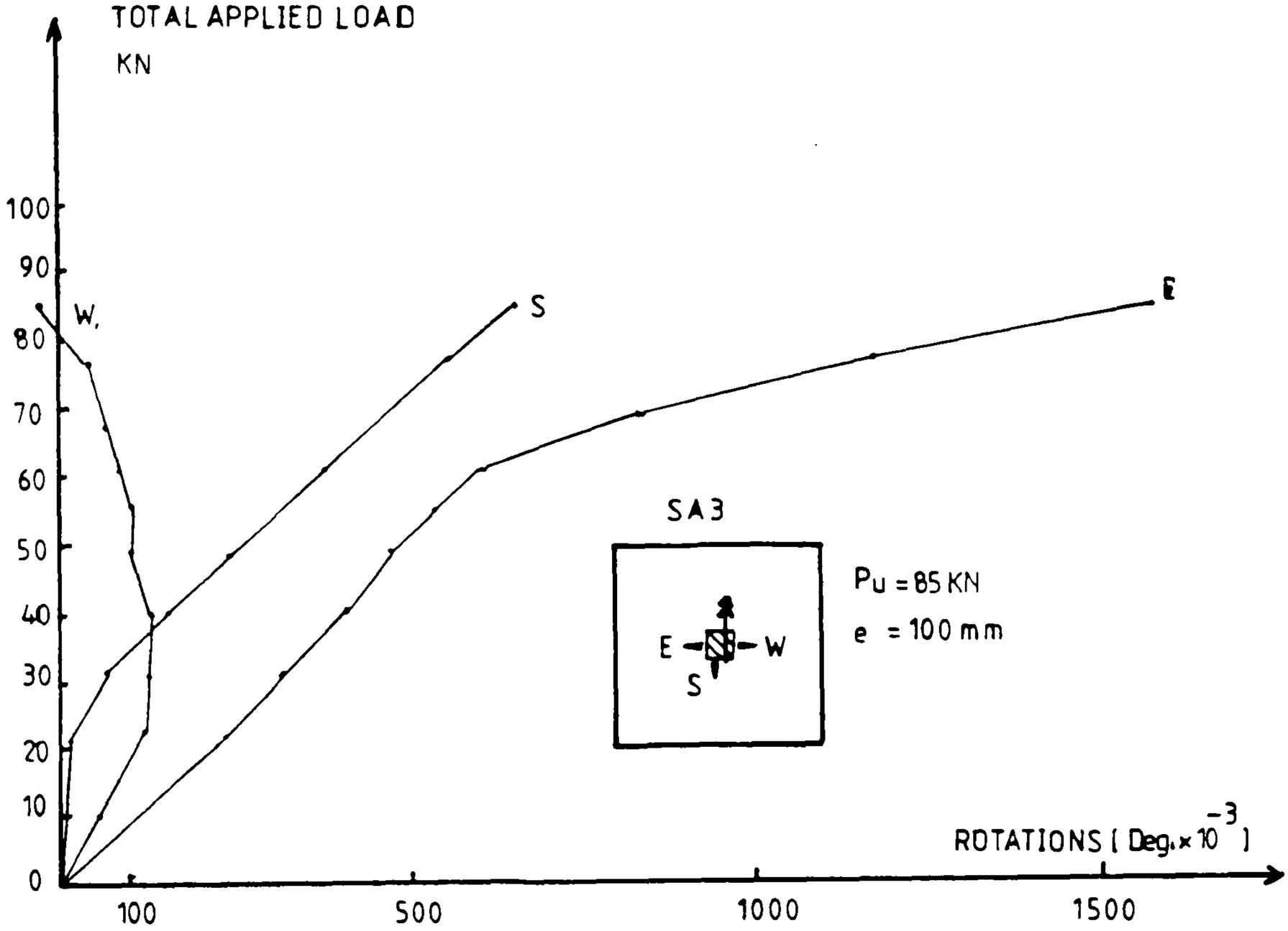

Fig.(3-12) Slab rotations

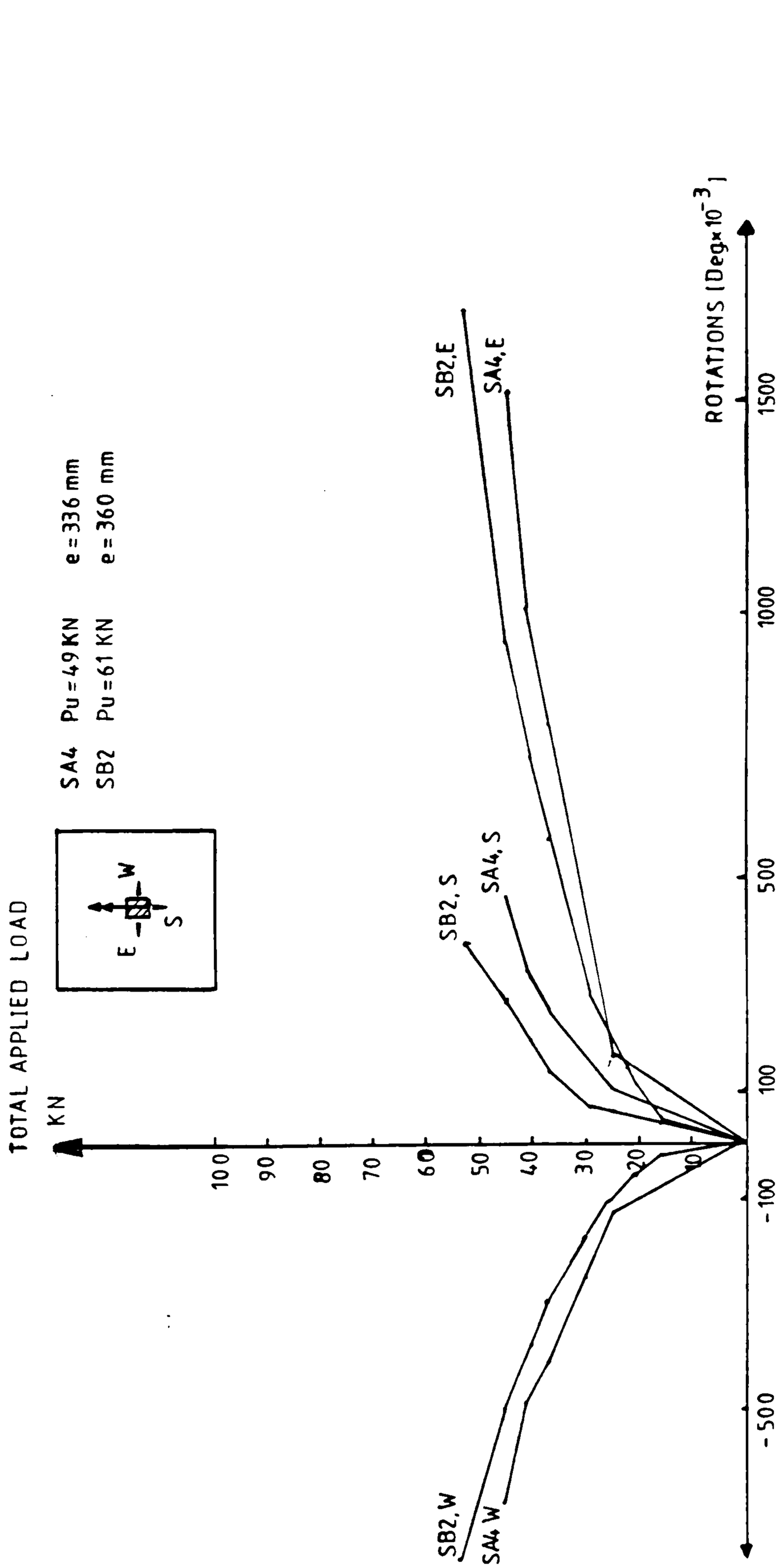

Fig.(3-13) Slab rotations

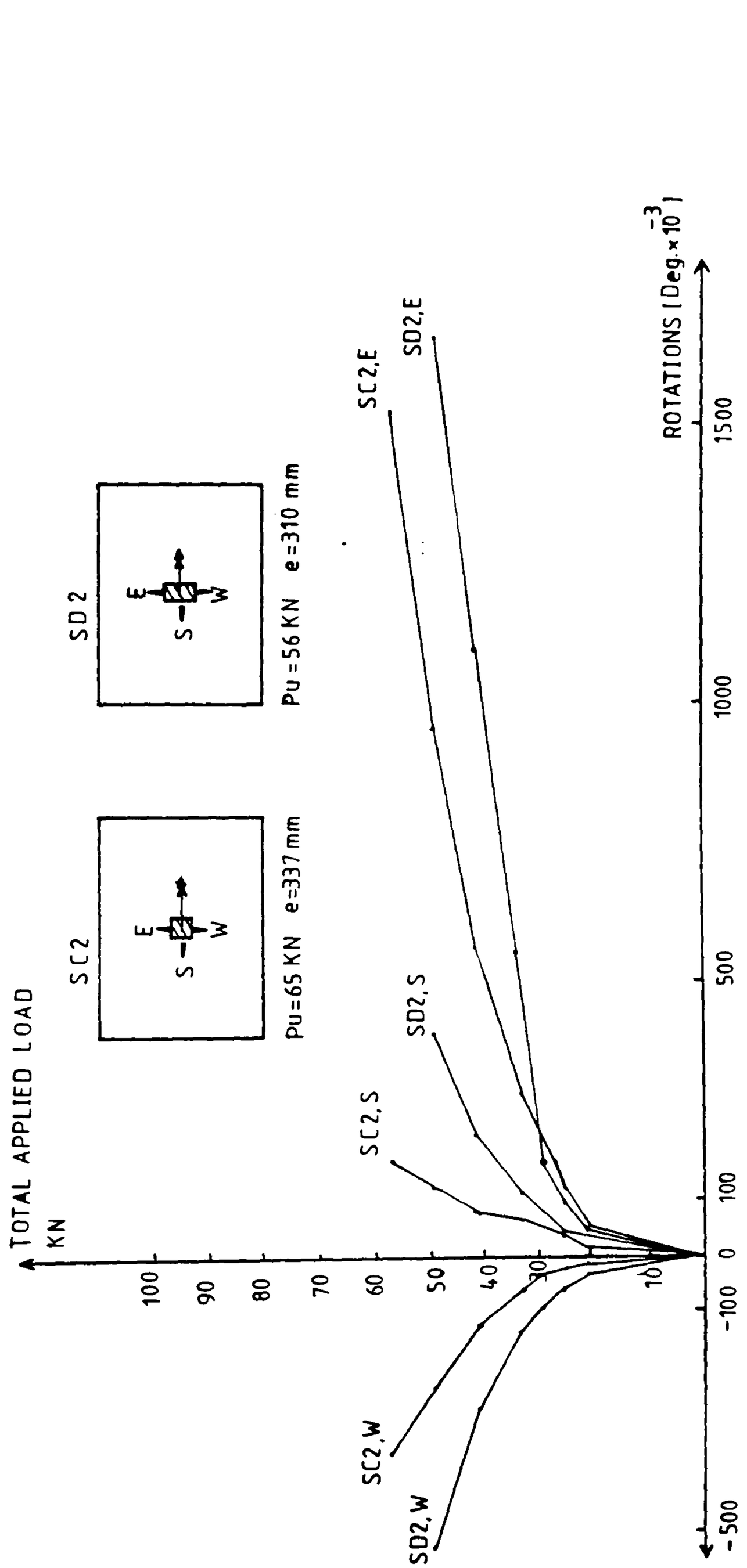

Fig.(3-14) Slab rotations

load,this may be due to a reduction of the joint stiffness at early stages of loading in eccentric slabs.

The joint rotations calculated as $\theta s=(\theta_E-\theta_W)/2$ plotted against the column moments are shown in Fig. (3-15), which shows that,increased eccentricity causes greater ultimate rotation of the slab-column joint.

During the test slab SA3 was unloaded and loaded again due to an error in the test procedure.

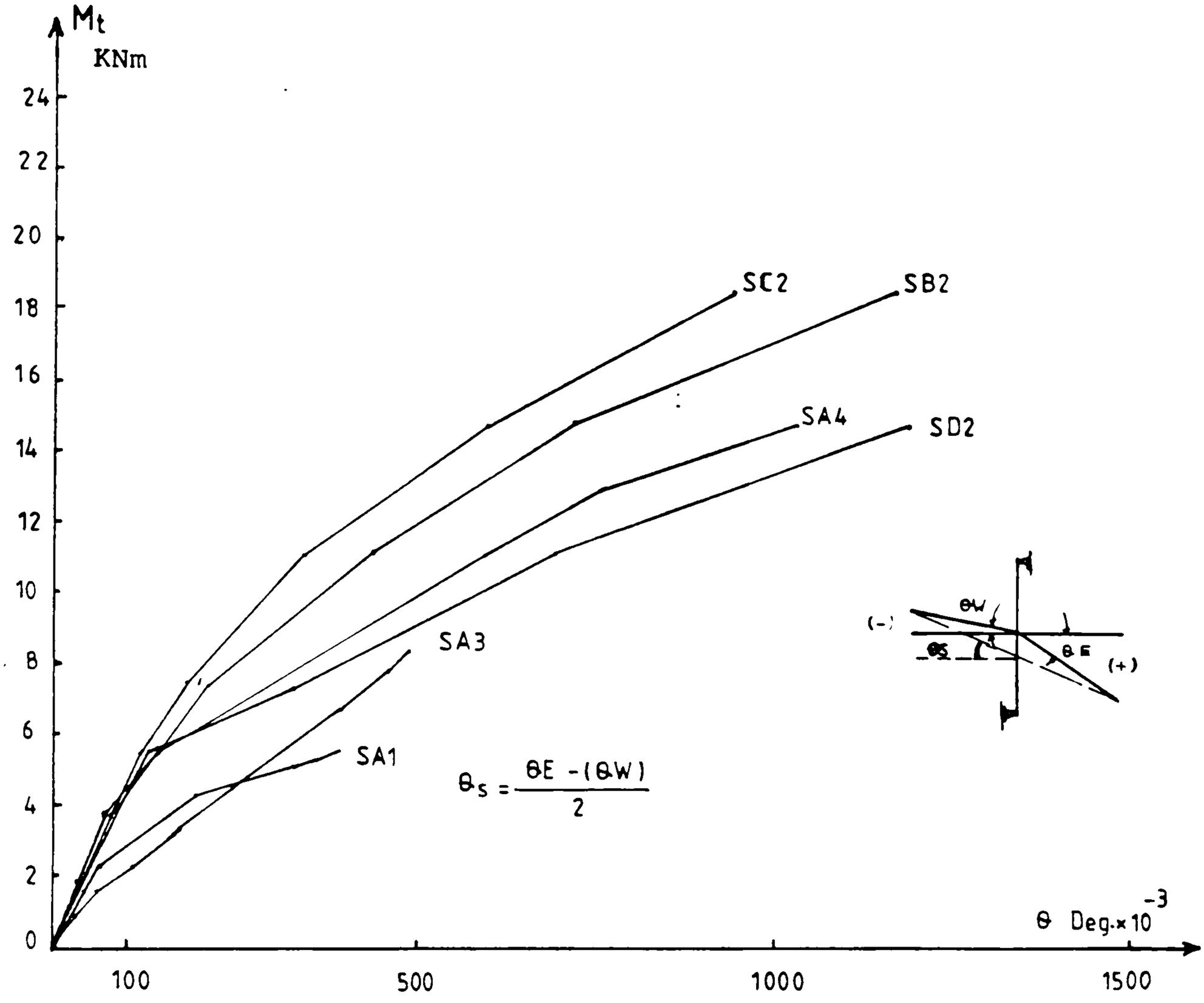

SLAB No	M_{tu} KNm	e mm	ρ %
SA1	5,55	52	0,55
SA3	8,46	100	0,55
SA4	16,65	336	0,55
SB2	22,2	360	1,00
SC2	22,2	337	0,72
SD2	17,57	310	0,72

Fig.(3-15) Slab rotations

CHAPTER FOUR

BEHAVIOUR OF CONCRETE

4-1 Concrete properties

This chapter summarizes some typical mechanical properties of concrete under uniaxial, biaxial, and triaxial states of stress. These data are essential for generalized mathematical modelling of concrete. They are of interest in relation to the complex stress states in slabs near columns, but a much simplified approach is used in the development of a punching theorem in Chapter Five.

4-1-1 Uniaxial loading

Typical stress-strain relationships for concrete subjected to uniaxial compression are shown in Fig.(4-1). The shapes of the curves are closely associated with the mechanism of internal microcracking. For a stress in the region up to about 30 percent of the maximum compressive strength f_c, the cracks existing in the concrete before loading remain nearly unchanged, and the concrete response is nearly linear elastic.

This level of stress has been termed the onset of localized cracking(33), and this occurs primarily due to bond breakdown at the aggregate-mortar matrix interface, after which the

material exhibits, distinct inelastic properties but still behaves in a relatively stable manner.

For stresses between 0.3 and $0.5f_c$ the bond cracks start to extend due to stress concentrations at the crack tips. For stresses between 0.5 and $0.75f_c$ some cracks at nearby aggregate surfaces start to bridge in the form of mortar cracks. At the same time other bond cracks continue to grow slowly. For compressive stresses above about $0.75f_c$ the largest cracks reach their critical lengths, and this stress level is termed the critical stress (59) (57). It corresponds to the minimal value of volumetric strain Fig.(4-1). When the maximum stress is reached, internal damage is accumulated, the compressive strain increases rapidly and the concrete enters the descending part of the stress-strain curve. The shape of the stress-strain curve is fairly similar for concretes of different strengths but the strain ε_{c1} at peak stress increases a little with the concrete compressive strength Fig.(4-2). A high-strength concrete behaves in a linear fashion to a relatively higher stress level than a low-strength concrete but all peak points are located close to the strain value of 0.002. Higher strength concretes tend to behave in a more brittle manner with the post peak stress dropping off more sharply than for concrete with lower strength.

As shown in Fig.(4-2), the initial modulus of elasticity of concrete is dependent on the compressive strength, and is generally taken as a function of the compressive strength ($Ec::\sqrt{fc}$ ACI 318-83, $Ec::\sqrt[3]{fc}$ CEB/FIP),

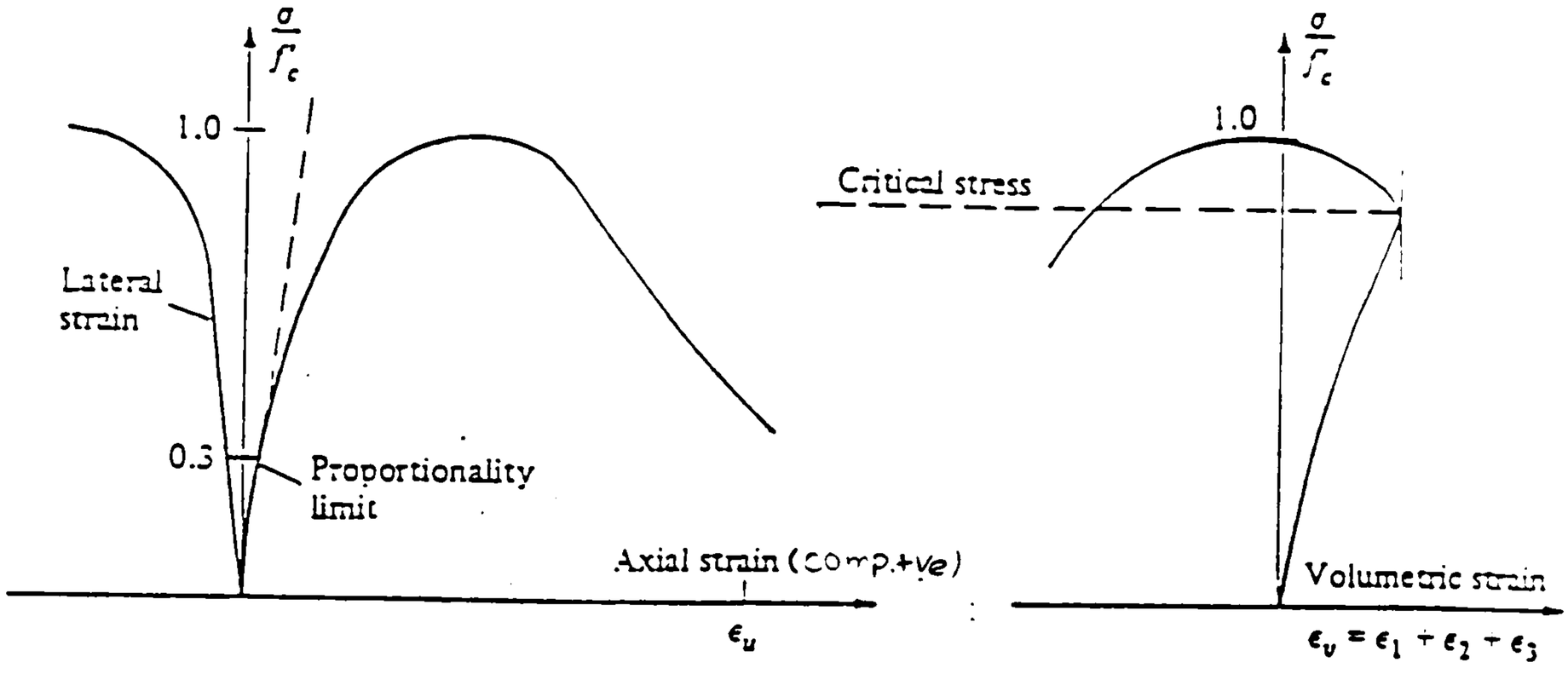

Fig.(4-1) Typical plot of compressive stress Vs axial,lateral,and volumetric strain (13)

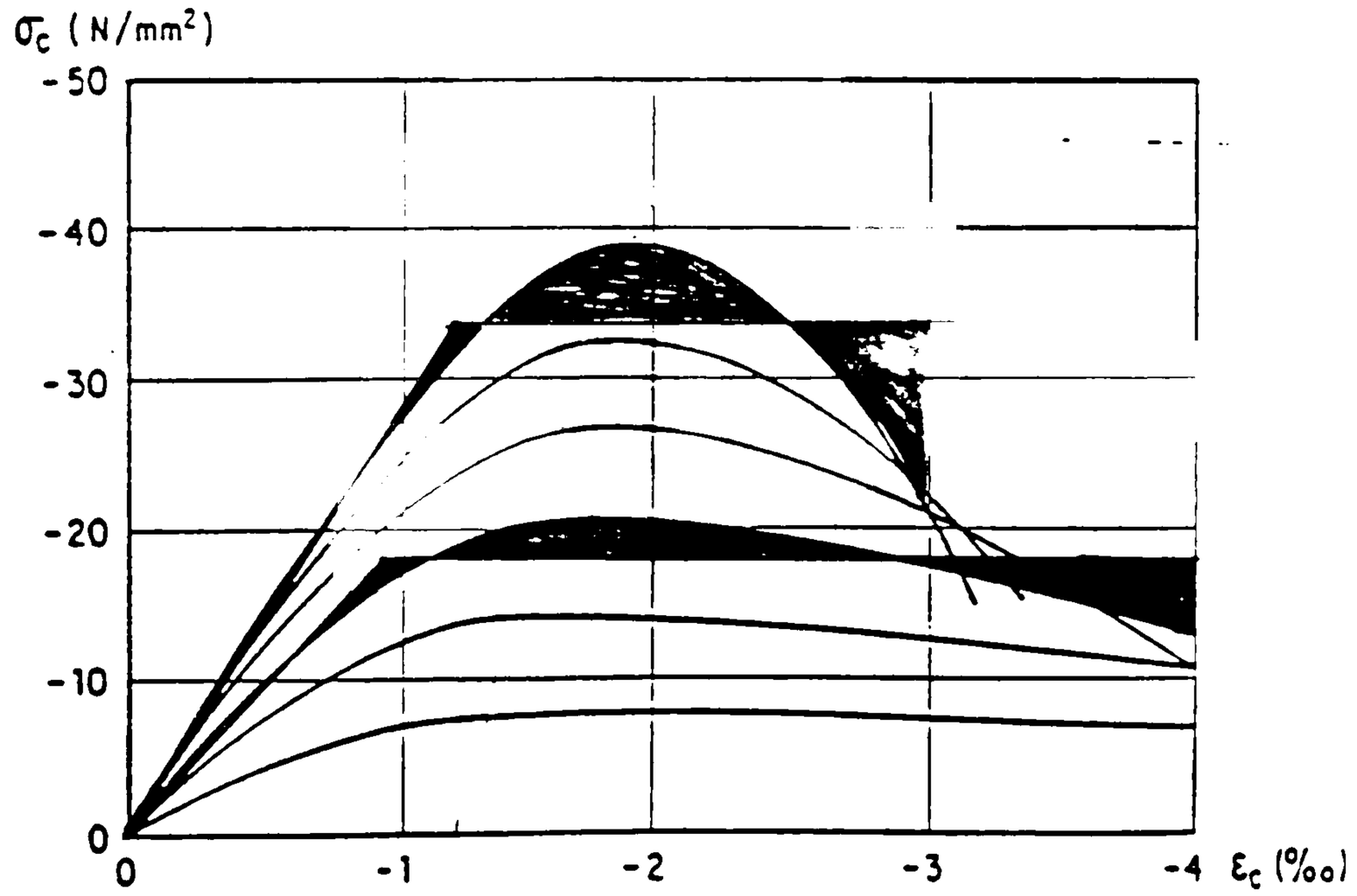

Fig.(4-2) Compressive stress-strain curves for different strength concretes (Wischers 1978) (68)

Fig.(4-3) shows stress-strain curves for concrete in uniaxial tension, all curves are nearly linear up to a relatively high stress level. At a stress about $0.75f_{ct}$ microcrack growth begins in a direction transverse to the stress. The ratio between uniaxial tensile and compressive strength may vary considerably but usually ranges from 0.05 to 0.1 . The modulus of elasticity under uniaxial tension is somewhat higher than in uniaxial compression.

In the present work, in order to calculate the neutral axis depth for a segment element of the slab a stress-strain relation for the concrete has to be known. To simplify the calculations, the uniaxial stress-strain curve for concrete in compression is approximated by the bi-linear relationship shown in Fig.(4-4) this curve is proposed in the CEB/FIP recommendations of 1970.[62] For higher strains it is assumed that the average stress remains constant and the descending branch of $\sigma : \varepsilon$ need not be defined. The assumption does however correctly imply a descending branch.

4-1-2 Biaxial loading

Figs.(4-5),(4-6) and (4-7) show typical stress-strain relationships of concrete under biaxial compression, combined tension and compression, and biaxial tension. As shown in Fig.(4-5) the strength of the concrete under biaxial compression is higher than the strength under uniaxial compression. A maximum strength increase of approximately 25 percent is observed at a stress ratio of

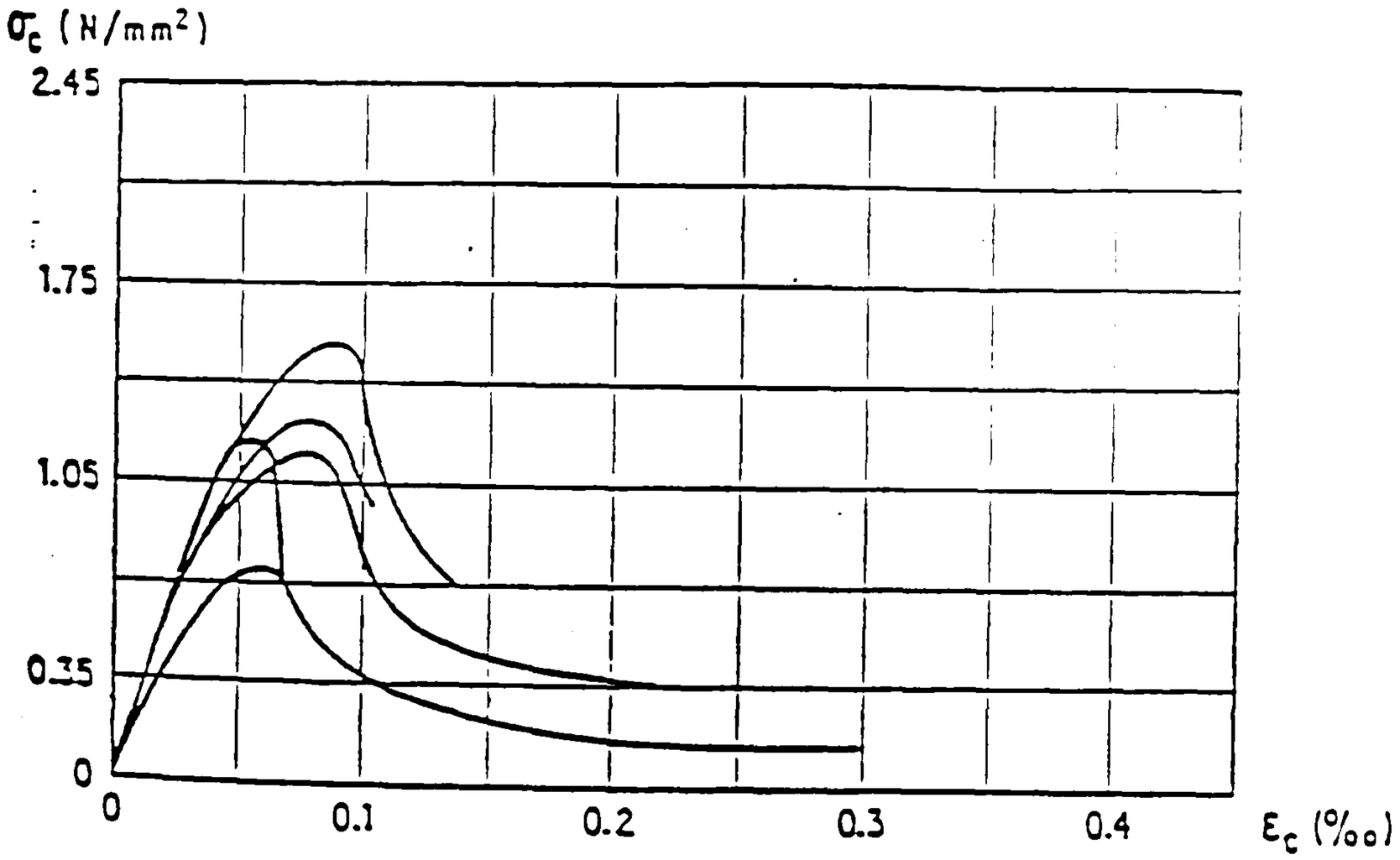

Fig.(4-3) Tensile stress-strain curves
(Hughes and Chapman 1966) (28)

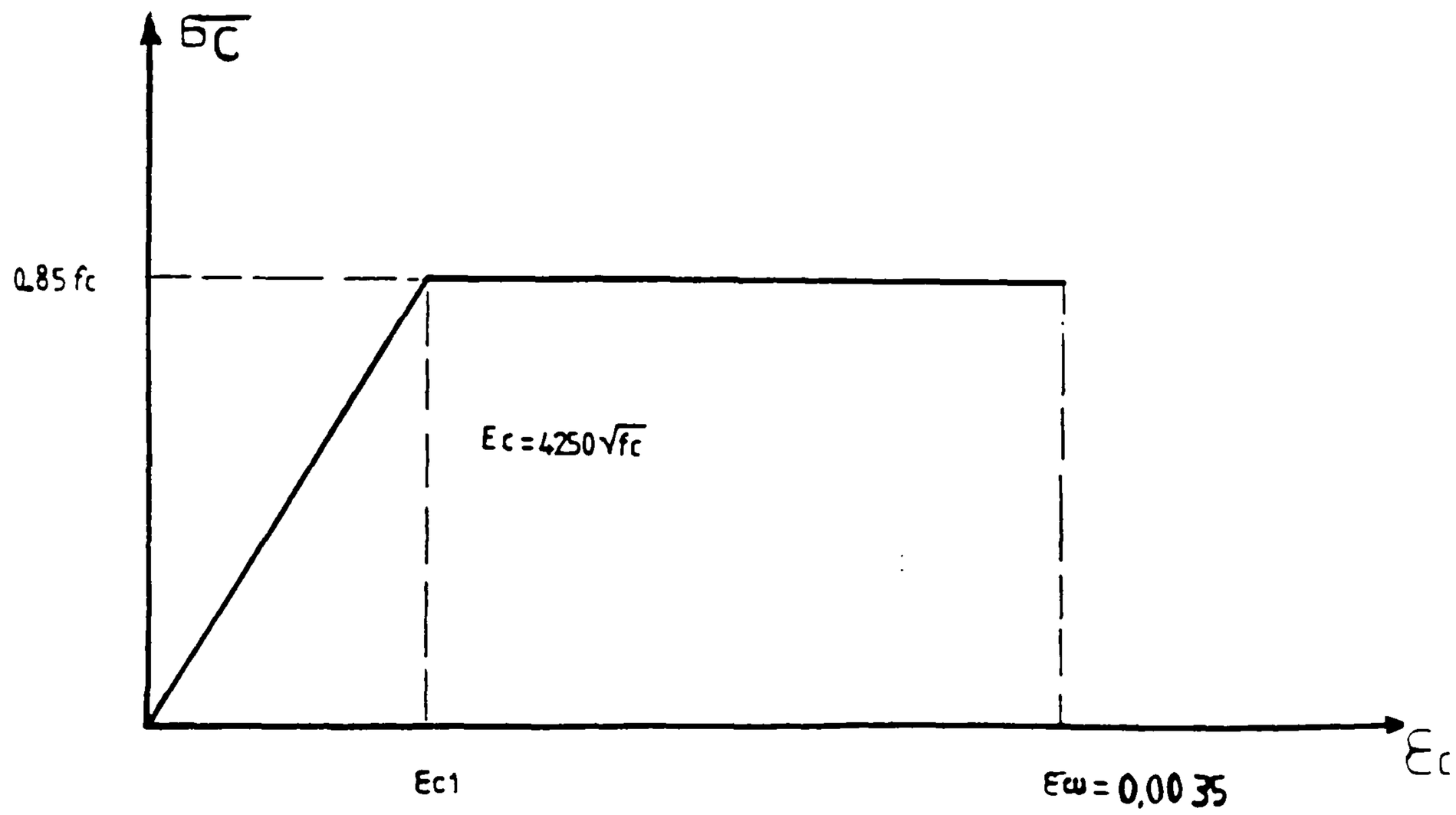

Fig.(4-4) The concrete stress-strain curve
(CEB/FIP 1970) (62)

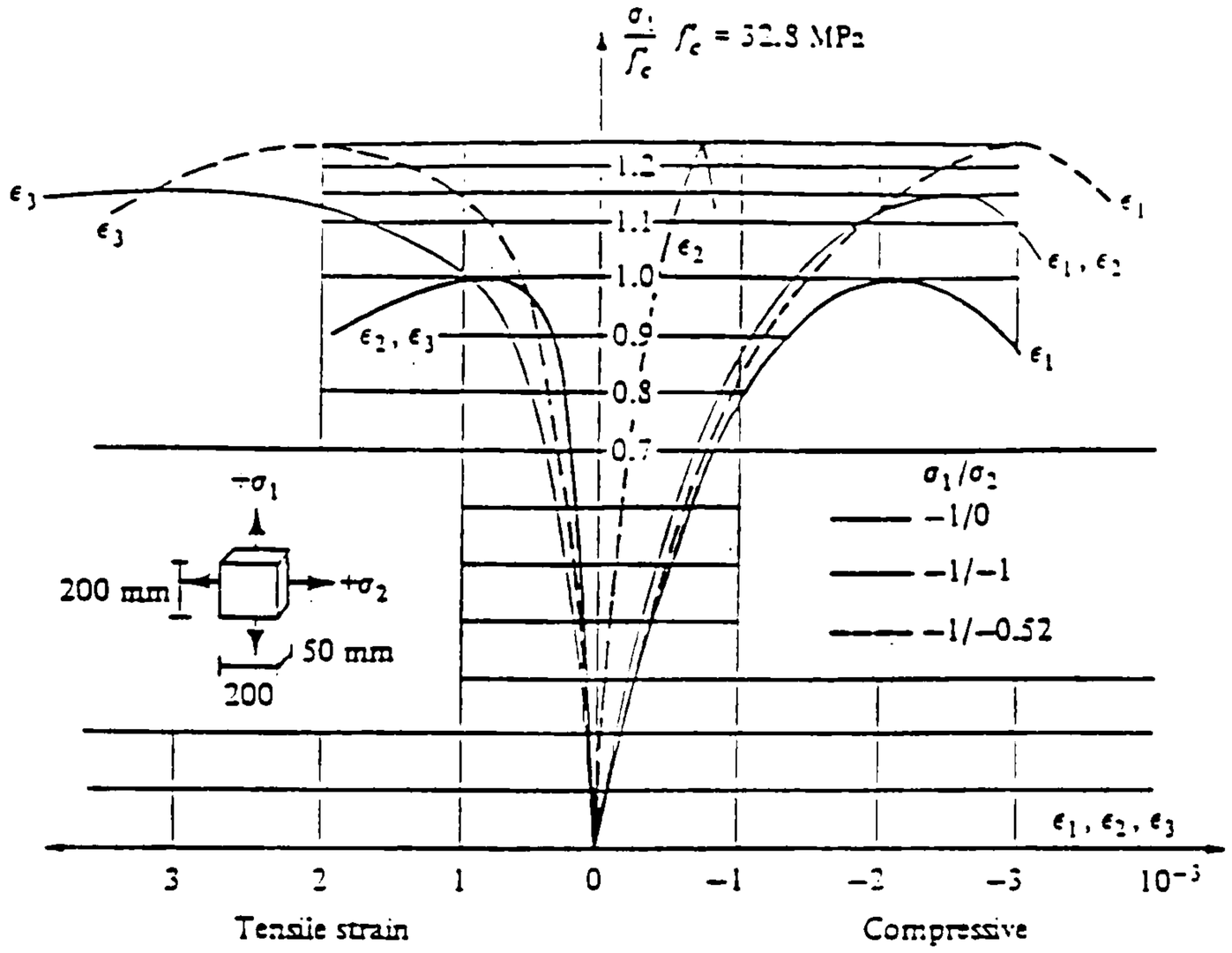

Fig.(4-5) Stress-strain relationships of concrete under biaxial-compression (Kupfer et al.,1969)(35)

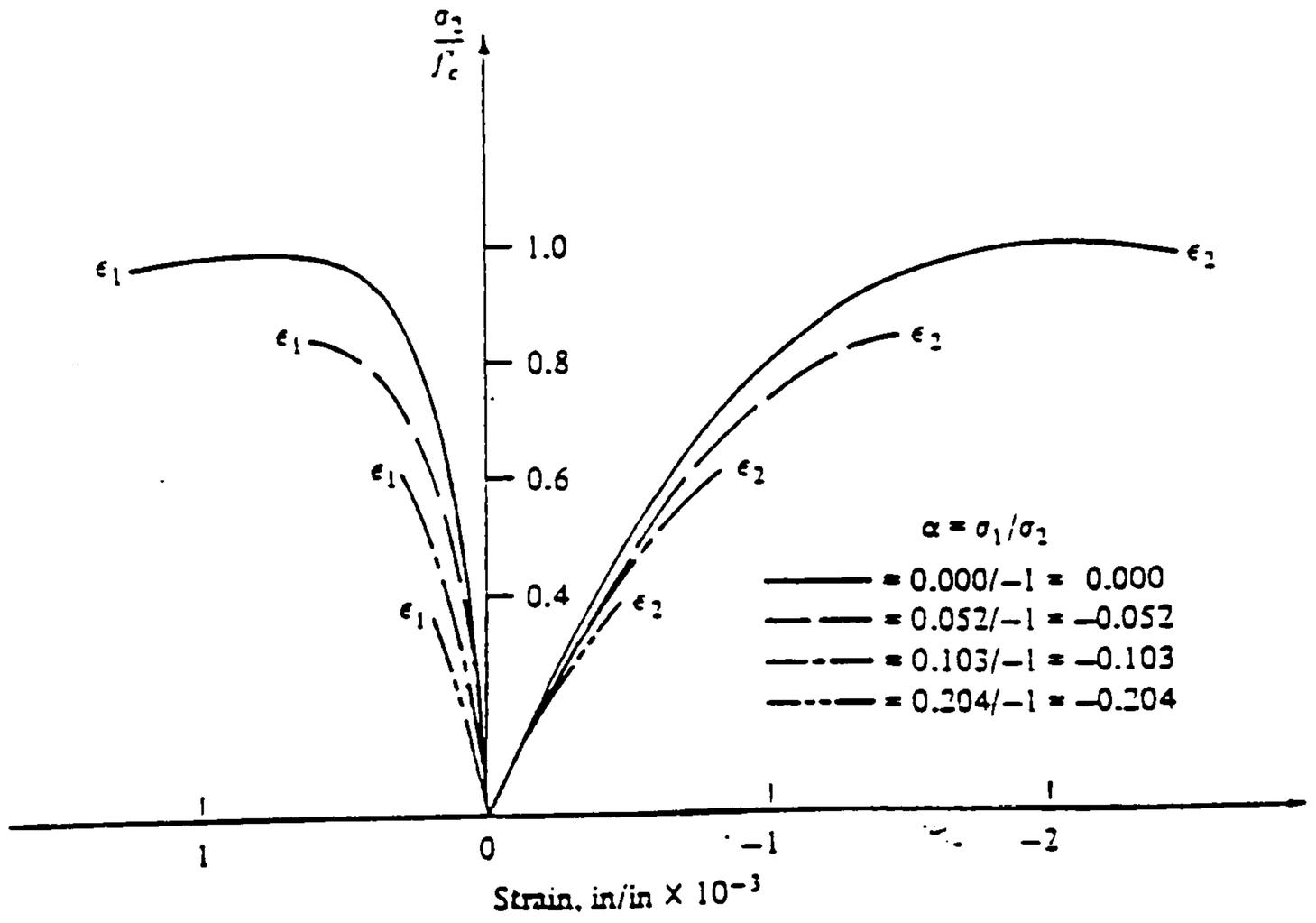

Fig.(4-6) Experimental stress-strain curves for biaxial tension-compression.(Kupfer et al.,1969.)(35)

($\sigma 2/\sigma 1=0.5$) and for the equal biaxial compression ($\sigma_2/\sigma_1=1$) an increase of 16 percent is achieved. Under biaxial compression-tension the compressive strength decreases as the tensile stress is increased Fig.(4-6). Under biaxial tension the strength of concrete is almost equal to its uniaxial tensile strength Fig.(4-8).

In biaxial compression-tension, as the tensile stress increases the magnitude at failure of both the principal compressive and tensile strains decrease Fig.(4-6)

For all these stress combinations, the failure of concrete occurs by tensile splitting with the fractured surface orthogonal to the direction of the maximum tensile stress or strain. Tensile strains are of crucial importance in the failure mechanism of concrete (Kupfer et al 1969) (35). Failure modes of biaxially loaded concrete are shown in Fig.(4-9).

Fig.(4-10) shows an approximated strength envelope for concrete which suggests a constant biaxial compressive strength of $1.2f_c$ for any stress ratio bigger than 0.2

4-1-3 Triaxial Loading

Fig.(4-11) shows typical stress-strain curves from triaxial tests by (Balmer-1949) (6). The tests were conducted at high confining-stress levels. The axial strength increases with increasing confining pressure and under very high confining stresses extremely high strengths have been recorded Fig.(4-11). The schematic shape of the failure surface of concrete subjected to triaxial loading is shown in Fig.(4-12).

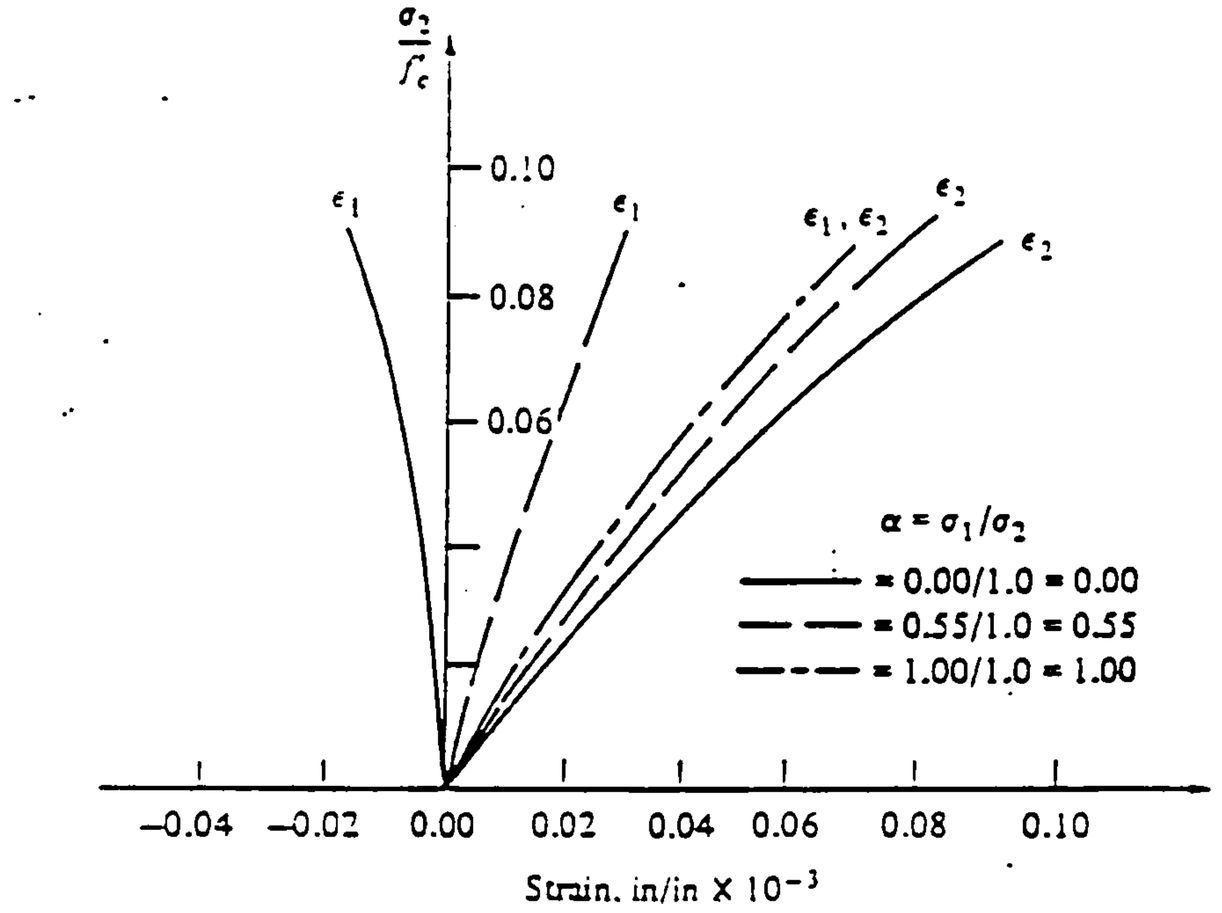

Fig.(4-7) Experimental stress-strain curves for biaxial tension. (Kupfer et al., 1969)(35)

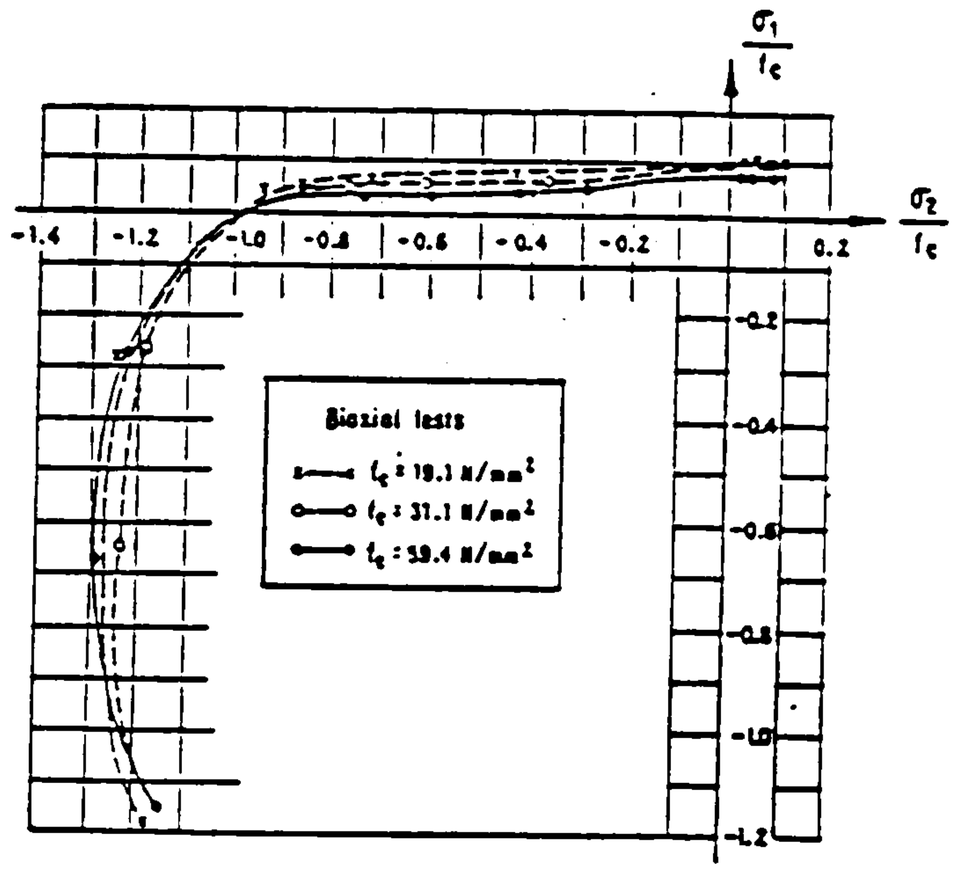

Fig.(4-8) Biaxial strength envelope of concrete (Kupfer et al ,1969)(35)

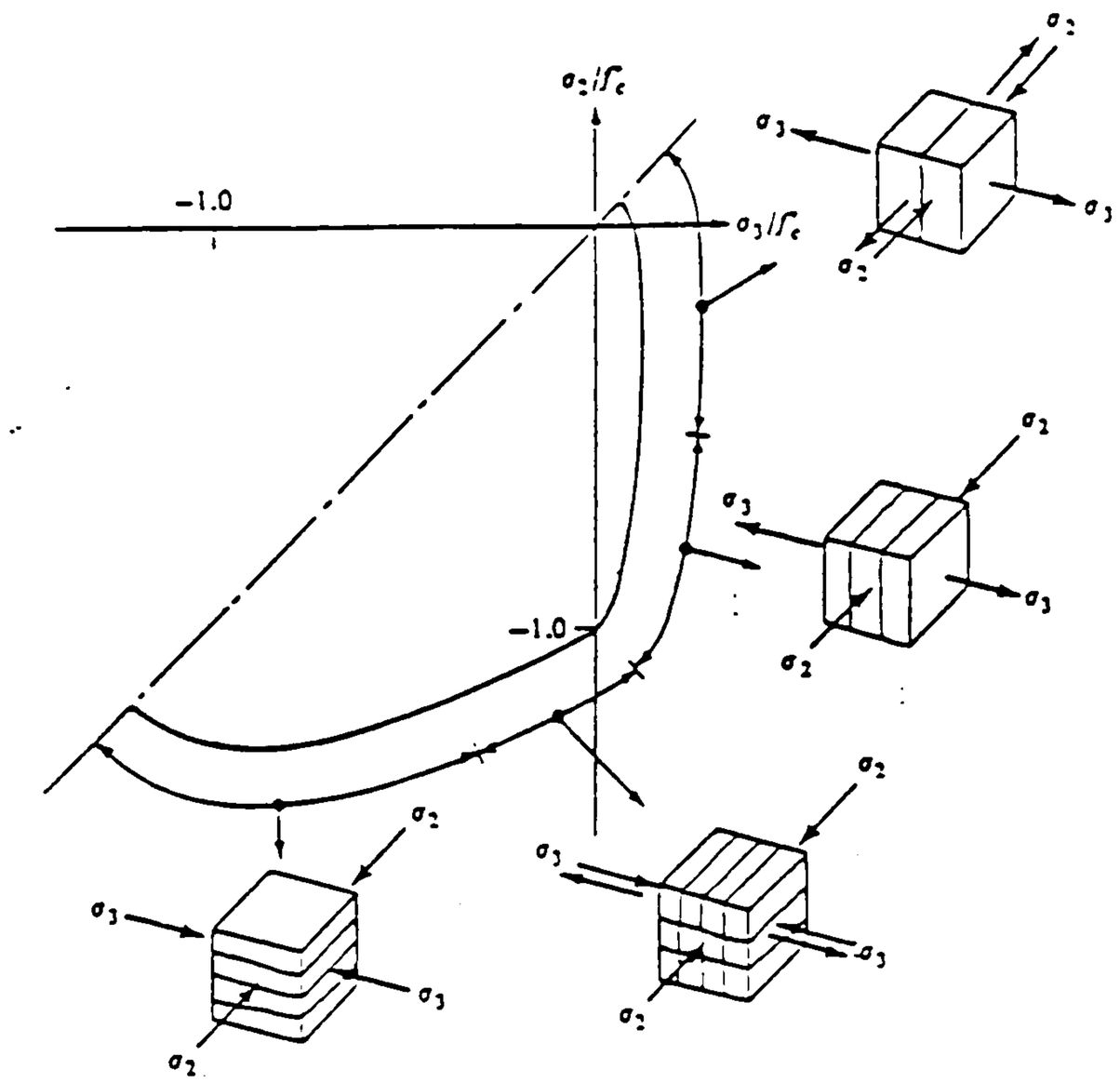

Fig.(4-9) Failure modes of biaxially loaded concrete (Nelissen,1972)(45)

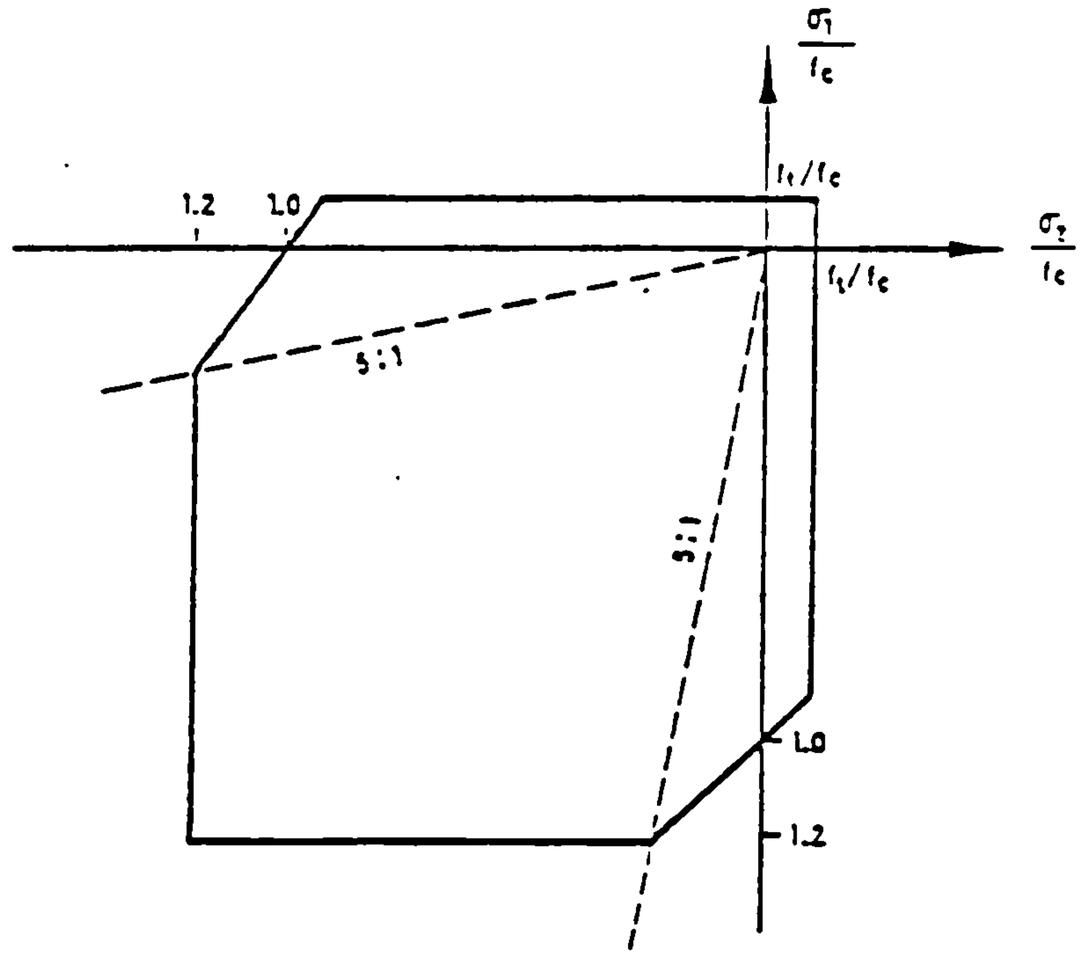

, Approximated biaxial strength envelope of concrete.

Fig.(4-10) Biaxial strength of concrete (Shehata 1985)(62)

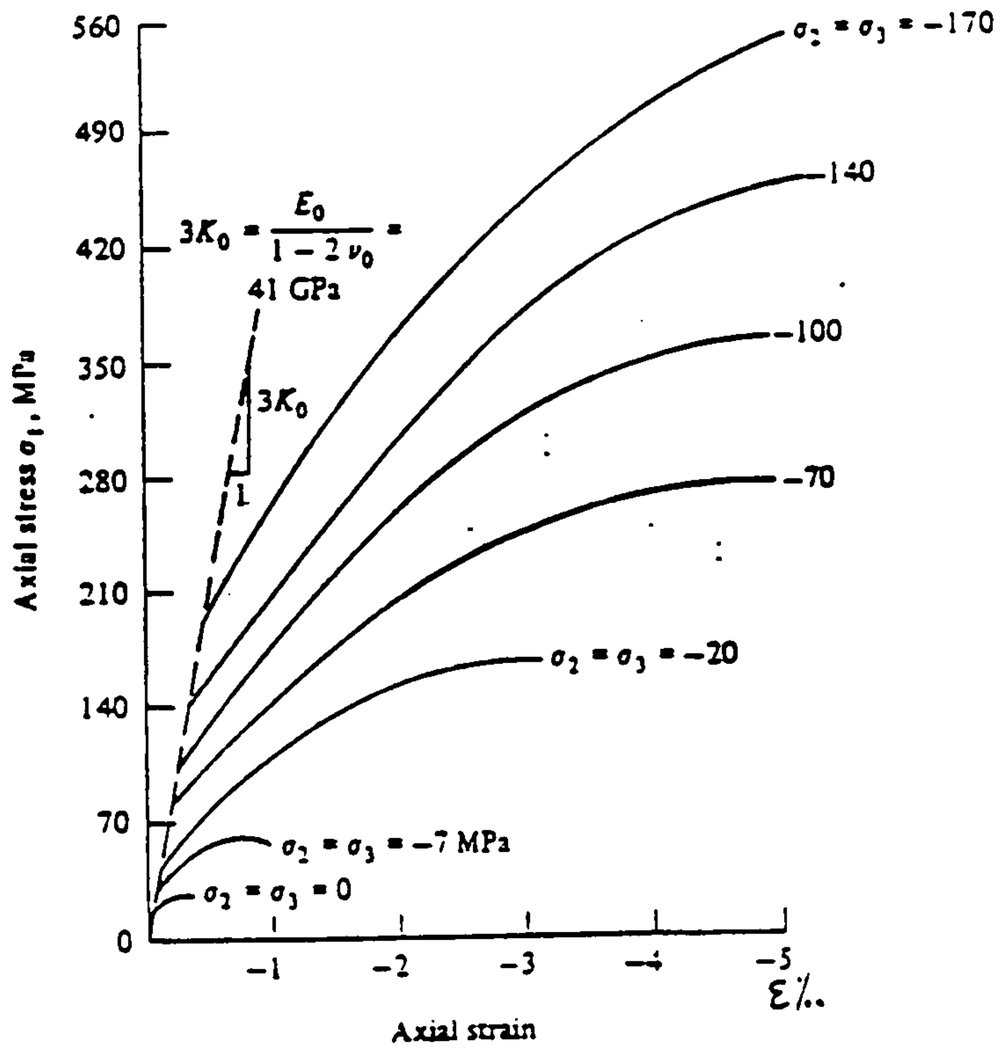

Fig.(4-11) Triaxial stress-strain relationship of concrete.(Balmer,1949) (6)

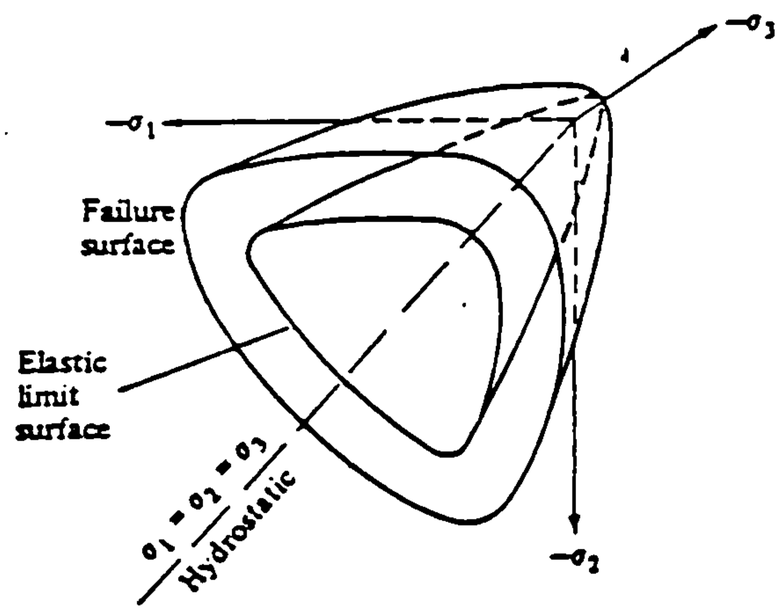

Fig.(4-12) Schematic failure surface of concrete in three-dimensional stress space (Chen 1982)(13)

With increasing hydrostatic pressure, the compaction of the cement paste becomes increasingly pronounced but this alone can not cause complete disruption of the concrete. An unloading from hydrostatic compression followed by a reloading in uniaxial compression shows that the uniaxial compressive strength has decreased to about 60 percent of its original value (Chinn and Zimmerman 1965) (12). The experimental studies of Mills and Zimmerman 1970 (36) have indicated that in triaxial tests the failure of the specimen is marked by a drop in the larger load and a corresponding increase in the smaller loads, so that determination of the exact point of failure is dependent on the rate of loading.

The stress-strain curve for concrete in triaxial compression is similar to that under biaxial compression, but in the former case the strains at failure are larger. The major failure plane in compressive triaxial tests appears to be the plane or planes defined by the minimum principal stress. Concrete behaviour under triaxial tension is assumed to be similar to biaxial tension behaviour and the tensile strength of the concrete under triaxial tension is approximately equal to the tensile strength in uniaxial tension. under a combined compressive-tensile stress state it is observed that the compressive strength of the concrete decreases as the tensile stress increases.

4-2 FAILURE CRITERIA OF CONCRETE

The concrete strength can be defined as the ultimate load-carrying capacity of a concrete element.

In general concrete failures can be divided into tensile failures defined by the formation of major cracks and the loss of tensile strength in the concrete normal to the crack direction, or compressive failure when many small cracks develop and the concrete element loses most of its strength.

The strength of the concrete under multiaxial stresses is a function of the state of stress, and can be predicted by considering the interaction of the various components of the state of stress.

One method of representing such a function is to use the principal stresses.

$$f\ (\sigma_1,\sigma_2,\sigma_3) = 0 \qquad (4.1)$$

Where σ_1, σ_2 and σ_3 are principal stresses. The three principal stresses σ_1, σ_2 and σ_3 can be expressed in terms of three principal stress invariants I_1, J_2 and J_3 and Eq.(4-1) can be replaced by

$$f\ (I_1,J_2,J_3) = 0 \qquad (4.2)$$

These three principal invariants will be used exclusively in formulating various criteria of failure for concrete, their definitions are as follows. The six stress invariants used in most failure criteria are as follows.

Stress Invariants: I_1, I_2, I_3

$$I_1 = \sigma_1 + \sigma_2 + \sigma_3 = 3\sigma_m \qquad (4.3)$$

$$I_2 = \sigma_1\sigma_2 + \sigma_2\sigma_3 + \sigma_1\sigma_3 \qquad (4.4)$$

$$I_3 = \sigma_1.\sigma_2.\sigma_3 \qquad (4.5)$$

Deviatoric Stress Invariants J_1, J_2, J_3

$$J_1 = S_1 + S_2 + S_3 = 0 \tag{4.6}$$

$$J_2 = 0.5(S_1^2+S_2^2+S_3^2) \tag{4.7}$$

$$J_3 = S_1.S_2.S_3 \tag{4.8}$$

Where

$$S_1 = \sigma_1 - \sigma_m \tag{4.9}$$

$$S_2 = \sigma_2 - \sigma_m \tag{4.10}$$

$$S_3 = \sigma_3 - \sigma_m \tag{4.11}$$

I_1 represents a purely hydrostatic pressure and J_2, J_3 represent the invariants of a state of pure shear.

Octahedral Stresses

The octahedral plane is the plane which makes equal angles with each of the principal-stress directions. The normal stress σ_{oc} on this plane is called the octahedral normal stress

$$\sigma_{oc} - I_1 /3 = \sigma_m \tag{4.12}$$

And the shear stress on the plane is called the octahedral shear stress τ_{oc}

$$\tau_{oc} = \sqrt{\frac{2}{3} J_2} \tag{4.13}$$

The direction of the octahedral shear is defined by the angle of similarity θ which is related to the invariant J3

$$\cos 3\theta = \frac{\sqrt{2}\ J_3}{\tau_{oc}^3} \tag{4.14}$$

$$\text{or } \cos\theta = \frac{\sigma_1 + \sigma_2 + \sigma_3}{2\sqrt{2}\,\tau_{oc}} \qquad (4.15)$$

Geometric interpretation of the stress state and invariants

The failure surface can be represented by geometrical interpretation of the stress state as a function

$$f(\xi, r, \theta) \qquad (4.16)$$

as shown in Fig.(4.13) where

$$\xi = \frac{1}{\sqrt{3}} I_1 = \sqrt{3}\,\sigma_m = \sqrt{3}\,\sigma_{oc} \qquad (4.17)$$

$$r = \sqrt{2J_2} = \sqrt{3}\,\tau_{oc} \qquad (4.18)$$

$$\cos 3\theta = \frac{2\sqrt{3}}{2} \frac{J_3}{J_2^{3/2}} = \frac{\sqrt{2}}{\tau_{oc}^3} J_3 \qquad (4.19)$$

Octahedral normal and shear strain

Definitions similar to those of the octahedral stresses can be used to define the octahedral strains as in Eq.(4.20) and (4.21)

$$\varepsilon_{oc} = (1/3)(\varepsilon_1 + \varepsilon_2 + \varepsilon_3) \qquad (4.20)$$

$$\gamma_{oc} = [(\varepsilon_1 - \varepsilon_2)^2 + (\varepsilon_2 - \varepsilon_3)^2 + (\varepsilon_3 - \varepsilon_1)^2]^{1/2} \qquad (4.21)$$

4-2-1 FAILURE CRITERION

Many failure criteria for concrete have been proposed, some of them will be discussed here.

Maximum-tensile stress criterion

The maximum tensile stress criterion of Rankine assumes that failure of the material takes place when the maximum principal stress inside the material reaches a value equal to the tensile strength of the material f_t. The equations for the fracture surface defined by this criterion are

$$\sigma_1 = f_t \quad \sigma_2 = f_t \quad \sigma_3 = f_t \tag{4.22}$$

The above equations are represented by three planes perpendicular to the principal stresses σ_1, σ_2, σ_3. The fracture surface can be fully described by using the variables ξ, r, θ or

I_1, J_2, θ within the range $0 \leqslant \theta \leqslant 60$ as follows

$$f\ (I_1, J_2, \ ) = 2\sqrt{3}\ \sqrt{J_2}\ \cos\ \theta + I_1 - 3f_t = 0 \tag{4.23}$$

or

$$f\ (r, \xi, \theta) = \sqrt{2}\ r\ \cos\ \theta + \xi - \sqrt{3} f_t = 0 \tag{4.24}$$

Fig.(4.14) shows the trace of the failure surface in the deviatoric plane containing the origin (plane π), and the tensile ($\theta=0^o$) and compressive ($\theta=60^o$) meridians of the fracture surface.

Rankine's theory is used to determine if a tensile type of failure has taken place in the concrete.

4-2-2 Mohr-Coulomb criterion

The Mohr-Coulomb theory assumes that failure takes place when the shearing stress (τ) on a plane reaches its limiting value, which is dependent only on the normal stress (σ) on the same plane.

$$\tau = f(\sigma) \qquad (4.25)$$

The envelope $f(\sigma)$ is an experimentally determined function, and can be represented as straight-line Fig.(4.15). The Mohr-coulomb criterion is given by Eq.(4.26)

$$\tau = C - \sigma\tan\phi \qquad (4.26)$$

Where C is the apparent cohesion and ϕ is the internal friction angle of the material.

Eq.(4.26) appears in the hydrostatic plane ($\theta=0^{o}$) as straight lines and in the deviatoric plane as a regular hexagon Fig.(4.16)

According to Mohr's criterion the intermediate principal stress has no influence on the failure. This means that the concrete strength in a biaxial compressive state is the same as that in uniaxial compression, while test results show an increase of about 20 percent of the concrete strength in biaxial compression.

4-2-3 Ottosen's Criterion (1977)

Ottosen (48) suggested a failure criterion involving the stress invariants I_1, J_2, and $\cos3\theta$ as follows

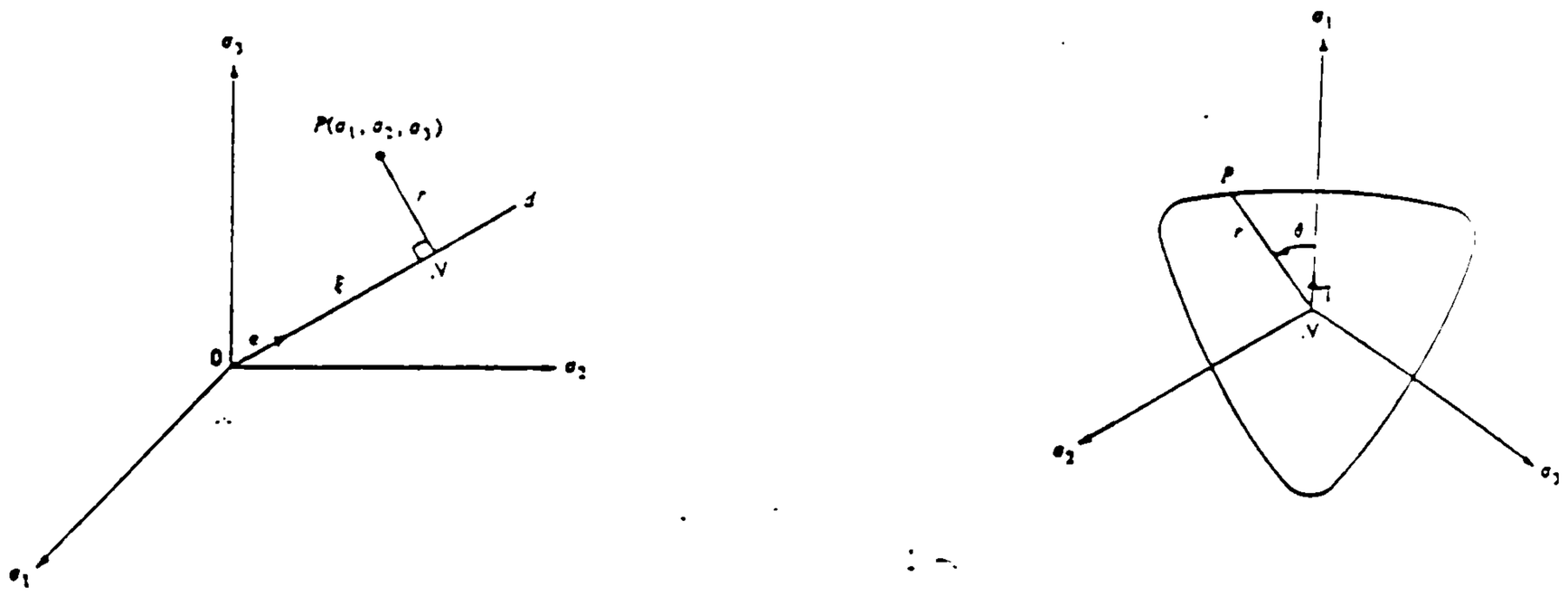

Fig.(4-13) Decomposition of stress in principal-stress space

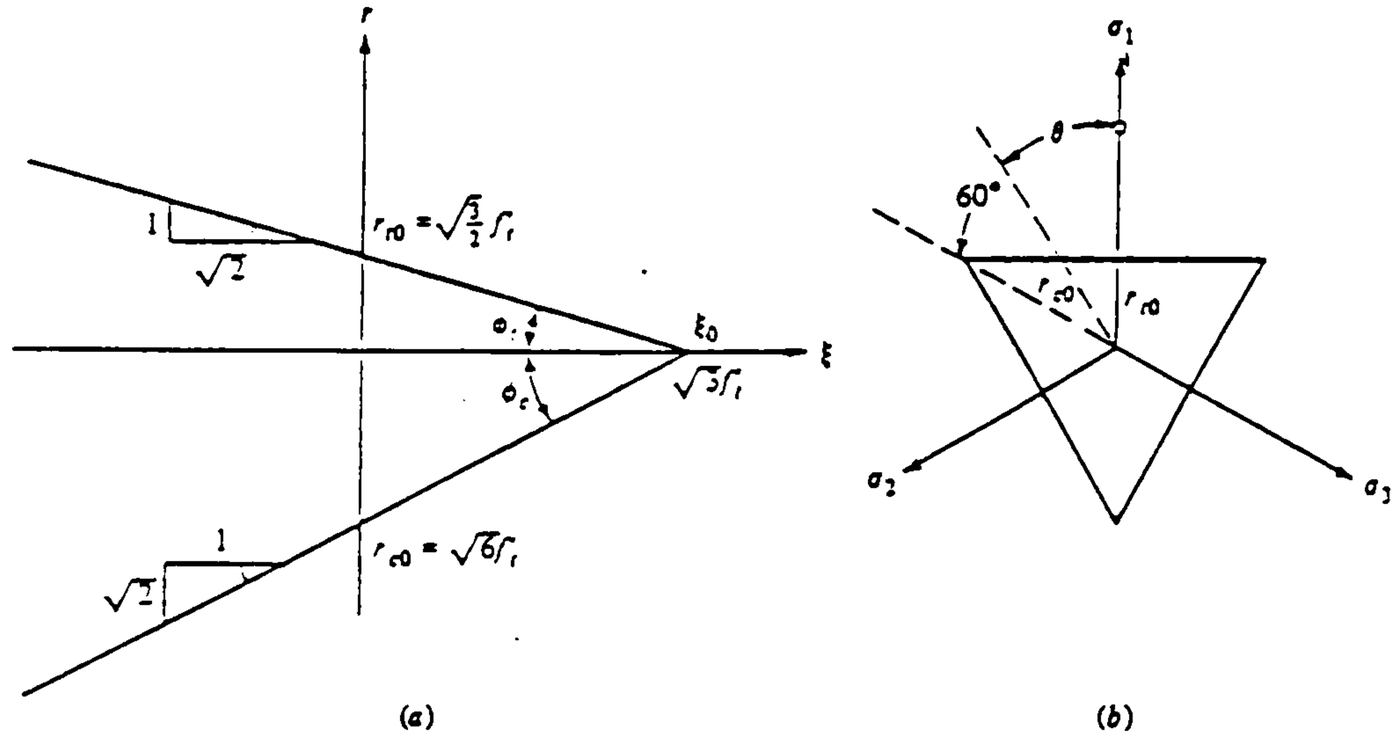

Fig.(4-14) Rankine's maximum-principal-stress criterion

a) Meridian plane $\Theta=0^{\circ}$

b) π Plane

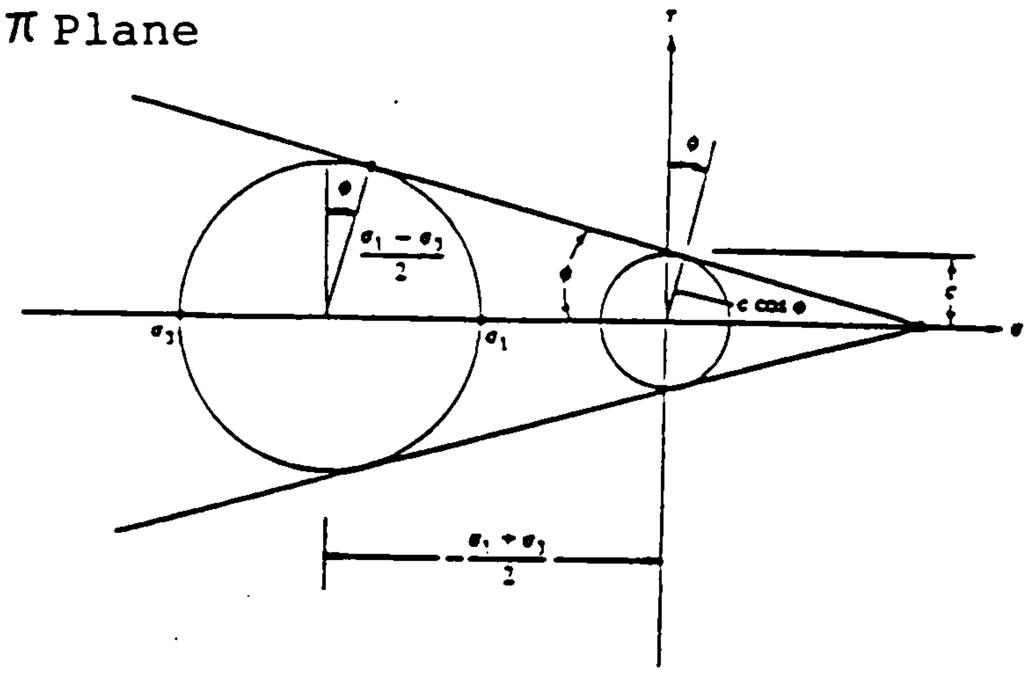

Fig.(4-15) Relationship between principal stresses for Mohr-Coulomb criterion

$$f\ (I_1, J_2, \cos 3\theta) = A\frac{J_2}{f_c} + \lambda\frac{\sqrt{J_2}}{f_c} + B\frac{I_1}{f_c} - 1 = 0 \qquad (4.27)$$

in which A and B are constants and λ is a function of $\cos 3\theta$,

$$\lambda = \lambda(\cos 3\theta) > 0$$

For A>0 and B>0 ,the failure surface of Eq.(4.27) has curved meridians, which are smooth and convex. From Eq.(4.27)

$$\frac{\sqrt{J_2}}{\sigma_c} = \frac{1}{2A}\left[-\lambda + \sqrt{\lambda^2 - 4A\left(B\frac{I_1}{\sigma_c} - 1\right)}\right] \qquad (4.28)$$

where the function, $\lambda=\lambda(\cos 3\theta)$ can be adequately represented in the form

$$\left.\begin{aligned} \lambda &= K_1 \cos[(1/3)\arccos(K_2\cos 3\theta) \quad \text{for } \cos 3\theta \geqslant 0\ ] \\ \lambda &= K_1 \cos[(\pi/3) - (1/3)\arccos(-K_2\cos 3\theta) \quad \text{for } \cos 3\theta \leqslant 0] \end{aligned}\right\} \qquad (4.29)$$

Here K_1 is a size factor and K2 is a shape factor ($0 \leqslant K_2 \leqslant 1$) Ottosen's is a four-parameter criterion and requires a computer for solution. Useful charts have been prepared by Ottosen (47) for design situations.

Fig.(4.17) shows the ability of the Ottosen's criterion to represent the experimental biaxial results of Kupfer,et.al.(35)

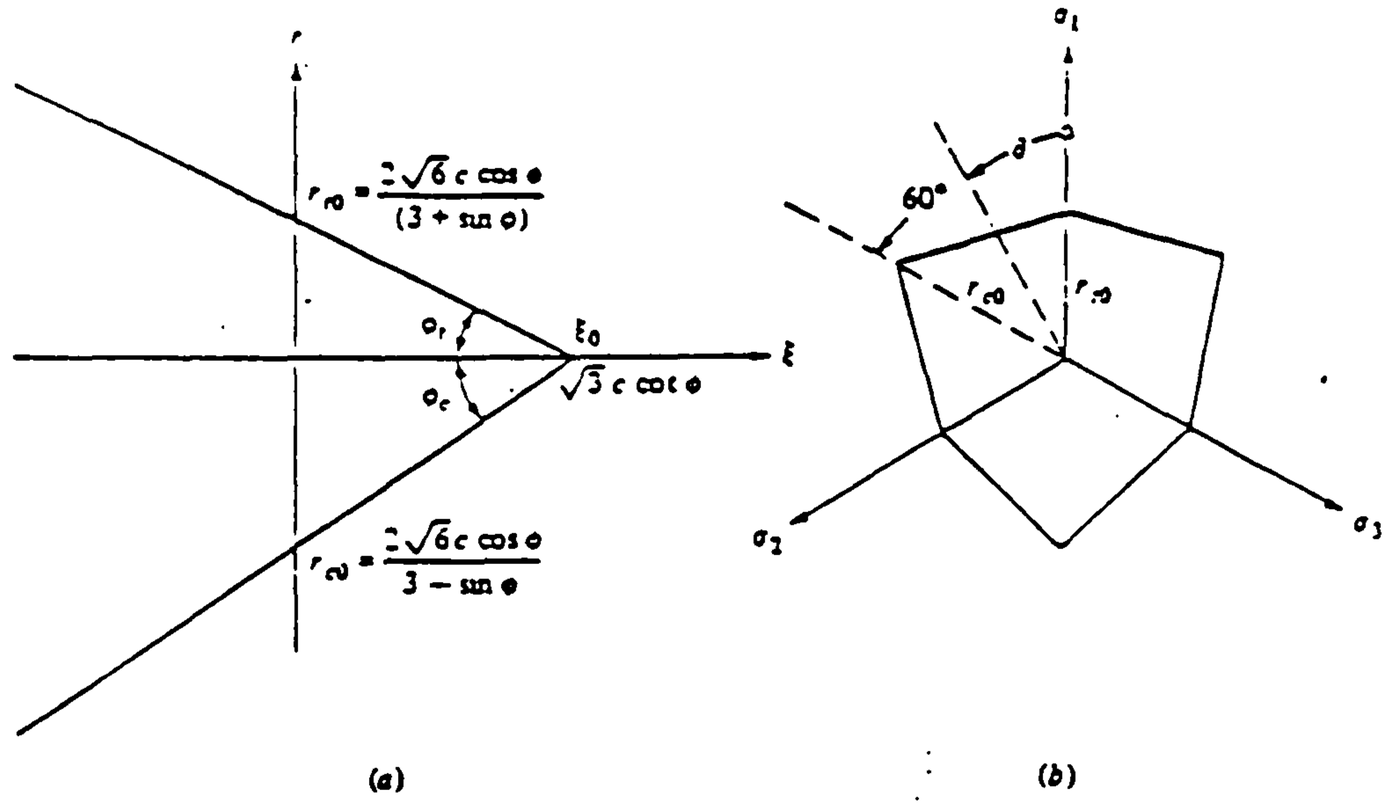

Fig.(4-16) Mohr-Coulomb criterion: (*a*) meridian plane, $\theta = 0°$; (*b*) π plane:

$$\tan\phi_t = \frac{2\sqrt{2}\sin\phi}{3 + \sin\phi} \qquad \tan\phi_c = \frac{2\sqrt{2}\sin\phi}{3 - \sin\phi}$$

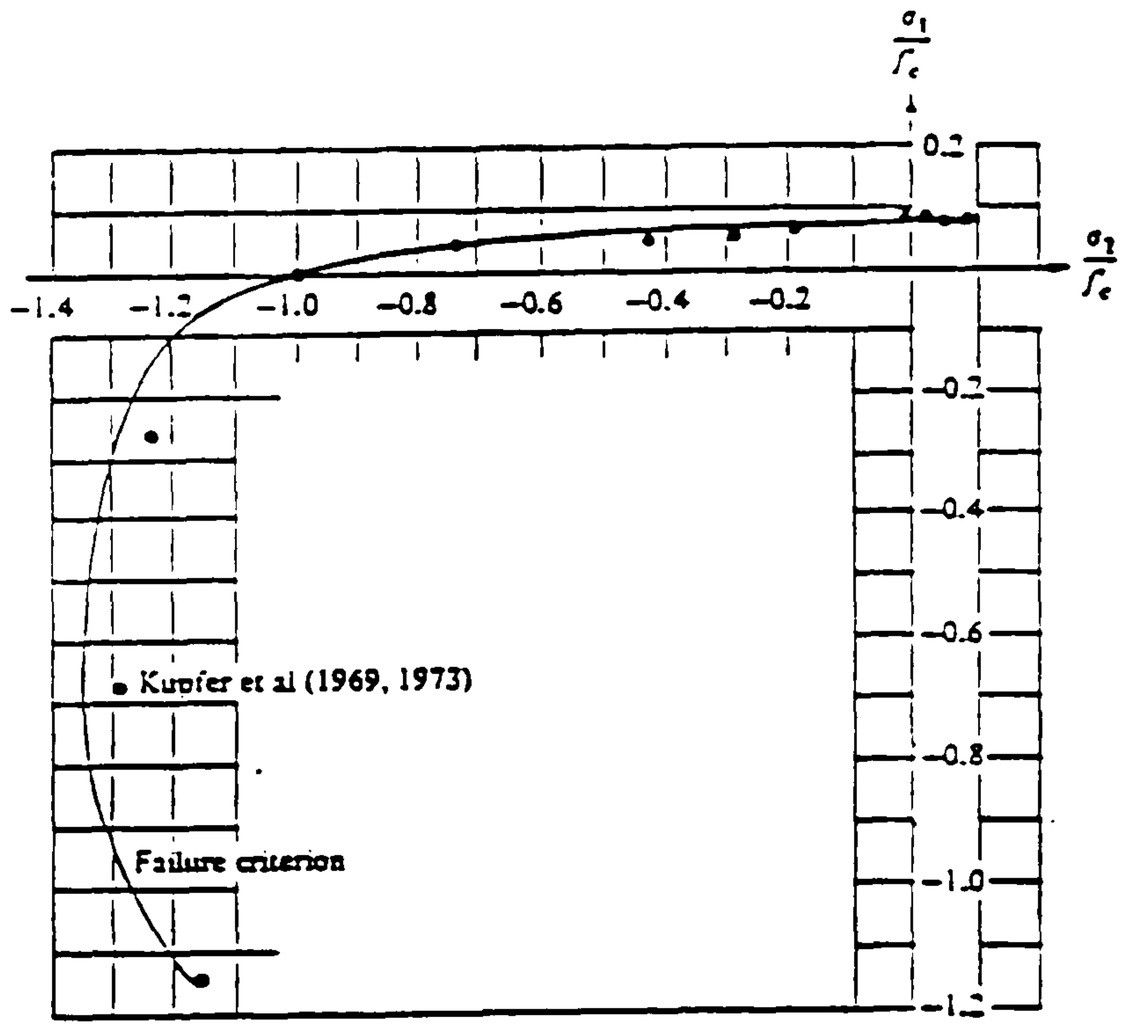

Fig.(4-17) Comparison between the Ottosen criterion ($f_t'/f_c' = 0.08$) and biaxial tests ($f_c' = 8.5$ kips/in^2 = 59.4 MPa). (Ottosen 1977)(48)

4-2-4 Kotsovos-Newman Criterion (1978)

Kotsovos and Newman (34) assumed that for design purposes concrete should be considered incapable of sustaining tensile stresses, they expressed the failure envelopes of Fig.(4-18) in terms of Octahedral stresses as follows.

$$\left.\begin{aligned} \frac{\tau_{oc}}{f_c} &= 1.417\frac{\sigma_o}{f_c} \qquad \text{for } \frac{\sigma_o}{f_c} \leqslant 0.283 \\ \frac{\tau_{oc}}{f_c} &= 0.671\frac{\sigma_o}{f_c} + 0.211 \qquad \text{for } \frac{\sigma_o}{f_c} > 0.283 \end{aligned}\right\} \quad (4.30)$$

$$\left.\begin{aligned} \frac{\tau_{oe}}{f_c} &= 0.707\frac{\sigma_o}{f_c} \qquad \text{for } \frac{\sigma_o}{f_c} \leqslant 0.624 \\ \frac{\tau_{oe}}{f_c} &= 0.496\frac{\sigma_o}{f_c} + 0.131 \qquad \text{for } \frac{\sigma_o}{f_c} > 0.624 \end{aligned}\right\} \quad (4.31)$$

In which τ_{oc} and τ_{oe} are the values of τ_o for $\sigma_1>\sigma_2=\sigma_3$ and $\sigma_1=\sigma_2>\sigma_3$ respectively.

For $\sigma_1>\sigma_2>\sigma_3$ σ_o can be predicted by interpolation using the Willam and Warnke (67) formula

$$\tau_o(\theta) = \frac{2\tau_{oc}(\tau_\alpha^2-\tau_{oe}^2)\cos\theta}{4(\tau_{oc}^2-\tau_{oe}^2)\cos^2\theta+(\tau_{oc}-2\tau_{oe})^2} +$$

$$\frac{\tau_{oc}(2\tau_{oe}-\tau_{oc})[4(\tau_{oc}^2-\tau_{oe}^2)\cos^2\theta+5\tau_{oe}-4\tau_{oc}\tau_{oe}]^{1/2}}{4(\tau_{oc}^2-\tau_{oe}^2)\cos^2\theta+(\tau_{oc}-2\tau_{oe})^2} \qquad (4.32)$$

in which τ_o, σ_o and θ are defined by equations (4.12), (4.13), (4.15) respectively.

4-2-5 Montague-Kormi Criterion (1982)

The failure criterion proposed by Montague and Kormi (42) assumes that, irrespective of the ratios of σ_1, σ_2 and σ_3, failure of concrete under a compressive stress state takes place when the unit volume energy causing shear distortion reaches a unique value equal to that which exists at failure in a uniaxial state of stress. The total energy stored in a concrete element under load is composed of two components E_σ and E_τ.

E_σ is related to the octahedral normal stress so defined by Eq.(4.12)

$$E_\sigma = 3\int_o^{\sigma_o} \sigma_o \, d\varepsilon_{oc} \qquad (4.33)$$

E_τ is related to the octahedral shear stress τ_o defined by Eq.(4.13)

$$E_\tau = 3 \int_0^{\tau_o} \tau_o \, d\gamma_{oc} \qquad (4.34)$$

The total energy is

$$E_T = E_\tau + E_\sigma \qquad (4.35)$$

During cracking a transfer of energy occurs between E_τ and E_σ, leading to an increase in the octahedral normal stress σ_o by σ_i (such that $\sigma^*=\sigma_o+\sigma_i$) and a reduction in the octahedral shear τ_o to τ^*. This transfer of loading is regarded as an irreversible process. By assuming the energy loss due to internal friction and temperature change is negligible, Eq.(4.35) can be written as

$$E_T = 3\int_0^{\sigma_o^*} \sigma_o \delta\varepsilon_o + 3\int_0^{\tau_o^*} \tau_o d\gamma_o \qquad (4.36)$$

To evaluate σ_c^* and τ_c^* Montague and Kormi used the functional stress-strain relationships obtained by Kotsovos and Newman (34)

$$\varepsilon_o = \frac{\sigma_o}{3\gamma_o} + a\sigma_o^b \tag{4.37}$$

$$\gamma_o = \frac{\tau_o}{2G_o} + c\tau_o^d \tag{4.38}$$

$$\frac{\sigma 1}{f_c} = \frac{k}{1 + l(\sigma_o/f_c)^m} \tag{4.39}$$

In which a,b,c,d,k,l,m and n are empirically derived constants stated in terms of f_c. For more details of these constants reference (42) can be consulted.

The total energy becomes

$$E_T = 3\left[\frac{\sigma_o^{*2}}{6k_o} + \frac{ab}{b+1}\sigma_c^{*(b+1)}\right] + 3\left[\frac{\tau_o^{*2}}{4G_o} + \frac{cd}{d+1}\tau_o^{*(d+1)}\right] \tag{4.40}$$

As a result of cracking, Eq(4.39) becomes

$$\frac{\sigma_c^*}{f_c} = \frac{\sigma_o}{f_c} - \frac{k}{1+l(\sigma_o/f_c)^m}\left(\frac{\tau_o^*}{f_c}\right)^n \tag{4.41}$$

Iterative solution of the simultaneous equations (4.40) and (4.41) gives the values of σ_o^* and τ_o^* for any given input energy E_T.

Solution of equations (4.40) and (4.41) for ($E_T = \overline{E_T}$) yields the unique value of τ_c^* for which $\overline{E_T}$ is given by the area under the uniaxial stress-strain characteristic

$$\overline{E_T} = \int_o^{f_c} \sigma 1 \; d\varepsilon_1 \qquad \sigma_2 = \sigma_3 = 0 \tag{4.42}$$

Having a unique value of τ_o^* defined, Eqs(4.40) and (4.41) can be solved for any state of stress $\sigma_1:\sigma_2:\sigma_3$ to determine their values at failure.

The failure criterion of Montague and Kormi predicts an enhancement in strength by a factor of 1.2 when concrete is subjected to equal biaxial compressive stress compared with uniaxial compressive stress Fig.(4.19)

4-3 SIZE EFFECTS

Size effects on the strength of concrete have been observed in different types of structure, and are related to different aspects of the material (i.e ratio of aggregate size to element dimension, type of loading, crack width, shrinkage, internal temperature of concrete during hardening, etc.). The interaction of the parameters makes the total size effect a complicated problem and for the present there seems to be no general method to evaluate the effect of the size of the structural element on its strength. Some analytical approaches and empirical equations have been developed for some specific practical cases.

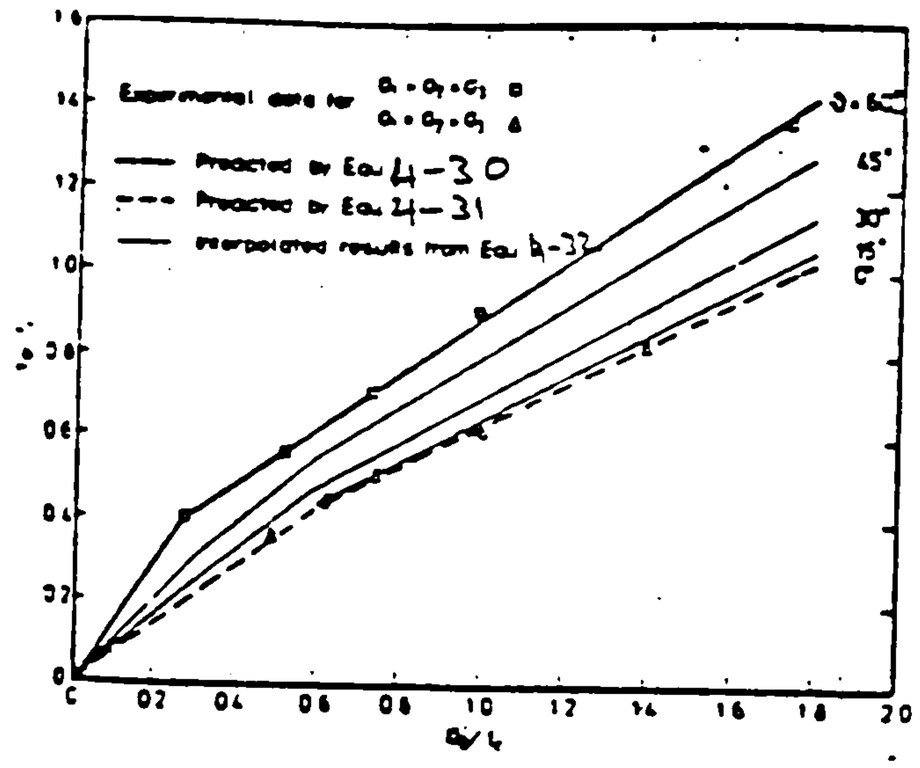

Fig.(4-18) Lower bound ultimate strength envelopes for concrete CA under multiaxial stress states (Kotsovos&Newman 1978)(34)

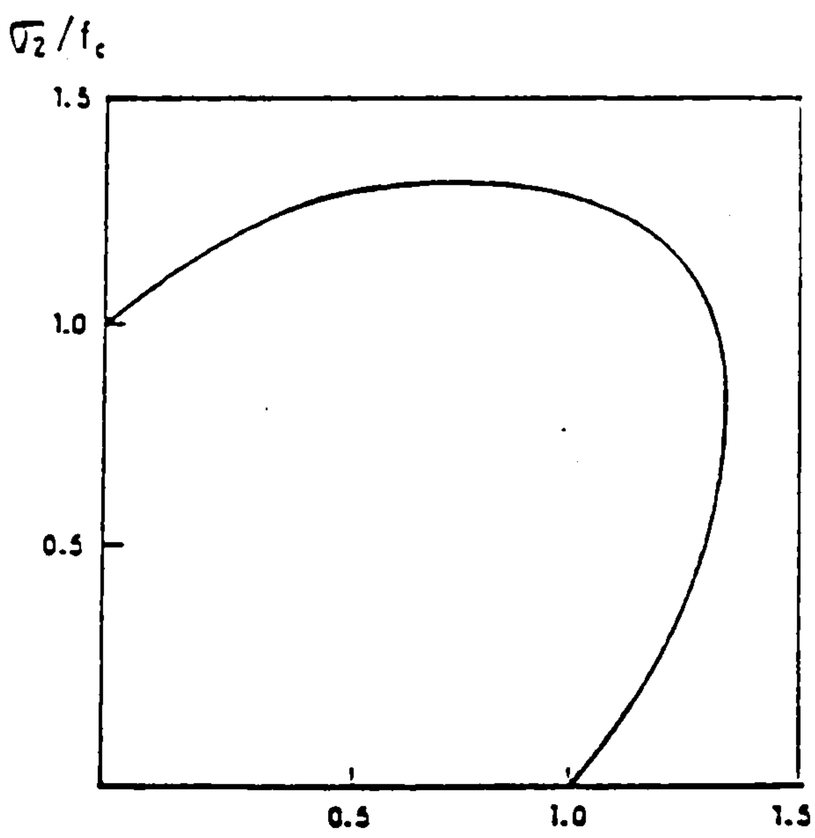

b) σ_1 σ_2 plane

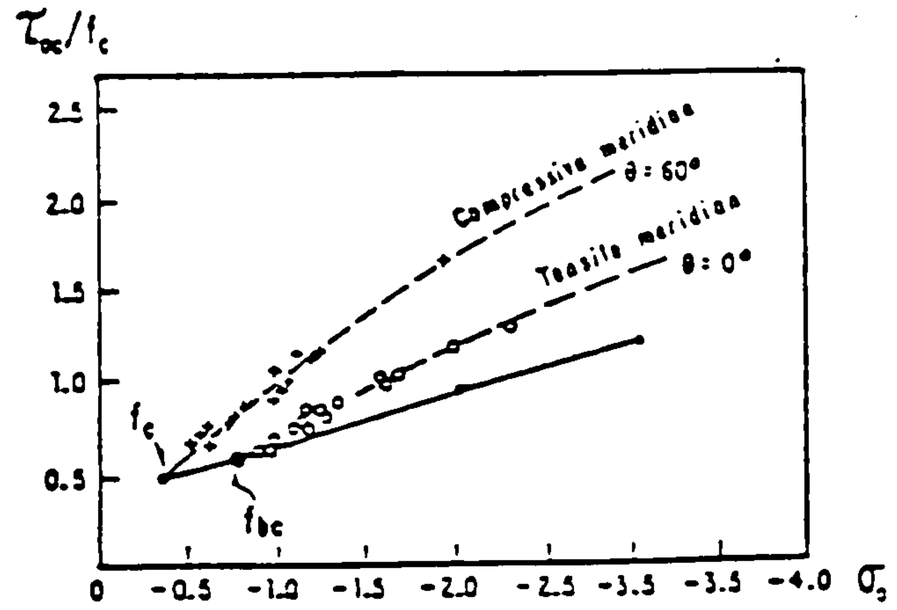

a) σ_{oc} τ_{oc} plane and test results of Mills and Zimmerman (1970)

Fig.(4-19) Failure surface traces for Montague and Kormi theory (1982) in the σ_{oc} τ_{oc} and σ_1 σ_2 planes (full lines)(42)

The classical fracture mechanics developed by Griffith (22) to treat the failure of glass has been applied to concrete in tension. Griffith used an elastic analysis to determine the release of strain energy (U) per unit increase in the area of fracture (A).

$$\frac{dU}{dA} = \frac{d}{dc}\left(\frac{\pi\ \sigma_o^2\ C^2}{2E}\right) = \frac{\pi\ \sigma_o^2\ C}{E} \qquad (4.43)$$

and he determined the work done in the course of crack formation

$$\frac{dW}{2A} = \frac{d}{dc}\ (2T_c) \qquad (4.44)$$

C is half of the crack length

σ_o is the uniform tensile stress normal to the plane of the crack

W is the work done in the course of crack formation

T is the surface energy per unit area of crack

Griffith then suggested that a crack would extend and lead to rupture when the rate of release of strain energy was at least equal to the rate of increase of surface energy i.e when

$$\frac{\pi\ \sigma_o^2\ C}{E} = 2T \qquad (4.45)$$

This gives the critical stress σ_c for a flawed material, i.e

one containing cracks, as

$$\sigma_c = \sqrt{\frac{2ET}{\pi\ c}} \qquad (4.46)$$

Various methods have been proposed to apply the ideas of fracture mechanics to concrete, but there seems to be a problem because in concrete the fracture front is not sharp but blunted by distributed cracking. However, fracture mechanics can give a simple idea of the probable influence of cracks, and can predict a scale effect in concrete in tension as a function of the flaw size or crack length.

The influence of scale on the shear resistance of members without shear reinforcement has been recognized from different sources (53,62,11,7).

In punching the size effect is probably related to the compressive stress concentration near the column.

A proposal developed by Bazant and Cao (7) uses the ratio d/aggregate size in a size factor

$$\xi = \sqrt{1 + (\lambda/\lambda_o)}$$

where λ= d/da is relative structure size (d/max. size of aggregate)

λ_o is empirical parameter characterizing the fracture energy of the material and shape of the structure.

According to Bazant and Cao's size-effect law, for a structure with a relatively small depth there is no influence of scale on

the nominal stress at failure Fig.(4.20). It seems that the proposal to use the ratio d/aggregate size is not very successful, Fig.(4.21) shows the scatter of the data for beams without shear reinforcement analysed by Bazant and Cao's formula.

Another proposal (53) is to relate the resistance to the effective depth (d) of the slab, Fig.(4.22) shows that the punching resistance is approximately proportional to $\sqrt[4]{1/d}$.

In this work the value of $V_{test}/x.c.\sigma_c.\sin\alpha$ from tests by the author and other researchers (30,56,20,43,51) is plotted against d see Fig.(4-23). A reasonable overall correlation is obtained with the square root ($\sqrt{1/d}$) relationship.

The function x cσ_c sinα is derived in the following chapter.

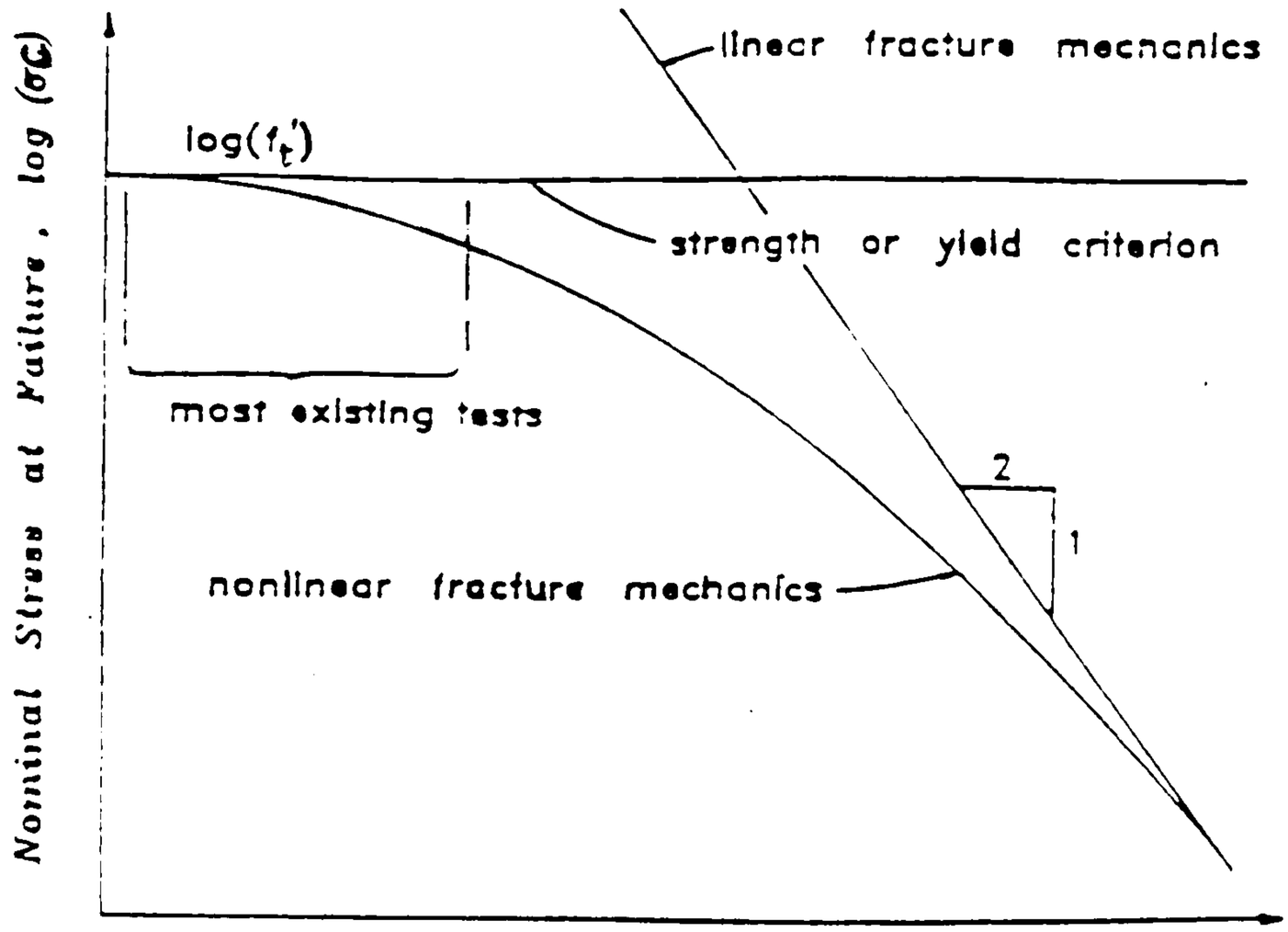

Fig.(4-20) Size-effect law for blunt fracture
(Bazant & Cao 1987) (7)

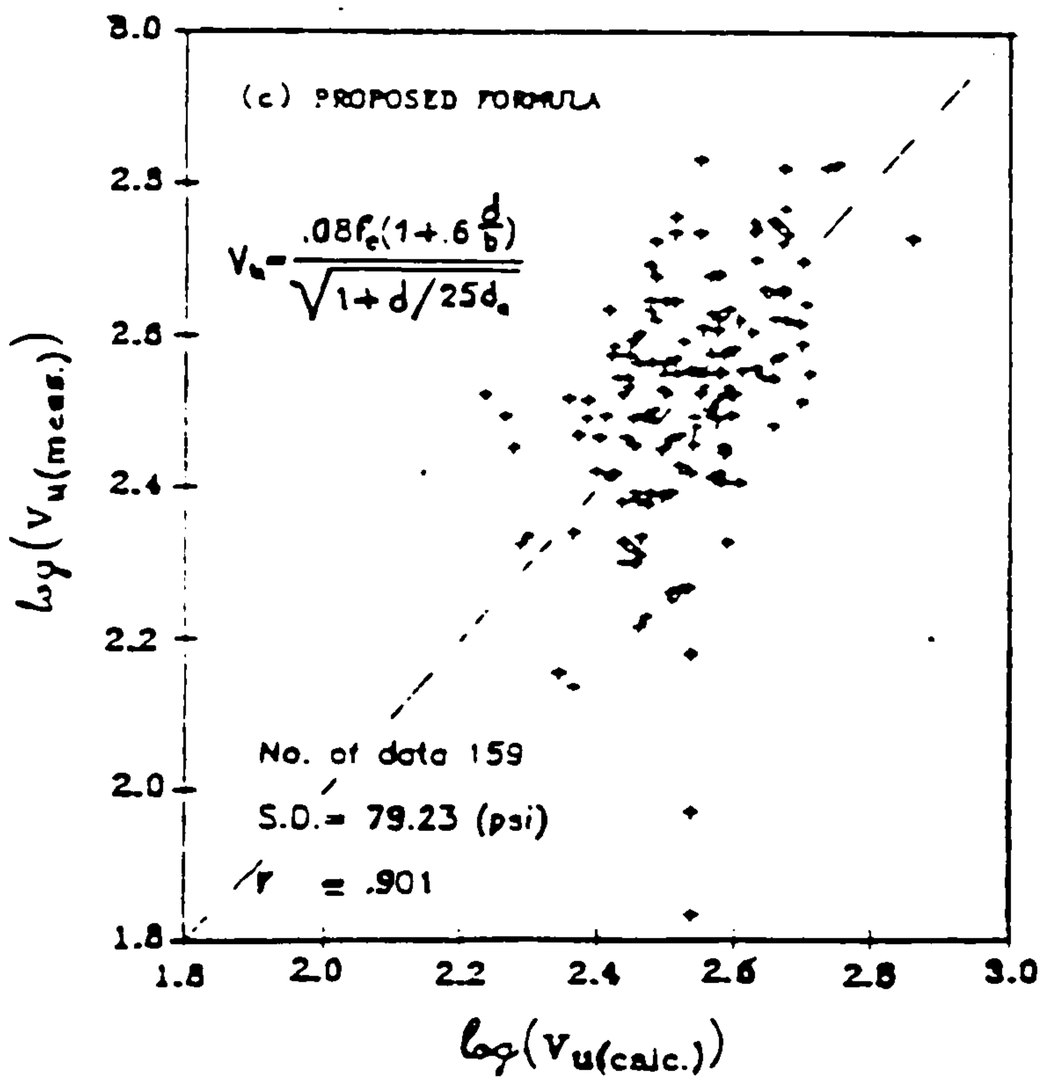

Fig.(4-21) Plot of measured versus calculated nominal shear strength values at ultimate load(Bazant& Cao 1987)(7)

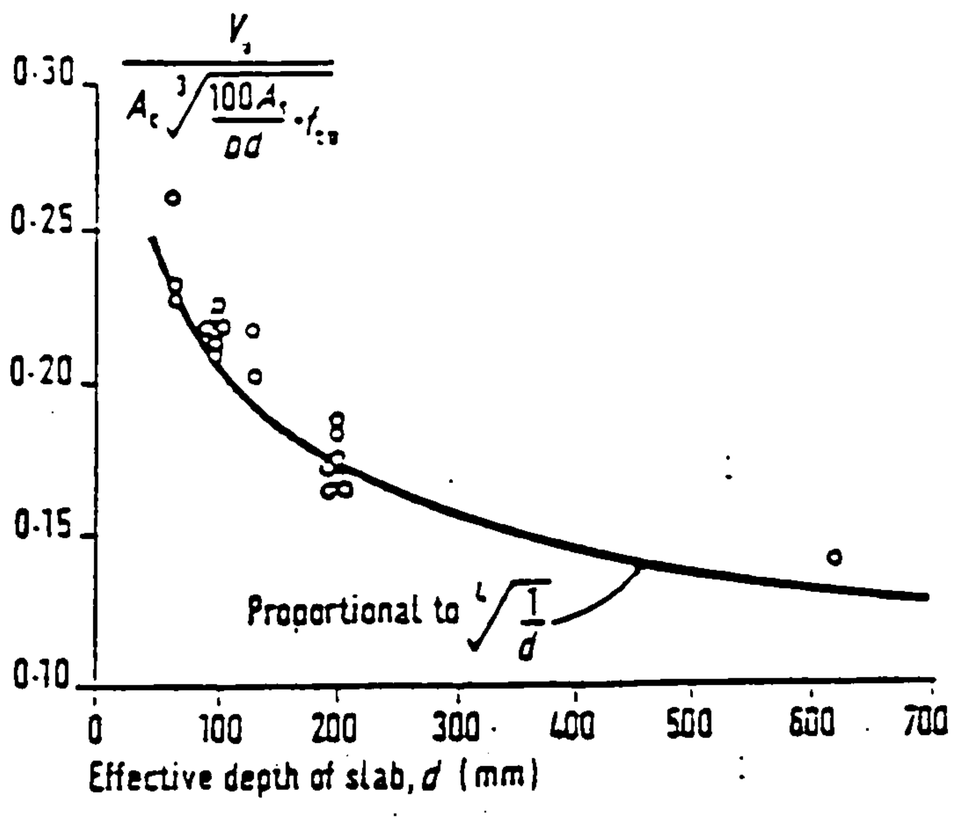

Fig.(4-22) Influence of slab depth on Punching resistance (Regan 1980)

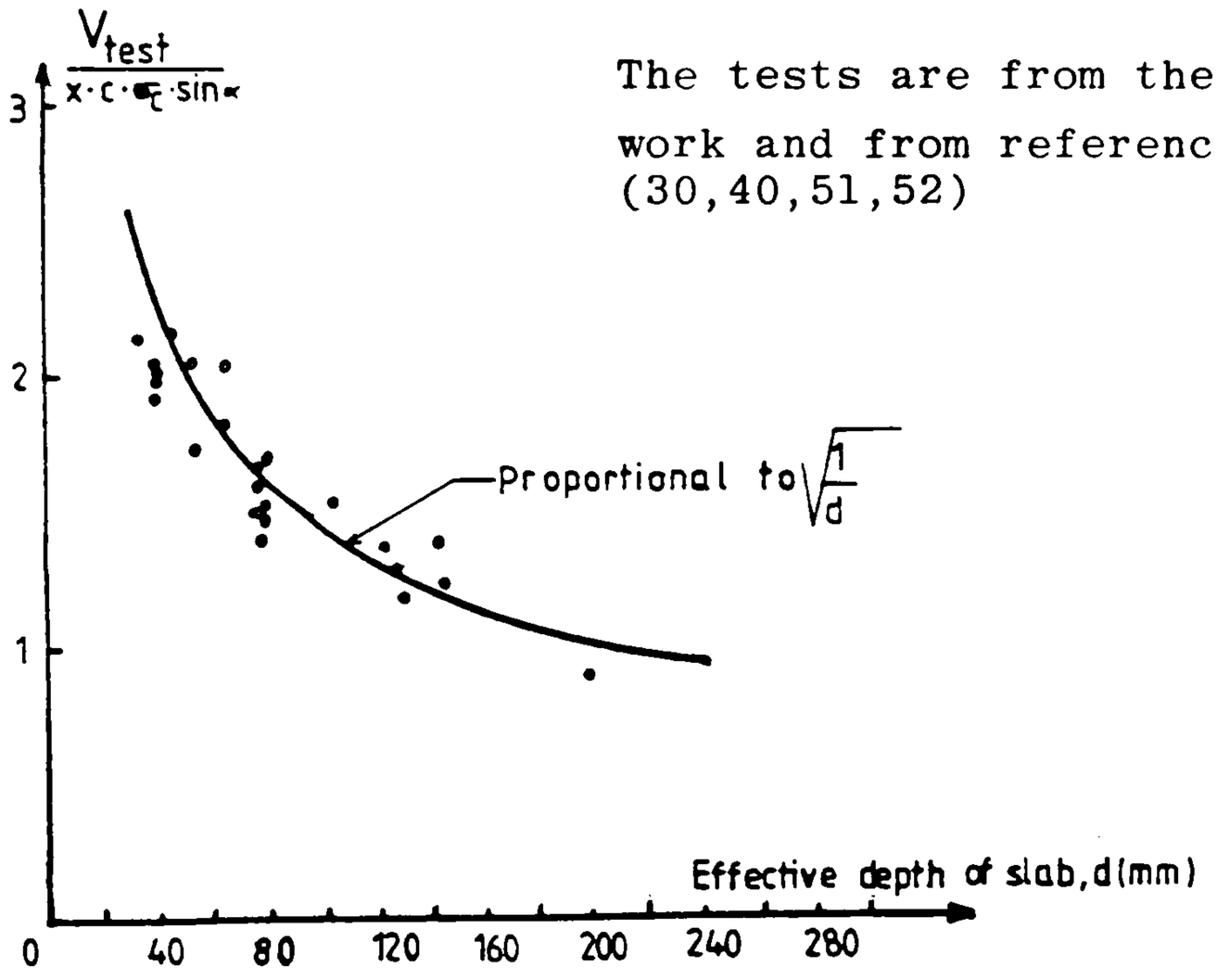

The tests are from the present work and from references (30,40,51,52)

Fig.(4-23) Influence of slab depth on punching resistance

CHAPTER FIVE

PUNCHING RESISTANCE

5-1 Proposed Model - Symmetric Punching

A great deal of information has been obtained from experimental investigations with respect to the qualitative effects of the numerous variables on the ultimate shearing strength. This information makes it possible to establish, a semi-theoretical approach for the ultimate strength reflecting the behaviour of the slabs with good accuracy. The model in the following represents the area of slabs around a column bounded by a circumferential line of contraflexure. The reinforcement is modelled as having radial and tangential resistances.

From tests it has been seen that at the first stages of loading no cracks are observed on the slab surface. Then as the load increases, cracks appear on the tension face, dividing the slab in the vicinity of the column into radial segments having almost linear deflection profiles see Fig.(3-1) and upon further increase of the loads, the cracks open up reducing the slab stiffness and resulting in large deflections. An inclined crack forms around the column well before punching occurs but does not have any major effect on the deflected shape of the slab so long as two-way flexural reinforcement is present. Finally the slab fails when the central cone is pushed through the slab.

The flexural crack pattern is considered to be represented well by dividing the slab into rigid segments, that rotate around centres of rotation, C.R. located at the column face on the level of the neutral axis Fig.(5-1a). This results in the reinforcement crossing the tangential crack at the column face yielding see Figures (5-1a)(3-10) as confirmed by Kinnunen and Nylander (30) and Anis (2).

The inclined crack caused by the radial shear stresses has an inclination approximately equal to 25^{o} see Fig.(5-1b) which value has been verified from the author's test specimens in the present work.

5-1-1 Neutral Axis of the segmental Element

In the proposed method of calculation of punching shear resistance, the slab is divided into four rigid segments. Each rigid segment shown in Fig.(5-2a) is subjected to the internal steel and concrete forces obtained from the rotation of the element around the centre of rotation C.R., and the external load. The forces on an element are:

- The external load $P\Delta\phi/2\pi$ acting on the circumference of the slab, where $\Delta\phi$ is the angle of the sector element.
- F_{ct} the radial resultant of the tangential forces in the concrete.
- F_{cr} the radial force in the concrete at the column face.
- F_{sr} the radial force in the steel cutting across the shear crack.

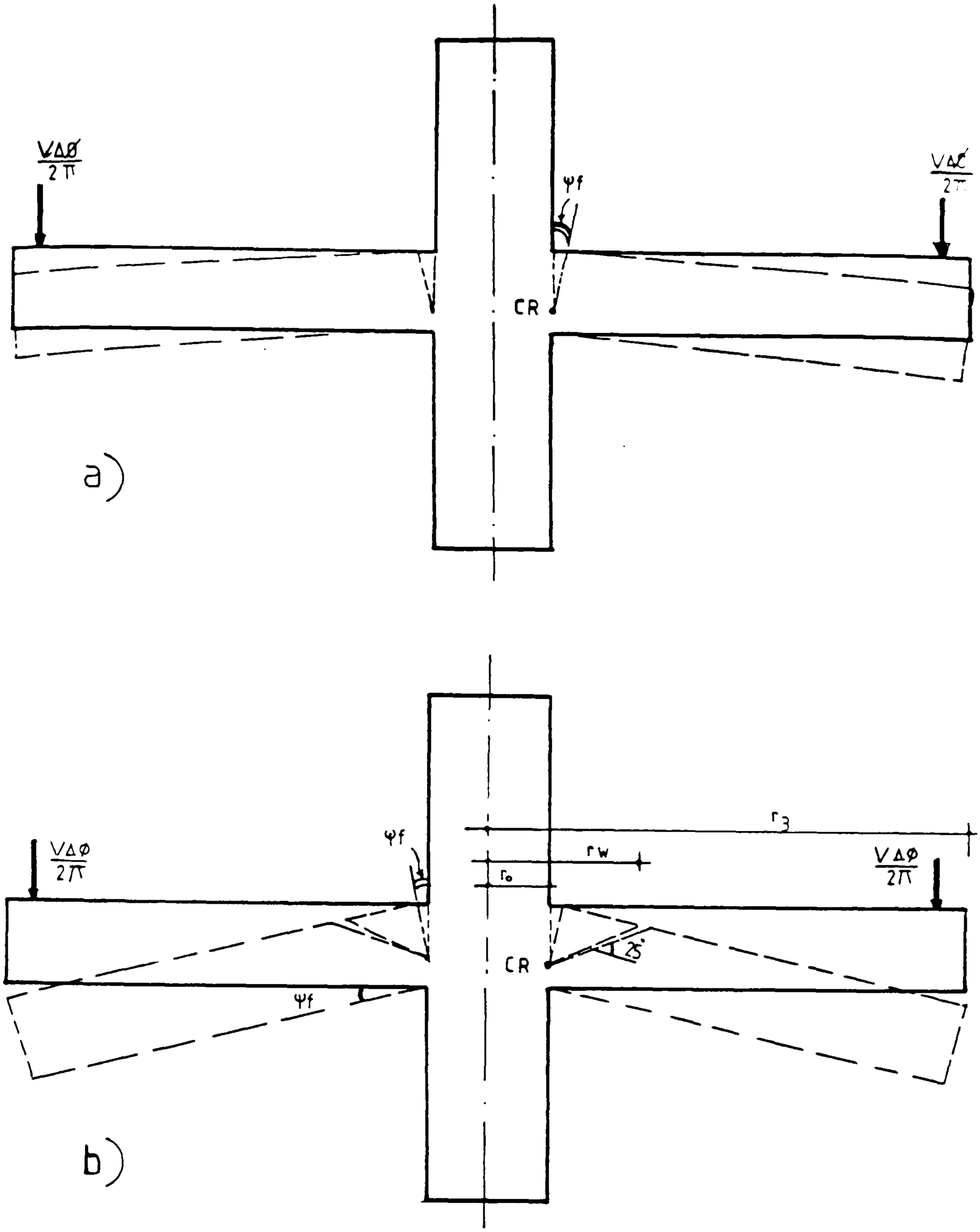

Fig.(5-1) Model of Slab Deformation

a) without shear crack b) with shear crack

$\Delta\phi$ = angle subtended by a radial segment

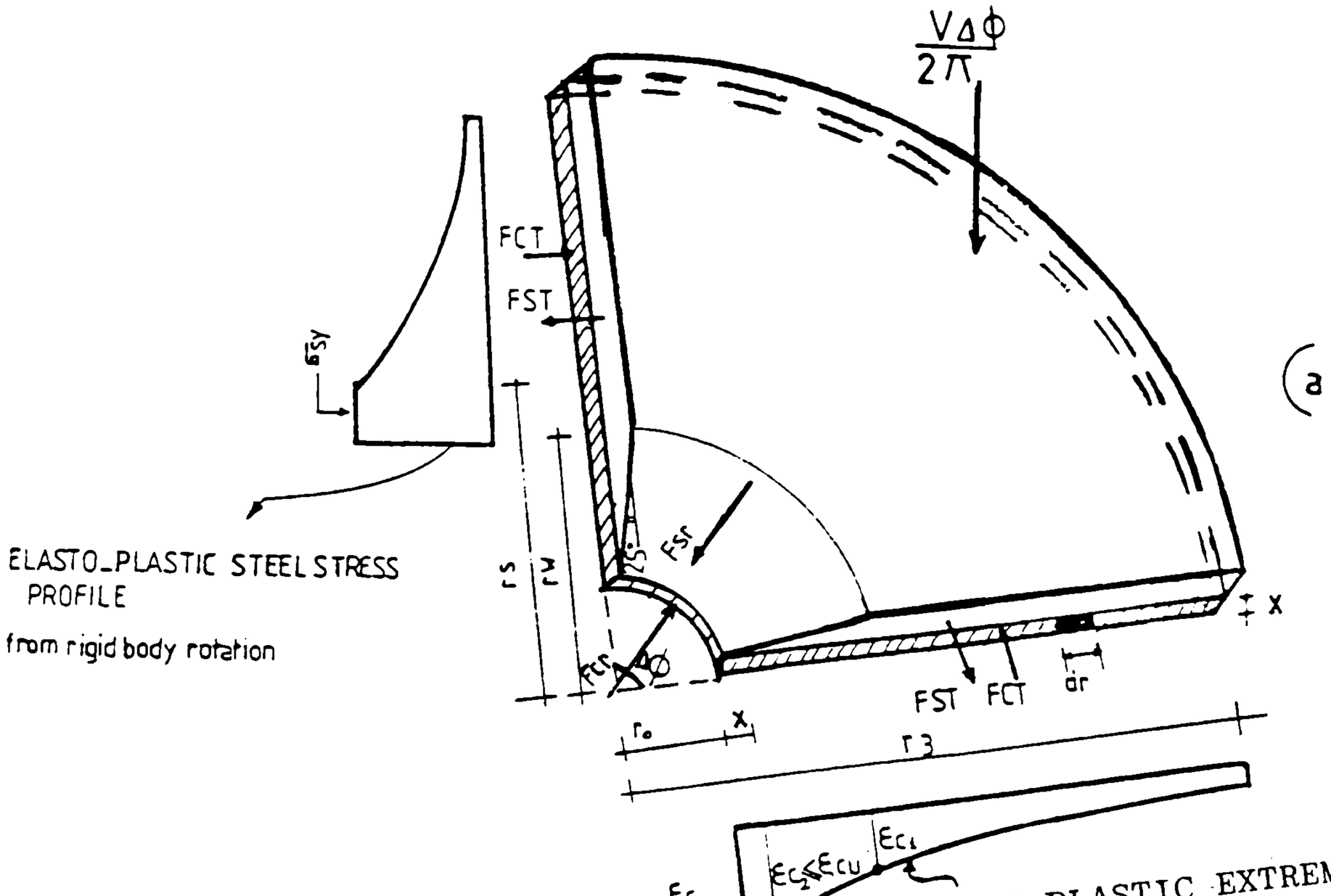

Fig.(5-2) Segment element with steel and concrete strain distributions together with concrete stress block along the radius

- F_{st} the resultant of the tangential forces in the steel.

Using the idealized stress-strain curve for concrete Fig.(4-3) and the strain profile for a rigid body rotation Fig.(5-2a), and also assuming that the radial concrete stress at the column face is known, as will be described later, the concrete forces on a rigid segment can be calculated from the rotation at failure ψ_f.

From the rigid body rotation, the tangential strain at the compressed face

$$\varepsilon_{ct} = \psi_f . x/r \qquad (5\text{-}1)$$

and the tangential concrete force obtained from the stress block associated with the concrete strain for an element at radius r and of width dr is

$$dF_{ct} = f_c \, K_c \, x \, K_x \, dr \qquad (5\text{-}2)$$

in the above equation K_c and K_x are functions of the extreme fibre concrete strain on the idealized stress-strain curve as shown in Fig.(5-2b) where

K_c is extreme fibre stress

K_x is average stress/extreme fibre stress

The values of K_c and K_x can be expressed in terms of ψ_f and r

$$r_{\varepsilon c1} = \psi_f . x/\varepsilon_{c1} \qquad (5\text{-}3)$$

$$r_{\varepsilon cu} = \psi_f . x/\varepsilon_{cu} \qquad (5\text{-}3')$$

For $r_o < r < r_{\varepsilon cu}$

$K_x = 0.85$

$K_c = 0.85$

For $r_{\varepsilon cu} < r < r_{\varepsilon c1}$

$$K_x = 0.5 + 0.35\left[\frac{(\psi_f x/r) - \varepsilon_{c1}}{(\varepsilon_{cu} - \varepsilon_{c1})}\right] \leqslant 0.85$$

$$K_c = 0.85$$

For $r_{\varepsilon c1} < r < r_3$

$$K_x = 0.5$$

$$K_c = 0.85\ \psi_f (x/\varepsilon_{c1}.r)$$

And F_{ct} can be calculated from Eq.(5-2) as

For $r_o > r_{\varepsilon c1}$

$$F_{ct} = 0.425\ f_c\ x^2\ (\psi_f/\varepsilon_{c1})\ \ln\ (r_3/r_o) \qquad (5\text{-}4)$$

For $r_{\varepsilon cu} \leqslant r_o \leqslant r_{\varepsilon c1}$

$$F_{ct} = 0.45\ f_c\ x\ \left[(r_{\varepsilon c1} - r_o) + \frac{\ln\left(\frac{r_{\varepsilon c1}}{r_o}\right) - \varepsilon_{c1}(r_{\varepsilon c1} - r_o)}{\varepsilon_{cu} - \varepsilon_{c1}} + x\frac{\psi_f}{\varepsilon_{c1}} \ln\left(\frac{r_3}{r_{\varepsilon c1}}\right)\right]$$

.... (5-5)

For $r_o \leqslant r_{\varepsilon cu}$

$$F_{ct} = f_c\ x\ [0.722(r_{\varepsilon cu} - r_o) + 0.425[r_{\varepsilon c1} - r_{\varepsilon cu} +$$

$$+ \frac{\ln\left(\frac{r_{\varepsilon c1}}{r_{\varepsilon cu}}\right) - \varepsilon_{c1}(r_{\varepsilon c1} - r_{\varepsilon cu})}{\varepsilon_{cu} - \varepsilon_{c1}} + x\frac{\psi_f}{\varepsilon_{c1}} \ln\left(\frac{r_3}{r_{\varepsilon c1}}\right)] \qquad (5\text{-}6)$$

For square slabs and square columns

$r_3 = 2A/\pi$

$r_o = 2a/\pi$

A is the slab length = 0.5 x span and

a is the side length of the column.

For rectangular slabs and columns r_o and r_3 should be taken as if the slabs had circular perimeters

$r_3 = (A + B)/\pi$

$r_o = (a + b)/\pi$

A = 0.5 x slab length

B = 0.5 x slab width

a and b are length and width of loaded area or column.

For continuous slabs r_3 should be taken at a distance where the radial bending moment is equal to zero (i.e. approx.0.25 span). The radial concrete force at the column face F_{cr} can be calculated as a first approximation as

$$F_{cr} = f_{cc}\ \xi \times c \qquad (5\text{-}7)$$

- $f_{cc} = 0.85\ f_c \times 1.2$

Where the factor 1.2 takes into consideration the effect of biaxial stresses near the column as described in section 4-1-2

- c is the length of the frontal bearing area of the radial segment shown in Fig.(5-2) c = column perimeter / 4 = $\pi r_o/2$

- ξ is the size coefficient defined in section 4-3

$$\xi = \sqrt{d/200}$$

Neglecting the differences between F_{cr} and its horizontal component

$$F_c^* = F_{cr} + F_{ct}\ \Delta\phi \qquad (5\text{-}8)$$

Using the idealized stress-strain curve for ordinary steel Fig. (5-3) and the failure rotation ψ_f from the rigid body rotation the tangential steel strain is defined as

$$\varepsilon_{st} = \psi_f \ (d/r) \ (1 - (x/d)) \qquad (5\text{-}9)$$

The radius at which the steel yields is

$$r_s = \psi_f \ (d/\varepsilon_{sy}) \ (1 - (x/d)) \qquad (5\text{-}10)$$

The total tangential steel force acting on the radial segment can be expressed as below

For the elastic state..... .....(a)

$r_s < r_w$

$$F_{st} = \int_{r_w}^{r_3} \rho_t \ \sigma_{st} \ d \ dr \qquad (5\text{-}11)$$

Where

σ_{st} is the steel stress in tangential direction.

$$F_{st} = \rho_t \ f_y \ d \ r_s \ \ln(r_3/r_w) \qquad (5\text{-}11')$$

The radial steel forces acting on the radial segment are given by

$$F_{sr} = \rho_r \ f_y \ d \ r_s \ \Delta\phi \qquad (5\text{-}12)$$

For the elasto-plastic state .....(b)

$r_s > r_w$

$$F_{st} = \rho_t \ f_y \ d((r_s - r_w) + r_s \ \ln(r_3/r_s)) \qquad (5\text{-}13)$$

$$F_{sr} = \rho_r \ f_y \ d \ r_w \ \Delta\phi \qquad (5\text{-}14)$$

where r_w is the radius at which the failure surface intersects the plane of the reinforcement. $r_w = r_o + (d-x)\cot 25^o$ (5-15)

where ρ_t is the ratio of tangential reinforcement

ρ_r is the ratio of radial reinforcement

d is the slab effective depth

The total radial steel force on the segment for either case (a) or (b) is

$$F_s^* = F_{sr} + F_{st}\ \Delta\phi \qquad (5\text{-}16)$$

To calculate the neutral axis depth in the slab segment the condition of equilibrium of the forces in the radial direction is applied

$$F_c^* - F_s^* = 0 \qquad (5\text{-}17)$$

Where F_c^* is found from eq.(5-8) and F_s^* from eq.(5-16).

In the calculations $\Delta\phi$ and ε_{sy} are taken as, $\Delta\phi$=1.57 radians and $\varepsilon_{sy} = f_y/E_s$.

For non-uniform arrangements of steel the ratio of reinforcement is taken as an average over the length and the width of the slab (i.e. $\rho = (\rho_x + \rho_y)/2$)

The rotations of the slab measured in the tests carried out for this thesis, and in other works (30) (52) indicate that the segment rotation ψ_f varied from 0.008 to 0.016 radians in those specimens which failed in shear. Within this range an increase or decrease in the value of the segment rotation of the order of 0.004 radians has little influence on the calculation of the neutral axis depth see Table (5-1). In the present work the segment rotation ψ_f is taken as 0.012 radians.

Table (5-1) The influence of segment rotation

on the neutral axis depth

ψ radian	x mm		
0.008	14.7	25.8	16.7
0.009	14.8	25.5	17.4
0.010	15.0	25.3	17.6
0.011	15.1	25.3	17.5
0.012	15.0	25.5	17.4
0.013	14.9	25.6	17.3
0.014	14.8	25.7	17.2
0.015	14.8	25.7	17.2
0.016	14.7	25.7	17.1
0.017	14.6	25.6	17.1
0.018	14.6	25.5	17.0
0.020	14.5	25.2	17.0
0.030	14.4	21.3	16.8
	SLAB B1 (PRESENT WORK) ρ = 1.00 % f_c= 27 N/mm^2 d = 62 mm ψ_f= 0.015 radian f_y= 530 N/mm^2	SLAB IA15a5 (Ref. 30) ρ = 0.8 % f_c= 26.8 N/mm^2 d = 117 mm ψ_f= 0.012 radian f_y= 450 N/mm^2	SLAB I5 (Ref. 52) ρ = 0.75 % f_c= 28.2 N/mm^2 d = 77 mm ψ_f= 0.017 radian f_y= 480 N/mm^2

5-1-2 Analysis of the Proposed Model and Failure Criteria.

After the internal forces acting on the rigid sector element have been formulated, the neutral axis depth can be found.

Referring to the model shown in Fig.(5-4) and using the vertical equilibrium condition :

$$V\Delta\phi/2\pi = F_{cr}\cdot\sin\alpha \qquad (5\text{-}18)$$

Where:

$$F_{cr} = \sigma_c\cdot x\cdot c\cdot\xi \qquad (5\text{-}19)$$

x is the neutral axis depth

c The length of the bearing area of the radial segment

ξ The size factor, which has been taken as $\sqrt{200/d}$ as in Section 4-3, with d in mm

σ_c is the concrete bearing capacity.

To make use of the equilibrium and compatibility equations so set up, a failure criterion is necessary. The distribution of stresses in the region of the slab-column joint is very complex and it must be expected that the strength of the concrete in this region is different from that in simple compression or shear alone. As has been mentioned in sections 4-1 and 4-2 the strength of concrete loaded in a certain direction is to a large degree dependent upon the magnitudes of the stresses in other directions. However in view of the complexity of the local stress distribution it is not possible to express the criterion of failure as a simple function of the ratios of tangential, radial and vertical stresses.

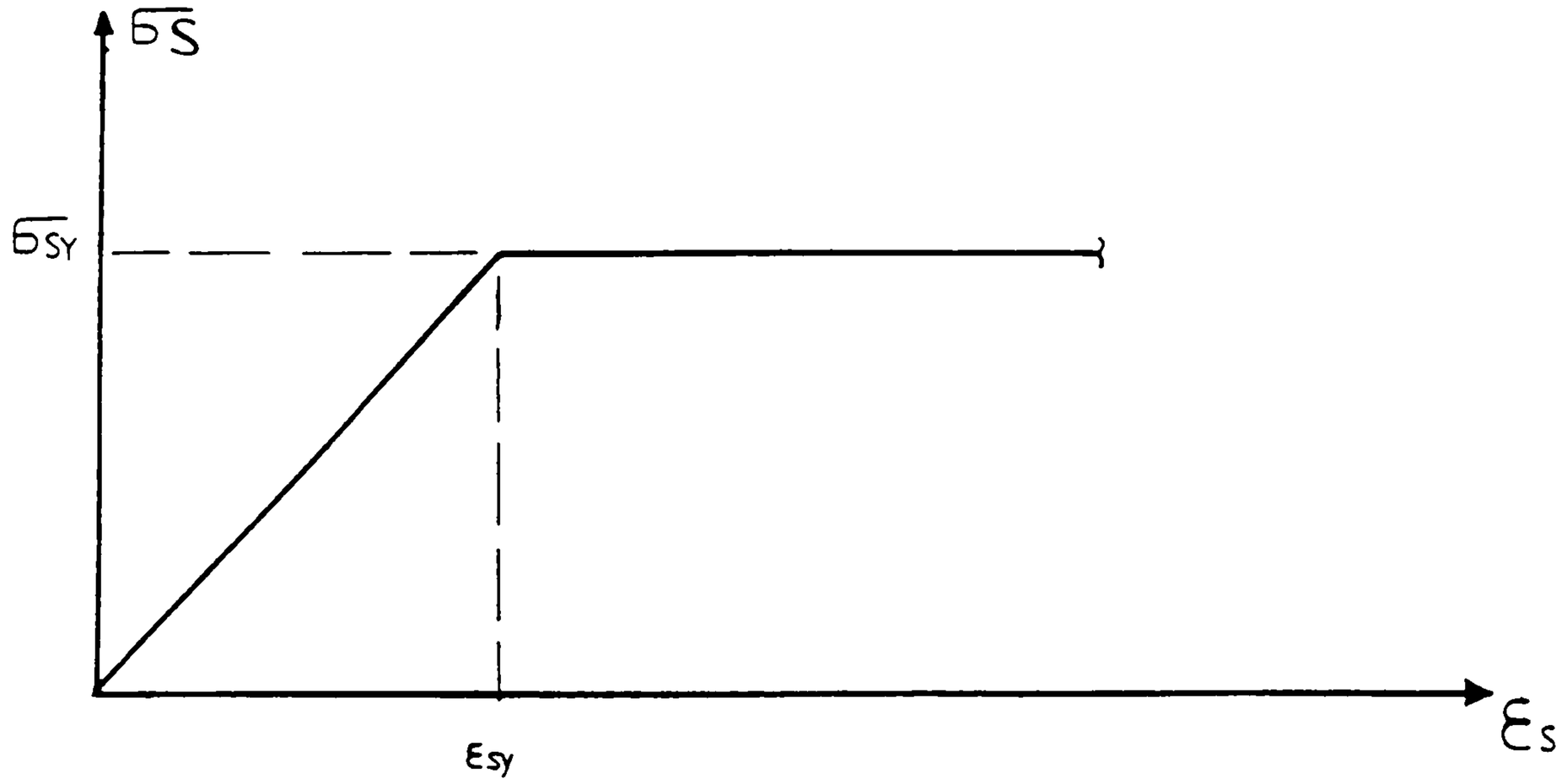

Fig.(5-3) Stress-strain curve for ordinary steel

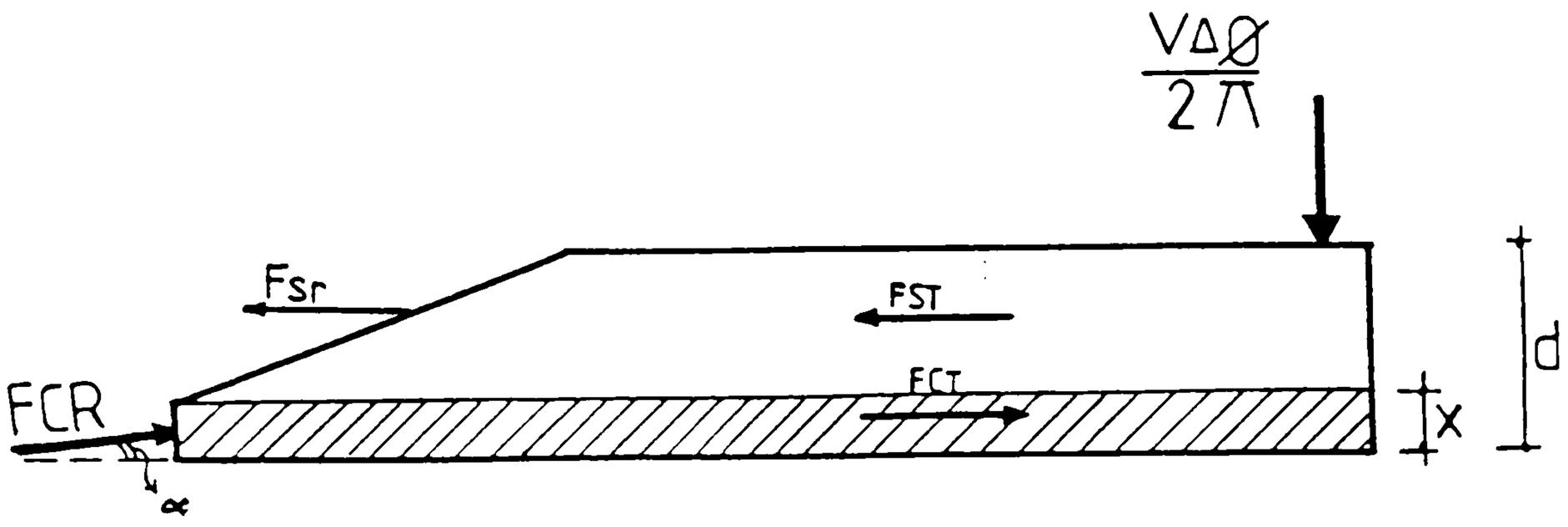

Fig.(5-4) Segment element

The failure takes the form of the front part of the radial segment failing to support the bearing force at the column face and test data show that the failure can be taken to occur when the angle of the compressive force (α) reaches 15^o see Figs.(5-4), (5-5) and the compressive stress at the front part of the radial segment reaches the stress limit determined on the basis of a statistical analysis of the available test data, as described below.

Fig.(5-5) shows the relationship between (σ_c/f_c) and (d/r_o) for some of the available test results. The values of σ_c have been calculated by equating $F_{cr} \cdot \sin 15^o$ to $V \cdot \Delta\phi/2\pi$.

The curve representing the relationship shown is :

$$\sigma_c/f_c = 1.43 \ln 3.33(d/r_o) \qquad (5\text{-}20)$$

This expression is applicable in the ranges $0.5 \leqslant \sigma_c/f_c \leqslant 3.5$ and $10 \leqslant f_c \leqslant 55$ N/mm^2.

The (σ_c/f_c) values calculated using equation (5-20) are in agreement with results obtained from six pyramid specimens tested by the author. The geometry and the test results are given in Table (5-2).

Using the vertical equilibrium condition equation (5-18), and the proposed failure criterion, the punching shear capacity of concentrically loaded reinforced concrete flat slabs can be calculated from the following equation :

$$V_u = 0.37 \cdot f_c \cdot \ln 3.33(d/r_o) \cdot x \cdot c_t \cdot \sqrt{200/d} \qquad (5\text{-}21)$$

Where :

c_t is the column perimeter.

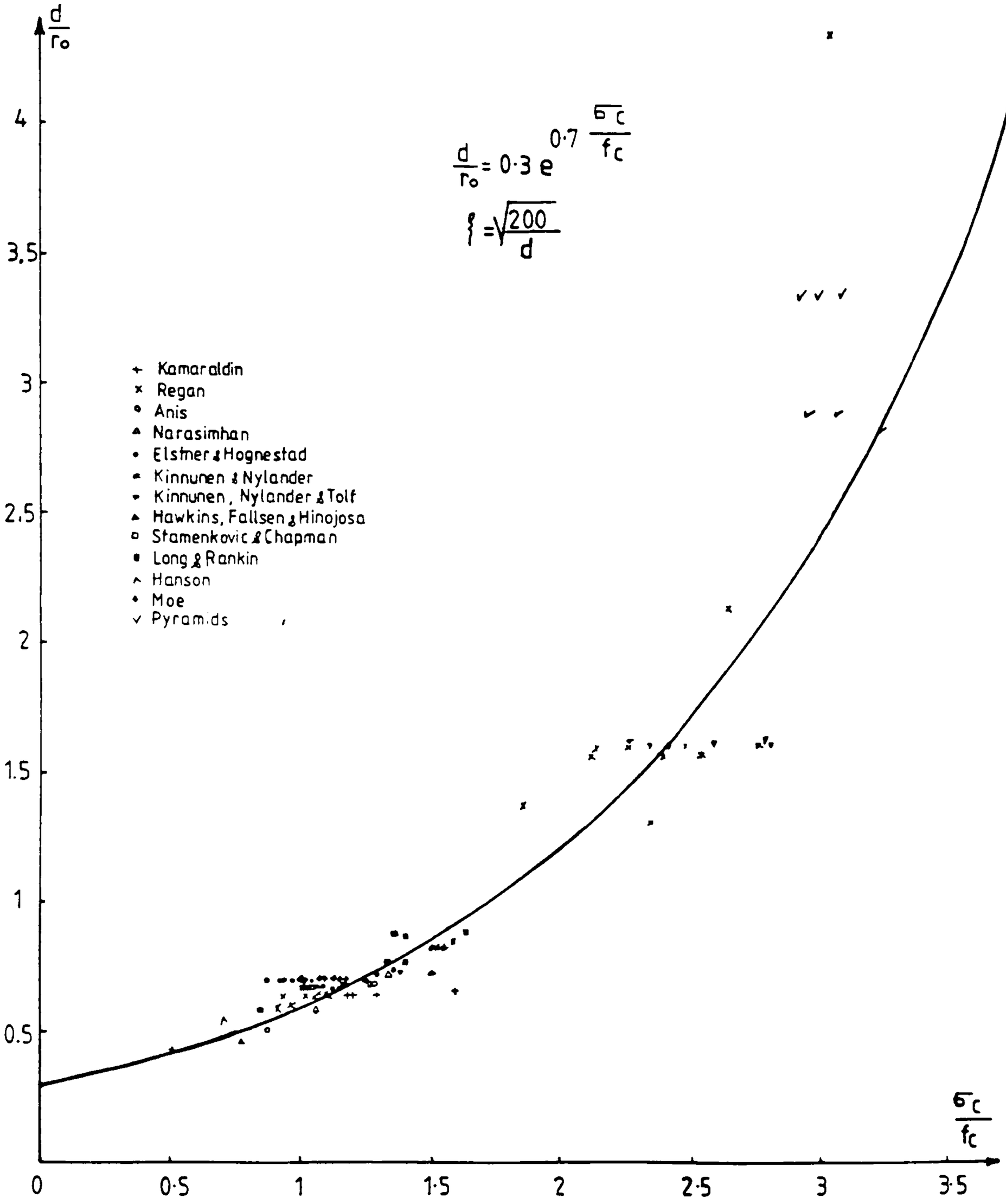

Fig.(5-5) Relationship between d/r_o and σ_c/f_c with $\alpha = 15^\circ$

Table (5-2) Pyramid Test Results

d/ro	∝ (0)	h (mm)	A_1=axb (mm^2)	A_2=b^1xa^1 (mm^2)	Ultimate load kN	$\frac{\sigma c}{fc}$ test	$\frac{\sigma c}{fc}$ cal
2.88	10	305	45x150	540x275	450	2.94	3.23
2.88	10	305	47x150	550x275	490	3.06	3.23
2.82	10	307	50x150	545x270	550	3.23	3.20
3.35	15	300	50x145	540x310	490	2.98	3.44
3.35	15	305	50x145	540x310	505	3.07	3.44
3.35	15	300	50x150	545x320	495	2.91	3.44

β = 40° fc = 22.7 N/mm^2

$$\frac{d}{r_o} = \frac{a' \cdot \pi}{2 \cdot b}$$

$$\varphi = \sqrt{\frac{200}{d}}$$

$$r_o = 2b/\pi$$

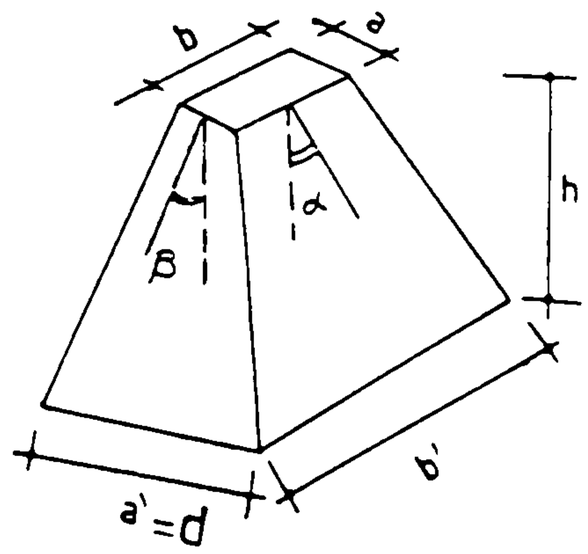

The test specimens were supported over the full area of their bases and loaded vertically in a test machine with its platens moving paralle to one another

5-2 Punching in the presence of transfer moments

A- Horizontal loading

Moments due to horizontal loads are transferred from the column to the slab by means of the bending, torsional resistances of the vertical slab-column interfaces and by uneven shear. Fig.(1-9a) shows the local yield-line mechanisms for an internal slab column connection under horizontal loading. The internal force system for a slab-column connection transferring pure moment is presented in Fig.(5-6) part b of which shows a section parallel to the plane of the external moment M while part c shows forces on a side segment of the slab. Assuming equal top and bottom steel, the forces acting in the transfer of the external moment from the column to the slab and shown in Fig. (5-6b) are the vertical resultants (F_v) of the compressive forces (F_{cr}) in the concrete acting at a lever arm of c, the horizontal resultants (F_H) of the compressive forces (F_{cr}) acting at a lever arm of (h-x), the steel forces (F_{s2}) with a lever arm h_o. The effects from Fig. (5-6c) are forces (F_{s1}) in the slab reinforcement with a lever arm h_o, and the components (F_e) of the compresive concrete forces acting between the segmental elements.

Assuming that the failure criterion for a slab under horizontal loading is the same as that for concentric loading as in Section (5-1-2) :

$$F_{cr} = 1.43\ Ln3.33(d/r_o)\ f_c \cdot x \cdot c\sqrt{200/d}$$

$$F_v = F_{cr}\ Sin\ \alpha$$

$F_H = F_{cr} \cos \alpha$

F_s^* = $F_{s1} + F_{s2}$ is the total steel force on segment 1 Fig.(5-2a) and it can be estimated as in equation (5-16).

The resisting moment can be expressed as

$$M_u = F_s^* h_o + F_v c + F_u(h-x) + F_e \delta \qquad (5\text{-}22)$$

Where : h is the slab thickness

h_o is the distance between the centres of top and bottom reinforcement

c is the column perimeter /4

x is the neutral axis depth

δ is the lever arm between the compresive concrete forces F_e.

It is difficult to estimate the resisting moment produced by the forces F_e (i.e. $F_e \cdot \delta$). The difficulty arises from estimating the lever arm between the forces. However since the forces are necessarily inclined the lever arm must be small and the moment may reasonably be neglected.

Available tests on flat slab-column assemblies under horizontal loading [Hanson & Hanson (A1,A3,B7,C8)(23), and Stamenkovic & Chapman (MI1,MI_r1)(63)] are compared with the predictions of equation (5-22).

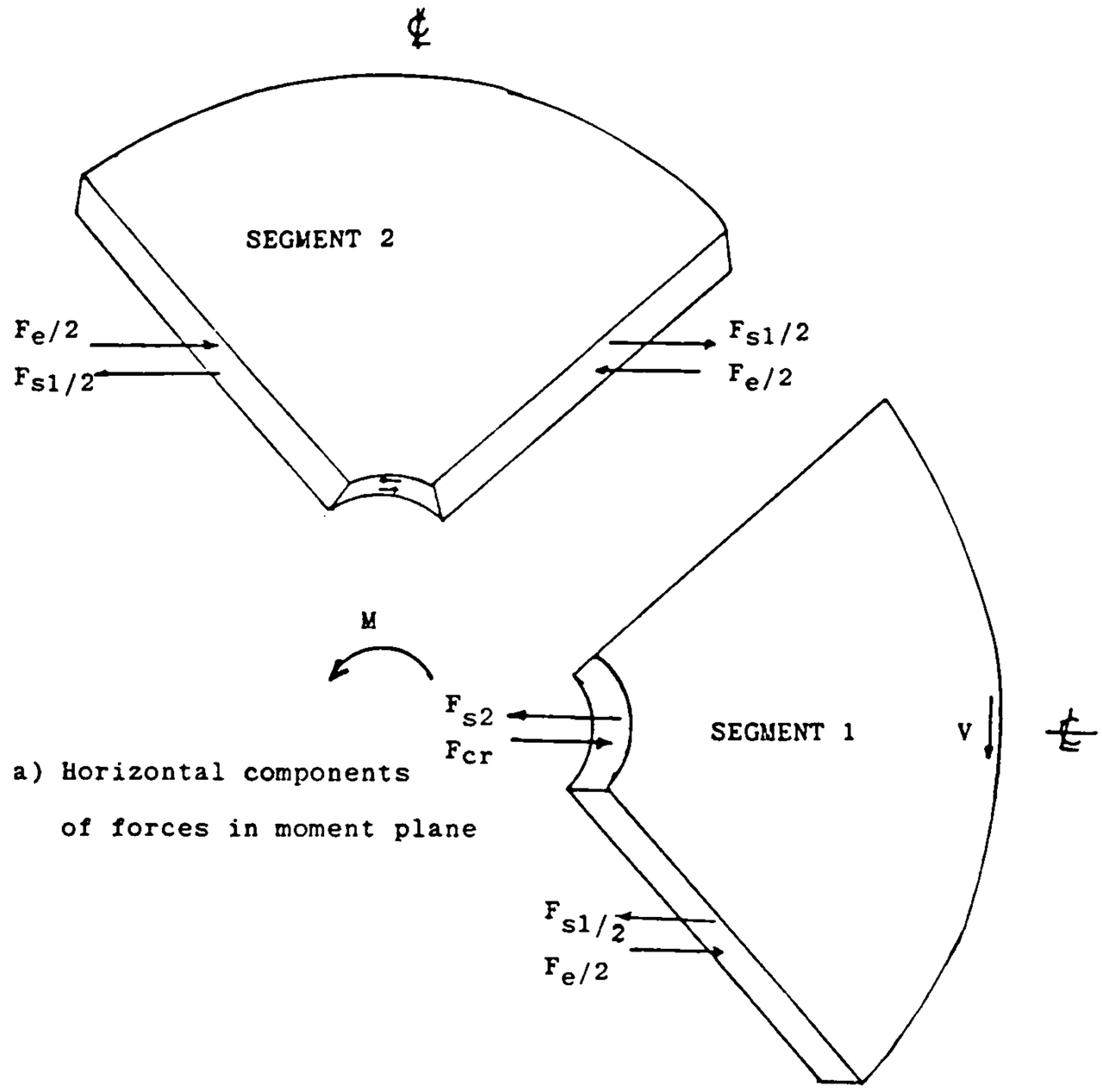

a) Horizontal components of forces in moment plane

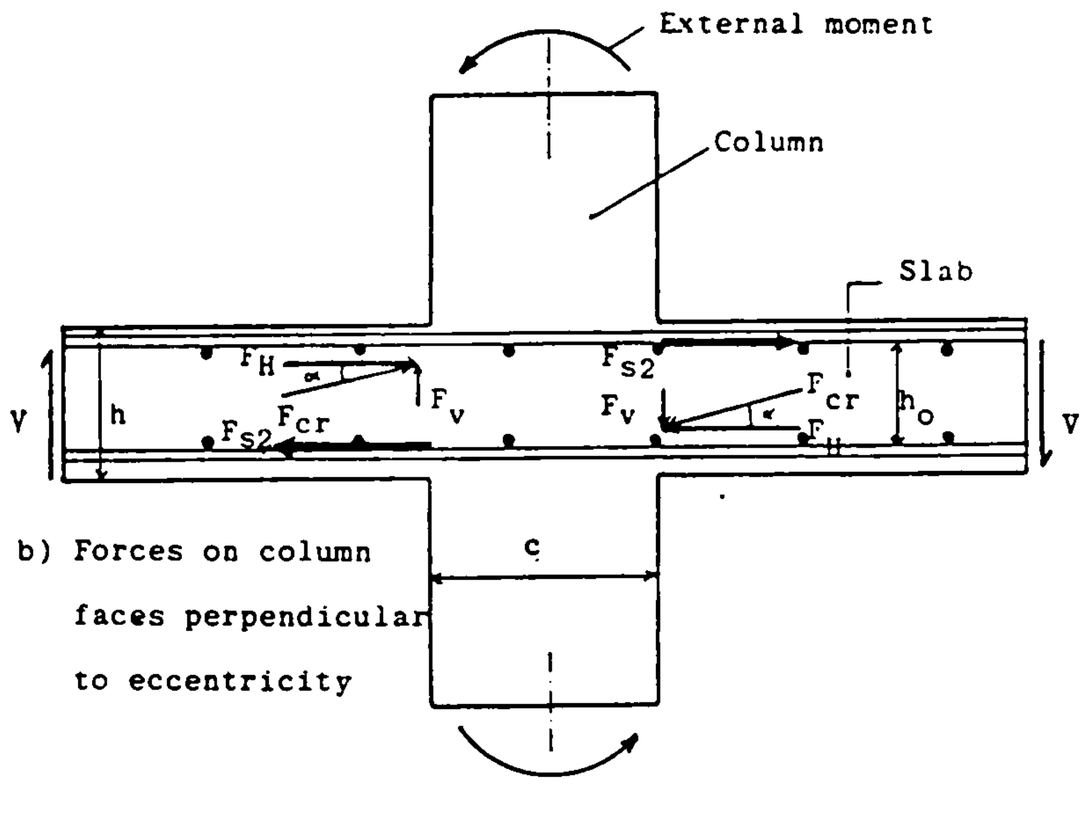

b) Forces on column faces perpendicular to eccentricity

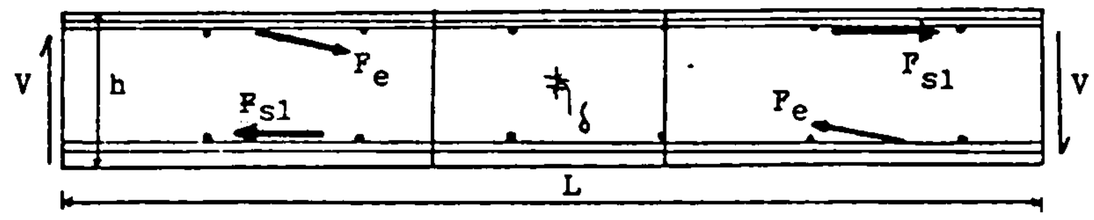

c) Forces on segment 2

Fig.(5-6) Internal forces balancing the external moment in a bending resistance test.

Table (5-3) shows a comparative analysis of the test moments and the moments calculated using equation (5-22) which shows satisfactory correlation between the two.

Slab No	h mm	h_o mm	c mm	F_s KN	M test KNm	M_u eqn5-22 KNm	M / M_u
Stamenkovic & Chapman							
MI1	76	36	127	200	18.40	17.03	1.08
MI_r1	76	36	114	189	18.60	15.72	1.18
Hanson & Hanson							
A1	76	36	152	341	22.33	24.26	0.92
A2	76	36	152	348	24.26	24.51	0.99
B7	76	36	228	334	35.68	29.52	1.20
C8	76	36	228	352	31.37	30.50	1.03

Table (5-3) Moment tests - comparison between calculated and test moments.

B- <u>Combined vertical and horizontal loading</u>

For combined vertical and horizontal loading an interaction curve can be derived in terms of V/V_u and M/M_u where : V and M are the observed failure load and moment, and V_u and M_u are calculated from equations (5-21) and (5-22) respectively.

From the preceding sections, the radial compression forces F_{cr} at the column face in the direction of the eccentricity is a linear function of the loading once the angle α at failure is assumed to be constant.

This applies to both concentric vertical loading and to pure moment loading. Then for any combination of vertical and moments loads :

" F_{cr} Sin $\alpha = k_1 V + k_2 M$ "

from which

$$\frac{V}{V_u} + \frac{M}{M_u} = 1 \qquad (5\text{-}23)$$

Satisfactory agreement is obtained between the calculated and the proposed values of the interaction formula, see Table (5-4) and Fig.(5-7).

Slab No	V KN	V_u KN	M KNm	M_u KNm	$\frac{V}{V_u} + \frac{M}{M_u}$
Hanson & Hanson					
A1	5.85	118.0	22.40	24.20	0.98
A2	4.90	117.0	24.80	24.50	1.05
B7	5.00	89.4	36.50	29.50	1.29
C8	5.70	91.7	31.40	30.50	1.09
A12	27.40	123.0	20.90	20.70	1.09
C17	32.10	91.0	25.20	22.10	1.49

Table (5-4) continued

Slab No	V KN	V_u KN	M KNm	M_u KNm	$\frac{V}{V_u} + \frac{M}{M_u}$
Anis					
B3	194.00	252.0	18.30	61.60	1.06
B4	142.00	248.0	26.70	61.00	1.01
B5	127.00	247.0	39.60	60.60	1.09
B6	117.00	256.0	54.40	62.40	1.35
B7	70.80	264.0	66.90	63.90	1.31
Stamenkovic & Chapman					
CI 1	86.00	123.0	7.50	18.65	1.10
2	61.00	111.0	10.30	17.30	1.14
3	35.00	104.0	14.20	16.50	1.19
4	21.00	103.0	19.80	16.40	1.41
MI 1			18.40	17.10	1.07
CI_r1	69.00	98.0	5.86	15.30	1.08
2	61.00	110.0	9.88	16.70	1.14
3	39.00	109.0	15.30	16.60	1.27
4	21.00	105.0	16.30	16.10	1.21
MI_r1			18.60	15.70	1.18
Kamaraldin					
SA1	109.00	109.0	5.60	18.30	1.30
SA3	85.00	115.0	8.50	18.95	1.18
SA4	49.00	108.0	16.40	18.20	1.35
SB2	61.00	128.0	21.90	22.80	1.45
SC2	65.00	127.0	21.90	21.40	1.53
SD2	56.00	116.0	17.36	20.10	1.34

Table (5-4) Results of slabs tested under combined vertical and horizontal loads.

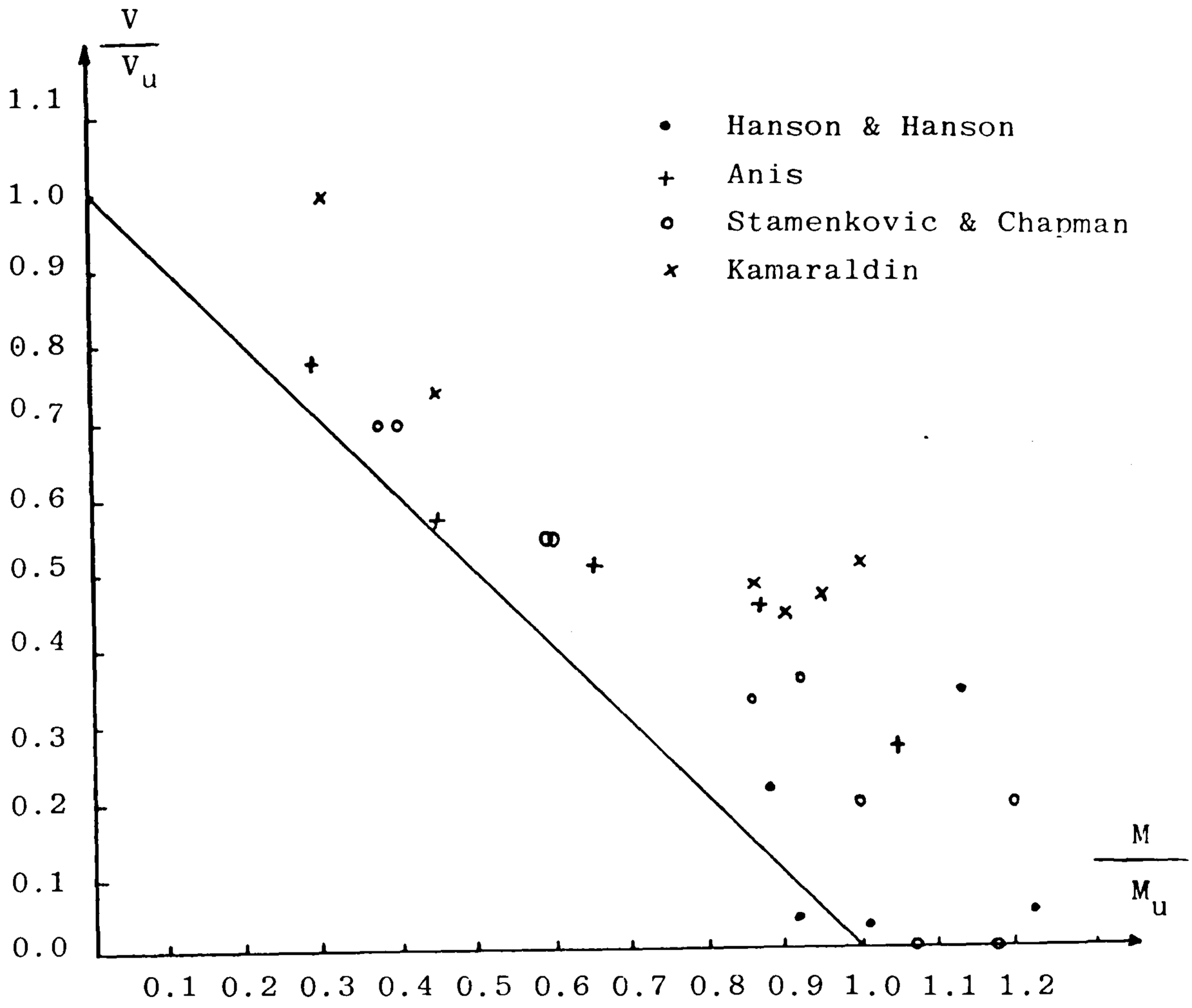

Fig. (5-7) Interaction curve - internal column

However, for practical purposes an empirical formula is developed in Section (5-2-1) for the calculation of eccentric punching resistance of internal slab-column connection.

5-2-1 Punching resistance of eccentrically loaded slabs

Moment transfer between slab and column occurs due to uneven distribution of live load, uneven spacing of columns, or in some cases lateral loads. Tests results have indicated that an increase in the moment (M_t) transferred between the slab and column produces a reduction in the punching strength. Assuming that the limiting concrete stress for eccentric loading is the same as that for concentric loading, the effect of eccentricity on the punching shear resistance may be formulated as :

$$\frac{V}{V_o} = \frac{1}{1 + K \cdot e}$$

Where : V_o is the shearing capacity of the slab
at zero eccentricity
V is eccentric punching load
e is the eccentricity of the load
K is coefficient dependent on variables other than eccentricity.

Fig. (5-8) shows the results of three series of tests of eccentrically loaded flat-slabs by, Stamenkovic and Chapman (63), Anis (2) and the author in the present work. The only variable in each series was the eccentricity (e) while the effective depth (d) and column dimensions were kept constant.

The values of "K" for the three series are found to be 1/206 , 1/302 and 1/240 . The main variables in the three series were the column dimensions and slab effective depths.

Experimental works by Hanson & Hanson (23) and the present study show that the effect of column dimensions on punching resistance is best represented by the column perimeter as the column shape has negligible influence. Fig. (5-9) shows the results of the tests by Hanson & Hanson (23) and Stamenkovic & Chapman (63) plotted against " e/c ", the trend in the graph follows that represented by :

$$\frac{V}{V_o} = f\left(\frac{1}{1 + e/c}\right)$$

Where c is column perimeter divided by 4

Further studies on available experimental works in the literature in conjunction with the test results produced in the course of the present study show that the effects of c and d may be incorporated in the above expression as :

$$\frac{V}{V_o} = \frac{1}{1 + \dfrac{e}{K_1(c + K_2 d)}}$$

In Fig. (5-10) values of V/V_o for 43 available test results on eccentrically loaded slabs are plotted against e/(c+3d) , the

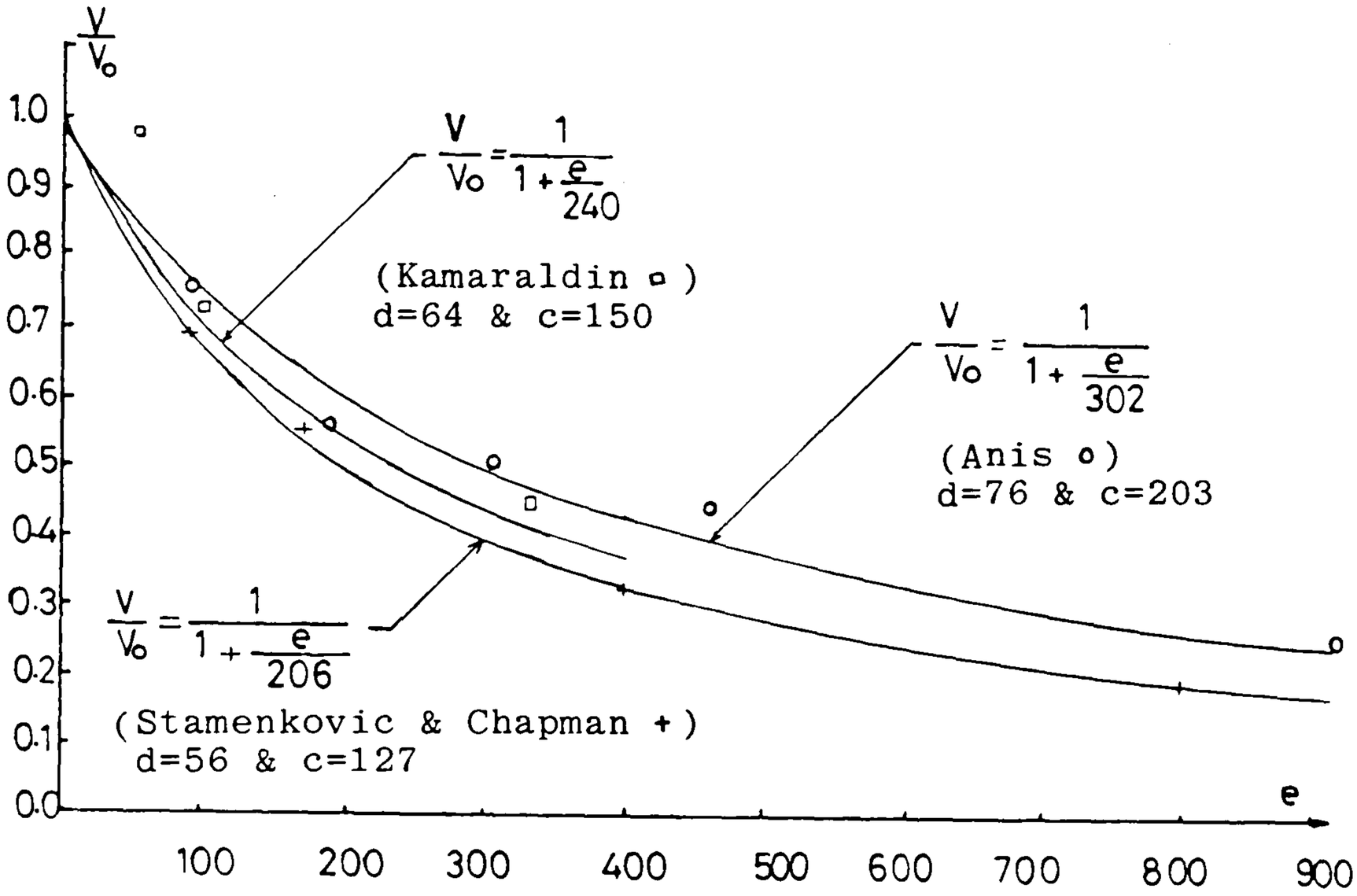

Fig. (5-8) Effect of eccentricity on punching shear resistance

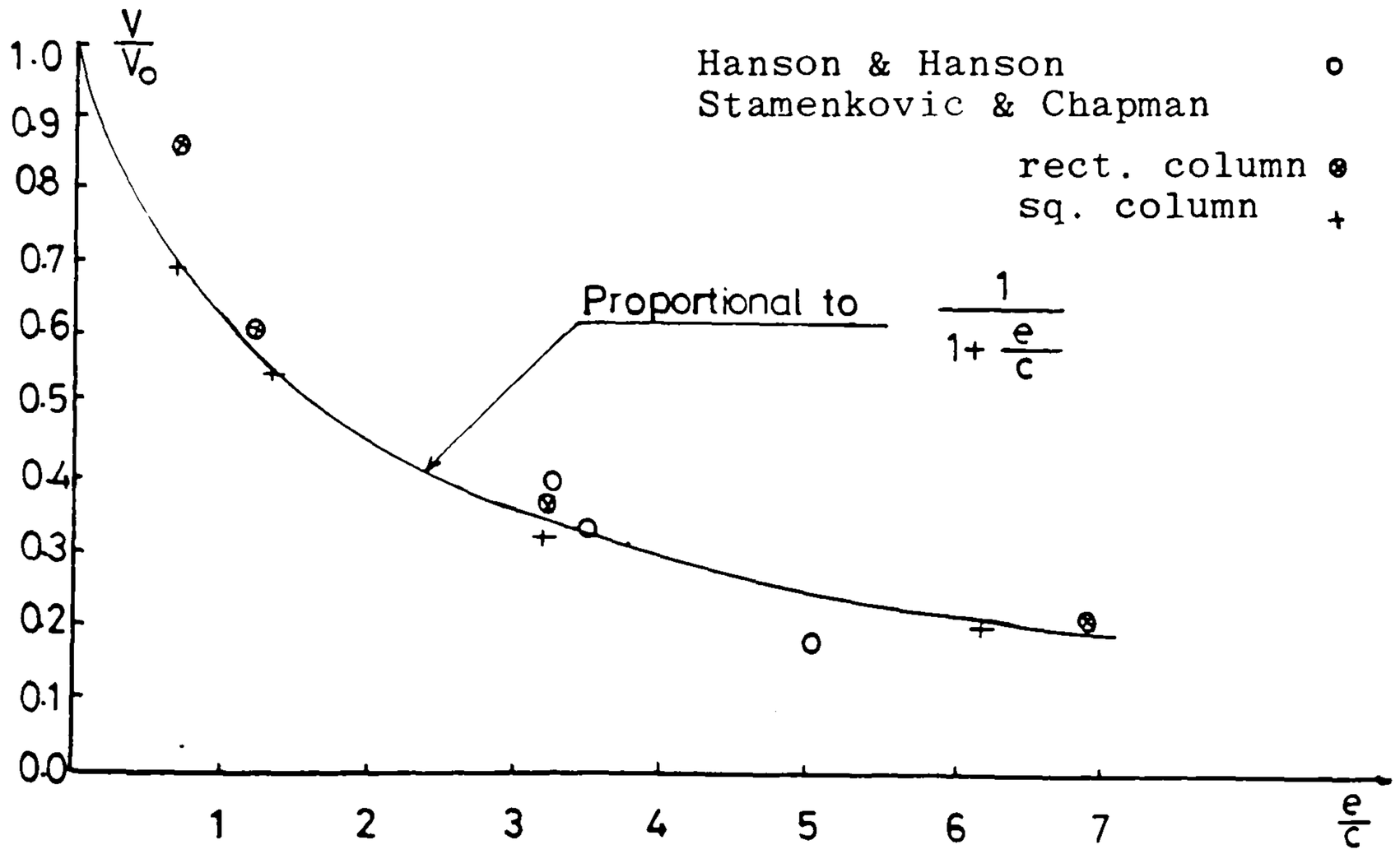

Fig. (5-9) Effect of combine e&c on punching shear resistance

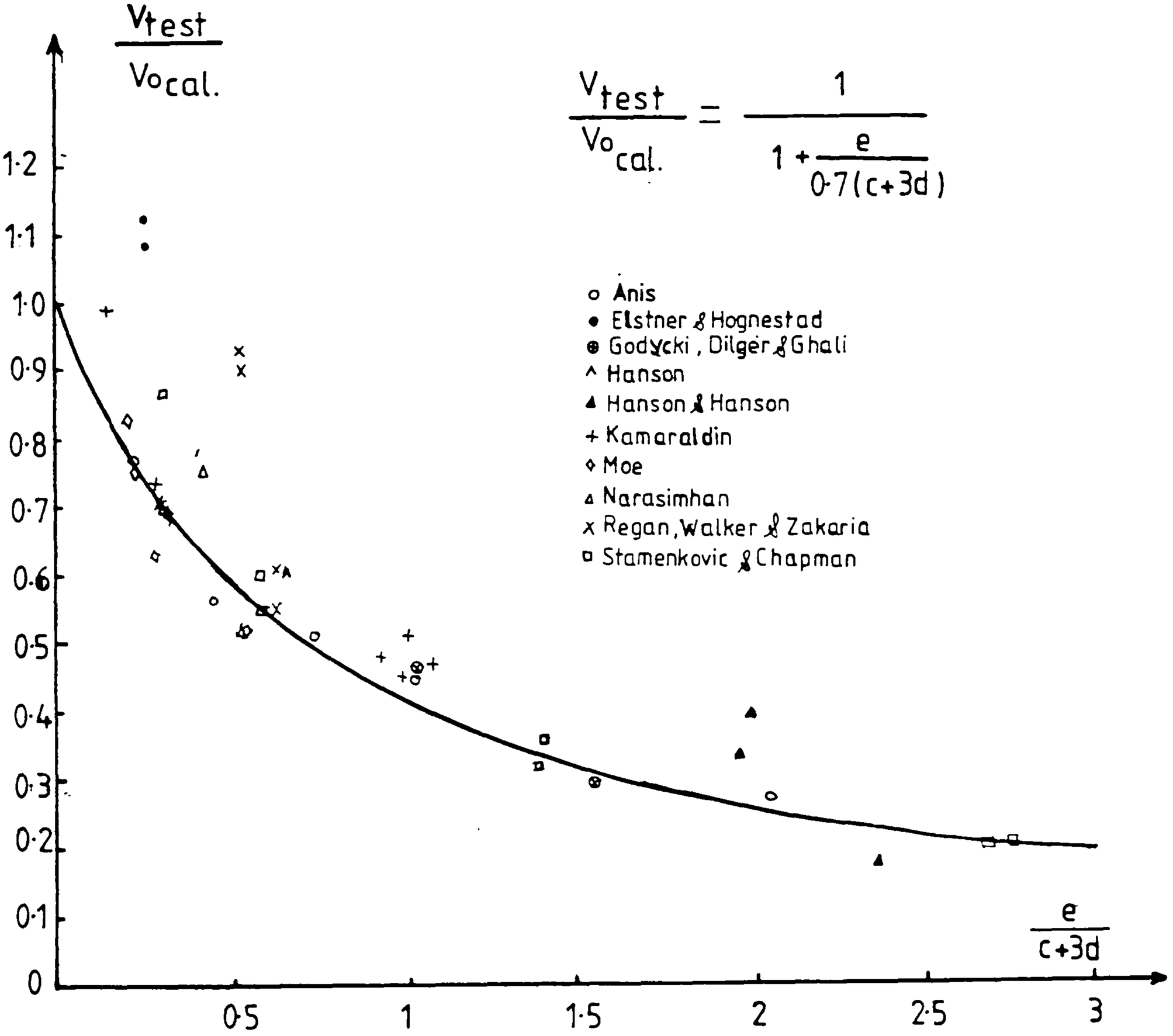

Fig.(5-10)Test results for internal slab-column connections under eccentric loading

best fit line for all the points is presented by the following equation in line with K1 & K2 values of 0.7 & 2.1 respectively.

$$\frac{V}{V_o} = \frac{1}{1 + \frac{e}{0.7(c+3d)}} \qquad (5\text{-}24)$$

The above equation is similar to that of BS8110 except that in BS8110, c is the column dimension in the direction of eccentricity.

5-3 Serviceability

The use of high-strength materials in structures results in shallow elements which may cause deflection problems. Such problems can be reduced if a relatively simple and accurate method exists for the computation of deflections.

Fig.(3-3) shows that the deflections of flat slabs are dependent on the type of loading and different variables of the slabs. To be able to obtain the deflections for eccentrically loaded slabs, the values of the joint rotation, (θ_j) and the slab effective stiffness (K_{se}) must be found.

The joint rotation is

$$\theta_j = M_t/K_{se}$$

Where M_t is the moment transferred between the slab and column

K_{se} is the slab effective stiffness

θ_j is the rotation of the slab-column joint, see Fig.(5-13)

The value of the transfer moment (M_t) maybe found by using the simple BS8110 equivalent frame method, as this method has been shown to give an adequate estimate of column moments.

The difference between the deflection of a flat slab structure and the equivalent beam-column frame is due to the relative lack of continuity between the slabs and columns. The slab-column frame is more flexible than a beam-column frame with the same EI values for its members see Fig.(5-11).

In the case of flat slabs the stiffness of the horizontal members of the frame should be obtained through the evaluation of an effective width of slab (b_e).

The calculation of a value for (K_{se}) is more of a problem because the stiffness of the strip reduces with increasing load due to the propagation of cracks. A method of finding the effective stiffness of the slab is to use the cracked section stiffness developed by Branson (10)

$$K_{se} = K_{sg}\left(\frac{M_{tcr}}{M_t}\right)^3 + K_{s\cdot cr}\left[1 - \left(\frac{M_{tcr}}{M_t}\right)^3\right] \qquad (5\text{-}25)$$

Where: $$K_{sg} = \frac{Ec\cdot b_e\cdot h^3}{1(1-\mu^2)}$$

is the gross uncracked stiffness of the slab

E_c is the initial tangent modulus of elasticity for concrete to be taken as $4250\sqrt{f_c}$ N/mm2

h is the slab thickness

b_e is the slab effective width to be taken as given by Stiglat(64)

$b_e = 0.22\ l + 2\ c_1 + 0.8\ c_2$ for $l_1 \geqslant 0.1 \cdot l$ or

$b_e = 0.6\ l + 2.5\ c_1\ 0.5\ c_2$ for $l_1 \leqslant 0.1 \cdot l$ see Fig.(5-12)

μ = Poisson's ratio

$K_{s \cdot cr} = \dfrac{12EI_{cr}}{l(1 - \mu^2)}$ is the fully cracked stiffness of the slab.

For a rectangular slab section:

$EI_{cr} = E_s . A_s . z . (d-x)$

x is neutral axis depth and can be calculated as

$x = d[\sqrt{(2+\alpha e \cdot \rho)\alpha e \cdot \rho} - \alpha e \cdot \rho]$

z = lever arm = $d-(x/3)$

$\rho = A_s/(b_e \cdot d)$ The ratio of reinforcement in the effective width

$\alpha_e = E_s/E_c$

E_s = Modulus of elasticity of steel

A reasonable estimate of M_{tcr} can be obtained if the behaviour of the joint is studied

In Fig.(5-13), M_t/θ_j curves are drawn for six slabs tested by the author in the present work, θ_j is taken as

$\theta_j = \theta_s - \theta_c$

where $\theta_s = (\theta_E + \theta_W)/2$

Where θ_E and θ_W are the rotations measured by the inclinometers on the slab surface

The rotation signs are positive clock-wise and negative anti clock-wise, see Fig.(5-13).

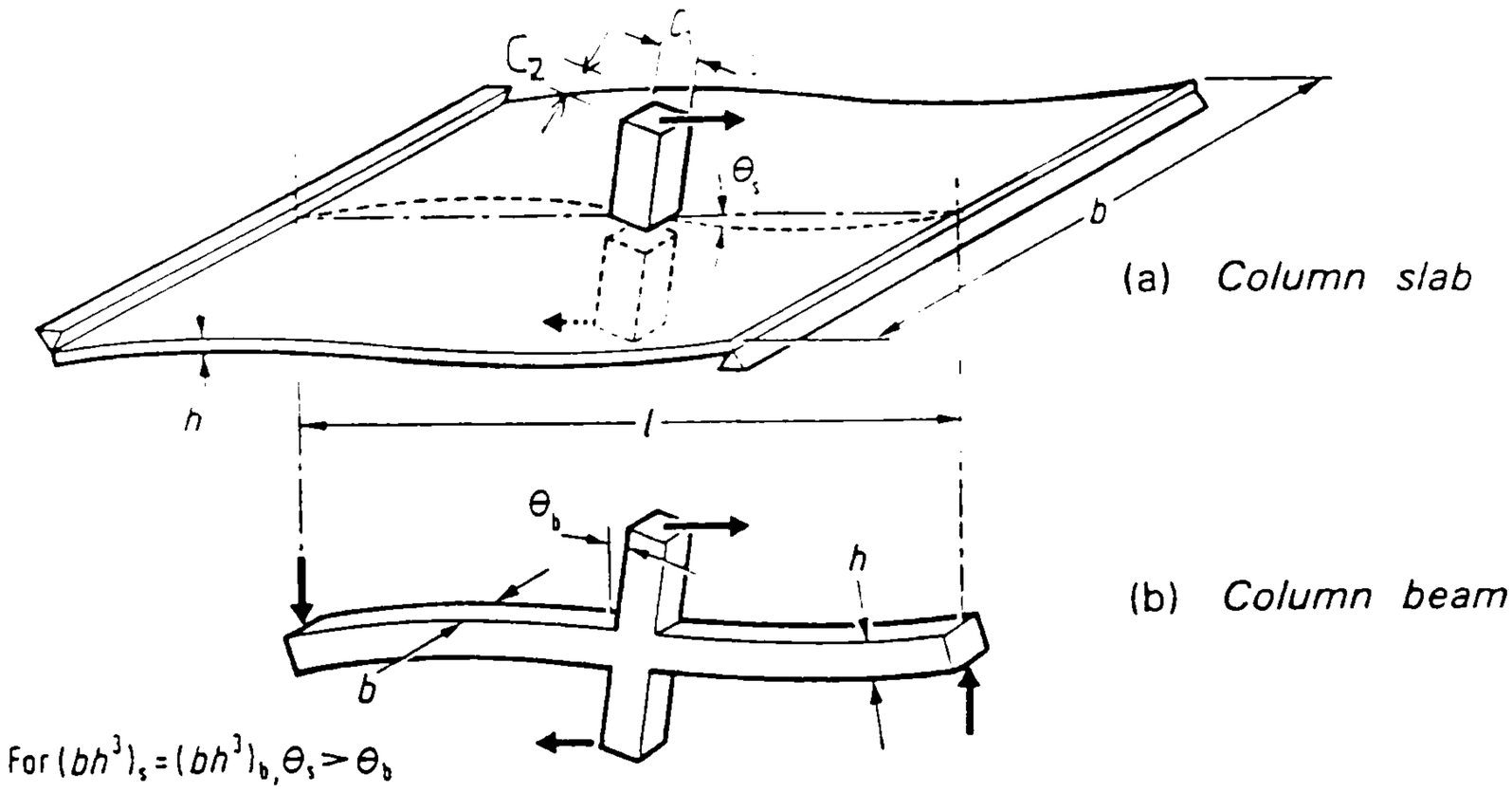

Fig.(5-11)Deformations of slab-columns and beam column structures

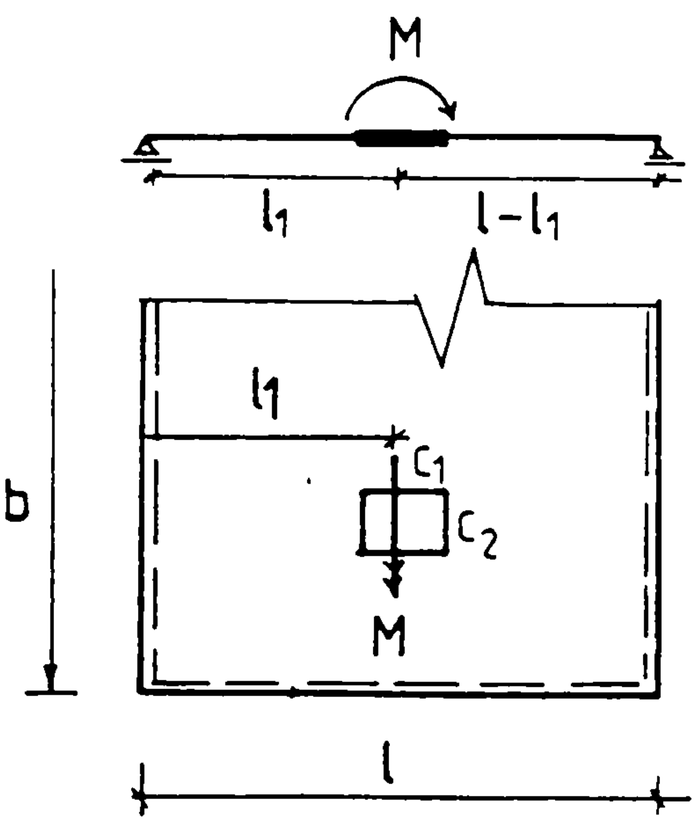

Fig.(5-12)Effective width in flat slab structure

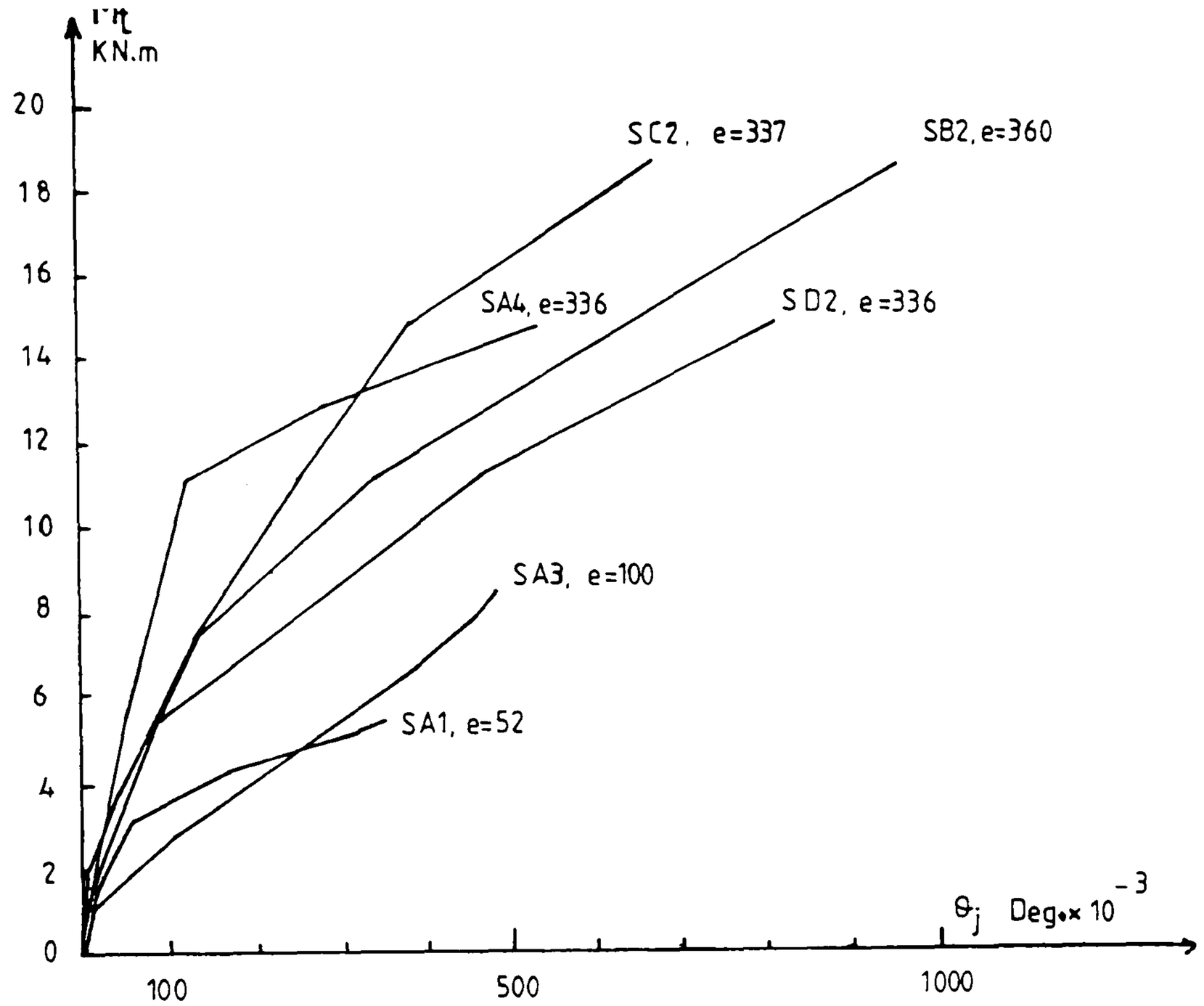

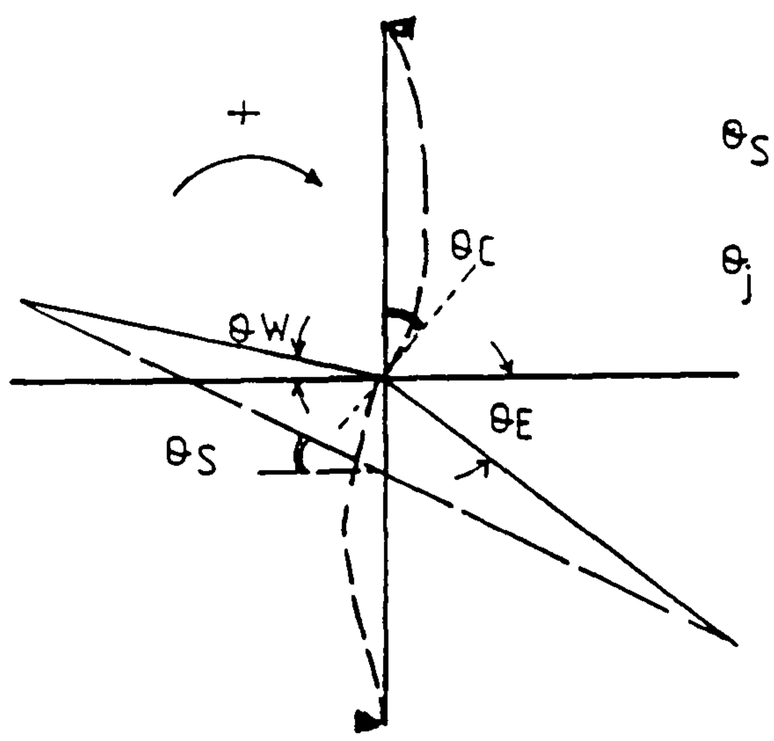

$$\theta_S = \frac{\theta_E + \theta_W}{2}$$

$$\theta_j = \theta_S - \theta_C$$

Fig. (5-13) M_t/θ_j curves for internal slab-column conections

Slabs SA1, and SA4 were similar but subjected to loads with different eccentricities. It is clear that there is no unique M_t/θ_j relationship and that the stiffness of the joint depends largely on the vertical load to which it is subjected.

It has been assumed that.

$$M_{cr} = \frac{P}{K_1} + \frac{M_{tcr}}{K_2}$$

where $M_{cr} = (f_{ctflex} \cdot h^2 \cdot b_e)/6$

$$f_{ctflex} = 0.6\sqrt{f_c} \cdot \sqrt{(200/d)}$$

$$\frac{f_{ctflex} \cdot h^2}{6} = \frac{P}{K_1} + \frac{M_{tcr}}{K_2 \cdot b_e}$$

In the absence of a transfer moment

$$\frac{f_{ctflex} \cdot h^2}{6} = \frac{P_{cr}}{K_1}$$

Where P_{cr} is the cracking load.

From the author's test data and Kinnunen & Nylander (30) K_1 was found to be approximately equal to 6. See Fig(5-14).

With K_1 known K_2 could be determined from slabs tested under eccentric loading by the author and Anis (2) and was found to be approximately equal to 4.5, see Table (5-5).

Table (5-5) Estimated value of K_2

Slab No	P_{cr} KN	M_{tcr} KNm	h mm	d mm	f_c N/mm^2	K_2
SA1	37	1.48	80	64	33	4.15
SA4	27	7.40	80	64	32	4.34
SB2	25	7.40	80	62	28	4.70
SC2	31	7.38	80	62	37	4.90
SD2	27	7.40	80	62	31	4.45
Anis Slabs						
B5	36	11.20	102	76	29.4	3.95
B6	32	14.80	102	76	31.8	3.93
B7	24	22.70	102	76	34.3	4.30

With K_1 and K_2 are known, M_{tcr} could be determined as:

$$M_{tcr} = \frac{f_{ctflex} \cdot h^2}{\frac{1.33}{b_e} + \frac{1}{e}} \qquad (5\text{-}26)$$

Where e is the load eccentricity = M_t/P

Once the effective stiffness is found for a particular load, its value can be used for the entire negative moment region of the slab. Deflections can be assessed from the equivalent frame moments, this negative moment stiffness and Branson's value for

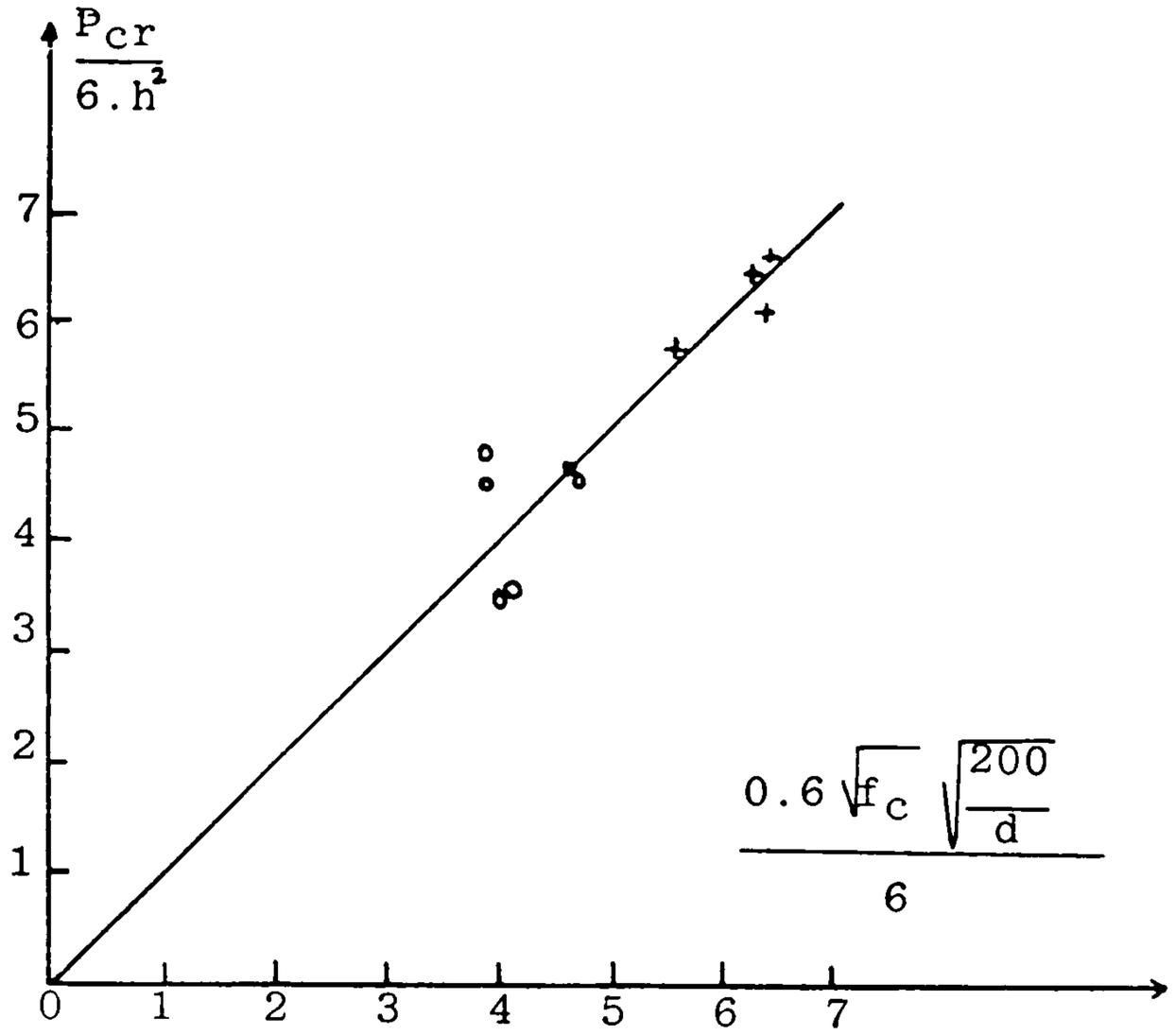

SLAB No	h mm	d mm	f_c N/mm^2	P_{cr} KN
The author's slabs +				
SA1	80	64	34	41
SB1	80	62	27	37
SC1	80	62	36	36
SD1	80	62	36	42
Kinnunen & Nylander's slabs o				
IA15a5	149	117	27.9	80
6	151	118	27.3	80
IA30a24	158	128	27.5	114
25	154	124	26.1	114
IA30d32	155	123	38	114
33	156	123	39.1	114

Fig. (5-14) P_{cr} and flexural stress relationship

the stiffness of the positive moment region.

To check the validity of the K_{se} values against test results, the joint rotation can be obtained as

$$\theta_j = \frac{M_t}{K_{se}} \qquad (5\text{-}27)$$

and compared with experimental rotations θ_j see Fig.(5-13). Comparisons with the present test data are given in Figs. (5-15), (5-16) and (5-17).

Due to a loading error the load on slab SA3 had to be released and the slab was reloaded again. The measured rotations may not be quite reliable.

5-3-1 Proposed deflection calculation procedure

In using the above proposals to calculate the deflection of a flat slab for a given load, the following steps are to be followed.

Step (i) Carry out equivalent frame analysis in accordance with BS 8110 recommendations.

Step (ii) Determine the moments transferred to columns (ie. M_t), load eccentricities at column positions (ie. $\frac{M_t}{V}$) and extents of positive and negative moment regions along the slab.

Step (iii) Calculate negative moment region stiffness (K_{se}) from equation 5-25 above.

Step (iv) Calculate positive moment region stiffness as

$$K_{se} = K_{sg} \left(\frac{M_{cr}}{M}\right)^3 + K_{scr} \left[1 - \left(\frac{M_{cr}}{M}\right)^3\right]$$

where $M_{cr} = (f_{ct\ flex} \cdot h^2 \cdot b_e)/6$

M is the positive moment

Step (v) Re-analyse the equivalent frame of step (i) using variable slab stiffnesses calculated in steps (iii) and (iv) to determine the slab deflection.

It may be noted that step (v) could be treated as the first stage of an iterative procedure of design including the determination of reinforcement.

CHAPTER SIX

TEST ANALYSIS

6-1 Introduction

In this chapter the results of tests on slabs by the Author of the present work and various other authors are compared with the failure loads calculated by the proposed method of analysis. These comparisons provide a valuable means of examining the validity of the assumptions used in the method of analysis, since the slabs tested exhibited a wide range of properties. Also the analysis is extended to compare the proposed method of predicting failure loads with other method proposed by various authors and Codes of Practice.

6-2 Concentric loading tests

The methods of testing and the experimental details of most of the tests have already been described briefly in chapter one. The details which are of relevance to the calculation of the failure loads are given in this section.

6-2-1 Slabs tested by Elstner and Hognestad

30 slabs were tested by Elstner and Hognestad (20). 15 have been reanalysed by the proposed method, the remaining ones have characteristics such as:

supports along two sides, supports at four corners, or shear reinforcement, which are not relevant in this analysis. The slabs were 1825 mm square and 152 mm thick. The main variables were the concrete strength, the ratio of tension reinforcement and the column size. Details of the tests and calculated results are given in table (6-2-1).

SLAB No	r_3 mm	r_o mm	C mm	ρ %	d mm	f_c N/mm^2	f_y N/mm^2	x mm	V_t KN	V_c KN	$\frac{V_c}{V_t}$
A1-a	1162	162	254	1.17	117	14.1	332	46.6	303	281	0.93
A1-b	1162	162	254	1.17	117	25.2	332	32.8	365	320	0.87
A1-e	1162	162	254	1.17	117	20.3	332	37.5	356	325	0.91
A2-a	1162	162	254	2.48	114	13.7	321	69.5	334	400	1.19
A2-b	1162	162	254	2.48	114	19.5	321	57.5	401	471	1.17
A2-c	1162	162	254	2.48	114	37.4	321	39.0	467	612	1.31
A7-b	1162	162	254	2.48	114	27.9	321	46.3	512	542	1.06
A3-a	1162	162	254	3.72	114	12.8	321	84.6	356	455	1.27
A3-b	1162	162	254	3.72	114	22.6	321	56.3	445	534	1.20
A3-c	1162	162	254	3.72	114	26.6	321	60.8	534	679	1.27
A3-d	1162	162	254	3.72	114	34.6	321	43.4	547	630	1.15
B-9	1162	162	254	2.24	103	43.9	341	30.5	505	518	1.02
B-11	1162	162	254	3.39	102	13.5	409	70.8	329	373	1.13
B-14	1162	162	254	3.39	102	50.6	326	35.1	579	693	1.19
A5	1162	227	356	2.47	114	27.8	321	45.8	534	452	0.85

Table (6-2-1) slabs tested by Elstner and Hognestad.

It is seen that a good agreement between the test and calculated failure loads was obtained for slabs having reasonable ratios of reinforcement which might arise in real structures.

6-2-2 Slabs tested by Moe

Moe (40) tested 31 slabs under concentric loading. The slabs were 1828 mm square with square columns and an overall thickness of 152 mm. Some of the slabs had holes in the vicinities of the columns and some of them had shear reinforcement. The proposed method is not applicable to these cases. Only 12 of the 31 tests were used in the present comparison. The main variables were the concrete strength, the column dimensions, the ratio of tensile reinforcement and in series "S" varying degrees of concentration of the tensile reinforcement inside the punching area. The details of the tests and the results of the analysis are shown in table (6-2-2). The tabulated results indicate that the proposed method of analysis gives a good agreement with the actual values.

SLAB No	r_3 mm	r_o mm	C mm	ρ %	d mm	f_c N/mm^2	f_y N/mm^2	x mm	V_t KN	V_c KN	$\frac{V_c}{V_t}$
M1	1150	194	305	1.50	114	21.2	488	46.3	440	394	0.90
H1	1150	162	254	1.15	114	26.6	333	30.7	379	343	0.90
S1-60	1150	162	254	1.06	114	23.8	407	33.8	396	338	0.85
S2-60	1150	162	254	1.06	114	22.5	407	34.9	362	330	0.91

Table (6-2-2) continued

S3-60	1150	162	254	1.06	114	23.0	407	34.4	370	332	0.90
S4-60	1150	162	254	1.06	114	24.3	407	33.3	340	340	1.00
S5-60	1150	162	254	1.05	114	22.2	399	34.1	318	318	1.00
S1-70	1150	162	254	1.06	114	25.0	491	34.7	400	364	0.91
S3-70	1150	162	254	1.06	114	25.0	491	34.1	385	358	0.93
S4-70	1150	162	254	1.06	114	25.8	491	28.2	380	306	0.80
S5-70	1150	162	254	1.05	114	23.0	482	35.4	342	342	1.00
R2	1150	97	152	1.37	98	26.6	333	28.1	317	303	0.95

Table (6-2-2) Slabs tested by Moe.

6-2-3 Slabs tested by Kinnunen and Nylander (30)

These tests were carried out on circular slabs having approximately 1710 mm diameter. The slabs were supported by tie-rods along the circumference and an upward vertical load was applied at the centrally placed column. The slabs had different types of tensile reinforcement, some of them had only ring reinforcement and these have not been considered as the radial resistance of the slabs were zero and the failure mechanism in this case is different from that of slabs having two way reinforcement. Only 6 tests of the two-way reinforced slabs are suitable for analysis as in the remaining slabs the column stub formwork accidentally penetrated the slab during casting.

The results of the analysis given in table (6-2-3) show good agreement between test and calculated failure loads.

SLAB No	r_3 mm	r_o mm	C mm	ρ %	d mm	f_c N/mm^2	f_y N/mm^2	x mm	V_t KN	V_c KN	$\frac{V_c}{V_t}$
IA15a5	885	75	118	0.80	117	26.8	450	25.5	260	255	0.98
6	855	75	118	0.79	118	26.2	463	26.5	280	260	0.93
IA30a24	855	150	235	1.01	128	26.4	464	34.2	438	410	0.94
25	855	150	235	1.04	124	25.1	460	34.6	416	385	0.92
IA30d32	855	150	235	0.49	123	25.6	457	21.4	263	243	0.92
33	855	150	235	0.48	125	26.6	470	21.8	263	261	0.99

Table (6-2-3) slabs tested by Kinnunen and Nylander.

6-2-4 Slabs tested by Kinnunen, Nylander and Tolf

16 tests are reported in reference (32). The test slabs were circular and supported on circular central columns. The investigation was carried out to study the influence of slab thickness, and the effect of shear reinforcement on punching shear strength. Some of the slabs thus had shear reinforcement. The proposed method is not applicable to these cases and only 6 tests were considered in the comparison. The test and calculated results are given in table (6-2-4).

SLAB No	r_3 mm	r_o mm	C mm	ρ %	d mm	f_c N/mm^2	f_y N/mm^2	x mm	V_t KN	V_c KN	$\frac{V_c}{V_t}$
1	600	62.5	98	0.80	100	28.6	706	22.4	216	219	1.01
3	600	62.5	98	0.81	99	22.9	701	26.2	194	205	1.05

Table (6-2-4) continued.

SLAB No	r_3 mm	r_o mm	C mm	ρ %	d mm	f_c N/mm^2	f_y N/mm^2	x mm	V_t KN	V_c KN	$\frac{V_c}{V_t}$
13	600	62.5	98	0.34	98	26.6	720	13.6	145	124	0.85
14	600	62.5	98	0.35	99	25.1	712	13.9	148	119	0.81
17	1200	125	196	0.34	200	25.4	668	33.9	489	418	0.85
18	1200	125	196	0.35	197	24.2	664	34.9	444	409	0.92

Table (6-2-4) slabs tested by Kinnunen, Nylander and Tolf.

6-2-5 Slabs tested by Hanson

10 Light-weight aggregate concrete slabs were tested by Hanson (24). Only one slab could be analysed by the proposed method, the remaining slabs had embedded ducts or shear reinforcement. The slab was 3660 mm square and supported by a 355 mm square central column. More details of the slab and the analysis results are listed in table (6-2-5).

SLAB No	r_3 mm	r_o mm	C mm	ρ %	d mm	f_c N/mm^2	f_y N/mm^2	x mm	V_t KN	V_c KN	$\frac{V_c}{V_t}$
B4	2330	226	355	0.94	162	22.2	450	52.7	556	592	1.06

Table (6-2-5) slab tested by Hanson

6-2-6 Slabs tested by Hawkings, Fa llsen and Hinojosa

Tow slabs are reported in reference (25). The slabs were 1825 mm square and 150 mm thick, the columns were square and centrally located. Test and calculated results are shown in table (6-2-6).

SLAB No	r_3 mm	r_o mm	C mm	ρ %	d mm	f_c N/mm^2	f_y N/mm^2	x mm	V_t KN	V_c KN	$\frac{V_c}{V_t}$
2	1162	247	388	1.11	117	26.3	411	32.9	352	296	0.84
9	1162	185	290	0.75	121	29.5	414	25.8	316	324	1.02

Table (6-2-6) slabs tested by Hawkins, Fallsen and Hinojosa.

6-2-7 <u>Slabs tested by Narasimhan</u>

Result of tests on square slabs carried out by Narasimham (43) are compared with the calculated values in the following. Since some of the concentrically loaded slabs had shear reinforcement,only two slabs are used in the present comparison. The slabs were 2 m square with 305 mm square columns. The details and the calculated and observed failure loads are given in table (6-2-7).

SLAB No	r_3 mm	r_o mm	C mm	ρ %	d mm	f_c N/mm^2	f_y N/mm^2	x mm	V_t KN	V_c KN	$\frac{V_c}{V_t}$
L7	1274	194	305	1.11	143	35.5	476	37.1	687	623	0.91
L9	1274	194	305	1.11	143	33.1	476	38.7	588	606	1.03

Table (6-2-7) slabs tested by Narasimham.

6-2-8 <u>Slabs tested by Stamenkovic and Chapman</u>

Two of the ten tests carried out by Stamenkovic and Chapman (63) on internal slab-column joints could be analysed

by the proposed method. The remaining ones were eccentrically loaded and will be analysed latter. The slabs were 914 mm square and 76 mm thick, reinforced with a top mesh only. Slab V/I/2 had a 127 mm square column while slab V/I/1 had a 76x152 mm column.

Table (6-2-7) shows good agreement between test and calculated failure loads.

SLAB No	r_3 mm	r_o mm	C mm	ρ %	d mm	f_c N/mm^2	f_y N/mm^2	x mm	V_t KN	V_c KN	$\frac{V_c}{V_t}$
V/I/2	582	80.0	127	1.17	56	25.9	434	14.1	117	109	0.93
V/Ir/1	582	72.5	114	1.17	56	25.2	414	13.8	109	105	0.96

Table (6-2-8) Slabs tested by Stamenkovic and Chapman

6-29 Slabs tested by Regan

The twenty eight tests reported in reference (56) are divided in five groups. All the tests were of slabs supported at four sides and subjected to concentrated loads at their centres.

The seven slabs of Group 1 were 2 m square and 100 mm thick. They were tested simply supported at four sides with spans of 1.83 m. Loads were applied through 200 mm square columns. The main variable in this group was the arrangement of the reinforcement.

The six slab specimens of group II were designed to study the size effect on punching resistance. The slabs were scaled linearly in the ratios 1.0, 0.64 and 0.32.

The slabs were square simply supported at four edges and loaded

through circular loading disks. The dimensions of the slabs were as follows.

SLAB No	h mm	d m	diameter of the loading disc mm	l mm	Span mm
II 1	250	200	250	2745	2575
II 2	160	128	160	1800	1630
II 3	160	128	160	1800	1630
II 4	80	64	80	900	730
II 5	80	64	80	900	730
II 6	80	64	80	900	730

Three of the six slabs reported in group III were analysed, they were circular with diameters of 1.5 m and 120 mm thick. The slabs were loaded centrally through 150 mm diameter steel plates and simply supported by eight tie bars situated in a circle of diameter equal to 1.37 m, the principal variables in this group were the concrete strength and the reinforcement ratio.

The four specimens of group IV were as shown in Fig.(6-1). The slabs were 100 mm thick. An upward load was applied at the centre through a 160 mm square plate and downward loads were applied at the four sides of a 1.83 m square, see Fig.(6-1). The principal variable in this group was the ratio between the central load (upward load) and the restraining moments at the edges of the 1.83 m square defined by the downward loads.

Slabs IV 1 had no boundary moments and the proposed method was not applied to this case.

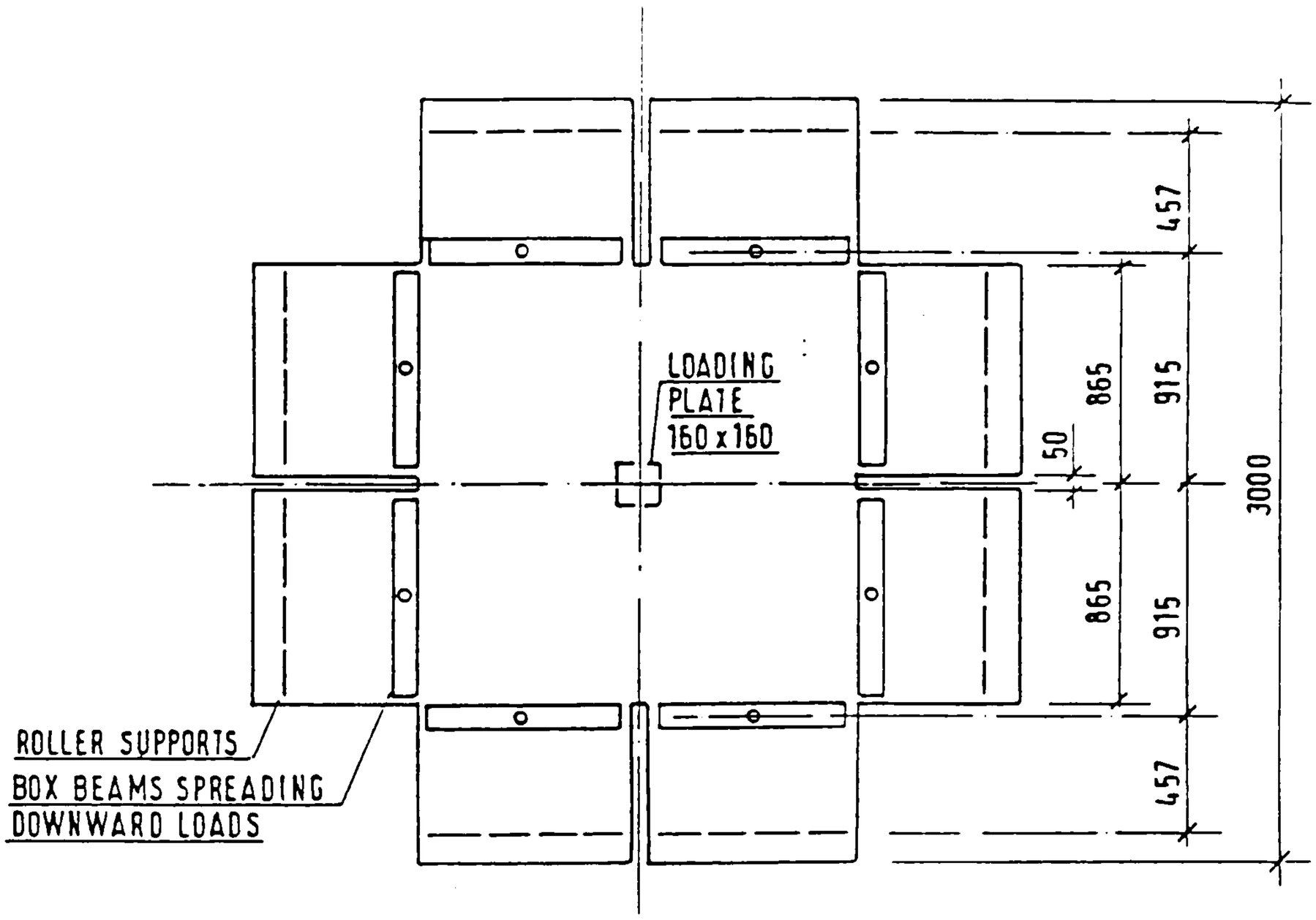

Fig.(6-1) Regan Loading systems of slabs group IV

The slabs of group V were 1.6 m square and 150 mm thick. They were simply supported at all four edges on spans of 1.5 mm, the principal variable between tests was the detail of the load area.

More details of the slabs in all groups and test results are given in table (6-2-9).

SLAB No	r_3 mm	r_o mm	C mm	ρ %	d mm	f_c N/mm^2	f_y N/mm^2	x mm	V_t KN	V_c KN	$\frac{V_c}{V_t}$
I 1	1165	127	200	1.20	77	25.8	500	23.2	204	200	0.98
I 2	1165	127	200	1.20	77	23.5	500	24.4	186	191	1.02
I 3	1165	127	200	0.92	77	27.5	500	19.4	204	178	0.89
I 4	1165	127	200	0.92	77	32.3	500	17.8	204	192	0.94
I 5	1165	127	200	0.75	79	28.2	480	17.4	175	168	0.96
I 6	1165	127	200	0.75	79	22.0	480	19.8	175	149	0.85
I 7	1165	127	200	0.80	79	30.5	480	17.3	196	181	0.92
II 1	1639	125	196	0.98	200	34.9	530	55.7	869	942	1.08
II 2	1038	80	126	0.98	128	33.3	485	31.1	402	404	1.00
II 3	1038	80	126	0.98	128	34.3	485	30.4	378	406	1.07
II 4	465	40	63	0.98	64	33.3	480	11.1	119	101	0.85
II 5	465	40	63	0.98	64	34.3	480	10.9	107	103	0.96
II 6	465	40	63	0.98	64	36.0	480	10.6	107	105	0.98
III 1	685	75	118	0.83	95	23.2	494	21.9	202	184	0.91
III 2	685	75	118	0.83	95	9.52	494	41.2	128	142	1.11
III 3	685	75	118	0.83	95	37.8	494	16.5	219	226	1.03
IV 2	583	102	160	1.31	80	34.0	525	20.1	236	245	1.03
IV 3	583	102	160	1.31	80	28.3	525	22.4	248	227	0.92
IV 4	583	102	160	1.31	80	31.3	525	21.1	260	237	0.91
V 1	955	27	42	0.80	118	34.3	628	26.2	179	193	1.07
V 2	955	85	133	0.80	118	32.2	628	26.0	289	313	1.08
V 3	955	55	86	0.80	118	32.4	628	26.6	274	276	1.00
V 4	955	65	102	0.80	118	36.2	628	24.4	294	309	1.05
V 5	955	75	118	0.80	118	32.9	628	25.8	294	306	1.04

Table (6-2-9) slabs tested by Regan.

6-2-10 Slabs tested by Rankin and Long

27 Slab-column specimens subjected to concentric vertical loading are reported in reference (51). Slabs with reinforcement indices $\rho\ f_y/f_c$ of less than 0.1 were predicted to fail in flexure. As a result the proposed method was not applicable to these cases and only 19 of these tests were suitable for analysis. The slabs were 700 mm square and simply supported at four edges with spans of 640 mm. The principal variable in the tests were the reinforcement ratio and the slab thickness. More details of the slabs and the test results are given in table (6-2-10).

SLAB No	r_3 mm	r_o mm	C mm	ρ %	d mm	f_c N/mm^2	f_y N/mm^2	x mm	V_t KN	V_c KN	$\frac{V_c}{V_t}$
3	407	63.7	100	0.691	40.5	30.7	530	6.9	56.55	52.08	0.92
4	407	63.7	100	0.821	40.5	34.8	530	7.1	56.18	60.76	1.08
5	407	63.7	100	0.833	40.5	34.8	530	7.3	57.27	62.44	1.09
6	407	63.7	100	1.026	40.5	34.8	530	7.9	65.80	63.44	0.97
7	407	63.7	100	1.163	40.5	26.7	530	9.6	70.94	66.92	0.94
8	407	63.7	100	1.292	40.5	26.7	530	10.2	71.09	71.52	1.00
9	407	63.7	100	1.454	40.5	26.7	530	10.4	78.60	65.48	0.83
11	407	63.7	100	0.802	40.5	29.9	530	7.5	55.00	55.16	1.00
12	407	63.7	100	1.107	40.5	29.9	530	8.9	67.06	65.48	0.98
14	407	63.7	100	0.691	40.5	34.0	530	6.6	52.45	55.16	1.05
15	407	63.7	100	1.994	40.5	34.0	530	11.4	84.84	95.28	1.12
2A	407	63.7	100	0.691	46.5	28.8	530	8.1	66.24	57.36	0.86
3A	407	63.7	100	1.293	46.5	28.8	530	11.3	89.72	80.00	0.98

Table (6-2-10) continued.

SLAB No	r_3 mm	r_o mm	C mm	ρ %	d mm	f_c N/mm^2	f_y N/mm^2	x mm	V_t KN	V_c KN	$\frac{V_c}{V_t}$
4A	407	63.7	100	1.992	46.5	30.9	530	13.8	97.43	104.8	1.07
3B	407	63.7	100	1.292	35.0	37.7	530	7.4	56.67	59.60	1.05
4B	407	63.7	100	1.994	35.0	30.9	530	10.3	72.52	67.68	0.93
2C	407	63.7	100	0.960	53.5	32.4	530	8.6	87.86	81.84	0.93
3C	407	63.7	100	1.228	53.5	32.4	530	12.1	124.1	115.1	0.93
4C	407	63.7	100	1.993	53.5	27.8	530	16.9	125.9	138.0	1.09

Table (6-2-10) slabs tested by Rankin and Long.

6-2-11 <u>Slabs tested by the Author in the present work</u>

The details of the four concentrically loaded slabs are given in chapter two. Moments were applied at the four edge of the slabs so, r_3 was calculated as $2(0.25l_x + 0.25l_y)/\pi$ where l_x and l_y are the spans in X and Y directions respectively.

r_o was considered as $(a + b)/\pi$ and $C=(a + b)/2$, where a and b are the column dimensions.

The results of the calculations and predicted failure loads are shown in table (6-2-11).

SLAB No	r_3 mm	r_o mm	C mm	ρ %	d mm	f_c N/mm^2	f_y N/mm^2	x mm	V_t KN	V_c KN	$\frac{V_c}{V_t}$
SA2	636	95.5	150	0.55	64	34	640	10.3	141	110	0.78
SB1	636	95.5	150	1.00	62	27	530	15.0	133	124	0.93

Table (6-2-11) continued.

SLAB No	r_3 mm	r_o mm	C mm	ρ %	d mm	f_c N/mm^2	f_y N/mm^2	x mm	V_t KN	V_c KN	$\frac{V_c}{V_t}$
SC1	795	95.5	150	0.72	62	36	530	11.2	129	123	0.96
SD1	795	95.5	150	0.72	62	36	530	11.2	127	123	0.97

Table (6-2-11) slabs tested by the Author.

6-3 ECCENTRIC LOADING TESTS

The predicted ultimate loads for eccentrically loaded slabs are defined by the following equation

$$V_{ec} = \frac{V_{cal}}{1 + \frac{e}{0.7(C+3d)}}$$

Where:

V_{cal} is the shear strength of a similar slab loaded concentrically

V_{ec} is the shear strength of the eccentrically loaded slabs

e is the load eccentricity.

C =(0.25 x column perimeter).

The results of tests carried out by the Author in the present work and from other researchers are analysed by the proposed formula in this Section.

6-3-1 Slabs tested by Elstner and Hognestad

Slabs A11 and A12 are reported in reference (20). The slabs were 1825 mm square with

356 mm square columns. The loads were intended to be applied eccentrically. It is doubtful whether the two slabs which were placed eccentrically under the testing machine in fact received any appreciable amount of eccentricity, since the columns were not free to move horizontally with respect to the machine. This may be why the calculated loads failure are smaller than the predicted ones, see table (6-3-1).

SLAB No	C mm	ρ %	d mm	f_c N/mm^2	f_y N/mm^2	x mm	e mm	V_t KN	V_c KN	V_{ec} KN	$\frac{V_{ec}}{V_t}$
A11	356	2.47	114.4	25.9	326	48.4	178	529	463	340	0.64
A12	356	2.47	114.4	28.4	326	45.9	178	529	482	355	0.67

Table (6-3-1) slabs tested by Elstner and Hognstad.

6-3-2 Slabs tested by Moe

The details of the test specimens and method of testing have already been given in chapters one and two. The results of the tests and analysis are shown in table (6-3-2). On inspection of the results, the proposed method of analysis gives reasonable agreement for all the slabs having small eccentricities of loading.

The average concrete strength of slabs M2A and M4A may not be quite reliable because the variation in strength between the various batches in the same slab. Slabs M4 and M5 failed in negative bending before the shear capacities were reached. It should be noted that the slabs were simply supported along all four edges and that the edges were free to lift in the case of

large eccentricity, therefore slabs M2A, M4A, M4, M5, M8 are irrelevant in the present comparison.

SLAB No	C mm	ρ %	d mm	f_{c_2} N/mm2	f_{y_2} N/mm2	x mm	e mm	V_t KN	V_c KN	V_{ec} KN	$\frac{V_{ec}}{V_t}$
M2	305	1.50	114	26.1	481	40.3	196	293	421	294	1.00
M3	305	1.50	114	23.0	481	43.4	338	207	399	229	1.10
M6	254	1.34	114	27.0	328	33.2	168	239	375	267	1.11
M7	254	1.34	114	26.9	328	34.5	61	311	366	320	1.02
M9	254	1.34	114	23.6	328	35.9	127	267	356	273	1.02
M10	254	1.34	114	21.2	328	38.3	308	178	341	196	1.10

Table (6-3-2)Slabs tested by Moe.

6-3-3 Slabs tested by Hanson and Hanson

Only seven of the seventeen test slabs reported in reference (23) could be analysed by the proposed method. Some of the remaining slabs had holes adjacent to the columns while the others were slabs with edge columns. The slabs were 1219x2133 mm with 76 mm thickness supported on central square or rectangular columns. The top and bottom ends of the column were provided with a hinged end condition. The load eccentricity was achieved by a variation in the vertical forces at the slab edges.

The result of the analysis and more data for these slabs are presented in table (6-3-3).

SLAB No	C mm	ρ %	d mm	f_c N/mm^2	f_y N/mm^2	x mm	e mm	V_t KN	V_c KN	V_{ec} KN	$\frac{V_{ec}}{V_t}$
A1	152	1.64	57	30.7	366	13.6	3891	5.85	118.0	6.5	1.10
A2	152	1.64	57	31.8	376	13.1	5056	4.90	117.0	5.0	1.02
B7	228	1.64	57	33.5	354	15.5	7297	5.00	89.4	3.3	0.66
C8	228	1.64	57	33.3	411	16.0	5602	5.70	91.7	3.4	0.60
A12	152	1.64	57	33.7	372	12.9	763	27.40	123.0	28.1	1.02
B16	228	1.64	57	30.9	341	15.1	795	35.10	80.3	21.0	0.60
C17	228	1.64	57	36.5	341	14.5	785	32.10	91.0	24.0	0.75

Table (6-3-3) slabs tested by Hanson and Hanson.

6-3-4 Slabs tested by Anis

6 Slabs were tested by Anis (2) under eccentric loading. Slab B1 was tested by the means of two horizontal forces acting at the top and bottom sides of the column stub, the slab failed in flexure. As a result only 5 slabs could be analysed by the proposed method. The slabs were 1520 mm square with 102 mm overall depth and central 203 mm square columns, they were supported at the edges and the loads were applied on the column, see Fig.(2-1). Some data concerning these slabs and the test results are presented in table (6-3-4).

SLAB No	C mm	ρ %	d mm	f_c N/mm^2	f_y N/mm^2	x mm	e mm	V_t KN	V_c KN	V_{ec} KN	$\frac{V_{ec}}{V_t}$
B3	203	2.19	76	30.4	330	25.4	94	194.0	252	192	0.99
B4	203	2.19	76	29.8	330	25.7	188	142.0	248	152	1.07
B5	203	2.19	76	29.0	330	26.1	312	127.0	247	122	0.96

Table (6-3-4) continued.

SLAB No	C mm	ρ %	d mm	f_c N/mm^2	f_y N/mm^2	x mm	e mm	V_t KN	V_c KN	V_{ec} KN	$\frac{V_{ec}}{V_t}$
B6	203	2.19	76	31.4	330	24.9	465	117.0	256	101	0.86
B7	203	2.19	76	33.8	330	23.9	945	70.8	264	64	0.90

Table (6-3-4) slabs tested by Anis.

6-3-5 <u>Slabs tested by Stamenkovic and Chapman</u>

Only eight of the ten eccentrically loaded slabs carried out by Stamenkovic and Chapman (63) are suitable for analysis. The slabs were 914 mm square with 76 mm thick, supported at the four edges. The slabs group CI had 127 mm central square columns while slabs CIr had 76x152 mm columns where the 152 mm was in the eccentricity direction. The vertical load was applied concentrically through the column, while the horizontal loads were applied at the top and bottom of the column. The properties of the slabs and the results of the analysis are given in table (6-3-5). The tabulated results indicate a good agreement between the actual and calculated failure loads.

SLAB No	C mm	ρ %	d mm	f_c N/mm^2	f_y N/mm^2	x mm	e mm	V_t KN	V_c KN	V_{ec} KN	$\frac{V_{ec}}{V_t}$
C/I/1	127	1.17	56	38.0	434	11.6	87	85	123	86	1.01
C/I/2	127	1.17	56	29.7	434	12.8	168	62	111	61	0.98
C/I/3	127	1.17	56	25.5	434	13.9	404	34	104	35	1.02
C/I/4	127	1.17	56	25.1	434	14.0	797	21	103	21	1.00
C/I/r_1	114	1.17	56	22.6	414	14.5	85	86	98	69	0.80

Table (6-3-5) continued.

SLAB No	C mm	ρ %	d mm	f_c N/mm^2	f_y N/mm^2	x mm	e mm	V_t KN	V_c KN	V_{ec} KN	$\frac{V_{ec}}{V_t}$
C/I/r_2	114	1.17	56	29.2	414	12.6	162	67	110	61	0.91
C/I/r_3	114	1.17	56	28.6	414	12.7	394	40	109	39	0.98
C/I/r_4	114	1.17	56	26.6	414	13.2	777	22	105	21	0.95

Table (6-3-5) slabs tested by Stamenkovic and Chapman.

6-3-6 Slabs tested by Hanson

Only slab C9 of the slabs reported in reference (24) could be analysed by the proposed method. This slab was 2285 mm square with a 508 mm square central column. Some data concerning this slab and the test result are presented in table (6-3-6).

SLAB No	C mm	ρ %	d mm	f_c N/mm^2	f_y N/mm^2	x mm	e mm	V_t KN	V_c KN	V_{ec} KN	$\frac{V_{ec}}{V_t}$
C9	400	0.63	162	23.3	423	38.4	559	283	445	234	0.83

Table (6-3-6) Slab tested by Hanson

6-3-7 Slab tested by Narasimham

Since most of the eccentrically loaded slabs tested by Narasimhan (43) had shear reinforcement, only slab L1 could be used in the comparison. The slab was 2285 mm square with a 305 mm square column. The slab properties and the analysis result are given in table (6-3-7) which shows a fair agreement between the test and predicted failure load.

SLAB No	C mm	ρ %	d mm	f_c N/mm^2	f_y N/mm^2	x mm	e mm	V_t KN	V_c KN	V_{ec} KN	$\frac{V_{ec}}{V_t}$
L1	305	1.11	143	26.6	398	42	300	400	534	337	0.84

Table(6-3-7) slab tested by Narasimhan.

6-3-8 Slabs tested by Regan, Walker, and Zakaria

These slabs are reported in reference (52). They were all 2 m square and 80 mm thick. The slabs were eccentrically loaded by upward forces applied to the columns which were provided with projection. The variables of the slabs were the size and shape of the columns. The slab details and analysis results are given in table (6-3-8).

SLAB No	C mm	ρ %	d mm	f_c N/mm^2	f_y N/mm^2	x mm	e mm	V_t KN	V_c KN	V_{ec} KN	$\frac{V_{ec}}{V_t}$
SM5	180	1.05	60	32.0	480	14.5	220	72	128	68	0.95
SM9	180	1.05	60	37.7	480	13.3	110	97	138	96	0.99
SM10	180	1.05	60	37.7	480	13.3	220	88	143	76	0.86
SM11	240	1.17	60	36.8	480	13.4	220	91	92	53	0.58
SM12	240	1.17	60	31.9	480	14.7	220	88	85	49	0.58

Table (6-3-8) slabs tested by Regan, Walker, and Zakaria.

6-3-9 slab tested by Godycki, Dilger and Ghali

Tests of two 1778 mm square slabs, 152 mm thick, are reported in reference (21). The slabs were subjected to vertical loads and moments applied through 305 mm central square columns. The principal variable in the tests was the

ratio of reinforcement. More details about the slabs and the tests results are presented in table (6-3-9).

SLAB No	C mm	ρ %	d mm	f_c N/mm^2	f_y N/mm^2	x mm	e mm	V_t KN	V_c KN	V_{ec} KN	V_{ec} / V_t
S.010	305	1.5	127	32.0	424	30.5	1068	132	428	126	0.95
S.005	305	0.5	127	30.9	424	20.8	704	132	282	114	0.86

Table (6-3-9) slabs tested by Godycki, Dilger and Ghali.

6-3-10 Slabs tested by the Author

Six slabs were tested by the Author in the present work. The slabs had different variables, column shape, ratio of reinforcement, span dimensions, and eccentricity of the load. Full details of the test specimens and method of testing have already been given in chapter two. The results of the analysis are given in table (6-3-10). The comparison between the calculated and observed failure loads shows good agreement and the proposed method of analysis is on the safe side.

SLAB No	C mm	ρ %	d mm	f_c N/mm^2	f_y N/mm^2	x mm	e mm	V_t KN	V_c KN	V_{ec} KN	V_{ec} / V_t
SA1	150	0.55	64	33	640	10.5	52	109	109	90	0.83
SA3	150	0.55	64	36	640	10.1	100	85	115	81	0.95
SA4	150	0.55	64	32	640	10.6	336	49	108	45	0.92
SB2	150	1.00	62	28	530	14.7	360	61	128	51	0.84
AC2	150	0.72	62	37	530	11.1	337	65	127	52	0.80
SD2	150	0.72	62	31	530	12.1	310	56	116	50	0.90

Table (6-3-9) slabs tested by the Author.

6-4 Comparison between the experimental data and predictions of existing methods from various sources

Most of the theoretical and experimental work carried out on punching shear resistance of reinforced concrete flat-slabs is reviewed in chapter one. The aim of this section is to compare the proposed solution with analytical solutions of other authors, and the recommendations given in the widely used codes of practice (The American ACI-318-83, The British BS8110 and CEB-FIP model code).

6-4-1 The following punching strength formulae are used in the present comparison, for concentrically loaded slabs.

6-4-1-1 Stamankovic and Chapman (63)

The punching shear resistance for slabs concentrically loaded is

$$V_{cal} = 0.9 \quad (4cd\sqrt{(f_c/145)} \cdot \left(\frac{15(1-0.07(c/d)}{1 + 5.25\,\dfrac{4cd\sqrt{(f_c/145)}}{V_{flex}}}\right)$$

Where:

c is the side length of the column,

V_{flex} is the flexural capacity of the slab.

In the present comparison V_{flex} was taken from the references where the slabs had been reported. Where the flexural capacities are not reported and for the author's slabs, V_{flex} was calculated as follows.

$$V_{flex} = \frac{2\ \pi\ m}{1 - (r_o/r_3)}$$

Where :

$$m = 0.9\ As\ f_y\ d(1 - 0.59\ \rho\ f_y/f_c)$$

$\rho = A_s/rd$ and $f_c = 0.85\ f_{cu}$

A_s being the area of the tensile reinforcement passing through the column face.

The results of the analysis are shown in table (6-4-1). Examining these tabulated results, it appears that the range of V_{cal}/V_{test} is from 0.64 to 1.32 and the ratio increases with increasing r/d. The lack of a size factor may have contributed to the scatter of the results.

SLAB No	r_o mm	r_3 mm	f_c N/mm^2	f_y N/mm^2	ρ %	r mm	d mm	V_f KN	V_c KN	V_t KN	$\frac{V_c}{V_t}$
A1a	162	1162	14.98	332	1.15	254	117	365	282	393	0.93
A1b	162	1162	26.77	332	1.15	254	117	390	346	365	0.95
A1c	162	1162	21.57	332	1.15	245	117	384	323	356	0.90
A2a	162	1162	14.55	321	2.47	254	114	590	315	334	0.94
A2b	162	1162	20.72	321	2.47	254	114	662	370	401	0.92
A2c	162	1162	39.73	321	2.47	254	114	743	484	467	1.03
A3a	162	1162	13.60	321	3.70	254	114	665	316	356	0.88
A3b	162	1162	24.00	321	3.70	254	114	915	334	445	0.75
A3c	162	1162	28.26	321	3.70	254	114	966	456	534	0.85
A3d	162	1162	36.76	321	3.70	254	114	1030	512	547	0.94

Table (6-4-1) continued.

SLAB No	r_o mm	r_3 mm	f_c N/mm^2	f_y N/mm^2	ρ %	r mm	d mm	V_f KN	V_c KN	V_t KN	$\frac{V_c}{V_t}$
A5	226	1162	29.50	321	2.47	356	114	771	514	534	0.96
A7	206	1162	29.64	321	2.47	254	114	713	431	512	0.84
B9	206	1162	46.60	341	2.00	254	103	658	450	505	0.89
B11	206	1162	14.34	409	3.00	254	102	702	292	329	0.88
B14	206	1162	53.76	326	3.00	254	102	923	517	579	0.89
Moe											
R2	97	1150	28.26	333	1.38	152	98	393	234	317	0.73
M1A	194	1150	22.52	488	1.50	305	114	649	412	440	0.94
H1	194	1150	28.26	333	1.36	264	114	361	333	379	0.88
S1-60	194	1150	25.28	407	1.06	254	114	398	338	396	0.85
S2-60	194	1150	23.90	407	1.53	254	114	409	329	362	0.90
S3-60	194	1150	24.43	407	2.30	254	114	399	332	370	0.89
S4-60	194	1150	25.80	407	3.45	254	114	359	323	340	0.95
S5-60	162	1150	23.58	399	1.06	254	114	379	320	318	1.00
S1-70	162	1150	26.56	491	1.06	254	114	470	365	400	0.91
S3-70	162	1150	26.56	491	2.30	254	114	472	356	385	0.95
S4-70	162	1150	27.41	491	3.45	254	114	463	361	380	0.95
S5-70	162	1150	24.43	482	1.06	254	114	450	348	342	1.02
Kinnunen & Nylander											
5	75	855	28.50	450	0.64	118	117	305	215	260	0.82
6	75	855	27.80	463	0.64	118	118	315	215	280	0.76
24	150	855	28.00	464	1.17	235	128	494	398	438	0.90
25	150	855	26.60	460	1.14	235	124	473	377	416	0.90
32	150	855	27.20	457	0.61	235	123	192	246	263	0.94
33	150	855	28.30	470	0.60	235	125	202	258	263	0.98

Table (6-4-1) continued.

SLAB No	r_o mm	r_3 mm	f_c N/mm^2	f_y N/mm^2	ρ %	r mm	d mm	V_f KN	V_c KN	V_t KN	$\frac{V_c}{V_t}$
Kinnunen, Nylander & Tolf											
1	62.5	600	30.40	706	0.80	98	100	313	174	216	0.80
3	62.5	600	24.30	701	0.81	98	99	298	156	194	0.80
13	62.5	600	28.30	720	0.35	98	98	143	131	145	0.90
14	62.5	600	26.70	712	0.34	98	99	140	129	148	0.87
17	125.0	1200	27.00	668	0.34	196	200	543	513	489	1.05
18	125.0	1200	25.70	664	0.35	196	197	535	498	444	1.12
Hanson											
B4	288	2330	23.60	450	0.94	355	162	777	649	490	1.32
Hawkins, Fallsen & Hinojosa											
2	247	1162	27.90	411	1.11	388	117	363	384	352	1.09
9	185	1162	31.30	414	0.75	290	121	343	365	316	1.15
Narasimhan											
L7	194	1274	37.70	476	1.11	305	143	673	596	687	0.86
L9	194	1274	35.10	476	1.11	305	143	668	586	588	0.99
Stamenkovic & Chapman											
V/I/2	80.8	582	27.54	434	1.37	127	56	91	81.5	117	0.69
V/Ir/1	72.5	582	26.70	414	1.72	114	56	108	115	109	1.06
Regan											
I1	127	1165	27.40	500	1.20	200	77	262	191	194	0.98
I2	127	1165	24.90	500	1.20	200	77	228	176	176	1.00
I3	127	1165	29.10	500	0.92	200	77	215	183	194	0.94
I4	127	1165	34.30	500	0.92	200	77	190	178	194	0.92
I5	127	1165	29.90	480	0.75	200	79	179	180	165	1.09

Table (6-4-1) continued.

SLAB No	r_o mm	r_3 mm	f_c N/mm^2	f_{y_2} N/mm^2	ρ %	r mm	d mm	V_f KN	V_c KN	V_t KN	$\frac{V_c}{V_t}$
I6	127	1165	23.30	480	0.75	200	79	156	152	165	0.92
I7	127	1165	32.30	480	0.80	200	79	170	172	186	0.93
II1	125	1639	37.00	530	0.98	196	200	1447	733	825	0.89
II2	80	1038	35.40	485	0.98	126	128	541	303	390	0.77
II3	80	1038	36.50	485	0.98	126	128	544	308	365	0.84
II4	40	465	35.40	480	0.98	63	64	129	75	117	0.64
II5	40	465	36.50	480	0.98	63	64	128	76	105	0.72
II6	40	465	38.40	480	0.98	63	64	128	77	105	0.73
III1	75	685	24.6	494	0.83	118	95	234	160	197	0.81
III2	75	685	10.10	494	0.83	118	95	186	108	123	0.88
III3	75	685	40.20	494	0.83	118	95	310	209	214	0.97
IV2	102	583	36.10	525	1.31	160	80	352	215	236	0.91
IV3	102	583	30.10	525	1.31	160	80	435	209	248	0.84
IV4	102	583	33.20	525	1.31	160	80	460	223	262	0.85
V2	85	955	34.20	620	0.80	133	118	474	280	280	1.00
V3	55	955	34.40	620	0.80	86	118	449	207	265	0.78
V4	65	955	38.50	620	0.80	102	118	459	243	285	0.85
V5	75	955	34.90	620	0.80	118	118	467	262	285	0.95
Rankin & Long											
3	63.6	407	32.6	530	0.69	100	40.5	50.5	47.4	56.5	0.83
4	63.6	407	37.0	530	0.82	100	40.5	46.2	54.2	56.2	0.96
5	63.6	407	37.0	530	0.88	100	40.5	69.0	45.1	57.3	0.78
6	63.6	407	37.0	530	1.02	100	40.5	80.3	59.1	65.6	0.90
7	63.6	407	28.3	530	1.16	100	40.5	79.3	54.0	71.0	0.76

Table (6-4-1) continued.

SLAB No	r_o mm	r_3 mm	f_c N/mm^2	f_y N/mm^2	ρ %	r mm	d mm	V_f KN	V_c KN	V_t KN	$\frac{V_c}{V_t}$
8	63.6	407	28.3	530	1.29	100	40.5	86.6	55.5	71.1	0.78
9	63.6	407	28.3	530	1.45	100	40.5	95.5	57.1	78.6	0.72
11	63.6	407	31.8	530	0.80	100	40.5	57.8	50.3	55.0	0.91
12	63.6	407	31.8	530	1.11	100	40.5	77.2	56.0	67.1	0.83
14	63.6	407	36.1	530	0.69	100	40.5	51.0	49.3	52.4	0.94
15	63.6	407	36.1	530	1.99	100	40.5	129.	68.0	84.4	0.80
2A	63.6	407	30.6	530	0.69	100	46.5	66.3	58.5	66.2	0.88
3A	63.6	407	30.6	530	1.29	100	46.5	116.	70.6	89.7	0.78
4A	63.6	407	32.8	530	1.99	100	46.5	166.	78.4	97.4	0.80
3B	63.6	407	40.0	530	1.29	100	35.0	67.9	51.1	56.7	0.90
4B	63.6	407	32.8	530	1.99	100	35.0	94.4	51.8	72.5	0.71
2C	63.6	407	34.4	530	0.69	100	53.5	88.3	75.7	87.8	0.86
3C	63.6	407	34.4	530	1.29	100	53.5	155.	90.5	124.	0.73
4C	63.6	407	29.6	530	1.99	100	53.5	215.	91.2	126.	0.72
Kamaraldin											
SA2	95	636	36.1	640	0.59	150	64	129	122	141	0.86
SB1	95	636	28.7	530	1.08	150	62	173	122	133	0.92
SC1	95	795	38.2	530	1.08	150	62	173	135	129	1.04
SD1	95	795	38.2	530	1.08	150	62	173	135	127	1.06

Table (6-4-1) Slabs analysed by Stamenkovic and Chapman's formula

6-4-1-2 Regan

The punching shear resistance suggested by Regan (53) is

$$V_{cal} = Ka \cdot Ksc \cdot \xi \sqrt[3]{(100As/bd) \cdot f_{cu}} \cdot 2.69\ d(\Sigma C + 7.85d)$$

Where

Ka = 0.13 for normal dense concrete

$$Ksc = 1.15 \sqrt{4\pi\ (\text{column area})(\text{column perimeter})^2}$$

$$\xi = \sqrt[4]{300/d} \quad \text{with d in mm}$$

(100As/bd) is the average of the percentages of tensile reinforcement in two orthogonal directions, where b is the width of Band I (see reference (53))

ΣC is the column perimeter.

The results of the analysis are shown in table (6-4-2). Regan's theory is on the safe side. The theory does not extend to slabs with flexural failure, as a result slabs 32 and 33 of reference (30) could be ignored.

SLAB No	d mm	ρ %	Ksc	f_{cu} N/mm^2	V_{cal} KN	V_{test} KN	$\frac{V_{cal}}{V_{test}}$
Elstner and Hognestad							
A1a	117	1.17	1	17.60	217	303	0.72
A1b	117	1.17	1	31.5	264	365	0.72
A1e	117	1.17	1	25.4	245	356	0.69
A2a	114	2.48	1	17.1	294	334	0.88
A2b	114	2.48	1	24.4	381	401	0.95
A2c	114	2.48	1	46.7	472	467	1.01
A3a	114	2.48	1	16.00	311	356	0.93

Table (6-4-2) continued.

SLAB No	d mm	ρ %	Ksc	f_{cu_2} N/mm^2	V_{cal} KN	V_{test} KN	$\frac{V_{cal}}{V_{test}}$
A3b	114	3.72	1	28.25	458	445	1.02
A3c	114	3.72	1	33.25	483	534	0.90
A3d	114	3.72	1	43.25	528	547	0.96
A5	114	2.48	1	34.75	490	534	0.92
A7	114	2.48	1	34.90	429	512	0.84
B9	103	2.24	1	33.25	361	505	0.71
B11	102	3.39	1	16.90	327	329	0.99
B14	102	3.39	1	63.25	507	579	0.88
MOe							
R2	114	1.37	1	33.25	272	317	0.86
M1A	114	1.50	1	26.50	365	440	0.83
H1	114	1.50	1	33.25	330	379	0.87
S1-60	114	1.06	1	30.00	306	396	0.77
S2-60	114	1.06	1	28.10	300	362	0.83
S3-60	114	1.06	1	28.75	302	370	0.82
S4-60	114	1.06	1	30.40	308	340	0.90
S5-60	114	1.05	1	27.75	298	318	0.94
S1-70	114	1.06	1	31.25	311	400	0.77
S3-70	114	1.06	1	32.25	314	385	0.81
S4-70	114	1.06	1	44.75	350	380	0.92
S5-70	114	1.05	1	28.75	301	342	0.88
Kinnunen & Nylander							
5	117	0.80	1.15	33.50	246	260	0.95
6	118	0.79	1.15	32.70	248	280	0.88

Table (6-4-2) continued.

SLAB No	d mm	ρ %	Ksc	f_{cu_2} N/mm^2	V_{cal} KN	V_{test} KN	$\frac{V_{cal}}{V_{test}}$
24	128	1.01	1.15	33.00	399	438	0.91
25	124	1.04	1.15	31.40	381	416	0.92
32	123	0.49	1.15	32.00	295	263	1.12
33	125	0.48	1.15	33.30	303	263	1.15
Kinnunen & Nylander & Tolf							
1	100	0.80	1.15	35.70	191	216	0.88
3	99	0.81	1.15	28.60	175	194	0.90
13	98	0.34	1.15	33.20	136	145	0.94
14	99	0.35	1.15	31.40	137	148	0.92
17	200	0.35	1.15	31.70	467	489	0.96
18	197	0.34	1.15	30.20	446	444	1.00
Hanson							
B4	162	0.94	1.00	27.70	528	490	1.07
Hawkins, Fallsen & Hinjosa							
2	117	1.11	1.00	32.90	424	352	1.20
9	121	0.75	1.00	36.90	339	316	1.07
Narasimhan							
L7	143	1.11	1.00	44.40	517	686	0.75
L9	143	1.11	1.00	41.40	505	588	0.86
Stamenkovic & Chapman							
V/I/2	56	1.17	1.00	32.40	95	117	0.81
V/Ir/1	56	1.17	0.96	31.50	88.8	109	0.88

Table (6-4-2) continued.

SLAB No	d mm	ρ %	Ksc	f_{cu_2} N/mm^2	V_{cal} KN	V_{test} KN	$\frac{V_{cal}}{V_{test}}$
Regan							
I1	77	1.20	1.00	32.20	180	194	0.93
I2	77	1.20	1.00	29.30	174	176	0.99
I3	77	0.92	1.00	34.30	168	194	0.86
I4	77	0.92	1.00	40.40	177	194	0.91
I5	79	0.75	1.00	35.20	163	165	0.99
I6	79	0.75	1.00	27.40	150	165	0.91
I7	79	0.80	1.00	38.00	171	186	0.92
II1	200	0.98	1.15	43.60	732	825	0.88
II2	128	0.98	1.15	41.60	331	390	0.85
II3	128	0.98	1.15	42.90	334	365	0.91
II4	64	0.98	1.15	41.60	98	117	0.84
II5	64	0.98	1.15	42.90	99	105	0.95
II6	64	0.98	1.15	45.20	101	105	0.96
III1	95	0.83	1.15	29.00	170	197	0.86
III2	95	0.83	1.15	11.90	127	123	1.03
III3	95	0.83	1.15	47.30	201	214	0.94
IV1	80	1.31	1.00	32.70	173	196	0.88
IV2	80	1.31	1.00	42.50	188	236	0.80
IV3	80	1.31	1.00	35.40	177	248	0.71
IV4	80	1.31	1.00	39.10	183	262	0.70
V2	118	0.80	1.15	40.20	278	280	0.99
V3	118	0.80	1.15	40.50	242	265	0.91
V4	118	0.80	1.00	45.30	230	285	0.80

Table (6-4-2) continued.

SLAB No	d mm	ρ %	Ksc	f_{cu_2} N/mm^2	V_{cal} KN	V_{test} KN	$\frac{V_{cal}}{V_{test}}$
V5	118	0.80	1.15	41.10	268	285	0.94
Rankin & Long							
3	40.5	0.691	1	38.4	50.0	56.55	0.88
4	40.5	0.821	1	34.5	51.1	56.18	0.91
5	40.5	0.833	1	34.5	52.4	57.27	0.91
6	40.5	1.026	1	34.5	51.1	65.58	0.78
7	40.5	1.163	1	37.1	58.8	70.94	0.83
8	40.5	1.292	1	37.1	61.0	71.09	0.86
9	40.5	1.454	1	37.1	63.3	78.60	0.81
11	40.5	0.802	1	37.4	52.1	55.00	0.95
12	40.5	1.107	1	37.4	58.0	67.00	0.86
14	40.5	0.691	1	42.5	51.7	52.45	0.98
15	40.5	1.994	1	42.5	73.7	84.84	0.87
2A	46.5	0.691	1	36.0	57.9	66.24	0.87
3A	46.5	1.293	1	36.0	71.3	89.72	0.79
4A	46.5	1.292	1	38.6	84.33	97.43	0.86
3B	35.0	1.292	1	47.1	55.60	56.67	0.98
4B	35.0	1.994	1	38.6	60.1	72.52	0.83
2C	53.5	0.690	1	40.5	71.6	87.86	0.81
3C	53.5	1.288	1	40.5	88.2	124.14	0.71
4C	53.5	1.993	1	34.8	97.0	125.94	0.77
Kamaraldin							
SA2	64.0	0.55	1	52.5	103.7	141.00	0.73
SB1	62.0	1.00	1	33.75	112.7	133.00	0.84

Table (6-4-2) continued.

SLAB No	d mm	ρ %	Ksc	f_{cu_2} N/mm2	V_{cal} KN	V_{test} KN	$\frac{V_{cal}}{V_{test}}$
SC1	62.0	0.72	1	45.00	111.2	129.00	0.86
SD1	62.0	0.72	0.96	45.00	106.7	127.00	0.84

Table (6-4-2) slabs analysed by Regan's formula.

6-4-1-3 <u>British Standard BS8110</u>

The code equations used are listed below.

$$V_C = 0.79\left(\frac{100\ As}{X\ d}\right)^{1/3}\ \left(\frac{400}{d}\right)^{1/4}$$

$$V_{cal} = V_c\ u\ d$$

For the purpose of making comparisons with test results the safety factor γ_m has been removed from the code equations.

u is the control perimeter at distance of 1.5d from the loaded area and has square corners whether the loaded area is rectangular or circular.

For concrete strength's greater than 25 N/mm^2 V_C may be multiplied by $(f_{cu}/25)^{1/3}$, the value of f_{cu} should not be taken greater than 40 N/mm^2.

400/d should not be taken as less than 1, and (100As/Xd) should not be taken greater than 3.

X is the side length of the shear perimeter.

The result of the analysis are shown in table (6-4-3). The tabulated results indicate that for slabs with flexural reinforcement concentrated in the punching area (slabs of group, S, reference (4) and slabs of group, I, reference (56)), BS8110 overestimates the influence of the ratio of reinforcement which results in a poor level of safety. Where concrete strength of tests is lower than grade C25, BS8110's general formula for punching shear resistance can give very significant overestimates of strength, this situation seems to be covered safely by the Code's limiting concrete made with normal-weight aggregate to be not below grade C25.

SLAB No	d mm	u mm	ρ %	f_{cu_2} N/mm^2	V_{cal} KN	V_{test} KN	$\frac{V_{cal}}{V_{test}}$
Elstner & Hognestad							
A1a	117	2420	1.17	17.6	320	303	1.06
A1b	117	2420	1.17	31.5	346	365	0.95
A1e	117	2420	1.17	24.5	320	356	0.90
A2a	114	2348	2.48	17.1	390	334	1.17
A2b	114	2348	2.48	24.4	390	401	0.97
A2c	114	2348	2.48	46.7	456	467	0.97
A3a	114	2348	3.72	16.00	417	356	1.17
A3b	114	2348	3.72	28.25	434	445	0.97
A3c	114	2348	3.72	33.25	458	534	0.86
A3d	114	2348	3.72	43.25	487	547	0.89
A5	114	2792	2.48	34.75	520	534	0.97
A7b	114	2384	2.48	34.90	444	512	0.87
B9	103	2252	2.24	33.25	370	505	0.73

Table (6-4-3) continued.

SLAB No	d mm	u mm	ρ %	f_{cu_2} N/mm^2	V_{cal} KN	V_{test} KN	$\frac{V_{cal}}{V_{test}}$
B11	102	2240	3.39	16.9	366	329	1.11
B14	102	2240	3.39	63.25	428	579	0.74
Moe							
R2	114	1976	1.06	33.25	273	317	0.86
M1A	114	2588	2.31	26.5	428	440	0.97
H1	114	2384	0.60	33.25	272	379	0.71
S1-60	114	2384	0.87	30.00	298	396	0.78
S2-60	114	2384	1.45	28.1	345	362	0.95
S3-60	114	2384	2.00	28.75	388	370	1.05
S4-60	114	2384	2.62	30.40	432	340	1.27
S5-60	114	2169	1.06	27.74	282	318	0.88
S1-70	114	2384	0.87	31.25	302	400	0.95
S3-70	114	2384	2.00	32.25	402	385	1.05
S4-70	114	2384	2.62	44.75	473	380	1.25
S5-70	114	2169	1.06	28.75	285	342	0.83
Kinnunen & Nylander							
5	117	2004	0.96	33.50	274	260	1.05
6	118	2016	0.96	32.75	275	280	0.96
24	128	2736	1.03	33.00	407	438	0.93
25	124	2688	1.08	31.40	391	416	0.94
32	123	2676	0.55	32.00	310	263	1.18
33	125	2700	0.54	33.30	320	263	1.21

Table (6-4-3) continued.

SLAB No	d mm	u mm	ρ %	f_{cu_2} N/mm^2	V_{cal} KN	V_{test} KN	$\frac{V_{cal}}{V_{test}}$
Kinnunen, Nylander & Tolf							
1	100	1700	0.80	35.75	198	216	0.92
3	99	1688	0.81	28.60	182	194	0.94
13	98	1676	0.34	33.25	142	145	0.97
14	99	1688	0.35	31.40	142	142	0.96
17	200	3400	0.35	31.75	487	487	1.00
18	197	3364	0.34	30.25	465	444	1.05
Hanson							
B4	162	3364	0.94	27.75	547	490	1.11
Hawkins, Fallsen & Hinjosa							
2	117	2956	1.11	32.90	421	352	1.20
9	121	2612	0.75	36.90	348	316	1.10
Narasimhan							
L7	143	2936	1.11	44.4	538	687	0.78
L9	143	2936	1.11	41.1	525	588	0.98
Stamenkovic & Chapman							
V/I/2	56	1180	1.17	32.40	98	118	0.84
V/Ir/1	56	1128	1.07	31.50	90	109	0.83
Regan							
I1	77	1724	2.12	32.2	221	194	1.14
I2	77	1724	1.18	29.3	176	176	1.00
I3	77	1724	1.18	34.3	186	194	0.96
I4	77	1724	0.90	40.4	179	194	0.92
I5	79	1748	1.31	35.2	200	165	1.21

Table (6-4-3) continued.

SLAB No	d mm	u mm	ρ %	f_{cu_2} N/mm^2	V_{cal} KN	V_{test} KN	$\frac{V_{cal}}{V_{test}}$
I6	79	1748	0.72	27.4	151	165	0.92
I7	79	1748	0.80	38.0	175	186	0.94
II1	200	3400	1.15	43.6	783	825	0.95
II2	128	2176	1.15	41.6	358	390	0.92
II3	128	2176	1.15	42.9	358	365	0.98
II4	64	1088	1.15	41.6	106	117	0.91
II5	64	1088	1.15	42.9	106	105	1.01
II6	64	1088	1.15	45.2	106	105	1.01
III1	95	1740	0.96	29.0	194	197	0.98
III2	95	1740	0.96	11.9	184	123	1.50
III3	95	1740	0.96	47.3	216	214	1.00
IV1	80	2096	1.47	32.7	246	196	1.25
IV2	80	1856	1.47	42.5	233	236	0.99
IV3	80	1824	1.47	35.4	220	248	0.88
Iv4	80	2016	1.47	39.1	251	262	0.96
V2	118	2096	0.80	40.2	288	280	1.02
V3	118	1856	0.80	40.5	255	265	0.96
V4	118	1824	0.80	45.3	250	285	0.88
V5	118	2016	0.80	41.1	277	285	0.97
Rankin & Long							
3	40.5	886	0.691	38.4	51.26	56.55	0.91
4	40.5	886	0.821	34.5	52.4	56.18	0.93
5	40.5	886	0.883	34.5	53.7	57.27	0.94
6	40.5	886	1.026	34.5	56.4	65.58	0.86

Table (6-4-3) continued.

SLAB No	d mm	u mm	ρ %	f_{cu} N/mm^2	V_{cal} KN	V_{test} KN	$\frac{V_{cal}}{V_{test}}$
7	40.5	886	1.163	37.1	60.3	70.94	0.85
8	40.5	886	1.292	37.1	62.4	71.09	0.88
9	40.5	886	1.454	37.1	64.9	78.60	0.83
11	40.5	886	0.802	37.4	53.4	55.00	0.97
12	40.5	886	1.107	37.4	59.4	67.06	0.88
14	40.5	886	0.691	42.5	52.0	52.45	0.99
15	40.5	886	1.991	42.5	74.0	84.84	0.87
2A	46.5	958	0.691	36.0	60.2	66.24	0.90
3A	46.5	958	1.293	36.0	74.1	89.72	0.83
4A	46.5	958	1.992	38.6	87.6	97.43	0.90
3B	35.0	820	1.292	47.1	53.1	56.67	0.94
4B	35.0	820	1.994	38.6	60.6	72.52	0.84
2C	53.5	1042	0.690	40.5	75.26	87.86	0.85
3C	53.5	1042	1.288	40.5	92.7	124.1	0.74
4C	53.5	1042	1.993	34.8	102.3	125.9	0.81
Kamaraldin							
SA2	64.0	1368	0.51	42.5	102	141.0	0.72
SB1	62.0	1344	1.44	33.75	131	133.0	0.98
SC1	62.0	1344	1.44	45.0	139	129.0	1.07
SD1	62.0	1344	1.44	45.0	137	127.0	1.08

Table (6-4-3) slabs analysed by BS8110.

6-4-1-4 ACI 318-83

The unfactored ultimate shear stress given by the ACI Code is

$$v_c = (1 + 2/\beta)(\sqrt{f_c}/6)$$

But not greater than $(\sqrt{f_c}/3)$ at the critical section.

β is the ratio of long side to short side of the concentrated load or reaction area.

The shear resistance is

$$V_{cal} = v_c \cdot u \cdot d$$

u is the perimeter of the critical section having the same shape as the loaded area and at a distance d/2 from the outline of the loaded area.

On inspection of the results given in table (6-4-4), the value of V_{cal}/V_{test} varies from 0.46 to 1.15, the scatter of results seems to be due to two factors.

1- The lack of a size factor - the ratio of V_{cal}/V_{test} tends to be high for thicker slabs.

2- The absence of the tension reinforcement influence in the code formula - the ratio of V_{cal}/V_{test} increases with decreasing reinforcement ratio.

SLAB No	d mm	u mm	β	f_c N/mm^2	V_{cal} KN	V_{test} KN	$\frac{V_{cal}}{V_{test}}$
Elstner & Hognestad							
A1a	117	1484	1	14.1	217	303	0.72
A1b	117	1484	1	25.2	290	365	0.79
A1c	117	1484	1	20.3	260	356	0.73

Table (6-4-4) continued.

SLAB No	d mm	u mm	β	f_c N/mm^2	V_{cal} KN	V_{test} KN	$\frac{V_{cal}}{V_{test}}$
A2a	114	1472	1	13.7	207	334	0.62
A2b	114	1472	1	19.5	246	401	0.61
A2c	114	1472	1	37.4	342	467	0.73
A3a	114	1472	1	12.8	199	356	0.56
A3b	114	1472	1	22.6	265	445	0.59
A3c	114	1472	1	26.6	288	534	0.54
A3d	114	1472	1	34.6	379	547	0.60
A5	114	1880	1	27.8	374	534	0.70
A7b	114	1472	1	27.9	295	512	0.57
B9	103	1428	1	43.9	324	505	0.64
B11	102	1424	1	13.5	178	329	0.54
B14	102	1424	1	50.6	344	579	0.54
Moe							
R2	114	1064	1	26.6	208	317	0.65
M1a	114	1676	1	21.2	293	440	0.66
H1	114	1472	1	26.6	288	379	0.76
S1-60	114	1472	1	23.8	273	396	0.69
S2-60	114	1472	1	22.5	265	362	0.73
S3-60	114	1472	1	23.0	268	370	0.72
S4-60	114	1472	1	24.3	276	340	0.81
S5-60	114	1472	1	22.2	263	318	0.83
S1-70	114	1472	1	25.0	280	400	0.70
S3-70	114	1472	1	25.8	284	385	0.74
S4-70	114	1472	1	23.8	273	380	0.72

Table (6-4-4) continued.

SLAB No	d mm	u mm	β	f_c N/mm^2	V_{cal} KN	V_{test} KN	$\frac{V_{cal}}{V_{test}}$
S5-70	114	1472	1	23.0	268	342	0.78
Kinnunen & Nylander							
5	117	839	1	26.8	169	260	0.65
6	118	842	1	26.2	169	280	0.60
24	128	1344	1	26.4	294	438	0.67
25	124	1332	1	25.1	276	416	0.66
32	123	1329	1	25.6	276	263	1.05
33	125	1335	1	26.6	287	263	1.09
Kinnunen, Nylander & Tolf							
1	100	707	1	28.6	126	216	0.58
3	99	704	1	22.9	111	194	0.57
13	98	700	1	26.6	118	145	0.81
14	99	704	1	25.1	116	142	0.82
17	200	1414	1	25.4	475	487	0.97
18	197	1404	1	24.2	453	465	0.97
Hanson							
B4	162	2068	1	22.2	526	490	1.07
Hawkins, Fallsen & Hinjosa							
2	117	2020	1	26.3	404	352	1.15
9	121	1644	1	29.5	360	316	1.14
Narasimhan							
L7	143	1792	1	35.5	509	687	0.74
L9	143	1792	1	33.1	491	588	0.84

Table (6-4-4) continued.

SLAB No	d mm	u mm	β	f_c N/mm^2	V_{cal} KN	V_{test} KN	$\frac{V_{cal}}{V_{test}}$
Stamenkovic & Chapman							
V/I/2	56	732	1	25.9	121	117	1.04
V/Ir/1	56	680	1	25.2	64	109	0.58
Regan							
I1	77	1108	1	25.8	144	194	0.74
I2	77	1108	1	23.5	138	176	0.78
I3	77	1108	1	27.5	149	194	0.77
I4	77	1108	1	32.3	162	194	0.83
I5	79	1108	1	28.2	151	165	0.92
I6	79	1108	1	22.0	133	165	0.81
I7	79	1108	1	30.5	157	186	0.84
II1	200	1413	1	34.9	557	825	0.67
II2	128	906	1	33.3	223	390	0.57
II3	128	906	1	34.3	226	365	0.62
II4	64	576	1	33.3	71	117	0.61
II5	64	576	1	34.3	72	105	0.68
II6	64	576	1	36.0	74	105	0.70
III1	95	770	1	23.2	117	197	0.60
III2	95	770	1	9.52	75.2	123	0.61
III3	95	770	1	37.8	150	214	0.70
IV1	80	960	1	26.2	131	196	0.67
IV2	80	960	1	34.0	149	236	0.63
IV3	80	960	1	28.3	137	248	0.55
IV4	80	960	1	31.3	143	262	0.54

Table (6-4-4) continued.

SLAB No	d mm	u mm	β	f_c N/mm^2	V_{cal} KN	V_{test} KN	$\frac{V_{cal}}{V_{test}}$
V2	118	904	1	32.2	202	280	0.72
V3	118	713	1	32.4	160	265	0.60
V4	118	880	1	36.2	208	285	0.73
V5	118	841	1	32.9	190	285	0.66
Rankin & Long							
3	40.4	562	1	30.7	42	56.5	0.74
4	40.5	562	1	34.8	44.7	56.2	0.79
5	40.5	562	1	34.8	44.7	57.3	0.78
6	40.5	562	1	34.8	44.7	65.6	0.68
7	40.5	562	1	26.7	39.2	70.9	0.55
8	40.5	562	1	26.7	39.2	71.1	0.54
9	40.5	562	1	26.7	39.2	78.6	0.49
11	40.5	562	1	29.9	41.5	55.0	0.75
12	40.5	562	1	29.9	41.5	67.1	0.62
14	40.5	562	1	34.0	44.2	52.4	0.84
15	40.5	562	1	34.0	44.2	84.8	0.52
2A	46.5	586	1	28.8	48.7	66.2	0.73
3A	46.5	586	1	28.8	48.7	89.7	0.54
4A	46.5	586	1	30.9	50.5	97.4	0.52
3B	35.0	540	1	37.9	38.7	56.67	0.68
4B	35.0	540	1	30.9	35.0	72.52	0.48
2C	53.5	614	1	32.4	62.3	87.8	0.71
3C	53.5	614	1	32.4	62.3	124.1	0.50
4C	53.5	614	1	27.8	57.8	125.9	0.46

Table (6-4-4) continued.

SLAB No	d mm	u mm	β	f_c N/mm^2	V_{cal} KN	V_{test} KN	$\frac{V_{cal}}{V_{test}}$
Kamaraldin							
SA2	64	856	1	34	106	141	0.75
SB1	62	846	1	27	91	133	0.68
SC1	62	846	1	36	105	129	0.81
SD1	62	848	1	36	105	127	0.83

Table (6-4-4) slabs analysed by ACI 318-83.

6-4-1-5 CEB-FIP

The punching shear load defined by CEB-FIP code for concrete structures is

$$V_{cal} = v_c \cdot u \cdot d$$

Where:

u is the length of the shortest curve at a minimum distance of 0.5d from the loaded area.

$v_c = 1.6\ Rc\ K\ (1 + 50\rho)$

$R_c = 0.052(f_c)^{2/3}$ is the characteristic concrete resistance

(The safety factor for material has been removed)

$K = 1.6 - d \not< 1$ (d in m)

$\rho = \sqrt{\rho_x . \rho_y} \not> 0.008$

In the calculations, the upper limit for the reinforcement ratio (ρ) was extended to 0.02 as proposed in the code complements (15), where the width for which ρ should be

calculated is extended to 2.5d to either side of a column.

The results of the comparisons are listed in table (6-4-5).

SLAB No	d mm	f_c N/mm^2	ρ %	u mm	V_{cal} KN	V_{test} KN	$\frac{V_{cal}}{V_{test}}$
Elstner & Hognestad							
A1a	117	14.1	1.17	1383	182	303	0.60
A1b	117	25.2	1.17	1383	266	365	0.73
A1c	117	20.3	1.17	1383	230	356	0.65
A2a	114	13.7	2.48	1374	217	334	0.65
A2b	114	19.5	2.48	1374	275	401	0.68
A2c	114	37.4	2.48	1374	421	467	0.90
A3a	114	12.8	3.72	1374	208	356	0.58
A3b	114	22.6	3.72	1374	303	445	0.68
A3c	114	26.6	3.72	1374	338	534	0.63
A3d	114	34.6	3.72	1374	401	547	0.73
A5	114	27.8	2.48	1782	462	534	0.86
A7b	114	27.9	2.48	1374	349	512	0.68
B9	103	43.9	2.48	1340	416	505	0.82
B11	102	13.5	3.39	1336	189	329	0.57
B14	102	50.6	3.39	1336	452	579	0.78
Moe							
R2	114	26.6	1.06	996	182	317	0.57
M1A	114	21.2	2.31	1570	332	440	0.57
H1	114	26.6	1.27	1374	276	379	0.73
S1-60	114	23.8	1.06	1374	240	396	0.61
S2-60	114	22.5	1.53	1374	276	362	0.74
S3-60	114	23.0	2.30	1374	307	370	0.83

Table (6-4-5) continued.

SLAB No	d mm	f_c N/mm^2	ρ %	u mm	V_{cal} KN	V_{test} KN	$\frac{V_{cal}}{V_{test}}$
S4-60	114	24.3	3.45	1374	318	340	0.93
S5-60	114	22.2	1.06	1374	229	318	0.72
S1-70	114	25.0	1.06	1374	248	400	0.62
S3-70	114	25.8	2.30	1374	331	385	0.86
S4-70	114	23.8	3.45	1374	314	380	0.83
S5-70	114	23.0	1.06	1374	235	342	0.69
Kinnunen & Nylander							
5	117	26.8	0.92	839	155	260	0.60
6	118	26.2	0.90	842	154	280	0.55
24	128	26.4	1.12	1344	285	438	0.65
25	124	25.1	1.18	1332	270	416	0.65
32	123	25.6	0.60	1329	222	263	0.84
35	125	26.64	0.58	1335	231	263	0.87
Kinnunen, Nylander & Tolf							
1	100	28.6	0.80	707	113	216	0.52
3	99	22.9	0.81	704	96	194	0.50
13	98	26.6	0.34	700	87	145	0.60
14	99	25.1	0.35	704	85	142	0.60
17	200	25.4	0.35	1414	304	487	0.62
18	197	25.2	0.34	1405	318	465	0.68
Hanson							
B4	162	22.2	0.94	1929	425	490	0.87

Table (6-4-5) continued.

SLAB No	d mm	f_c N/mm^2	ρ %	u mm	V_{cal} KN	V_{test} KN	$\frac{V_{cal}}{V_{test}}$
Hawkins, Fallsen & Hinjosa							
2	117	26.3	1.11	1919	372	352	1.06
9	121	29.5	0.75	1540	294	316	0.93
Narasimhan							
L7	143	35.5	1.11	1669	474	687	0.69
L9	143	33.1	1.11	1669	453	588	0.77
Starnenkovic & Chapman							
V/I/2	56	25.9	1.29	684	69	117	0.59
V/Ir/1	56	25.2	1.00	632	57	109	0.53
Regan							
I1	77	25.8	2.12	1042	174	194	0.90
I2	77	23.5	1.18	1042	130	176	0.74
I3	77	27.5	1.18	1042	144	194	0.74
I4	77	32.3	0.90	1042	146	194	0.75
I5	79	28.2	1.31	1048	157	165	0.95
I6	79	22.0	0.72	1048	109	165	0.66
I7	79	30.5	0.80	1048	140	186	0.75
II1	200	34.9	1.15	1413	541	825	0.66
II2	128	33.3	1.15	906	226	390	0.58
II3	128	34.3	1.15	906	231	365	0.63
II4	64	33.3	1.15	576	75	117	0.64
II5	64	34.3	1.15	576	77	105	0.73
II6	64	36.0	1.15	576	79	105	0.75
III1	95	23.2	0.96	770	108	197	0.55

Table (6-4-5) continued.

SLAB No	d mm	f_c N/mm^2	ρ %	u mm	V_{cal} KN	V_{test} KN	$\frac{V_{cal}}{V_{test}}$
III2	95	9.52	0.96	770	59	123	0.48
III3	95	37.8	0.96	770	149	214	0.70
IV1	80	26.2	1.47	891	135	196	0.69
IV2	80	34.0	1.47	891	160	236	0.68
IV3	80	28.3	1.47	891	142	248	0.57
IV4	80	31.3	1.47	891	152	262	0.58
V2	118	32.2	0.80	904	182	280	0.65
V3	118	32.4	0.80	713	144	265	0.54
V4	118	36.2	0.80	779	170	285	0.59
V5	118	32.9	0.80	841	172	285	0.60
Rankin & Long							
3	40.5	30.7	0.691	527	35.7	56.6	0.63
4	40.5	34.8	0.821	527	40.6	56.2	0.72
5	40.5	34.8	0.883	527	41.5	57.3	0.73
6	40.5	34.8	1.026	527	43.6	65.6	0.66
7	40.5	34.8	1.163	527	38.25	70.9	0.54
8	40.5	26.7	1.292	527	39.8	71.0	0.56
9	40.5	26.7	1.454	527	41.7	78.6	0.53
11	40.5	26.7	0.802	527	36.5	55.0	0.66
12	40.5	29.9	1.107	527	40.5	67.1	0.60
14	40.5	34.0	0.691	527	38.2	52.45	0.73
15	40.5	34.0	1.994	527	56.7	84.84	0.67
2A	46.5	28.8	0.691	546	40.6	66.24	0.61
3A	46.5	28.8	1.293	546	49.6	89.72	0.55

Table (6-4-5) continued.

SLAB No	d mm	f_c N/mm^2	ρ %	u mm	V_{cal} KN	V_{test} KN	$\frac{V_{cal}}{V_{test}}$
4A	46.5	30.8	1.992	546	52.0	97.43	0.53
3B	35.0	37.8	1.292	510	42.1	56.67	0.74
4B	35.0	30.8	1.994	510	44.6	72.52	0.62
2C	53.5	32.4	0.690	568	52.2	87.86	0.59
3C	53.5	32.4	1.288	568	63.8	124.1	0.51
4C	53.5	27.8	1.993	568	70.1	125.9	0.55
Kamaraldin							
SA2	64	34	0.84	801	95	141	0.68
SB1	62	27	1.58	795	99	133	0.75
SC1	62	36	1.58	795	120	129	0.93
SD1	62	36	1.58	795	120	127	0.94

Table (6-4-5) slabs analysed by CEB-FIP code.

6-4-2 Punching shear formulae used in the present comparison for eccentrically loaded slabs

6-4-2-1 Stamankovic and Chapman

The ultimate strength under combined loading can be calculated from the following proposed interaction formula:

$$\frac{V_{cal}}{V_{test}} + \frac{M_{cal}}{M_{test}} = 1$$

Where V_{cal} and M_{cal} are given in section (1-3-3-4) the results in table (6-4-6) for slabs analysed by the above formula are on the safe side and in some cases conservative.

Slab No	f_c N/mm^2	ρ %	d mm	V_{test} KN	M_{test} KN m	V_u Kn	M_u KN m	$\frac{V_c}{V_t}+\frac{M_c}{M_t}$
Elster & Hognestad								
A11	25.9	24.7	114	529	94.2	466	164.7	0.59
A12	28.4	2.47	114	529	94.2	469	170.6	0.60
Meo								
M2	26.1	1.50	114	292	57.2	416	120.7	0.85
M3	23.0	1.50	114	207	69.9	412	110.2	0.88
M6	26.8	1.34	114	239	40.1	325	84.5	0.83
M7	25.3	1.34	114	311	19.0	334	80.7	0.86
Ma	23.6	1.34	114	267	33.9	326	76.4	0.79
M10	21.2	1.34	114	178	54.8	316	70.7	0.75
Anis								
B3	30.4	2.19	76	192	18.0	194	45.8	0.72
B4	29.8	2.19	76	140	26.3	191	45.1	0.76
B5	29.0	2.19	76	126	39.3	191	44.3	0.55
B6	31.4	2.19	76	116	53.9	194	46.9	0.57
B7	33.8	2.19	76	70	66.1	200	49.5	0.60
Stamenkovic & Chapman								
C/I/1	36.0	1.17	56	84.5	7.3	100	19.2	0.82
C/I/2	29.7	1.17	56	62.3	10.5	93.7	16.7	0.77
C/I/3	25.5	1.17	56	33.8	13.6	88.7	15.1	0.78
C/I/4	25.1	1.17	56	20.9	16.6	88.2	14.9	0.74

Table (6-4-6) continued.

Slab No	f_c N/mm^2	ρ %	d mm	V_{test} KN	M_{test} KN m	V_u Kn	M_u KN m	$\frac{V_c}{V_t}+\frac{M_c}{M_t}$
MI1	28.1	1.17	56	00.0	18.4	0.00	16.1	0.88
CIr1	22.6	1.17	56	85.7	7.3	83.7	14.0	0.65
CIr2	29..2	1.17	56	67.3	10.8	92.0	15.8	0.71
CIr3	28.6	1.17	56	39.9	15.7	91.3	15.6	0.69
CIr4	26.6	1.17	56	21.6	16.8	88.9	15.1	0.74
MIr1	26.0	1.17	56	00.0	18.6	0.00	14.9	0.81
Hanson								
C-9	23.7	1.50	162	283	158.0	774	148.8	0.70
Narasimhan								
L1	26.6	1.11	143	400	120.0	495	153.6	0.63
Godycki, Dilger & Ghali								
S010	32.0	1.00	127	132	135.4	413	138.0	0.77
S005	30.9	0.50	127	132	92.9	298	121.6	0.83
Hanson & Hanson								
A1	30.7	1.64	57	5.74	22.3	97.8	17.6	0.76
A2	31.8	1.64	57	4.80	24.2	100	18.2	0.72
B7	33.5	1.64	57	4.89	35.7	107	32.7	0.88
C8	33.3	1.64	57	5.60	31.4	122	31.7	0.97
A12	33.7	1.64	57	26.8	20.5	375	22.8	0.62
B16	30.9	1.64	57	34.4	27.3	39.7	31.6	0.60
C17	36.5	1.64	57	31.5	24.7	28.7	40.9	0.59
Regan, Walker & Zakaria								
SM5	32.0	1.05	60	72	15.8	110	21.4	0.72
SM9	37.7	1.05	60	97	10.7	114	24.1	0.77

Table (6-4-6) continued.

Slab No	f_c N/mm^2	ρ %	d mm	V_{test} KN	M_{test} KN m	V_u Kn	M_u KN m	$\frac{V_c}{V_t} + \frac{M_c}{M_t}$
SM10	37.7	1.05	60	88	19.4	114	24.1	0.64
SM11	36.8	1.34	60	91	20.0	111	40.3	0.76
SM12	31.9	1.34	60	88	19.4	112	37.9	0.77
Kamaraldin								
SA1	33	0.59	64	109	5.66	119	19.4	0.83
SA3	36	0.59	64	85	8.50	120	20.7	0.90
SA4	32	0.59	64	49	16.50	116	19.8	0.80
SB2	28	1.08	62	61	22.00	122	18.1	0.58
SC2	37	1.08	62	65	22.00	133	22.8	0.68
SD2	31	1.08	62	56	17.4	140	20.9	0.81

Table (6-4-6) Eccentrically loaded slabs analysed by Stamankovic and Chapmans formula.

6-4-2-2 Regan

The ultimate shear capacity for slabs eccentrically loaded, suggested by Regan for practical purposes is

$$V_{ecal} = \frac{V_{ocal}}{1 + \frac{1.5e}{\sqrt{(c_1 + 2d)(c_2 + 2d)}}}$$

Where e is the load eccentricity

V_{ocal} is the punching shear load given in section (6-4-1-2)

c_1 and c_2 are the column dimensions.

The results of the analysis are listed in table (6-4-7).

Slab No	$C_1 x C_2$ mm	d mm	f_{cu_2} N/mm^2	ρ %	e mm	V_{oc} KN	V_t KN	V_{ec} KN	V_{ec} / V_t
A11	356x356	114	31.0	2.47	178	498	529	341	0.64
A12	356x356	114	34.1	2.47	178	515	529	353	0.60
Moe									
M2	305x305	114	31.3	1.50	196	386	292	248	0.85
M3	305x305	114	27.6	1.5	338	370	207	189	0.92
M6	305x305	114	32.2	1.34	168	375	239	254	1.06
M7	254x254	114	30.4	1.34	61	333	311	280	0.90
M9	254x254	114	28.3	1.34	127	325	267	233	0.87
M10	254x254	114	25.4	1.34	308	314	178	160	0.90
Hanson & Hanson									
A1	152x152	57	36.8	1.64	3891	125	54.7	5.45	0.95
A2	152x152	57	38.2	1.64	5056	126	4.80	4.26	0.89
B7	152x305	57	40.2	1.64	7297	159	4.89	4.70	0.96
C8	305x152	57	40.0	1.64	5602	159	5.60	6.07	1.08
A12	152x152	57	40.4	1.64	736	128	26.87	24.1	0.89
B16	152x305	57	37.1	1.64	795	155	34.38	33.9	0.98
C17	305x152	57	43.8	1.64	785	164	31.49	36.2	1.15
Anis									
B3	203x203	76	36.5	2.19	94	225	192	161	0.84
B4	203x203	76	35.7	2.19	188	225	140	125	0.89
B5	203x203	76	34.8	2.19	312	222	126	96	0.76
B6	203x203	76	37.7	2.19	465	228	116	77	0.66
B7	203x203	76	40.5	2.19	945	234	70	47	0.67

Table (6-4-7) continued.

Slab No	$C_1 x C_2$ mm	d mm	f_{cu_2} N/mm^2	ρ %	e mm	V_{oc} KN	V_t KN	V_{ec} KN	$\frac{V_{ec}}{V_t}$
Stamenkovic & Chapman									
CI1	127x127	56	43.2	1.17	87	104	84.5	67	0.79
CI2	127x127	56	35.6	1.17	168	98	62.3	48	0.76
CI3	127x127	56	30.6	1.17	404	93	33.8	26.3	0.78
CI4	127x127	56	30.1	1.17	797	92	20.9	15.3	0.73
CIr1	76x152	56	27.1	1.17	85	81	85.7	51.0	0.60
CIr2	76x152	56	35.0	1.17	162	88	67.3	42.0	0.62
CIr3	76x152	56	34.3	1.17	394	88	39.9	24.0	0.60
CIr4	76x152	56	31.9	1.17	777	85	21.6	13.60	0.63
Hanson									
C9	508x508	162	28.4	0.63	571	568	283	280	0.99
Narasimhan									
L1	303x303	143	31.9	1.11	492	461	400	205	0.51
Godycki, Digler & Ghali									
S010	305x303	127	38.4	1.00	1068	412	132	106	0.80
S005	305x305	127	37.1	0.50	704	323	132	111	0.85
Regan									
SM5	240x120	60	38.4	1.05	220	122	72	60	0.83
SM9	240x120	60	45.2	1.05	110	129	97	83	0.85
SM10	240x120	60	45.2	1.05	220	129	88	61	0.69
SM11	240x240	60	44.2	1.34	220	174	91	91	1.00
SM12	240x240	60	38.3	1.34	220	166	88	87	0.98

Table (6-4-7) continued.

Slab No	$C_1 x C_2$ mm	d mm	f_{cu_2} N/mm^2	ρ %	e mm	V_{oc} KN	V_t KN	V_{ec} KN	$\frac{V_{ec}}{V_t}$
Kamaraldin									
SA1	150x150	64	39.6	0.55	52	101	109	79	0.72
SA3	150x150	64	43.2	0.55	100	104	85	68	0.79
SA4	150x150	64	38.4	0.55	334	100	49	36	0.72
SB2	150x150	62	33.6	1.00	360	113	61	38	0.62
SC2	150x150	62	44.4	0.72	337	111	65	39	0.60
SD2	200x100	62	37.2	0.72	310	100	56	37	0.65

Table (6-4-7) Eccentrically loaded slabs analysed by Regan's formula

6-4-2-3 BS 8110

The BS 8110 equation used for the calculation of eccentric punching loads is given below

$$V_{ecal} = \frac{V_{ocal}}{1 + \frac{1.5\ e}{X}}$$

Where V_{ocal} is given in section (6-4-1-3)

e is the load eccentricity

X is the length of the side of the shear perimeter parallel to the eccentricity.

The results of the comparison are shown in table (6-4-8).

It can be seen that, BS 8110 yields unsafe results for slabs with rectangular columns see table 6-4-8, Hanson & Hanson's slabs C8, C17 and the author's slab SD2, and for slabs with extra reinforcement through the columns, Regan's slab SM11.

Slab No	x mm	d mm	f_{cu_2} N/mm^2	ρ %	e mm	V_{oc} KN	V_t KN	V_{ec} KN	$\frac{V_{ec}}{V_t}$
Elstner & Hognstad									
A11	698	114	31.0	2.47	178	465	529	336	0.63
A12	698	114	34.1	2.47	178	480	529	347	0.65
Moe									
M2	647	114	31.3	1.50	196	366	292	251	0.86
M3	647	114	27.6	1.50	338	351	207	196	0.95
M6	647	114	32.2	1.34	168	356	239	256	1.07
M7	596	114	30.4	1.34	61	322	311	279	0.90
M9	596	114	28.3	1.34	127	314	267	237	0.89
M10	596	114	25.4	1.34	308	303	178	172	0.96
Hanson & Hanson									
A1	323	57	36.8	1.64	3891	119	5.74	6.24	1.09
A2	323	57	38.2	1.64	5056	120	4.80	4.90	1.02
B7	323	57	40.2	1.64	7297	122	4.89	3.49	0.71
C8	476	57	40.0	1.64	5602	180	5.60	9.60	1.72
A12	323	57	40.4	1.64	763	122	26.9	26.8	1.00
B16	323	57	37.1	1.64	795	119	34.4	25.4	0.74
C17	476	57	43.8	1.64	785	180	31.5	51.8	1.64
Anis									
B3	431	76	36.5	2.32	94	218	192	164	0.85
B4	431	76	35.7	2.32	188	217	140	131	0.94
B5	431	76	34.8	2.32	312	215	126	103	0.82
B6	431	76	37.7	2.32	465	221	116	84	0.73
B7	431	76	40.5	2.32	945	225	70	52	0.75

Table (6-4-8) continued.

Slab No	X mm	d mm	f_{cu_2} N/mm^2	ρ %	e mm	V_{oc} KN	V_t KN	V_{ec} KN	$\frac{V_{ec}}{V_t}$
Stamenkovic & Chapman									
CI1	295	56	43.2	1.18	87	98	84.5	68	0.80
CI2	295	56	35.6	1.18	168	94	62.3	51	0.81
CI3	295	56	30.6	1.18	404	90	33.8	29.5	0.87
CI4	295	56	30.1	1.18	797	89	20.9	17.6	0.84
CIr1	320	56	27.1	1.36	85	98	85.7	70.0	0.82
CIr2	320	56	35.0	1.36	162	107	67.3	61.0	0.90
CIr3	320	56	34.3	1.36	394	106	39.9	37.0	0.93
CIr4	320	56	31.9	1.36	777	104	21.6	22.4	1.04
Hanson									
C9	994	162	28.4	0.63	571	531	280	285	1.02
Narasimhan									
L1	734	143	31.9	1.11	492	448	205	245	1.19
Godycki, Dilger & Ghali									
S010	686	127	38.4	1.03	1068	397	132	119	0.90
S005	686	127	37.1	0.44	704	296	132	116	0.88
Regan									
SM5	420	60	38.4	1.00	220	137	72	77	1.07
SM9	420	60	45.2	1.00	110	139	97	100	1.03
SM10	420	60	45.2	1.00	220	139	88	78	0.88
SM11	420	60	44.2	2.39	220	186	91	104	1.14
SM12	420	60	38.3	1.00	220	137	88	77	0.88

Table (6-4-8) continued.

Slab No	X mm	d mm	f_{cu_2} N/mm^2	ρ %	e mm	V_{oc} KN	V_t KN	V_{ec} KN	$\frac{V_{ec}}{V_t}$
Kamaraldin									
SA1	342	64	39.6	0.51	52	108	109	88	0.81
SA3	342	64	43.2	0.51	100	108	85	75	0.88
SA4	342	64	38.4	0.51	336	107	49	43	0.88
SB2	336	62	33.6	1.44	360	113	61	43	0.71
SC2	336	62	44.4	1.44	337	119	65	47	0.73
SD2	386	62	37.2	1.44	310	145	56	66	1.17

Table (6-4-8) Eccentrically loaded slabs analysed by BS 8110.

6-4-2-4 ACI 318-83

The ACI assumed distribution of shear stress around an internal column is shown in Fig. (1-30).

The eccentric punching shear load is

$$V_{ecal} = \frac{V_{ocal}}{1 + \frac{6\ \gamma_v\ e\ (X+Y)}{X^2 + d^2 + 3XY}}$$

Where

V_{ocal} is given in Section (6-4-1-4)

$X = c_1 + d$

$Y = c_2 + d$

c_1 and c_2 are the column dimensions

e is the load eccentricity

$$\gamma_v = 1 - \frac{1}{1 + \sqrt[2/3]{(X/Y)}}$$

is the fraction of the moment transferred by uneven shear, and X is the width of the face of the critical section resisting the moment.

The results of the analysis are shown in table (6-4-9), and indicate that the ACI code is conservative with respect to the treatment of eccentricity.

Slab No	c_1 mm	c_2 mm	d mm	f_c N/mm^2	e mm	V_{oc} KN	V_t KN	V_{ec} KN	$\frac{V_{ec}}{V_t}$
Elstner & Hognestad									
A11	356	356	114	25.9	179	363	529	250	0.40
A12	356	356	114	28.9	178	381	529	263	0.50
Moe									
M2	305	305	114	26.1	196	325	292	209	0.72
M3	305	305	114	23.0	338	305	207	156	0.75
M6	305	305	114	26.88	168	330	239	224	0.94
M7	254	254	114	25.3	61	281	311	235	0.75
M9	245	254	114	23.6	127	271	267	193	0.72
M10	254	254	114	21.2	308	257	178	130	0.73
Hanson & Hanson									
A1	152	152	57	30.7	3891	88	5.74	3.84	0.67
A2	152	152	57	31.8	5056	89	4.80	3.00	0.63
B7	152	305	57	33.5	7297	126	4.89	3.11	0.63
C8	305	152	57	33.3	5602	125	5.60	4.83	0.86
A12	152	152	57	33.7	736	92	26.87	23.8	0.88
B16	152	305	57	30.9	795	121	34.38	22.8	0.66
C17	305	152	57	36.5	785	131	31.49	29.2	0.93

Table (6-4-9) continued.

Slab No	c_1 mm	c_2 mm	d mm	f_c N/mm^2	e mm	V_{oc} KN	V_t KN	V_{ec} KN	$\frac{V_{ec}}{V_t}$
Anis									
B3	203	203	76	30.4	94	156	192	111	0.58
B4	203	203	76	29.8	188	154	140	86	0.61
B5	203	203	76	29.0	312	152	126	66	0.52
B6	203	203	76	31.4	465	158	116	53	0.46
B7	203	203	76	33.8	945	164	70	33	0.47
Stamenkovic & Chapman									
CI1	127	127	56	36.0	87	82	84.5	53.0	0.62
CI2	127	127	56	29.7	168	74	62.3	36.0	0.57
CI3	127	127	56	25.5	404	70	33.8	19.5	0.58
CI4	127	127	56	25.1	797	68	20.9	13.3	0.64
CIr1	152	76	56	22.6	85	60	85.7	37.2	0.43
CIr2	152	76	56	29.2	162	69	67.3	32.0	0.47
CIr3	152	76	56	28.6	394	68	39.9	17.7	0.44
CIr4	152	76	56	26.6	777	65	21.6	9.85	0.45
Hanson									
C9	508	508	162	23.7	568	704	283	469	1.65
Narasimhan									
L1	305	305	143	26.6	461	440	400	199	0.50
Godycki, Dilger & Ghali									
S010	305	305	127	32.0	1068	414	132	106	0.80
S005	305	305	127	30.9	704	406	132	139	1.05

Table (6-4-9) continued.

Slab No	c_1 mm	c_2 mm	d mm	f_c N/mm^2	e mm	V_{oc} KN	V_t KN	V_{ec} KN	$\frac{V_{ec}}{V_t}$
Regan									
SM5	240	120	60	32.0	220	109	72	50.7	0.70
SM9	240	120	60	37.7	110	118	97	75.0	0.77
SM10	240	120	60	37.7	220	118	88	55.0	0.62
SM11	240	240	60	36.8	220	146	91	78.0	0.82
SM12	240	240	60	31.9	220	135	88	71.0	0.81
Kamaraldin									
SA1	150	150	64	33.0	52	105	109	82	0.75
SA3	150	150	64	36.0	100	110	85	71	0.84
SA4	150	150	64	32.0	336	103	49	36	0.74
SB2	150	150	62	28.0	360	93	61	31	0.51
SC2	150	150	62	37.0	337	107	65	38	0.58
SD2	200	100	62	32.0	310	97	56	35	0.62

Table (6-4-9) eccentric slabs analysed by ACI-83.

6-4-2-5 CEB-FIP

The eccentric punching shear load for a rectangular column is

$$V_{ecal} = \frac{V_{ocal}}{1 + \frac{1.5\ e_x + 1.5\ e_y}{\sqrt{(c_1 + d)(c_2 + d)}}}$$

Where V_{ocal} is given in section (6-4-1-5)

c_1, c_2 are column dimensions

e_x and e_y are load eccentricities in x and y directions.

The results of the analysis are listed in table (6-4-10).

Slab No	c_1 mm	c_2 mm	d mm	f_c N/mm^2	e mm	V_{oc} KN	V_t KN	V_{ec} KN	$\frac{V_{ec}}{V_t}$
A11	356	356	114	25.9	178	438	529	279	0.53
A12	356	356	114	28.4	178	466	529	297	0.56
Moe									
M2	305	305	114	26.1	196	355	292	209	0.71
M3	305	305	114	23.0	338	142	207	142	0.68
M6	305	305	114	26.8	168	333	239	149	0.62
M7	254	254	114	25.3	61	278	311	222	0.72
M9	254	254	114	23.6	127	265	267	175	0.65
M10	254	254	114	21.2	308	247	178	109	0.61
Hanson & Hanson									
A1	152	152	57	30.7	3891	103	5.74	5.25	0.91
A2	152	152	57	31.8	5056	105	4.8	2.81	0.58
B7	152	305	57	33.5	7297	151	4.89	3.70	0.76
C8	305	152	57	33.3	5602	151	5.60	4.78	0.80
A12	152	152	57	33.7	763	109	26.8	16.8	0.63
B16	152	305	57	30.9	795	143	34.4	26.8	0.77
C17	365	152	57	36.5	785	160	31.5	30.3	0.96
Anis									
B3	203	203	76	30.4	94	193	192	128	0.76
B4	203	203	76	29.8	188	195	140	97	0.69
B5	203	203	76	29.0	312	191	126	71	0.56

Table (6-4-10) continued.

Slab No	c_1 mm	c_2 mm	d mm	f_c N/mm^2	e mm	V_{oc} KN	V_t KN	V_{ec} KN	$\frac{V_{ec}}{V_t}$
B6	203	203	76	31.4	465	201	116	57	0.49
B7	203	203	76	33.8	945	211	70	34.7	0.49
Stamenkovic & Chapman									
CI1	127	127	56	36.8	87	86	84.5	52.2	0.59
CI2	127	127	56	29.7	168	77	62.3	32.4	0.52
CI3	127	127	56	25.5	404	69	33.8	16.0	0.47
CI4	127	127	56	25.1	797	69	20.9	9.15	0.44
CIr1	152	67	56	22.6	85	72	85.7	45.5	0.53
CIr2	152	76	56	29.2	162	85	67.3	40.4	0.60
CIr3	152	76	56	28.6	394	84	39.9	22.7	0.57
CIr4	152	76	56	26.6	777	80	21.6	12.7	0.59
Hanson									
C9	508	508	162	23.7	568	533	283	234	0.83
Narasimhan									
L1	305	305	143	26.6	461	400	400	157	0.39
Godycki, Dilger & Ghali									
S010	305	305	127	32.0	1068	393	132	83	0.63
S005	305	305	127	30.9	704	335	132	97	0.74
Regan									
SM5	240	120	60	32.0	220	109	72	45	0.62
SM9	240	120	60	37.7	110	122	97	71	0.73

Table (6-4-10) continued.

Slab No	c_1 mm	c_2 mm	d mm	f_c N/mm^2	e mm	V_{oc} KN	V_t KN	V_{ec} KN	$\frac{V_{ec}}{V_t}$
SM10	240	120	60	37.7	220	122	88	63	0.71
SM11	240	240	60	36.8	220	186	91	89	0.97
SM12	240	240	60	31.9	220	169	88	80	0.91
Kamaraldin									
SA1	150	150	64	33.0	52	95	109	70	0.64
SA3	150	150	64	36.0	100	101	85	59	0.70
SA4	150	150	64	32.0	336	94	49	28	0.57
SB2	150	150	62	28.0	360	124	61	35	0.57
SC2	150	150	62	37.0	337	149	65	44	0.68
SD2	200	100	62	31.0	310	133	56	41	0.73

Table (6-4-10) eccentric slabs analysed by CEB-FIP.

Comparison between experimental punching shear loads reported in the literature including tests from the present study and predictions of the existing theories, code recommendations, and the proposed theory are presented in Figs (6-2) to (6-7).

These show that the proposed method of calculating the punching shear resistance of reinforced concrete flat slab structures yield more accurate predictions than those existing.

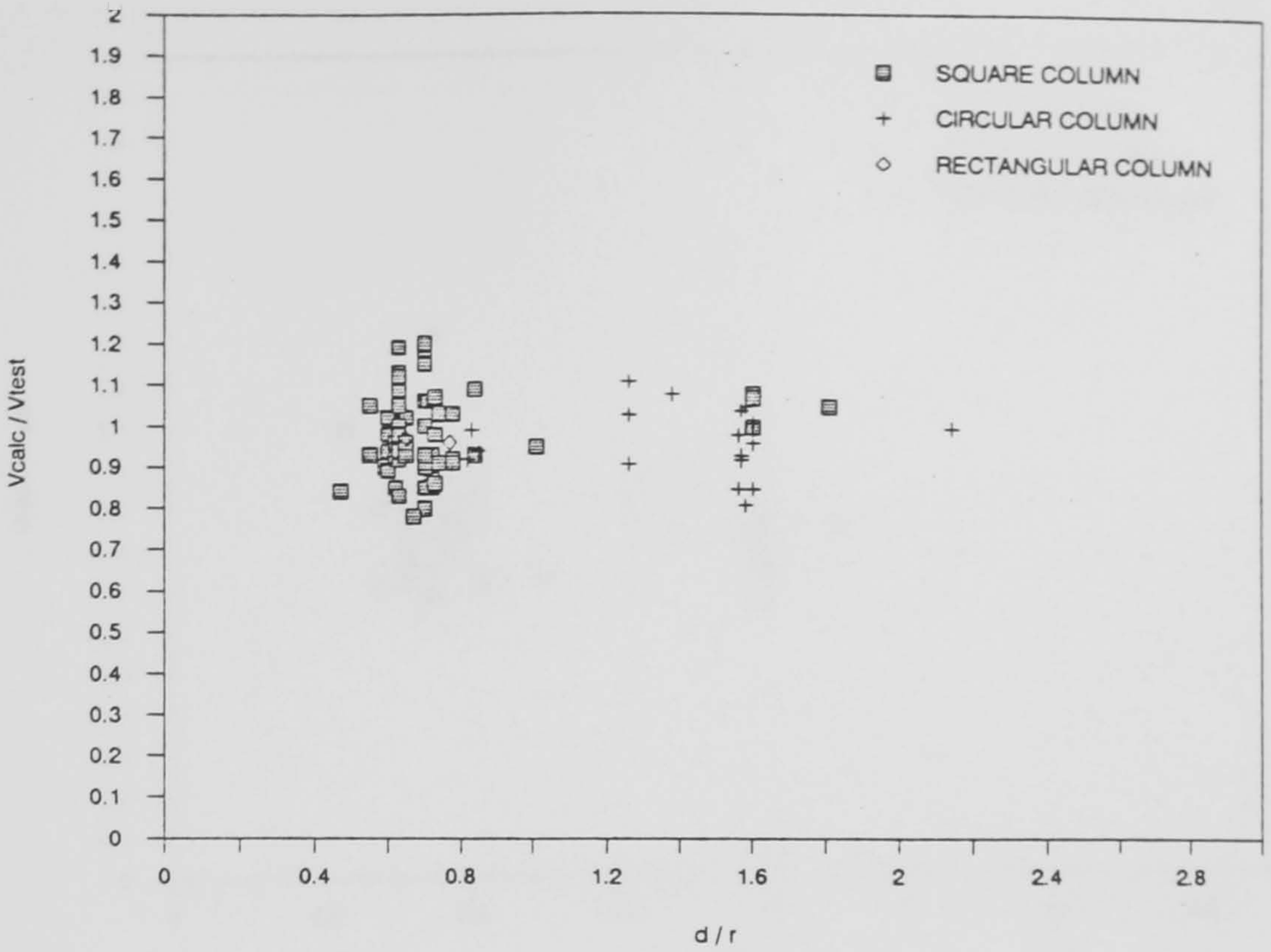

a) Concentrically loaded slabs

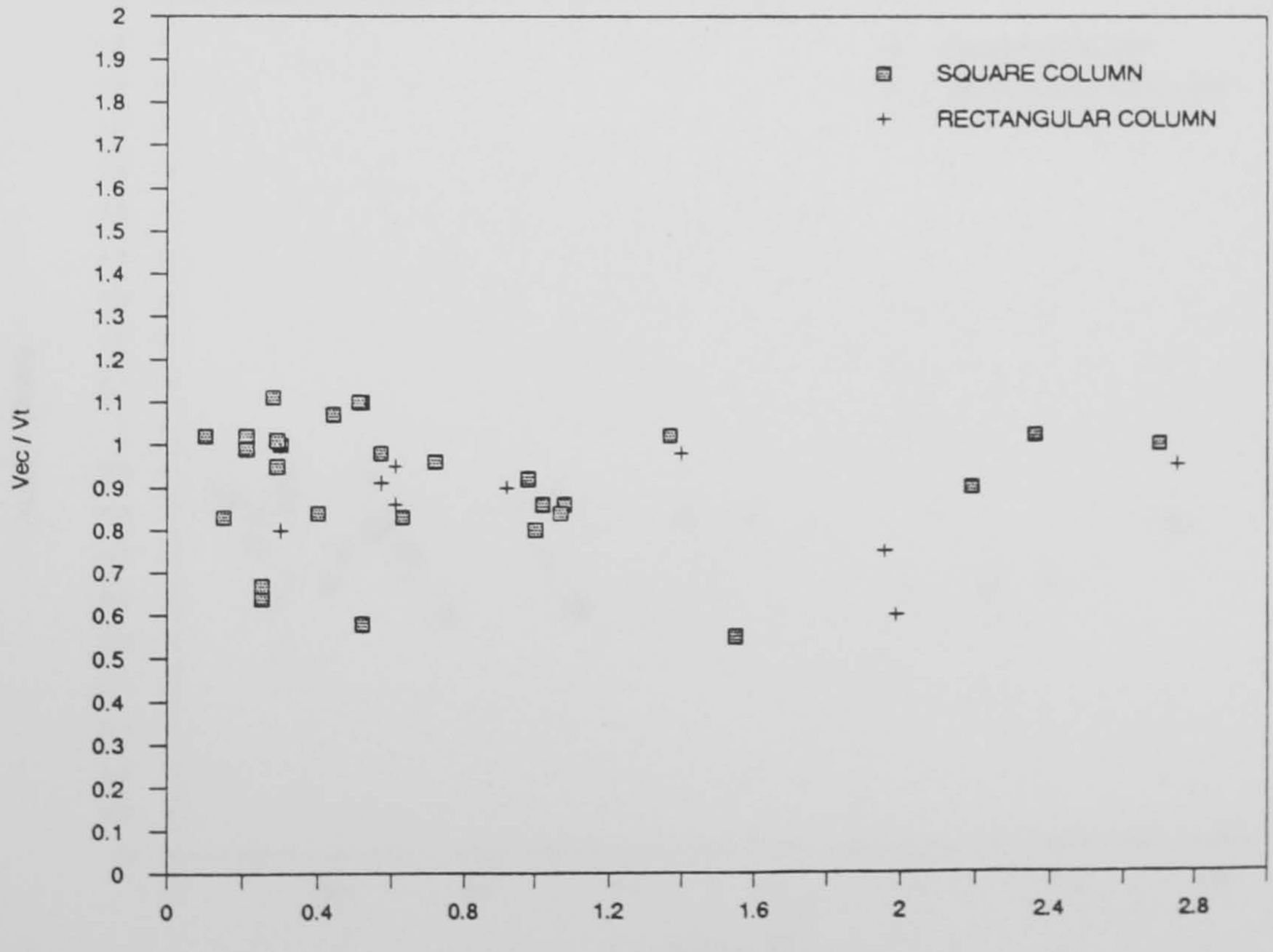

b) Eccentrically loaded slabs

Fig.(6-2) Comparison of test results with the author's formulae

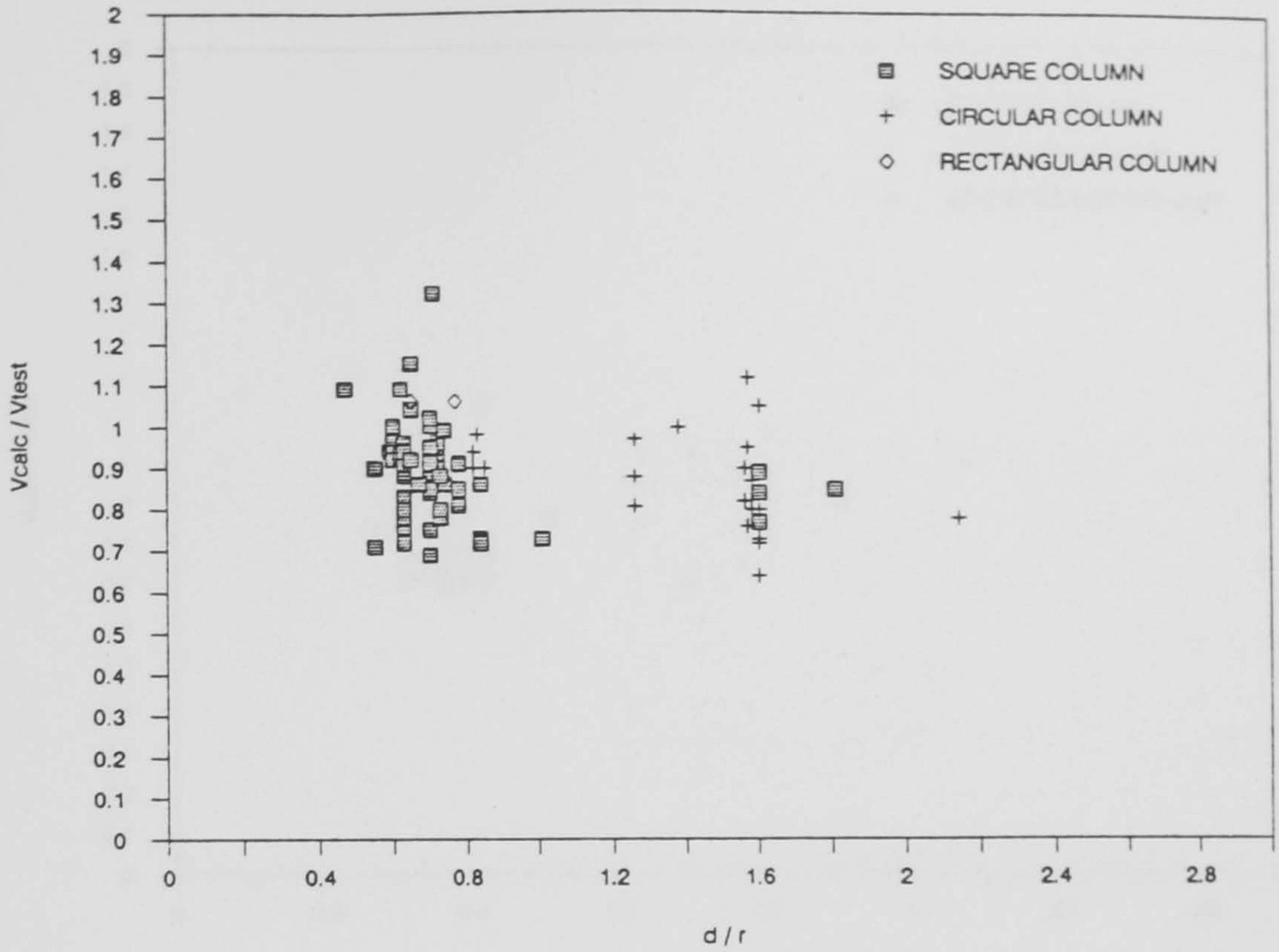

a) Concentrically loaded slabs

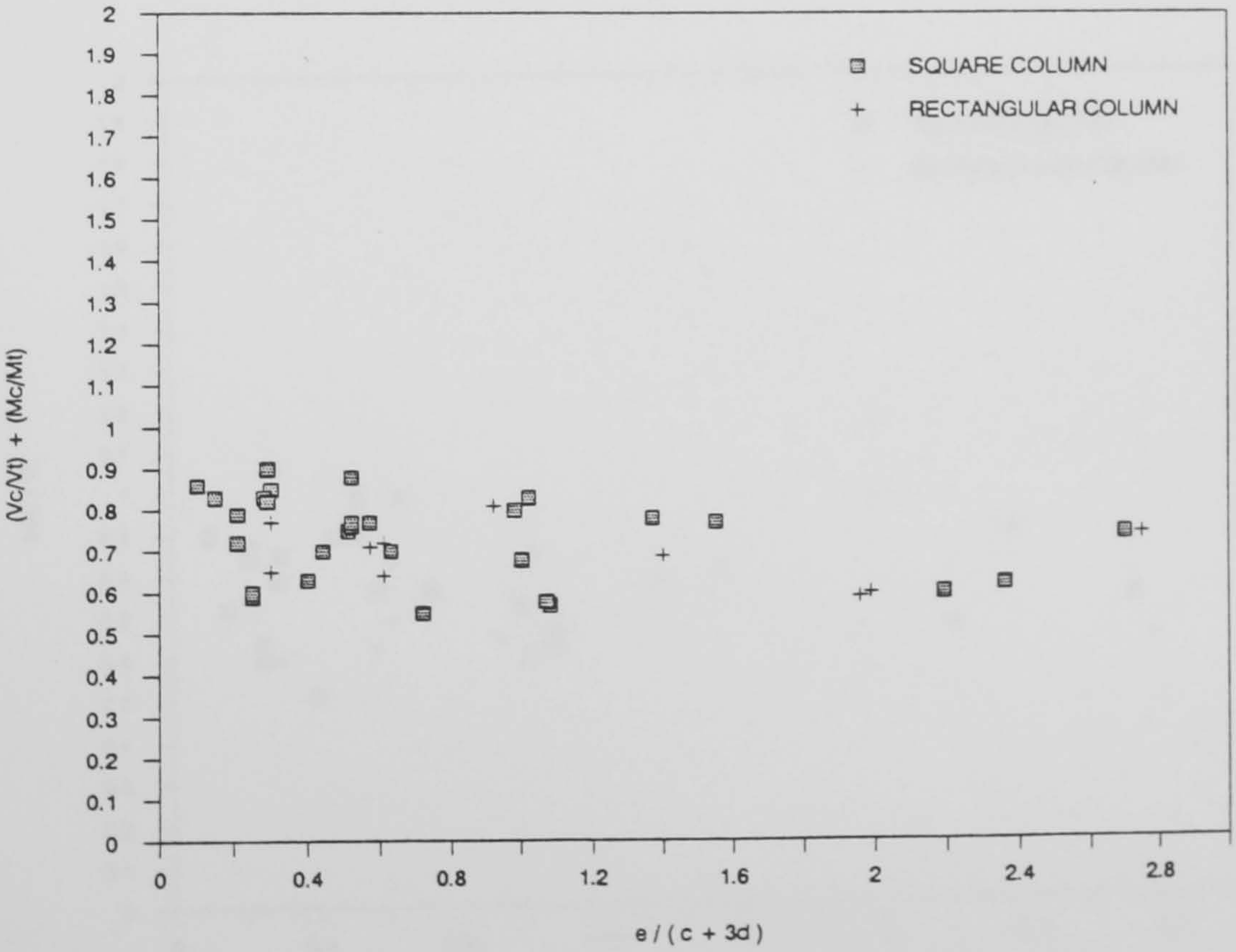

b) Eccentrically loaded slabs

Fig.(6-3) Comparison of test results with Stamenkovic and Chapman's formulae

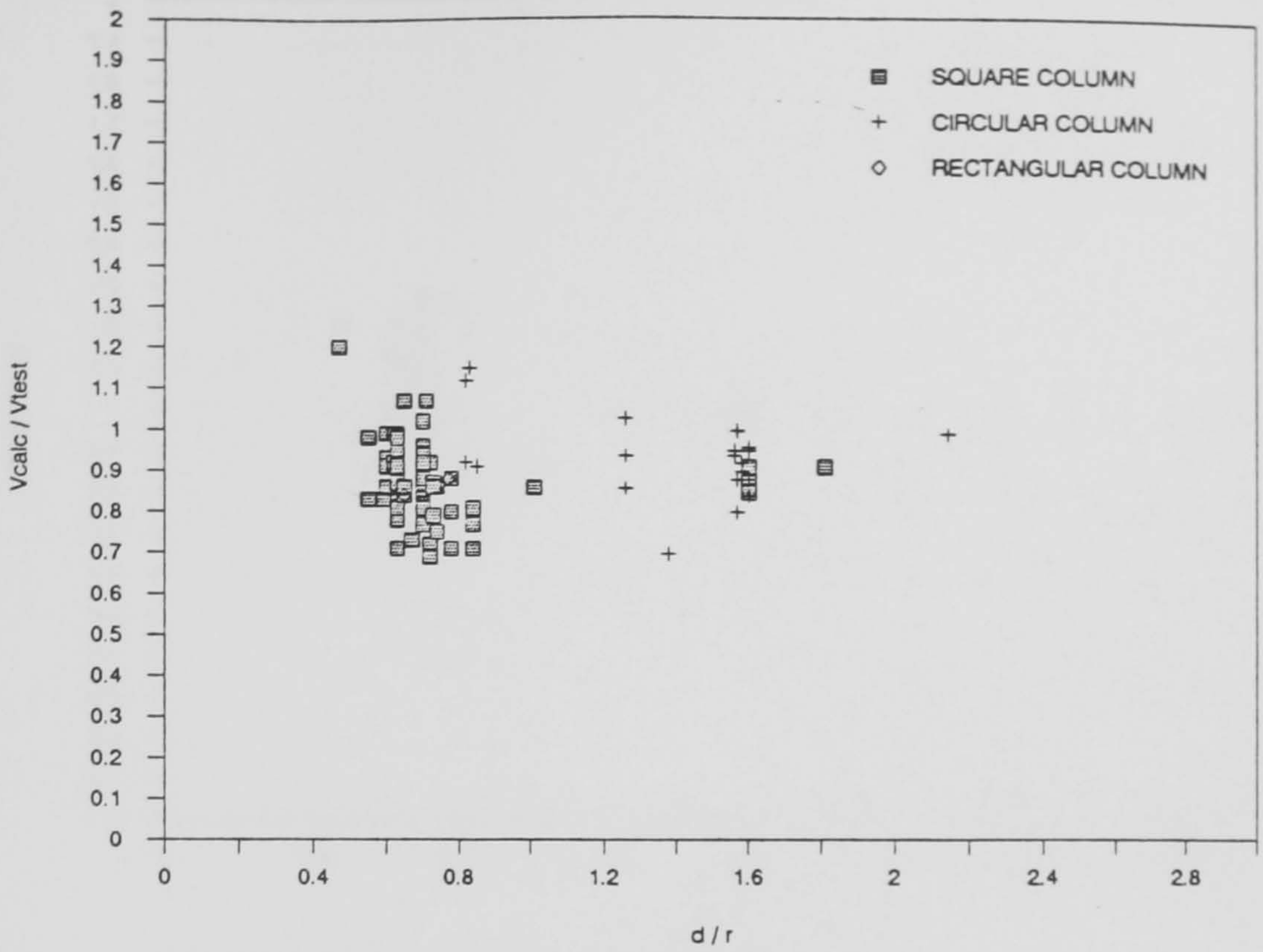

a) Concentrically loaded slabs

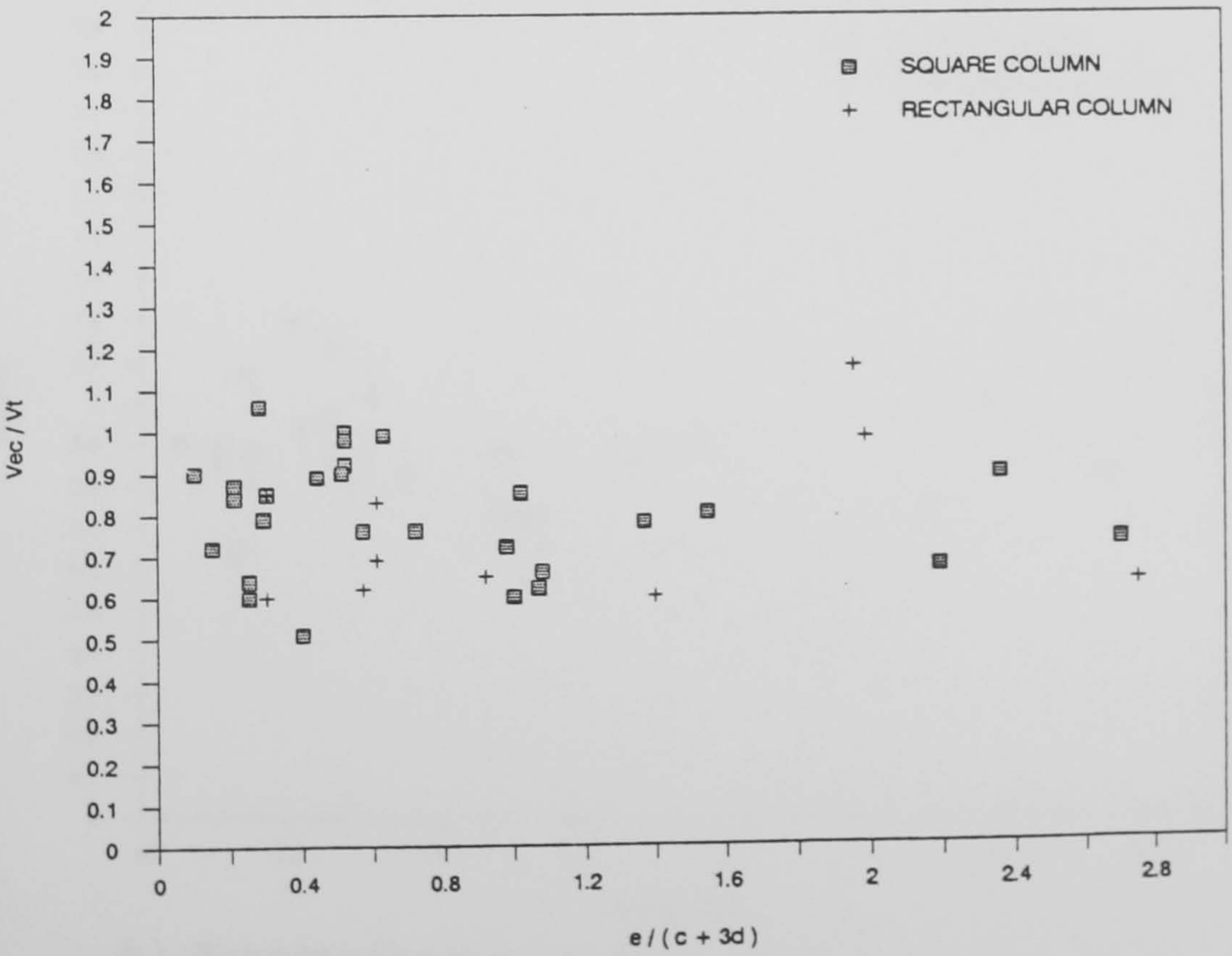

b) eccentrically loaded slabs

Fig.(6-4) Comparison of test results with Regan's formulae

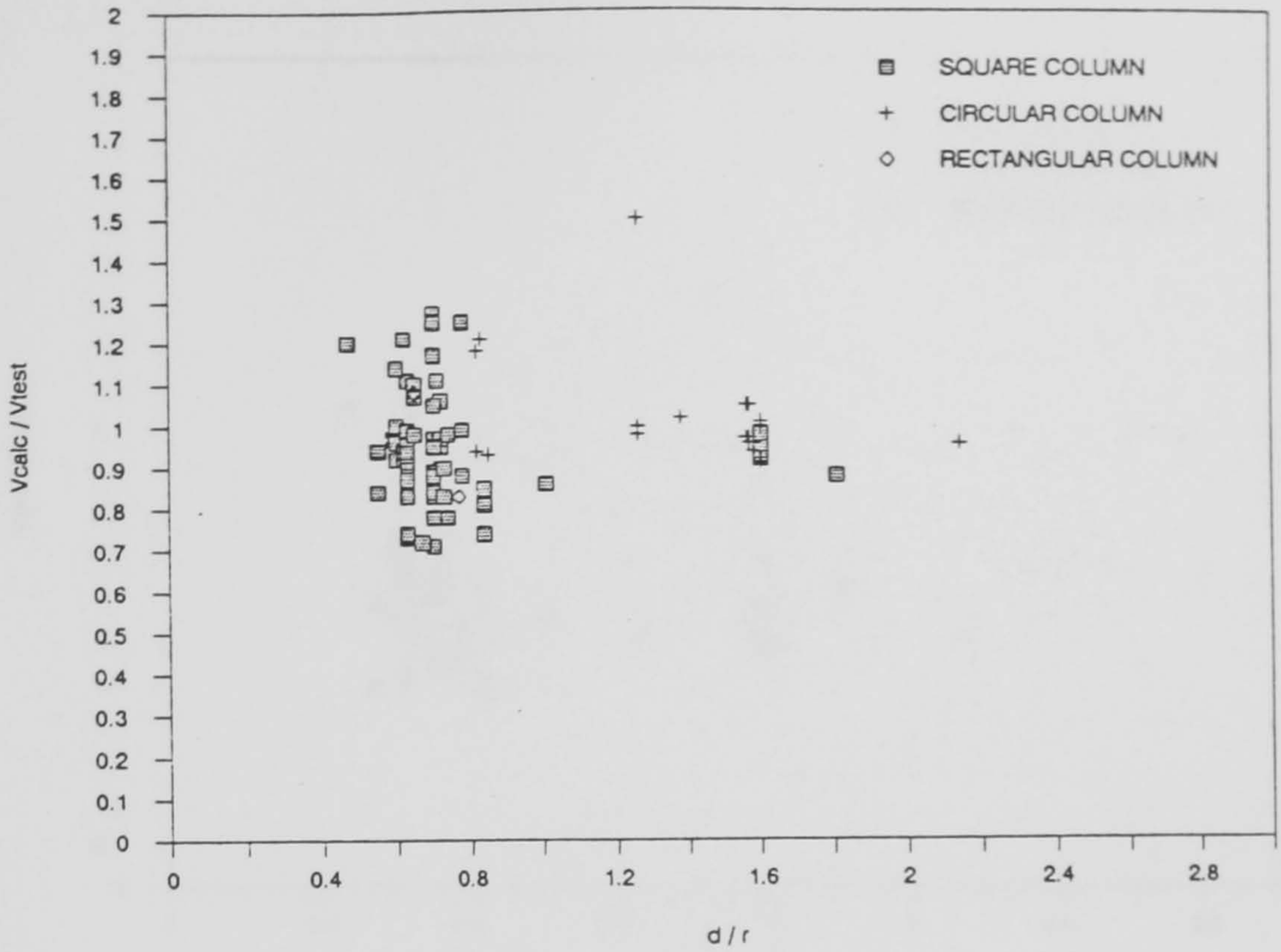

a) Concentrically loaded slabs

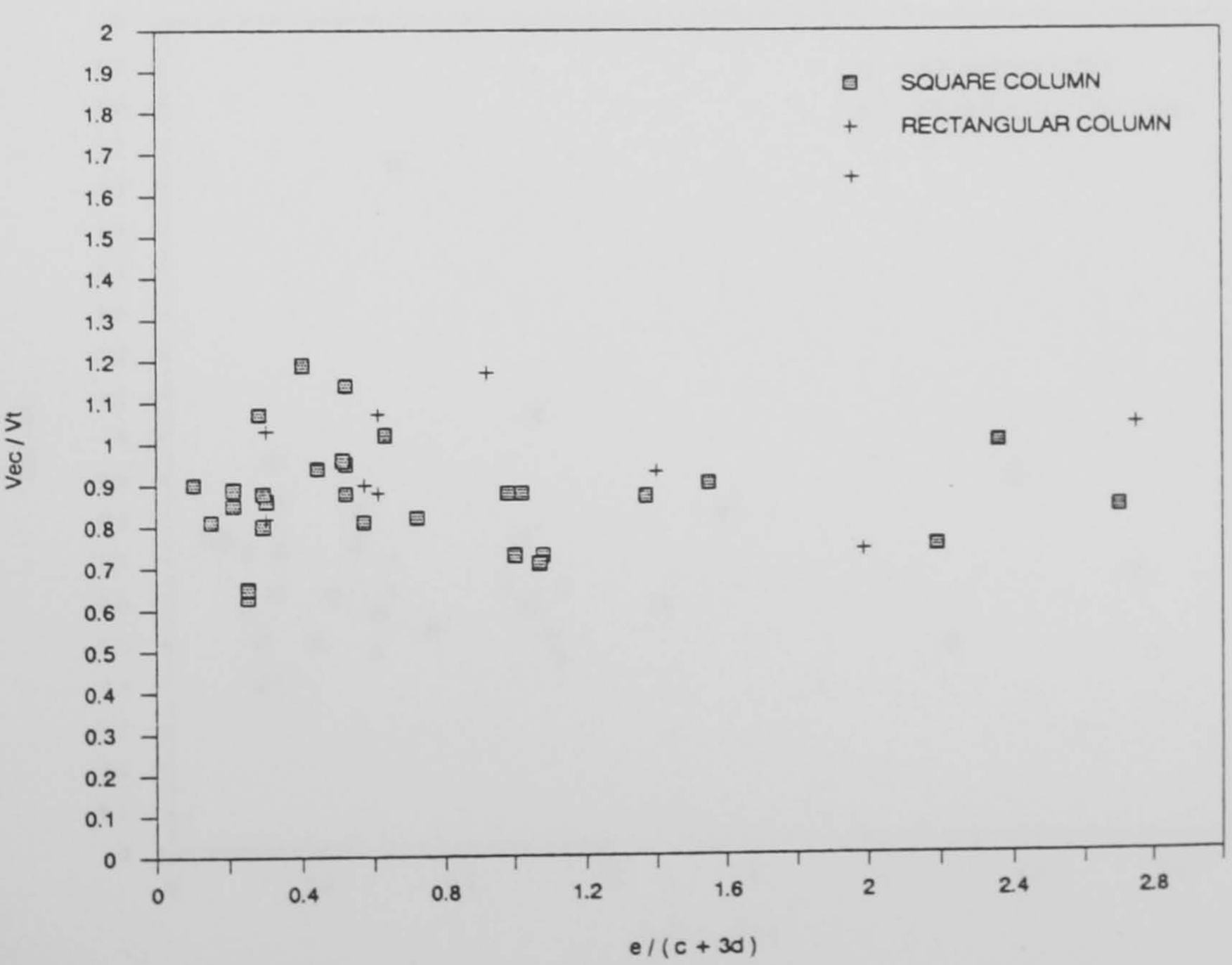

b) Eccentrically loaded slabs

Fig.(6-5) Comparison of test results with BS 8110

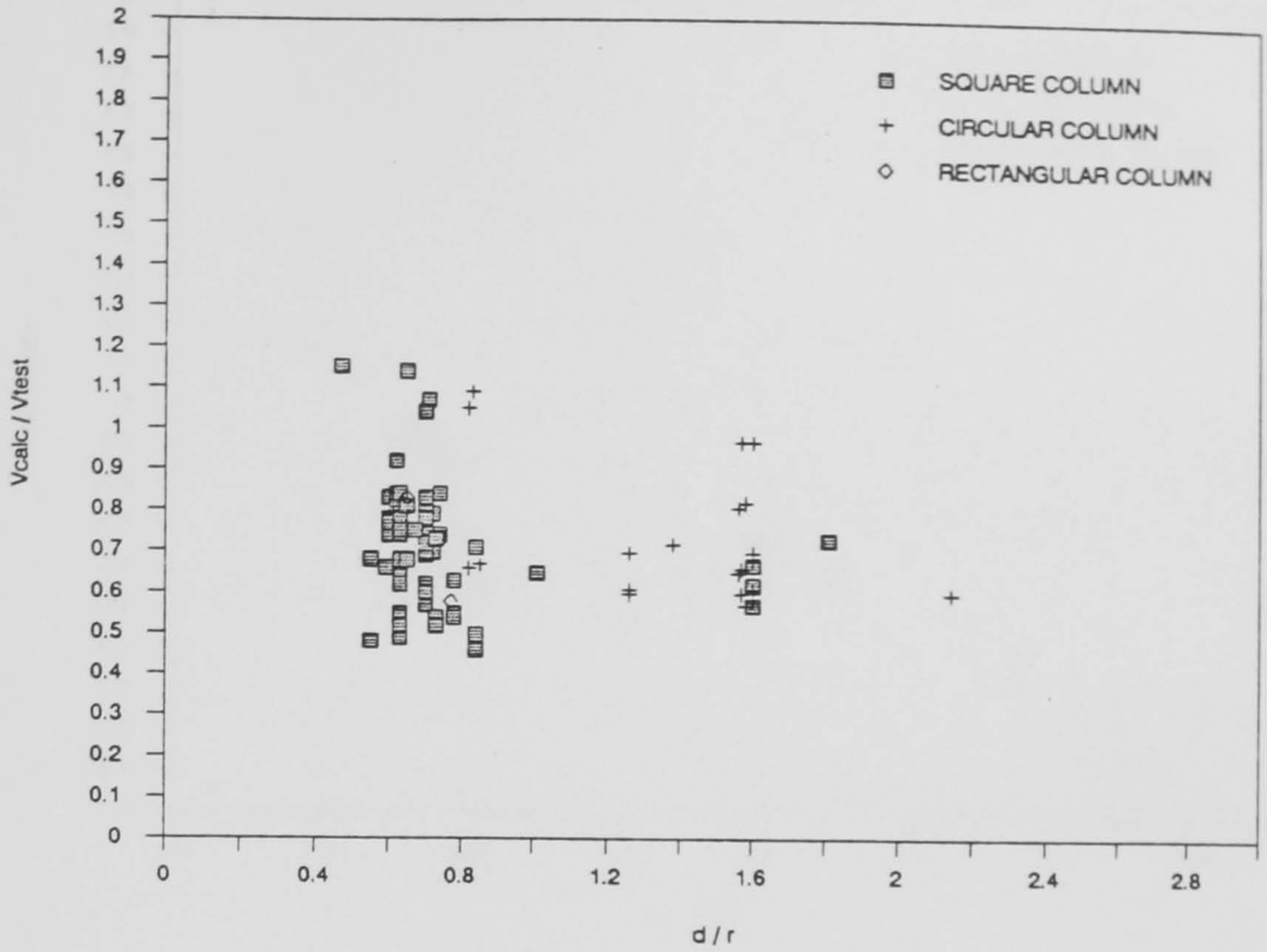

a) Concentrically loaded slabs

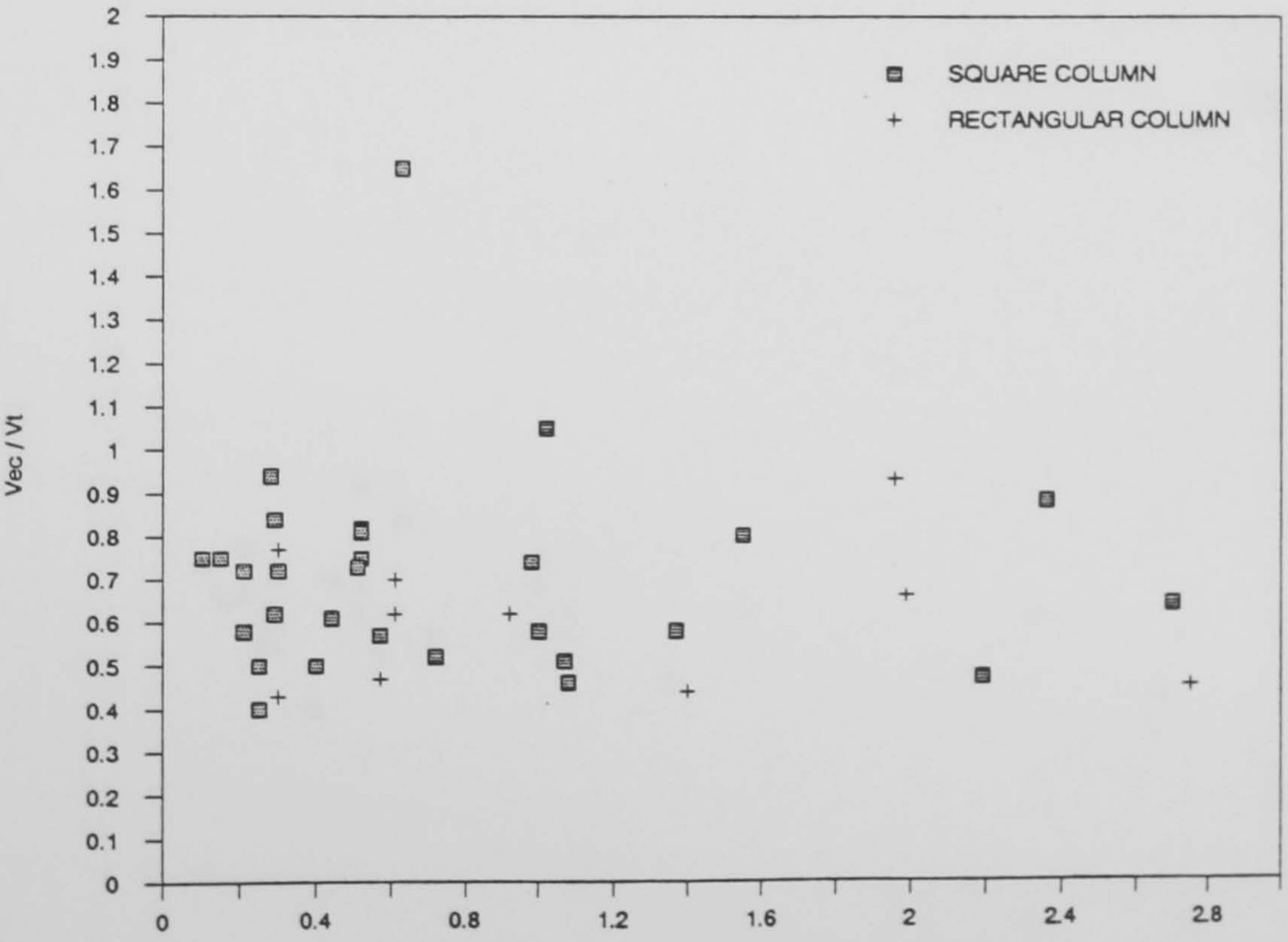

b) Eccentrically loaded slabs

Fig.(6-6) Comparison of test results with ACI 318-83

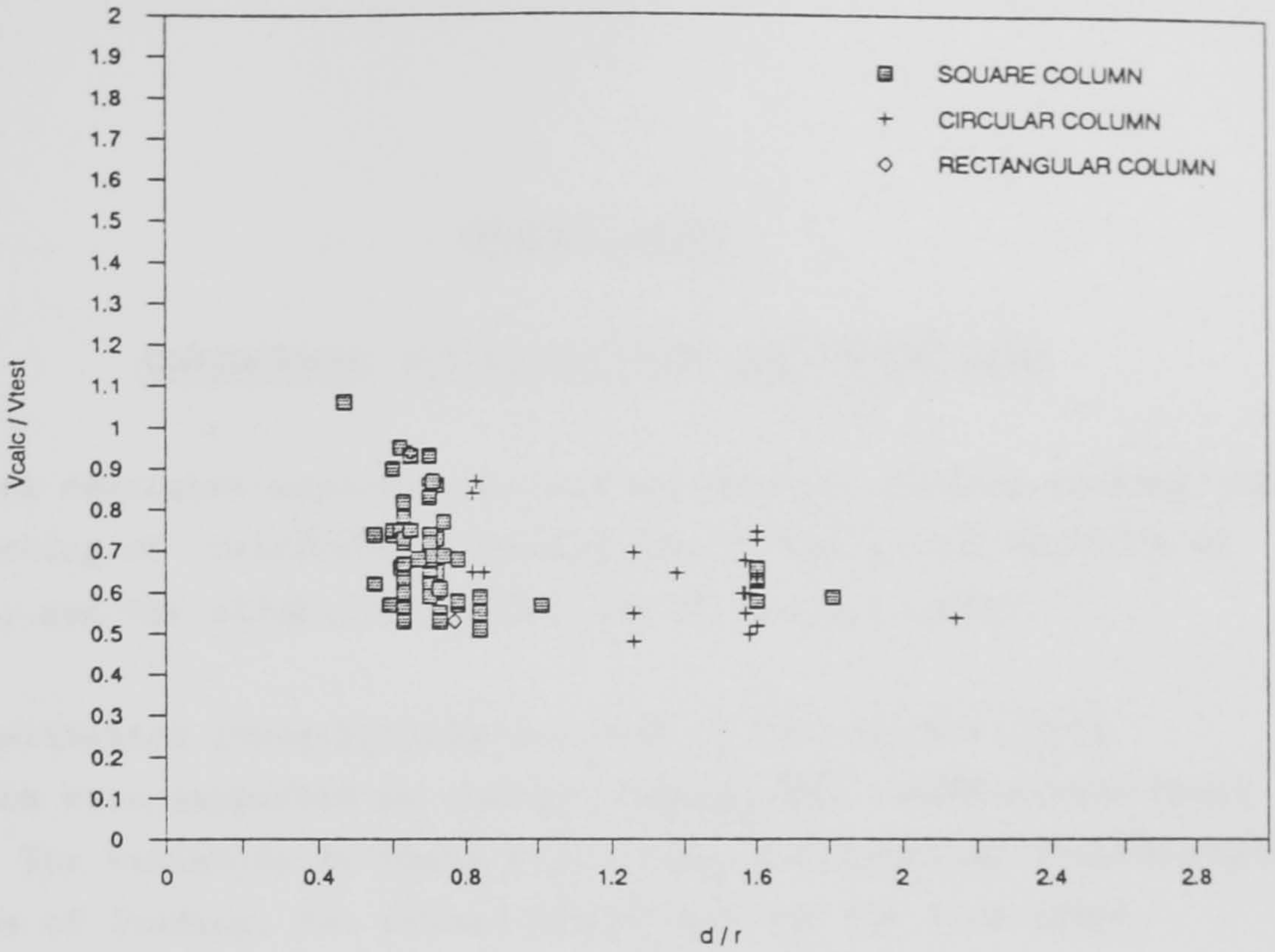

a) Concentrically loaded slabs

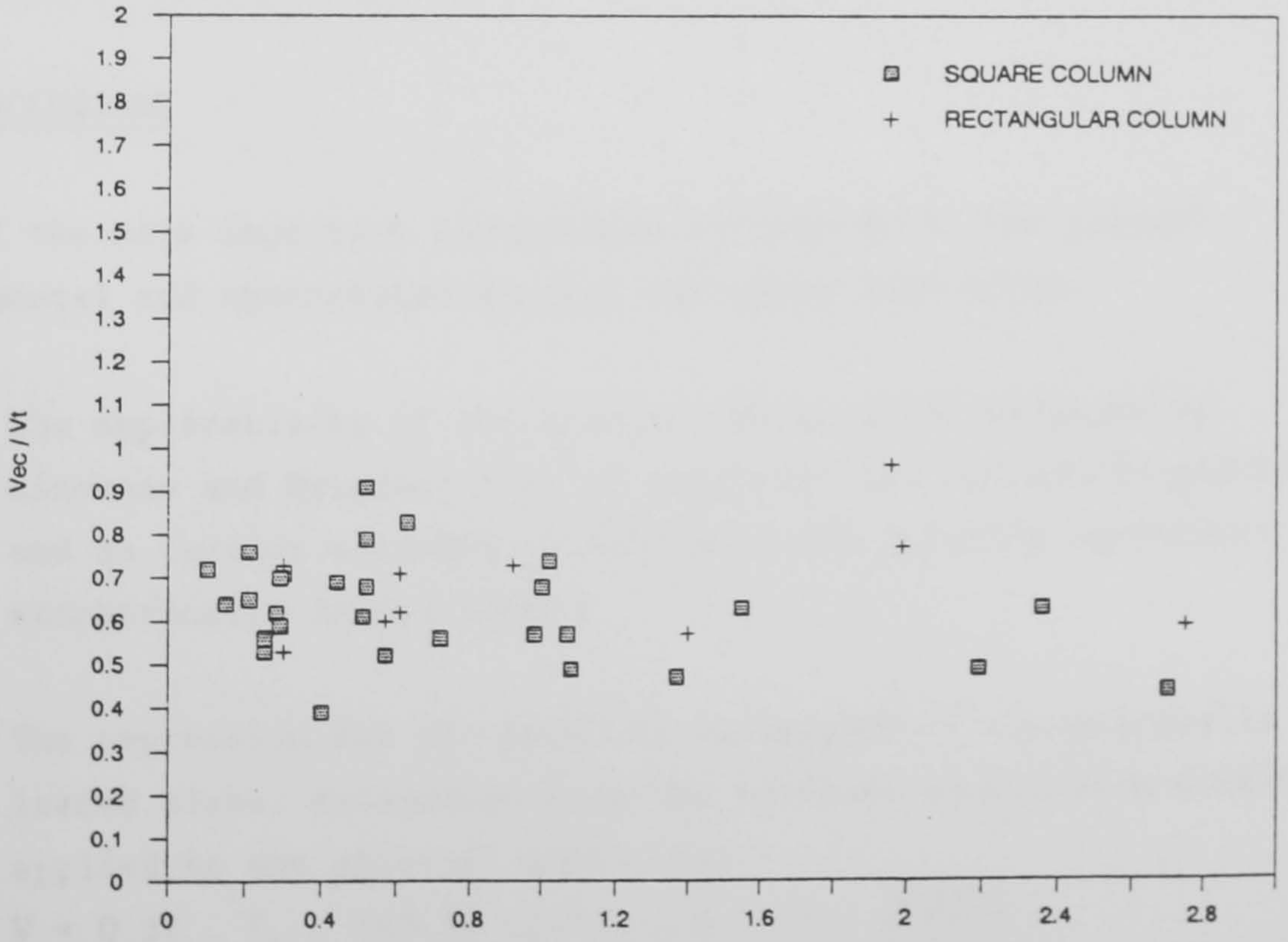

b) Eccentrically loaded slabs

Fig.(6-7) Comparison of test results with CEB-FIP

CHAPTER SEVEN

CONCLUSIONS AND SUGGESTIONS FOR FUTURE WORK

This work describes experimental and theoretical studies dealing with the punching of reinforced concrete flat-slabs in the vicinity of columns, and the effective stiffnesses of cracked slabs.

The experimental investigation was made on 10 concrete slabs. The slabs were supported on central columns and loaded around their edges. The variables in these tests were, the ratio of reinforcement, the type of loading, the column dimensions and the slab shape.

The theoretical investigation of punching strength was verified by comparisons with the results of tests on 99 concentrically loaded and 43 eccentrically loaded slabs.

7-1 CONCLUSIONS

Some of the more important conclusions arrived at in the present experimental and theoretical studies are summarized below.

1- The applicability of the physical model first proposed by Kinnunen and Nylander (30) is confirmed for concentric punching and is further extended to determine the punching resistance of eccentrically loaded slabs.

2- The expression for the punching resistance of concentrically loaded slabs, determined from the vertical equilibrium condition applied to the physical model, is:

$$V = 0.37 \cdot f_c \cdot 1n3.33\,(d/r_o) \cdot x \cdot c_t \cdot \sqrt{200/d}$$

Where $r_o = c_t/2\pi$

c_t is the column perimeter

3- The punching shear resistance is consistent with the radial compressive stress in the concrete at the column face reaching a limiting value:

$\sigma_c/f_c = 1.43 \ln 3.33 (d/r_o)$

and being inclined at an angle of $15^\bullet$ to the plane of the slab.

4- The scale effect of the slab effective depth may best be represented by square root of "d/200", where "d" is in "mm".

5- Ultimate moment strength of internal slab-column connection under horizontal loading can be calculated from equation (5-22).

$$M_u = F_s^* h_o + F_v c + F_H (h-x)$$

6- Ultimate strength of internal slab-column connection under combined vertical and horizontal loading is given by the proposed equation (5-23).

$$\frac{V}{V_u} + \frac{M}{M_u} = 1$$

7- The decreasing effect of progressive eccentricity on the punching shear resistance can be formulated as:

$$\frac{V}{V_o} = \frac{1}{1 + \dfrac{e}{0.7\ (c + 3d)}}$$

8- The column shape has a negligible effect on the punching shear resistance for eccentrically and concentrically loaded slabs provided the length of the column perimeter is constant.

9- Experimental evidence in the present work and from other sources indicates that the assumptions made, expressions developed and failure criterion proposed in the present study yield realistic predictions of the punching shear resistance of concentrically and eccentrically loaded reinforced concrete flat slabs.

10- The test results indicate that slab-column joint is not rigid and that there is a relative rotation between the two members.

11- The BS8110 definition of the ratio of flexural reinforcement as being that for a width only equal to that of the column plus "1.5d" to either side of it, can result in unsafety (0.25 x span to either side of column centre) is more realistic.

Also the use of the dimension of a shear perimeter parallel to the eccentricity in calculating eccentric punching shear resistance as recommended in BS8110 may give unsatisfactory results for slabs with rectangular columns. (Column perimeter/4 is preferable).

12- The use of concrete compressive strength as the only factor in determining the punching shear resistance as suggested by ACI - 318-83 may lead to unsafe results for thick slabs on large columns.

13- The deflection of eccentrically loaded slabs can be estimated by using the method described in section 5-3.

7-2 SUGGESTIONS FOR FUTURE RESEARCH

Since this work deals only with internal slab column connections of ordinary reinforced concrete slabs with no shear reinforcement, further work to extend the theory to the following cases is recommended.

- Eccentric and concentric punching in prestressed slabs.

- Punching shear in slabs with shear reinforcement.
- Punching at edge and corner columns.

More experimental work on internal and external connections having different variables is required.
Among those variables that should be included in further tests are slabs with different column shapes and eccentricities of the applied load.

REFERENCES

==========

1. Andrä H.P., Zum Tragverhalten des Auflagerbereichs von flachdecken, Dr Ing. thesis, Universitat Stuttgart 1982

2. Anis, N.N., Shear strength of reinforced concrete flat slabs without shear reinforcement, PhD Thesis, Imperial College London, 1970.

3. ACI 318M-83 Building code requirements for reinforced concrete, American Concrete Institute, Detroit, 1983.

4. ACI 318-83 Commentary on Building code requirements for reinforced concrete.American Concrete Institute, Detroit, 1983

5. ACI-ASCE Committee 428, Progress Report on code clauses for limit Design, ACI,Journal Vol 65 No 9 September 1968 pp 713-720

6. Balmer,G.G. Shearing strength of concrete under high triaxial stress, computation of Mohr's Envelope as a curve, Struct.Res.Lab.Rep.Sp-23 Denver, Colo. October 1949.

7. Bazant,Z.P., and Cao,Z., Size effect in punching shear failure of slabs, ACI structural Journal, January/Fibruary 1987 pp.44-53.

8. Braestrup M.W., Punching shear in concrete slabs, IABSE Colloqium, Copenhagen, 1979, introductory report Oct. 1978, pp 115-136.

9. Braestrup M.W., Ten lectures on concrete plasticity, Course given in Nanjin, China, October 1982.

10. Branson D.E Instantaneous and time dependent deflections of simple and continuous reinforced concrete beams, HPR Report No 7 part 1 Alabama highway department, Bureau of public roads, Aug. 1963, pp 78

11. BS 8110 Structural use of concrete. British Standards Institute, London, 1985

12. Chinn,J., and R.M.Zimmerman, Behavior of plain concrete under various high triaxial compression loading conditions, Air force weapons lab. tech. rep. WLTR64-163 Kirtland Air force base Albuquerque, N.Mex. 1965.

13. Chen W.F., Plasticity in reinforced concrete, McGraw-Hill book company 1982

14. Comite Euro-International du Beton "Concrete under multiaxial states of stress, constitutive equation for practical design" Bulletin d'information No 156 Juin. 1983.

15.CEB-FIP model Code for concrete structures Comite Euro-International du Beton 1978.

16. Comite Euro-International du Beton, Punching shear of reinforced concrete, A state of art report by P.E.Regan and M.W.Braestrup, Bulletin d'Information No 168, Jan. 1985.

17. Corley,W.G., and Jirsa,J.O., Equivalent frame analysis for slab design ACI.Journal November 1970 pp.875-884.

18. Deutscher Ausschuss für Stahlbeton, Heft 240, Hilfsmittel zur Berechnung der Schnittgrössen und Formänderungen von Stahlbetontragwerken nach Din 1045: 1972, Berlin 1976.

19. DIN 1045, Beton und Stahlbeton Bemessung und Ausführung, Deutsches Institut für Normung, Berlin, Dec. 1978.

20. Elstner, R.C. and Hognestad,E.,Shearing strength of reinforced concrete slabs, ACI Journal, 1956, July ,pp29-58.

21. Godycki, Dilger, and Ghali, Behaviour of reinforced concrete slab-column connections subjected to static loadings. Archivum Inzynierii Ladowej. Technical university Lodz Tom XXIII Z. 2/1977

22. Griffith,A.A., The phenomena of rupture and flow in solids,philosophical transactions, Royal Society of London Series A, V221, 1920 pp.163-198.

23. Hanson N., and Hanson J., Shear and moment transfer between concrete slabs and columns, Portland Cement Association, Development Department Bulletin D129 January, 1968.

24. Hanson, J.,M., Influence of embedded service ducts on strength of flat-plate structure, Research and development bulletin, Portland cement association 1970

25. Hawkins N. M., Fallsen H. B. and Hinojosa R. C., Influence of column rectangularity on the behaviourof flat plate structures, Publication SP-30, ACI Detroit, 1971, pp 127-146

26. Hognestad,E., Elstner,R. and Hanson,J. Shear strength of reinforced structural light-weight concrete slabs, ACI Journal Vol. 61 June 1964, pp.643-656

27. Hughes, B.P., Limit state theory for reinforced concrete design. Third edition, Pitman London 1980.

28. Hughes,B.P., and Chapman,G.P., The complete stress-strain curve for concrete in direct tension, RILEM Bull. 30,1966 pp 95-97.

29. Jones,L.L. and Wood,R.H., Yield line analysis of slabs, Chatto & Windus London 1967.

30. Kinnunen, S., and Nylander, H., Punching of concrete slabs without shear reinforcement, Meddelande Nr 38. Institutionen for Byggnadsstatik, Kungliga Tekniska Hogskolan, Stockholm, Sweden, 1960.

31. Kinnunen, S.,Punching of concrete slabs with two-way reinforcement, Meddelande Nr 41, Institutionen for Byggnadsstatik, Kungliga Tekniska Hogskolan, Stockholm, Sweden, 1963.

32. Kinnunen, Nylander, & Tolf, Undersokningar rorande genomstansning vid. Institutionen for byggnadsstatik, KTH, Journal of the Nordic concrete federation. 10 Nordiska Betongforskningsmotet 21-23 Aug. 1978 pp 25-26.

33. Kotsovos,M.D. and Newman,J.B., behaviour of concrete under multiaxial stress, ACI Journal Sept. 1977, pp 444-446

34. Kotsovos,M.D., and J.B.Newman, Generalized stress-strain relation for concrete J.Eng.Mech.DIV. ASCE vol 104 No EM4 proc. pap. 13922 pp845-856 August 1978.

35. Kupfer,H., Hilsdorf,H.K., and Rusch,H., Behaviour of concrete under Biaxial stresses,ACI Journal Vol 66 No 8 August 1969 pp 656-666.

36. Laddie,L., Mills, and, Zimmerman, R.M, Compressive strength of plain concrete under multiaxial loading conditions ACI Journal October 1970.pp 802-807

37. Long,A.E. A two-phase approach to the prediction of the punching strength of slabs. ACI Journal Feb. 1975, pp 37-45.

38. Long A.E., and Masterson D.M., Improved experimental procedure for determining the punching strength of reinforced concrete flat slab structures, ACI publication SP-42 Vol.2 pp 921-935

39. Mehrain,M., and Aalami,B., Rotational stiffness of concrete slabs. ACI, Journal September 1974 pp.429-435.

40. Moe, J., Shearing strength of reinforced concrete slabs and footings under concentrated loads, Portland Cement Association, Bulletin D47,April 1961.

41. Mohammed,I.A. and Popov,E.P., Effective stiffness of a plate subjected to a local edge moment Proccedings, Second U.S. National Congress of Applied Mechanics, 1954.

42. Montague,P., and Kormi,K., Constitutive relationships and failure criterion for concrete based on fundamental material properties, Magazine of Concrete Research vol.34 No 118 March 1982 pp.35-43.

43. Narasimhan, Shear reinforcement in reinforced concrete column heads, PhD thesis, Imperial College, London, 1971.

44. Negrutiu,R., Elastic Analysis of Flat Slab Structures. Analiza elastica a structurelor cu dale. Editora Academiei Republicii Socialiste Romania 1976.

45. Nelissen,L.J.M., Biaxial testing of normal concrete, Heron Delft vol.18 No 1 1972.

46. Nölting D. Des Durchstanzen von Platten aus Stahlbeton Tragverhalten Berechnung,Bemessung,Heft 62,Institut fur Baustoffe, Massivbau und Brandschutz, Technischen Universitat Braunschweing, 1984.

47. Ottosen,N.S., Failure and elasticity of concrete, Dan. Atom. Energy comm. Res. Establ. Riso Eng. Dept. Riso-M-1801, Roskilde, Denmark, July 1975.

48. Ottosen,N.S., A failure criterion for concrete, Journal of the Eng. Mech. Div. ASCE vol. 103 No EM4 pp.527-535 August 1977

49. Pecknold,D.A., Slab effective width for eqivalent frame analysis.ACI Journal April 1975 pp.135-137.

50. Petcu V., Stanculescu G., and Pancaldi U., Punching strength predictions for two-way reinforced concrete slabs. Revue Romanie de sciences Techniques, serie de Mecanique Appliquee, Vol. 24 No 2 Mar./Apr. 1979, pp 263-281.

51. Rankin G.I.B, and Long,A.E Predicting the punching strength of conventional slab-column specimens, Proc. Instn Civ. Engrs, Part 1,82, Apr.1987, pp 327-346

52. Regan P.E, Walker P.R, and Zakaria K.A.A, Tests of reinforced concrete flat slabs, Technical note, The Polytechnic of Central London Octber 1978.

53. Regan, P.E.,Behaviour of reinforced concrete flat slabs CIRIA report No 89, 1980.

54. Regan P.E., Punching shear in prestressed concrete slab bridges, Structures Research Group, Polytechnic of Central London, Jan. 1983.

55. Regan,P.E., Shear combs, reinforcement against punching. The Structural Engineer vol. 63B No.4 December 1985, pp 76-84.

56. Regan, P.E., Symmetric punching of reinforced concrete slabs, Magazine of concrete research Vol. 38 No. 136 Sept.1986, pp115-128

57. Richart,F.E.A.,Brandtzaeg and Brown,R.L., The failure of plain and spirally reinforced concrete in compression Univ.Ill.Eng.Exp.ST.Bull. 190 April 1926.

58. Richart,F.E.A.Brandtzaeg, and Brown,R.L., A study of the failure of of concrete under combined compressive stresses University Ill. Eng. Exp. St. Bull. 185 1928.

59. Rusch, H., Physical problems in the testing of concrete, Library translation No 86 Cement and concrete Association London 1960.

60. Scott, D.B.,Alexander and Simmonds. S.H., Shear-moment transfer in slab-column connections, Structural Engineering Report No 141 University of Alberta July 1986.

61. Shehata I.A., Punching of prestressed and non-prestressed reinforced concrete flat slabs, MPhil thesis, Polytechnic of Central London Sept. 1982.

62. Shehata, I.M., Theory of punching in concrete slabs PhD, thesis. The Polytechnic of Central London, 1985.

63. Stamenkovic, A., and Chapman, J.C., Local strength of flat slabs at column heads, CIRIA report NO 39.August 1972.

64. Stiglat, K. Der plattenstreifen unter dem angriff von Flächenmomenten, Mitwirkende plattenbreiten, die Bautechnik, Vol.4, Berlin, 1963.

65. Whitney,C.S., Ultimate shear strength of reinforced concrete flat slabs, footings, beams, and frame members with out shear reinforcement, ACI Journal Vol.54 No 4 October 1957, pp 265-298.

66. Whittle,R.T., Design of reinforced concrete flat slabs to BS 8110, CIRIA report 110, 1985.

67. Willam,K.J., and Warnke,E.P., Constitutive models for the triaxial behaviour of concrete, IABSE, 1975.

68. Wischers G., Application of effects of compressive loads on concrete, Betotech Ber, 2 and 3 Duesseldarf.

69. Yamazaki, J. Shear and moment tansfer between reinforced concrete flat plates and columns, PhD thesis, University of Washington Seattle, 1975.

70. Rankin G.I.B. and Long A.E., Predicting the enhanced punching strength of interior slab-column connections, Proceedings, Institution of Civil Engineers, Part 1, 1987, 82, Dec, pp 1165-1186.

71. Long A.E. and Masterson D.M., Improved experimental apparatus for determining the punching strength of reinforced concrete flat slab structures. Internal Report No. 55, Dept. of Civil Engineering, Queen's University Belfast, March 1973.

NOTATION

The notation which follows is for the author's experimental work and theoretical approach. The symbols relating to other researchers work and codes of practice are given in the text.

A	Slab length
A_s	Area of steel
a	Length of loaded area (or column)
B	Slab width
b	Width of loaded area (or column)
b_e	Effective width of slab
C	The length of the bearing area of a radial segment
d	Effective thickness or depth
E_c	Modulus of elasticity of concrete
E_s	Modulus of elasticity of steel
e	Eccentricity of the applied load
F_{ct}	Tangential concrete force
F_{st}	Tangential steel force
F_{sr}	Radial steel force
F_{cr}	Radial concrete force
F_c	Total radial concrete force
F_s	Total radial steel force
f_c	Cylinder strength of concrete
f_{cu}	Cube strength of concrete
f_t	Concrete tensile strength

$f_{ct,flex}$ Flexural tensile strength of concrete

f_y Yield stress of steel

H Horizontal load

h Overall thickness or depth

K_x, K_c coefficients (functions of the concrete strain and the idealised stress-strain curve)

l Span length

M Positive moment at midspan

M_t Moment transferred to column

M_{cr} Moment to cause first crack to develop

M_{tcr} Transfer moment at first cracking of slab

M_1, M_2 Negative moments at supports

m Moment per unit width

P Applied vertical load

P_{cr} Vertical load at first cracking of slab

r_o Radius of a column (or loaded area)

r_3 Radius of slab

r_w Punching radius

r_s Radius at which tangential reinforcement yields

V Vertical load

V_{flex} Flexural capacity of slab

V_{test} Experimental ultimate load (in some tables V_t)

$V_{cal} = V_{ocal}$ Calculated ultimate concentric punching load (in some tables given as V_c and V_{oc})

$V_{ecal} = V_{ec}$ Calculated ultimate eccentric punching load

x Neutral axis depth

z Lever arm

α	Angle between radial compression at column face and mean plane of slab
$\Delta\phi$	Sectorial angle of a radial segment
ε	Normal strain
ε_{c1}	$= 0.85f_c/(4250\sqrt{f_c})$
ε_{ct}	Concrete tangential strain
ε_{cu}	Ultimate strain of concrete (0.0035)
ε_{st}	Steel tangential strain
ε_{sy}	Strain in the steel corresponding to f_y
ψ_{ft}	Rotation at failure of a radial segment
ρ	Reinforcement ratio
ρ_r	Ratio of radial reinforcement
ρ_t	Ratio of tangential reinforcement
σ	Normal stress
σ_c	Concrete bearing stress
σ_{sr}	Steel stress in radial direction
σ_{st}	Steel stress in tangential direction
$\sigma_1, \sigma_2, \sigma_3$	Principal stress
τ	Shear stress
θ_s	Slab rotation
θ_c	Column rotation
θ_j	Joint rotation
ξ	Depth factor
::	Proportional to

APPENDIX A

The experimental work included six square and four rectangular slabs. Four slabs were tested concentrically while six slabs were tested eccentrically. The loads were applied in stages, after each stage of loading a set of deflection and rotations readings was taken. The positions of the dial gauges and the spirit level inclinometers are shown in figures A1. A2, A3.The dial gauge and the inclinometer readings are listed in tables (A). In the following tables all deflections are in mm while the rotations are in degrees.

Table A1 Slabs deflection

V	deflection								
KN	1	2	3	4	5	6	7	8	9
25	0.53	0.35	0.15	0.04	0.02	0.03	0.37	0.82	1.12
37	0.36	0.28	0.81	0.11	-0.30	0.88	0.47	0.93	1.22
49	1.47	0.98	0.48	0.37	-0.41	0.68	0.95	2.06	3.93
61	3.17	2.13	1.00	0.80	-1.69	2.22	1.39	3.98	4.33
69	5.14	3.44	1.99	1.08	-1.07	2.49	2.25	5.08	7.38
77	5.53	3.72	2.12	1.19	-0.87	2.73	2.44	5.47	7.87
85	6.06	4.09	2.30	1.20	-1.04	2.46	2.79	6.20	8.89
89	6.69	4.43	2.46	1.05	-1.40	1.86	3.18	6.99	10.04
93	6.88	4.58	2.54	1.02	-1.50	1.68	3.33	7.28	10.51

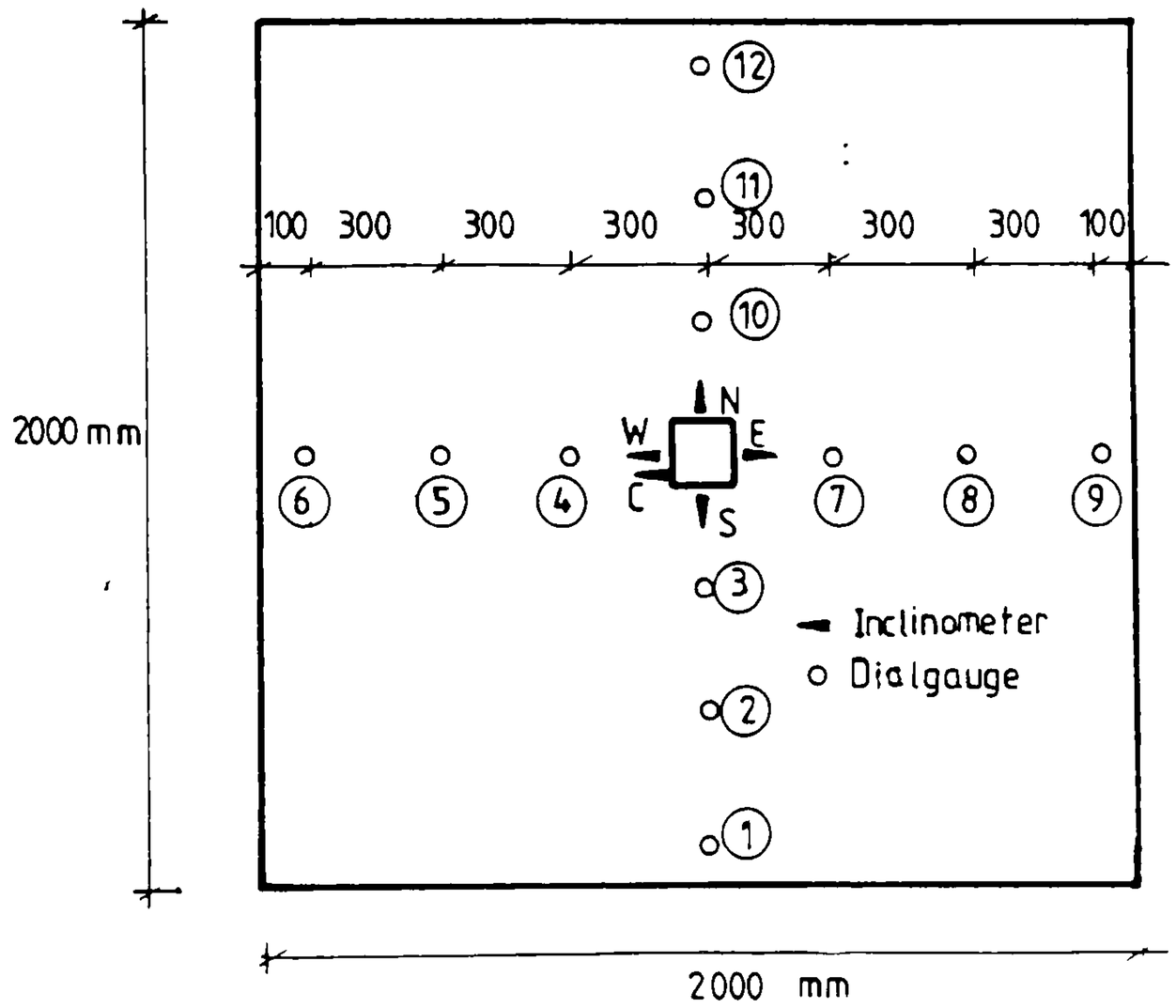

Fig. A1 Inclinometer and dial-gauge positions on slabs (SA1,SA2,SA3,SA4,SB1,SB2)

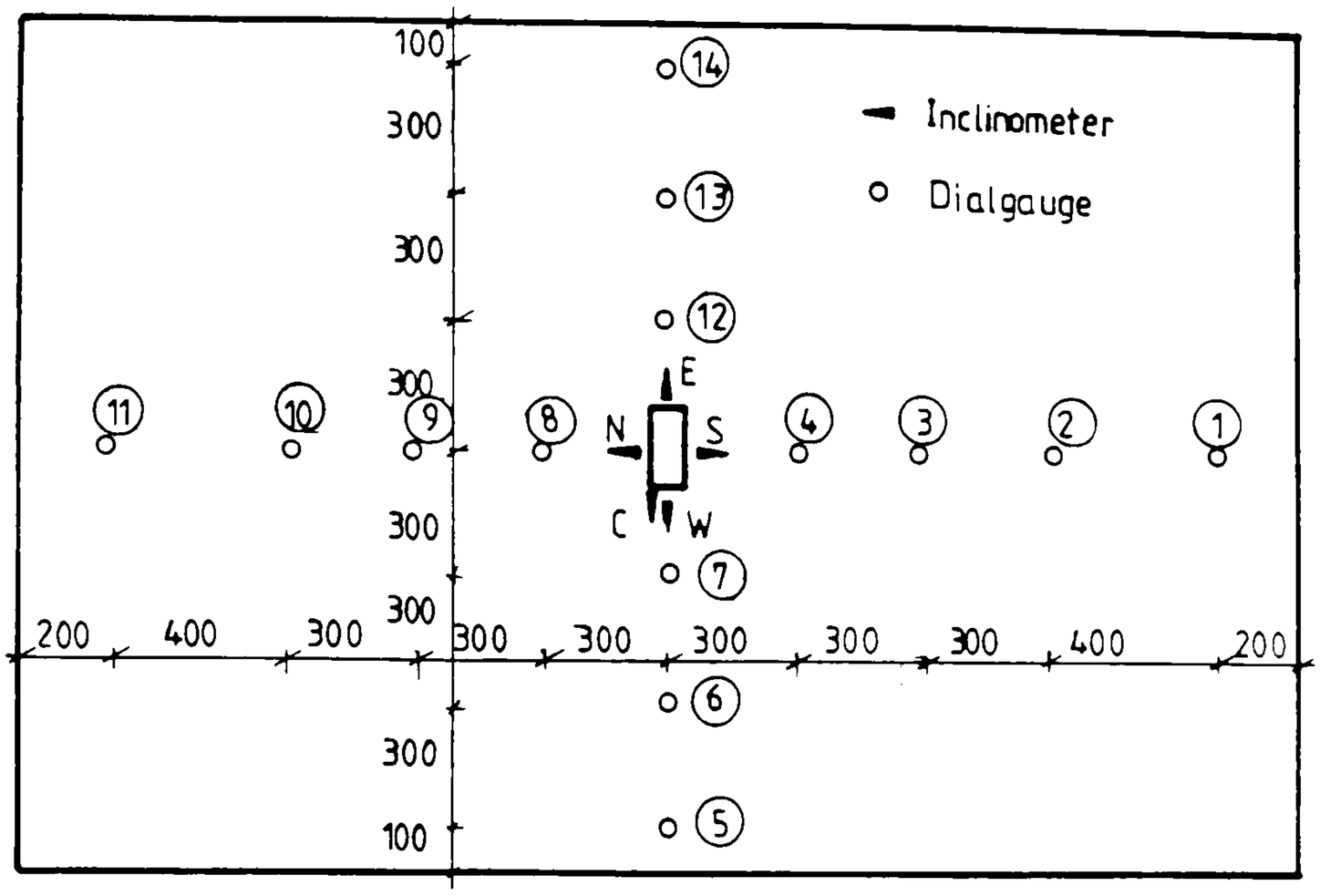

Fig. A2 Inclinometer and dial-gauge positions on slabs (SD1,SD2)

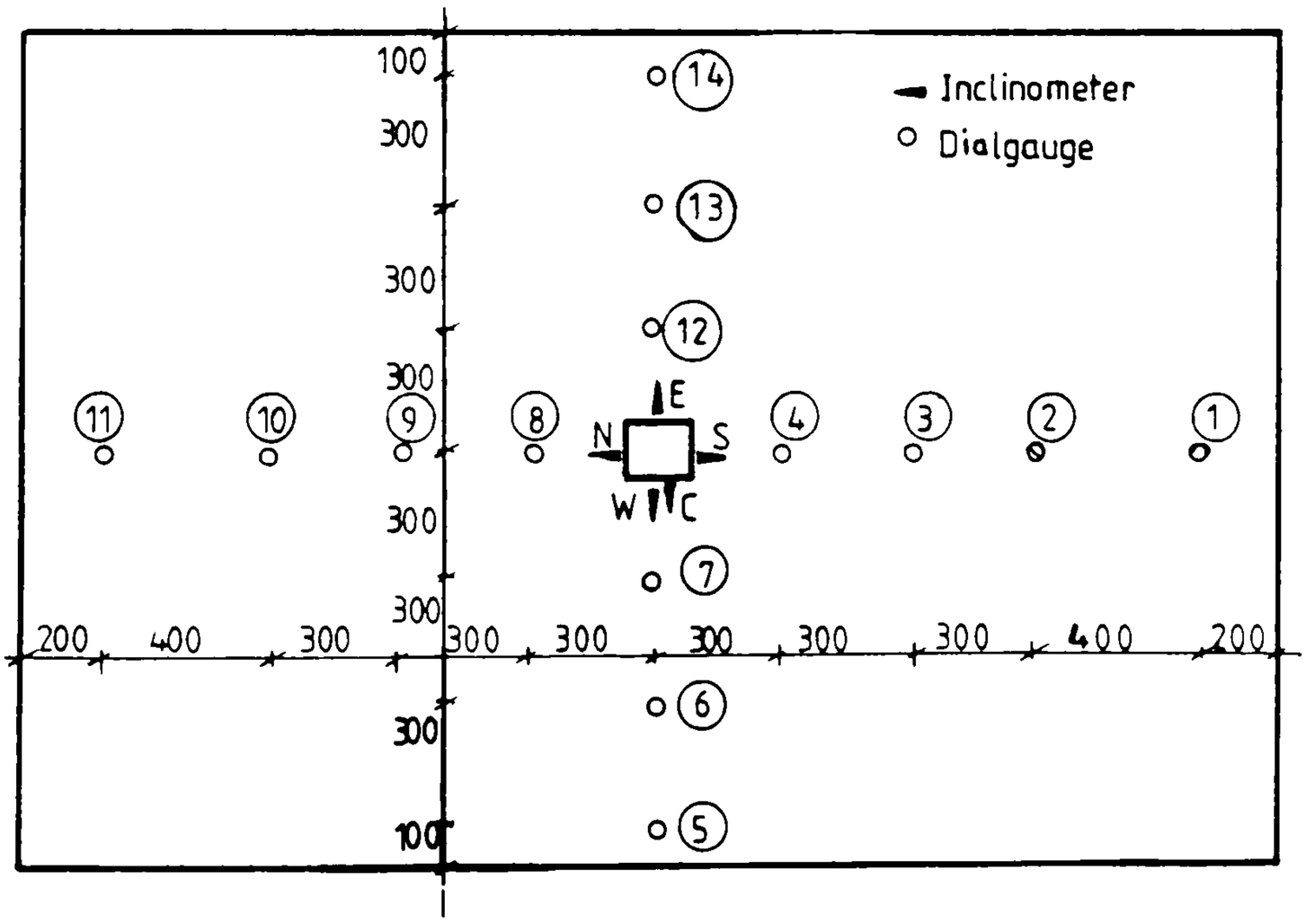

Fig. A3 Inclinometers and dial-gauge positions on slabs (SC1,SC2)

Table A1 - slab SA1 continued.

V	deflection								
KN	1	2	3	4	5	6	7	8	9
97	7.17	4.80	2.65	0.97	-1.66	1.43	3.59	7.86	11.25
101	7.83	5.33	2.88	0.94	-1.78	1.17	3.99	8.75	12.47
105	7.93	5.44	2.92	0.91	-1.88	0.97	4.21	9.18	13.09

Table A1 - slab SA1.

V	deflection								
KN	1	2	3	4	5	6	7	8	9
25	1.00	0.03	0.04	0.11	0.25	1.35	0.14	0.24	0.49
37	1.26	0.23	0.16	0.30	0.61	1.92	0.30	0.54	0.91
49	2.30	0.54	0.47	0.56	1.23	2.83	0.58	1.09	1.70
61	3.93	1.23	0.96	1.01	2.26	4.44	1.12	2.24	3.46
69	4.29	2.33	1.08	1.18	2.61	4.90	1.25	2.65	4.17
77	4.72	2.59	1.27	1.38	2.99	5.41	1.46	3.05	4.46
85	5.04	2.84	1.38	1.47	3.16	5.59	1.57	3.24	4.86
89	5.82	3.43	1.67	1.74	3.71	6.29	1.83	3.76	5.55
93	6.16	3.70	1.80	1.86	3.95	6.61	1.97	3.98	5.77
97	6.43	3.95	1.93	1.99	4.22	6.96	2.11	4.31	6.21
101	7.71	4.19	1.05	2.13	4.48	7.29	2.25	4.58	6.56
105	7.14	4.50	2.22	2.32	4.86	7.83	2.45	4.92	7.10
109	7.46	4.77	2.31	2.49	5.20	8.25	2.58	5.33	7.65

Table A1 - slab SA2 continued.

V	deflection								
KN	1	2	3	4	5	6	7	8	9
113	7.88	5.11	2.49	2.68	5.56	8.72	2.77	5.67	8.11
117	8.21	5.40	2.65	2.89	5.98	9.26	2.94	6.05	8.59
121	8.62	5.71	2.78	3.10	6.42	9.91	3.12	6.49	9.19
125	9.07	6.08	2.98	3.31	6.82	10.37	3.41	6.98	9.86
129	9.55	6.49	3.24	3.61	7.38	11.13	3.79	7.55	10.63
133	10.07	6.92	3.46	3.85	7.82	11.66	4.14	8.22	11.51
137	10.49	7.34	3.72	4.25	8.44	12.39	4.88	9.55	13.19

Table A1 - slab SA2.

V	deflection								
KN	1	2	3	4	5	6	7	8	9
22	0.34	0.24	0.05	-2.92	-5.10	-7.39	2.51	5.17	7.90
31	0.95	0.67	0.26	-3.00	-5.30	-7.79	2.83	5.80	8.75
40	1.99	1.33	0.51	-3.09	-5.50	-8.13	3.11	6.49	9.71
49	3.78	2.49	1.01	-3.17	-5.37	-7.95	3.25	7.47	11.29
55	4.13	2.76	1.10	-5.00	-7.05	-9.41	3.33	8.08	12.23
69	6.24	4.27	1.74	-5.63	-8.35	-12.12	3.43	10.16	16.87
77	6.80	4.87	2.02	-5.77	-9.65	-12.71	3.86	11.82	19.40
85	7.75	5.52	2.48	-5.79	-9.69	-12.88	4.58	13.39	21.74

Table A1 - slab SA3.

V	deflection								
KN	1	2	3	4	5	6	7	8	9
25	0.49	0.31	0.13	-0.34	-0.46	-2.35	1.40	4.22	4.99
37	2.46	1.64	0.64	-1.56	-4.36	-6.84	3.90	10.10	14.05
41	2.89	1.93	0.78	-2.16	-5.59	-9.01	4.88	12.31	17.52
45	3.54	2.37	0.97	-2.83	-8.11	-11.50	6.14	15.33	22.32

Table A1 - slab SA4.

V	deflection								
KN	1	2	3	4	5	6	7	8	9
17	0.20	0.04	0.03	-0.40	-0.24	-0.09	0.22	0.46	0.73
21	0.27	0.05	0.09	-1.02	-0.60	-0.25	0.54	1.19	1.85
25	0.31	0.07	0.12	-1.66	-1.03	-0.42	0.85	1.90	2.90
29	0.36	0.08	0.13	-2.46	-1.52	-0.65	1.25	2.72	4.15
37	0.39	0.09	0.15	-4.88	-3.06	-1.36	2.42	5.66	8.71
45	0.42	0.11	0.16	-7.80	-4.93	-2.23	3.79	8.96	13.82
53	0.43	0.21	0.17	-12.27	-7.79	-3.59	5.80	13.68	21.11

Table A1 - slab SB2.

V	deflection								
KN	1	2	3	4	5	6	10	11	12
25	0.63	0.45	0.21	0.27	0.51	0.73	0.43	0.89	1.32
37	1.42	1.03	0.47	0.56	1.08	1.50	0.81	1.71	2.50
49	2.28	1.65	0.75	0.83	1.64	2.25	1.18	2.52	3.69
61	3.12	2.26	1.04	1.12	2.22	3.00	1.56	3.21	4.64
73	4.34	3.15	1.44	1.58	3.15	4.26	2.04	4.38	6.32
85	5.04	3.68	1.69	1.70	3.38	4.55	2.14	4.60	6.56
93	5.72	4.26	2.03	1.91	3.75	5.02	2.46	5.12	7.19
101	6.48	4.86	2.31	2.14	4.23	5.60	2.72	5.72	7.99
109	7.33	5.48	2.59	2.45	4.80	6.39	3.03	6.30	8.71
117	8.36	6.27	3.03	3.03	5.87	7.77	3.46	7.18	9.92

Table A1 slab SB1.

V	deflection										
KN	1	2	3	4	5	6	7	8	9	10	11
21	0.12	0.13	0.10	0.04	0.54	0.39	0.21	0.15	0.29	0.46	0.65
57	5.17	3.50	2.24	0.86	3.41	2.33	1.13	0.83	2.12	3.38	5.05
69	5.93	4.06	2.62	1.02	3.78	2.62	1.28	1.02	1.02	2.58	4.07
81	7.65	5.29	3.38	1.33	4.69	3.15	1.53	1.35	3.43	5.41	7.95
93	10.57	6.62	4.24	1.67	5.69	3.89	1.87	1.81	4.57	7.19	10.55
105	11.49	7.96	5.08	2.01	6.64	4.62	2.22	2.20	5.55	8.73	12.71
113	12.88	8.93	5.74	2.29	7.37	5.18	2.49	2.53	6.30	9.90	14.34
121	14.31	10.06	6.43	2.59	8.19	5.85	2.81	2.92	8.21	11.28	16.25

Table A1 slab SC1.

V	deflection										
KN	1	2	3	4	5	6	7	8	9	10	11
19	-0.21	-0.14	-0.08	-0.07	0.19	0.18	0.08	0.30	0.62	0.95	1.39
23	0.34	0.26	0.17	0.05	0.36	0.32	0.16	0.41	0.85	1.28	1.87
27	1.28	0.92	0.60	0.23	0.82	0.50	0.26	0.60	1.32	2.00	2.91
31	2.80	1.96	1.27	0.50	0.92	0.75	0.39	0.86	1.95	3.02	4.40
35	3.91	2.73	1.74	0.68	1.30	1.05	0.55	1.20	2.78	4.32	6.31
39	5.86	5.05	2.57	0.99	2.08	2.61	0.83	1.75	4.06	6.34	8.24
47	7.88	5.46	3.46	1.35	2.88	2.91	1.13	2.25	5.25	8.22	11.9
55	10.10	7.01	4.46	1.74	4.02	3.78	1.54	2.83	6.60	10.34	14.9
67	11.86	8.26	5.26	2.06	5.00	4.58	1.93	3.45	8.04	12.47	18.1
79	13.60	9.51	6.07	2.41	6.64	5.31	2.32	4.06	9.41	14.67	23.2

Table A1 slab SD1.

V	deflections													
KN	1	2	3	4	5	6	7	8	9	10	11	12	13	14
19	-0.16	-0.12	-0.08	-0.03	-0.58	-0.3	-0.10	0.24	0.42	0.63	0.87	0.26	0.56	0.83
23	-0.03	0.00	-0.03	-0.01	-1.29	-0.73	-0.25	0.38	0.75	1.14	1.60	0.55	1.22	1.80
27	-0.24	0.19	0.11	0.06	-2.09	-1.21	-0.41	0.54	1.11	1.71	2.40	0.85	1.97	2.92
31	0.67	0.47	0.32	0.13	-3.02	-1.77	-0.63	0.69	1.50	2.31	3.27	1.23	2.85	4.23
39	1.85	1.26	0.83	0.31	-5.45	-3.32	-1.28	1.08	2.46	3.87	5.53	2.23	5.17	7.83
51	3.41	2.28	1.49	0.54	-9.01	-5.59	-2.36	1.43	3.42	5.33	7.67	3.58	8.33	12.68
55	5.20	3.44	2.26	0.83	-14.22	-9.03	-3.91	1.95	4.52	7.22	10.39	4.14	13.07	19.89

Table A1 Slab SC2

V	deflections													
KN	1	2	3	4	5	6	7	8	9	10	11	12	13	14
19	0.40	0.29	0.19	0.09	-0.47	-0.28	-0.13	-0.04	0.10	0.16	0.25	0.18	0.46	0.70
23	0.70	0.52	0.33	-0.14	-1.04	-0.62	0.25	0.18	0.39	0.69	1.00	0.42	1.01	1.54
27	1.08	0.81	0.51	0.22	-1.69	-0.99	-0.41	0.39	0.86	1.39	1.95	0.72	1.69	2.57
31	1.83	1.37	0.85	0.37	-2.44	-1.44	-0.59	0.52	1.19	1.86	2.67	1.06	2.47	3.77
39	3.94	2.85	1.78	0.75	-4.73	-2.84	-1.19	0.91	2.13	3.40	4.84	2.11	4.87	7.50
47	6.60	4.83	3.01	1.31	-8.52	-5.20	-2.21	1.38	3.16	4.91	7.17	3.85	8.59	13.23

Table A1 Slab SD2

Table A2 Slabs rotation

V KN	M_t KN m	Rotation			
		W	E	S	C
25	0.74	0.025	0.072	0.012	-0.014
37	1.48	0.052	0.128	0.019	-0.019
49	2.22	0.058	0.189	0.032	-0.021
61	2.77	0.159	0.210	0.040	-0.025
69	3.33	0.220	0.221	0.074	-0.026
77	3.70	0.240	0.268	0.103	-0.029
85	4.25	0.225	0.530	0.120	-0.033
89	4.62	0.185	0.766	0.133	-0.037
93	4.81	0.178	0.800	0.141	-0.038
97	5.00	0.161	0.820	0.155	-0.039
101	5.18	0.138	0.874	0.178	-0.040
105	5.55	0.137	0.930	0.189	-0.048

Table A2 - slab SA1.

V KN	Rotation			
	N	W	S	E
25	0.032	0.012	0.008	0.016
37	0.080	0.049	0.027	0.045
49	0.195	0.119	0.107	0.112
61	0.343	0.235	0.200	0.238
69	0.370	0.266	0.209	0.279
77	0.434	0.307	0.278	0.325

Table A2 - slab SA2 continued.

V	Rotation			
KN	N	W	S	E
85	0.487	0.332	0.312	0.344
89	0.570	0.427	0.382	0.426
93	0.600	0.466	0.412	0.755
97	0.620	0.510	0.430	0.800
101	0.746	0.557	0.458	0.852
105	0.746	0.640	0.504	0.922
109	0.800	0.697	0.542	0.993
113	0.840	0.759	0.583	1.040
117	0.938	0.845	0.630	1.110
121	1.020	0.992	0.679	1.198
125	1.105	1.000	0.719	1.280
129	1.246	1.100	0.779	1.390
133	1.410	1.200	0.833	1.460
137	1.610	1.385	0.891	1.529

Table A2 - slab SA2.

V	Mt	Rotation				
KN	KN m	W	E	S	N	C
22	0.736	0.067	0.127	0.016	0.014	0.030
31	1.472	0.068	0.203	0.064	0.068	0.067
40	2.208	0.080	0.296	0.136	0.163	0.108
49	2.760	0.086	0.362	0.266	0.283	0.138
55	3.312	0.086	0.423	0.316	0.345	0.168
69	6.624	-0.021	0.863	0.516	0.552	0.442
77	7.728	-0.083	1.000	0.656	0.559	0.541
85	8.464	-0.087	1.029	0.684	0.763	0.558

Table A2 - slab SA3.

V	Mt	Rotation				
KN	KN m	W	E	S	N	C
25	4.35	-0.070	0.290	0.04	0.028	-0.209
37	9.05	-0.500	0.810	0.130	0.226	-0.250
41	10.56	-0.719	0.890	0.180	0.439	-0.480
45	12.07	-0.967	1.130	0.250	0.547	-0.510

Table A2 - slab SA4.

V	Mt	Rotation			
KN	KN m	W	N	E	C
17	1.85	-0.016	0.040	0.045	-0.011
21	3.70	-0.057	0.050	0.110	-0.020
25	5.55	-0.097	0.060	0.467	-0.037
29	7.40	-0.157	0.070	0.550	-0.057
37	11.1	-0.307	0.140	0.563	-0.097
45	14.8	-0.495	0.252	0.940	-0.140
53	18.5	-0.787	0.380	1.569	-0.228

Table A2 - slab SB2.

V	Rotation	
KN	W	S
25	0.050	0.041
37	0.113	0.094
49	0.156	0.162
61	0.222	0.312
73	0.357	0.394
85	0.600	0.467
93	0.670	0.548
101	0.723	0.648
109	0.800	0.766
117	0.910	0.939

Table A2 slab SB1.

V	Rotation	
KN	W	S
21	0.038	0.029
57	0.224	0.189
69	0.258	0.226
81	0.319	0.279
93	0.414	0.367
105	0.519	0.462
113	0.595	0.525
121	0.696	0.582

Table A2 slab SC1.

V	Mt	Rotation			
KN	KN m	W	N	E	C
19	1.85	-0.015	0.013	0.084	-0.024
23	3.70	-0.017	0.037	0.120	-0.038
27	5.55	-0.038	0.050	0.200	-0.056
31	7.40	-0.064	0.060	0.292	-0.073
39	11.1	-0.174	0.074	0.553	-0.119
51	14.8	-0.240	0.121	0.947	-0.212
55	18.5	-0.360	0.171	1.539	-0.276

Table A2 slab SC2.

V	Mt	Rotation			
KN	KN m	W	N	E	C
19	1.85	-0.029	0.009	0.040	-0.011
23	3.70	-0.060	0.040	0.090	-0.027
27	5.55	-0.099	0.080	0.168	-0.039
31	7.40	-0.146	0.114	0.541	-0.050
39	11.1	-0.286	0.202	0.800	-0.085
47	14.8	-0.532	0.351	1.378	-0.143

Table A2 slab SD2.

V	Rotation	
KN	W	S
19	0.012	0.053
23	0.025	0.073
27	0.046	0.120
31	0.072	0.176
35	0.105	0.244
39	0.170	0.354
47	0.240	0.459
55	0.343	0.588
67	0.441	0.741
79	0.543	0.879

Table A2 slab SD1.